Towards the Manufacturing of Microfluidic Devices:
Fluid Flow in Multilayer Devices as a Test Case

by

Samuel N. Korb

S.B. in Mechanical Engineering, 2004
Massachusetts Institute of Technology

Submitted to the Department of Mechanical Engineering
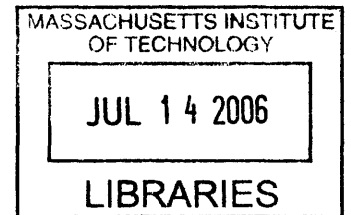in Partial Fulfillment of the Requirements for the Degree of

Master of Science in Mechanical Engineering

at the

Massachusetts Institute of Technology

June 2006

© 2006 Massachusetts Institute of Technology
All rights reserved

Signature of Author: ....
Department of Mechanical Engineering
May 12, 2006

Certified by: ....
Jung-Hoon Chun
Professor of Mechanical Engineering
Thesis Supervisor

Accepted by: ....
Lallit Anand
Professor of Mechanical Engineering
Chair, Department Committee on Graduate Students

Towards the Manufacturing of Microfluidic Devices:
Fluid Flow in Multilayer Devices as a Test Case

by

Samuel N. Korb

Submitted to the Department of Mechanical Engineering on May 12, 2006 in Partial Fulfillment
of the Requirements for the Degree of Master of Science in Mechanical Engineering

ABSTRACT

In this work, the area of microfluidics is analyzed for advances that could be made in the manufacturing of a microfluidic device, and then one area – the alignment of multilayer devices – is selected for greater focus.

Microfluidics is an emerging technology receiving much attention to date for its potential in biological, chemical, and medical applications. It could bring costs savings and contamination-reducing disposable parts, but only if certain hurdles relating to the design and fabrication of the devices are overcome. In order to better understand the manufacturing issues, a survey of the applications is presented, with a focus on the functional requirements for the fabrication of the devices. Then, a survey of the techniques currently in use to create microfluidic devices is presented, again focusing on the issues related to their fabrication and scalability to large-volume manufacturing.

In order to address the issues that arise during the surveys, two new directions are submitted. First, a "test device" is proposed. This test device will consist of a variety of sample features characteristic of many different types of microfluidic devices, in a range of carefully selected dimensions. The test device serves as a tool for evaluating different processes for relative capabilities in creating the microfluidic structures.

Second, multilayer devices, an area of concern that will arise as the field moves forward, is explored further. Specifically, the impact on fluid flow parameters of alignment of the two layers, a process currently performed manually, is investigated. A theoretical model of the scenario, which acts as a pressure barrier to laminar flow in a rectangular channel, is established, identifying the parameter of interest, the coefficient of pressure loss across the multilayer joint between layers. Then a series of sample multilayer parts with target dimensions of 100 μm x 100 μm x 3 mm is constructed. The pressure loss coefficients were obtained as a function of the cross-sectional area of the joint, from as small as 0.71 for very large joints up to over 1000 for joints that are only 30 μm of the channel in width. Failure pressure for the devices was found to be on the order of 140 kPa.

Thesis Supervisor: Jung-Hoon Chun
Title: Professor of Mechanical Engineering

Acknowledgements

My plan had been to seek maximum productivity and circumvent the Acknowledgements section, based largely on the inevitability of forgetting someone or other, but as the writing draws to a close and I feel more proud of what I have created, I am seized by nostalgia and feel compelled to correct the omission and give thanks where they are due.

This thesis is not merely a culmination of its writing, nor the two years of research of the manufacturing of microfluidic device, but instead my entire time at MIT. I feel that I've tried to learn from everyone I've come into contact with both inside and beyond the Institute, and in ways both obvious and subtle, I think each interaction has added to this work. So to everyone I've had the good fortune to interact with, and particularly the minute subset of you who will read these words, thank you.

Four individuals bear mention by name.

Professor Jung-Hoon Chun, my advisor, I am grateful to for believing in me and for sharing his many insights and humor.

JP Urbanski has been consistently helpful, and without his advice, I would still be in the lab trying to build a working device.

Kunal Thaker is both bright and capable, and his assistance with the Testing Platform was crucial to my research.

Kurt Broderick, the guru of the EML, was ever cheerful in the face of my constant barrage of questions, and I could not have succeeded without his help.

SNK
Spring 2006

"If you will it, it is no dream."
Herzl

3

Contents

List of Figures

8

1 Introduction

For any process in which a fluid is used, where the focus is not on bulk movement of the fluid, it is better to use less of that fluid. This is the basic tenant underlying the field of microfluidics. If blood is to be analyzed, it is safer for the patient to have one drop withdrawn instead of a test tube. If pharmaceuticals are being developed, it is less time consuming to use nanoliters of possible drug candidates instead of milliliters. And if an expensive reagent is used in an assay, it is cheaper to use less fluid. These factors are what drive the development of microfluidic devices. For this reason, for over thirty years, researchers have been trying to shrink the ways in which we work with fluids.

The challenge before the field is not only how to make devices smaller, but how to duplicate the macro-scale processes reliably at the micro-scale and how to fabricate them affordably at large volume. That is, if a drop of blood cannot sufficiently be analyzed for the presence of pathogens, then the microfluidic device is worth only as much as the plastic from which it is formed. Similarly, if the device is expensive, unpredictable, or worse, both, then microfluidics will never fulfill its promise.

A caveat is raised by the first sentence of this section: not all fluids are headed in a micro-direction. In fluid applications where the focus is on bulk transport of the fluid through the system or fabrication of large quantities of product, micro-applications will never be justified.

Microfluidics has been widely studied, and many different functions have been achieved. Simultaneously, methods for creating the devices and focusing on problems of manufacturing have been addressed. For this reason, the microfluidics area is referred to as an "emerging technology" [Fiorini 2005]. This implies that the fundamental technologies have proved successful in creating working prototypes of the technology, and that great promise is shown for applications for the technology. However, many steps forward remain to be made before microfluidic devices can available for a wider use. The traditional manufacturing rubrics of cost,

cycle time, and quality can be applied: at present, microfluidics fails to satisfy any of them sufficiently. At present, the majority of the microfluidic fabrication is still on a prototyping level with low repeatability. In this usage, repeatability is taken to mean similarity between successive parts created in the same process flow. But there are many potential long-term gains, so if these barriers can be overcome, the microfluidics market could explode.

In some ways, the development of microfluidics parallels the development of Micro Electro-Mechanical Systems, or MEMS [Verpoorte 2003]. Many diverse applications were demonstrated with the technology, but there are only a few applications where MEMS are used widely. One is in the acceleration detectors for automobile airbags. There are some higher-cost commercialized MEMS devices, such as high-end pressure sensors, like those produced by Kulite, or the Digital Light Processing (DLP) Chip produced by Texas Instruments for use in projectors, which has a wide array of fast-responding rockers with mirrors mounted to each. Each mirror represents a pixel in the final outputted image. MEMS have achieved far less market penetration than was initially hoped.

The concern with microfluidics is similar – that despite the large potential for innovation, the technology will face difficulties in being commercialized. The risk is more on the side of working out effective fabrication technology, and less on discovering the applications that MEMS face. In addition to the manufacturing issues discussed above, adoption of a new technology like microfluidics might face resistance if it perceived as new and unproven. Pharmaceuticals provide a telling example: while it is true that if microfluidic processes were implemented, they could provide a substantial savings in reagents consumed, there are currently billions of dollars invested worldwide in the current platform using mini-wells: robotics, sensors, handling devices, libraries, and everything else set up around high-throughput screening (HTS) processes, discussed in greater depth in Section 2.2.1. Further, if they could be made "backward compatible" (a term borrowed from computer software that implies the ability of a new technology to interface with existing infrastructure), for example microfluidic plates that are the same overall size as the mini-plates so the same robots can be used, then that would be an additional boon.

There is the possibility of a microfluidic "killer application," like the airbag sensors were for MEMS, that is able to selectively penetrate the market, but even this would be less than what the emerging technology is theoretically capable of achieving. Our hope in this area is to apply

our knowledge of manufacturing processes to improve the methods of fabrication of the devices, with the goal of facilitating the widespread adoption of microfluidics. To that end, a review of the applications that show promise for the adaptation to microfluidics is conducted, with the focus on the functional requirements for the potential devices that might be created to address those applications.

Secondarily, a survey is conducted of the current fabrication processes in use for creating microfluidic devices. While the fact that microfluidics have not broken into the big time suggests that more could be done to improve the processes, it is important to assess where they are at present, their relative strengths and weaknesses, and in particular their areas for improvement. It is hoped that by presenting the functional requirements of the applications and then the current capabilities side by side, areas of focus for future directions will be highlighted.

Next, given the current wide variety of process choices, a metric is proposed to facilitate the relative comparison of the different methods. Referred to as a "test device," it would feature characteristic features of typical microfluidic devices. It would be reproduced using the various methods of fabrication, and then measured to determine the process capabilities of the various methods on a standard rubric.

Next, given the increasing importance of multilayer devices, that area was selected for additional focus. A theoretical model of the fluid flow parameters, specifically the relationship between volumetric rate of flow and pressure drop, will be presented for the fluid flow in a multilayer microfluidic channel. The microscopic length-scale of the devices confines the flow inside the devices to the laminar regime, whereas most of the empirical models that exist for the macroscopic cases are for the turbulent case, requiring some adaptation as well as necessitating experimental verification of the model. In addition, a conceptual model for some of the alignment issues present in multilayer devices will be discussed. Using the soft lithography technique, a device was created that will be presented, as well as the flow parameters that were measured in the device.

One decision that was made early on was to limit the focus of the research to polymer-based devices. Microfluidic devices have been created in silicon, as well as glass, but the processing for these rigid devices by and large has a long cycle time, and the price can be steep. Conversely, polymer devices are cheap enough to be disposable, which is important to any process that could be sensitive to contamination, like many of the biological applications.

12

Toward the beginning of this section, there was a discussion of how microfluidics are only best if they can reliably reproduce the same functionality seen in the macro-scale. It should be noted that this, however, is part of an adaptive paradigm for the conception of microfluidics. That is, the statement assumes that the only areas where microfluidics will be successful are areas where macrofluidics have gone first and paved the way. It is also conceivable that completely new applications that were previously not possible at the macro-scale could be devised and implemented in the microfluidic regime. Unfortunately, that level of speculation is beyond the scope of this thesis, but it is a point that should be remembered when assessing the field of microfluidics for potential innovation.

2   Survey of Microfluidic Applications

The promise of microfluidics is great, possibly bringing great improvements in savings and efficiency to many different fluid processes [Nguyen 2002]. The applications can be grouped into the following categories:

- Assays
- Pharmaceutical Drug Discovery
- Genomics and Proteomics
- Cytology and Biotechnology
- Drug Delivery
- Surface Patterning

In the following sections, each of these applications will be discussed in greater detail. As can be seen, many of these have roots in biology and chemistry, with some extensions into optics and electrical engineering.

Throughout this survey, particular attention will be paid to the functional components of each fluidic process, as it currently exists in the macro-scale, to gain familiarity with what specific functions the micro-incarnation would have to mimic. From there, it becomes possible to draw up a list of key characteristics where tolerances have to be tightly controlled in order to insure a proper functioning of the device. It is in those areas that the bulk of the manufacturing research should be focused, in order to provide the specific functionalities required with acceptable quality and repeatability. By understanding the functional components of the processes in the abstract, it becomes possible to manipulate the methods of achieving those functions to create the best possible manifestation of the same functions on the micro-scale. This conception methodology is adapted from Suh [2001].

2.1 Assays

In the most general sense, an assay is a means of determining an unknown property of a substance, often the presence or concentration of a component substance in a mixture. An example of an assay might be detecting if a sample of air or water is tainted with a particular toxin or other agent. One of the areas where microfluidics are hoped to excel is exactly in this notion of an instant diagnostic test. Many different types of substances could be quickly checked for the incidence of other materials. This could be beneficial to healthcare workers in the field, checking the blood of a patient for disease markers, or to wildlife caretakers, checking drinking water for animals to make sure solute concentrations are within acceptable levels.

In the next sections, the functional view of an assay will be presented, as well as sub-areas of assays, including one case study that has already been recast in the microfluidic regime.

2.1.1 Functions of an Assay

In Figure 2-1, a graphic flow of an assay is presented.
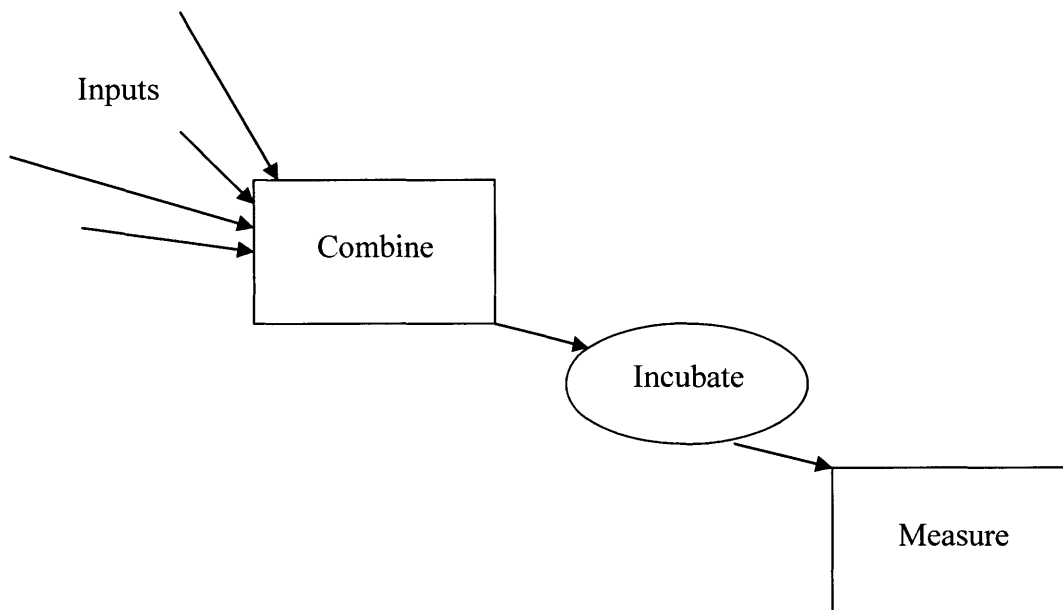
Figure 2-1: Components of an Assay.

The first thing to happen in an assay is that one or more substances are introduced as inputs. Typically, there is at least one sample to be interrogated, and at least one reagent that will combine with the sample in order to facilitate the eventual measurement.

Then, the inputs are combined. This can happen simply, or in particular sequences or at specific ratios. Next, the mixture is incubated, to provide an opportunity for the components to react. Here too, this might be as simple as agitating the fluid to promote physical mixing, or it might require some time for the reaction to progress, or it might require the additional of external stimuli such as heat.

Finally, the reaction must be measured in some fashion to detect the presence or concentration of the target substance. This most often occurs optically, via a color change or a fluorescence of the reaction, but it could be accomplished by electrically detecting a change in resistivity, or by some other measurement of a physical property due to the reaction between the reagent and the sample.

Typically, this is the end of the functionality, as the primary purpose of an assay is accomplished by the measurement step. However, in some cases, it might be necessary to further process the sample, in which case an output would need to be created. Also, during the combination step, it may be necessary to purify the target, particularly if other similar compounds are part of the sample that might cause cross-contamination.

These are the general functional blocks of an assay. Any microfluidic device that seeks to perform an assay must at a minimum be able to achieve these functions.

2.1.2 Types of Assays

Under the general heading of assays, there are various subcategories that refer to particular classes of assays. Bioassays typically involve an organism, such as a single-celled bacterium. The organism serves as the recipient for the target substance, and the intent of the assay is to measure the effects of the substance on the organism [Voldman 1999].

Another type is an immunoassay, in which particular organic or inorganic compounds may be identified within a mixture. In particular, immunoassays take advantage of relationships between molecules that are similar enough in shape to bind together favorably. In these relationships, the target is referred to as an antigen, and its homolog is called the antibody. By attaching the antibody to other molecules, such as a larger molecule or a magnetic molecule, the immunoassay can sequester the target antigen, either by mechanical straining or by using a magnet. A detailed understanding of the particular chemistries involved is necessary to design a

16

particular assay, but from the point of view of a microfluidic device designer, the same functionalities of inputs, combination, incubation, and detection apply.

One particular application, the Enzyme-Linked Immunosorbent Assay, will be discussed in greater detail in the next section, again focusing on the functions that will need to be replicated at the micro-scale in order to reliably recreate the same process.

2.1.3 Enzyme-Linked Immunosorbent Assay (ELISA)

This assay is an example of an immunoassay. The process is described graphically in Figure 2-2, and in the text below.
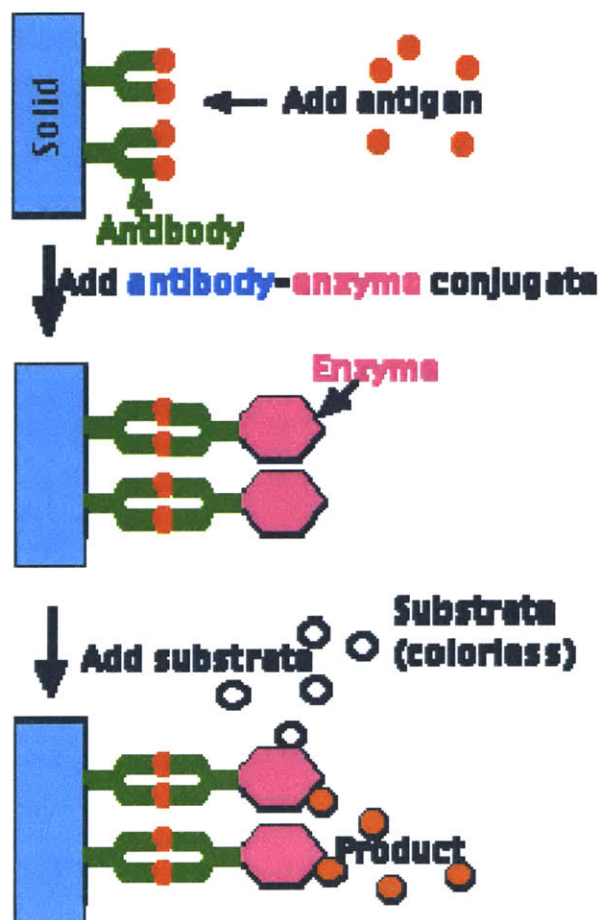
Figure 2-2: The ELISA Process, from Kimball [2006].

First, the surface, represented in Figure 2-2 as the solid, is coated with an antibody – the green Y-shape on the left. Then, the target antigen, portrayed here as the red circles, is added to the solution. Once there, it binds selectively to the antibody. In a step that is not shown, the solution is then washed, carrying away molecules that were not the right fit and did not bind,

17

replacing them with clean fluid. Next, the second antibody is added. This antibody is bound to an enzyme. The enzyme here is the pink hexagon. The antibody is only able to bind to the antigen, which was previously bound to the antibody attached to the substrate. Another wash occurs, removing the excess un-bound enzyme-linked antibody. The remaining structure is a layered arrangement of enzymes linked to antibodies bound to antigens bound to antibodies bound to the surface. The last step is to add a reagent that is originally colorless, but that is converted by the enzyme to a colored product, which can be detected by optical means. Color change implies enzymes, which in turn imply the presence of the antigen.

Turning an eye to functionality, the same general framework for an assay is present, with the purification step included, but the particular requirements for this method impose a few additional constraints. First, multiple inputs must be introduced at different times, based on the composition. Secondly, the device must have the capacity to perform the two washes that are critical to prevent false positives. Whatever material is used must be compatible with the first antibody to allow for bonding, or the surface chemistry of the material might need to be altered with some sort of additive. Finally, in order to detect the color change, there must be sufficient surface area in the device to create a threshold amount of product, and the material must be transparent in order to permit observation and detection. Eteshola [2001] created a prototype microfluidic ELISA device.

2.2 Pharmaceutical Drug Discovery

The route to a new medication, an arduous process starting from at most a hint of what directions to purse and continuing all the way through human trials, collectively referred to as pharmaceutical development, goes through a stage known as a drug discovery. This occurs fairly early on, when a target has been selected and a vast library has been assembled.

The target can be any sort of compound, molecule, or agent known to cause detrimental effects to humans. At present, much of the research is done on protein targets that are key actors in diseases or other conditions. The library is a huge repository of candidate molecules that may prove effective in fighting the target. Libraries can be developed in different manners, but most balance a mix of randomness to introduce diversity with some prior knowledge of successful compounds that may have worked with similar targets in the past.

18

The actual process used to evaluate the library's effectiveness on the target is HTS. HTS is known as a "brute-force approach," as it tests every single chemical in the library against the target. There are two types of screenings: target screening and cross-screening. Target screening is the first step, described in the previous paragraph, and cross-screening is performed further down the line. In a cross-screen, there are already a few potential hits, and these are crossed against other targets or compounds from the body to gain a better understanding of the total effect of the potential drug. That is, merely because a chemical shows effectiveness with one target, it might not be enough to justify further development. For example, a chemical that obliterates a target protein would seem to have promise, until it is discovered to have that effect on any protein it encounters. In that case, it would cause much more harm than good if used as a pharmaceutical. It is these molecular side-effects that a cross-screen attempts to deduce.

2.2.1 High-Throughput Screening

At the macro-scale, HTS is performed on plates serviced by robots similar to those in Figure 2-3.
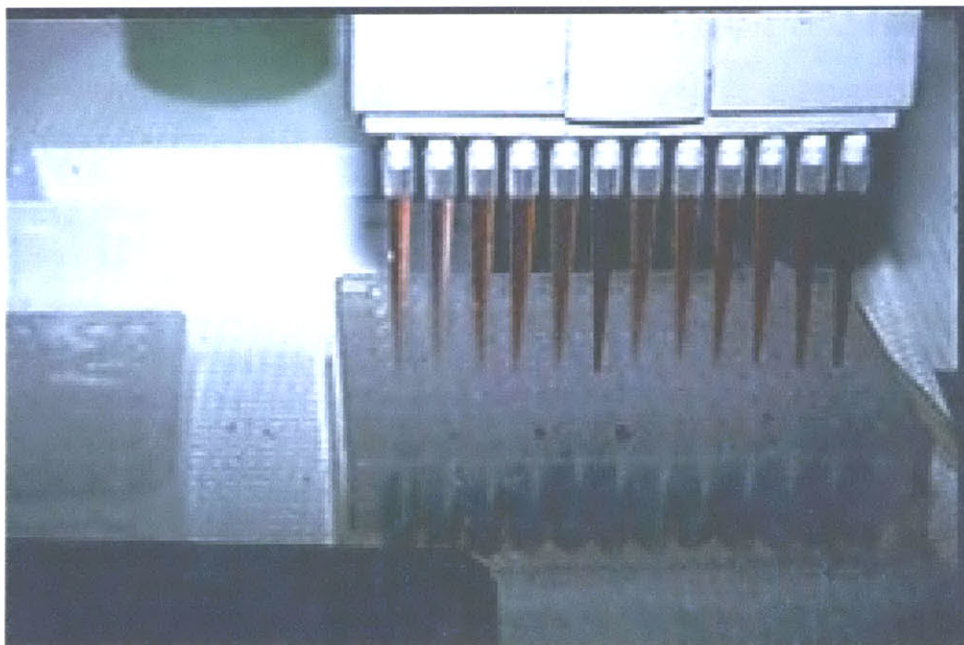
Figure 2-3: High-Throughput Screening Plate and Robot. From Michigan [2006].

The plate is the basic component of the screen. A plate contains many small wells, into which the target and the library element are deposited, usually with some non-reactive solvent as well. The robots that typically perform the HTS have a few different end-effectors. The one

pictured in Figure 2-3 is a series of pipettes, allowing the rapid delivery of fluid to multiple wells simultaneously. Other robotic appendages are hands that pick up the plates and move them from deposition locations to incubation locations, and possibly onto detection locations.

HTS can be viewed as a massively parallel set of assays. Each reaction that takes place inside each well in the plate is itself an assay. However, where assays typically look for the presence of a substance using known reactions, the screen looks for the incidence of a reaction using known reactants. The massively parallel nature of the screen puts additional pressures on the usual inputs-combine-incubate-detect functions of the equipment, as will be discussed after a brief explanation of the process flow.

The process consists of pre-filling the wells of the plates with the library of compounds and the solvent, after which the target is inserted into every well. After incubation, the measurement takes place, either by machine or manually with a human operator examining the plate. The method of detection is almost universally optical, since introducing other probes would greatly increase the costs. Finally, the potential hits are often extracted from the first set of plates in order to create a second-stage screen. The purpose of this second screen is to compare the results of the potential hits from the first screen side by side.

The functions of a microfluidic incarnation would be similar. It would need to pre-fill the test compartments with the components of the library, which would require a high degree of addressability within the device, and distribute the target to each of the test sites without contamination between different library elements. These two steps could be interchanged, i.e. the target could be distributed uniformly first and then the library applied thereafter. Then, after incubation, optical measurement must be possible, usually requiring a transparent material for the device. Finally, potential matches must be able to be selectively removed, requiring the same degree of addressability as for the library distribution, but in reverse. Daub [2004] describes the issues of adapting HTS to microfluidics in greater detail.

2.3 Genomics and Proteomics

Genomics is the study of the genome, the sequence of nucleic acids that make up deoxyribonucleic acid (DNA). Proteomics is the study of proteins, strings of amino acids that are transcribed from DNA. Since many of the processes used in working with DNA and proteins are similar, the two areas have been grouped under the same general category.

20

Practically, laboratory techniques in genomics and proteomics seek to discover more about the structure or makeup of DNA strands and proteins found in the body via physical manipulation. For DNA, the end goal is typically sequencing, or determining the order of nucleotide bases in the chain. There are four nucleotide bases, adenine, thymine, guanine, and cytosine, abbreviated A, T, G, and C, respectively, and their arrangement determines the workings of the organism. The genome is the full set of DNA within an organism, and the well-publicized Human Genome Project [2006] was an attempt to determine the sequence of the human DNA. The list of bases fully describes the DNA strand, so the laboratory tests seek to find that sequence.

The sequencing procedure begins with DNA extraction. The DNA normally is found inside the nucleus of the cell, so both the cell and the nucleus must be breached to isolate the DNA. Bursting a cell is also known as lysing.

Once the specific strand has been isolated, it has to be replicated many times over to create a sufficient volume of the same strand to allow the subsequent tests to have accurate results. The most common method of replication is known as the polymerase chain reaction, or PCR. PCR takes advantage of the natural ability of particular enzymes in the cell, known as polymerase, to duplicate the DNA of the cell. The full set of DNA in a cell must be duplicated every time a cell divides, so all that is necessary to artificially promote replication is to provide favorable conditions and the polymerase molecule in sufficient volume, and the natural replication mechanism takes over from there. PCR will be described in more detail in the next section.

In order to perform the sequencing, the DNA molecule is actually replicated with the inclusion of modified bases. This is known as the Sanger technique [Sanger 2006]. A solution is prepared containing the strand to be sequenced, replication enzymes known as DNA polymerases, the four bases used to build the DNA strands, and a small amount of specially modified bases. The modified bases can be inserted into the chain being built by the polymerase, but they then terminate the replication by interacting with and inhibiting the polymerase. The modified bases also carry a fluorescent marker. The sample contains all four of modified A, modified T, modified G, and modified C, and each of those is keyed to fluoresce at a different color wavelength. When the polymerases go to work, every so often, they will use a modified base that suddenly terminates the processing. Then, if the sample can be sorted by length and

viewed under a fluorescent light source, it will reveal a clear presentation of which base is at which position in the original strand.

The processes used to sort the strands by length are essentially filters that force the solution of sub-strands through a medium that inhibits the flow. If either the inhibition of the filter or the attraction of the force is proportional to the length of the strand, then, after running the filter for a long enough period of time, the sub-strands will have separated from one another, and the relative position in the filter will be the relative length of strand.

The motive force for most of the filters is electrical: a cathode is inserted into one end of the channel, and an anode into the other. The strands themselves have a charge, and thus the electric field created by the voltage drop between the electrodes will push them along.

What sets the different methods apart is the medium of filtration. A common macro-scale process is known as gel electrophoresis. The sample is deposited at one end of a large block of agarose gel, a substance derived from seaweed. The molecules can diffuse through the gel, but in doing so, they are forced to meander around the gel molecules. The longer the chain, the more laborious each evasion, leading to the requisite separation. The different side strands appear as bands after running the current for a while, which can give either relative measures of length, or can be compared against a calibrated ladder sample with known components.
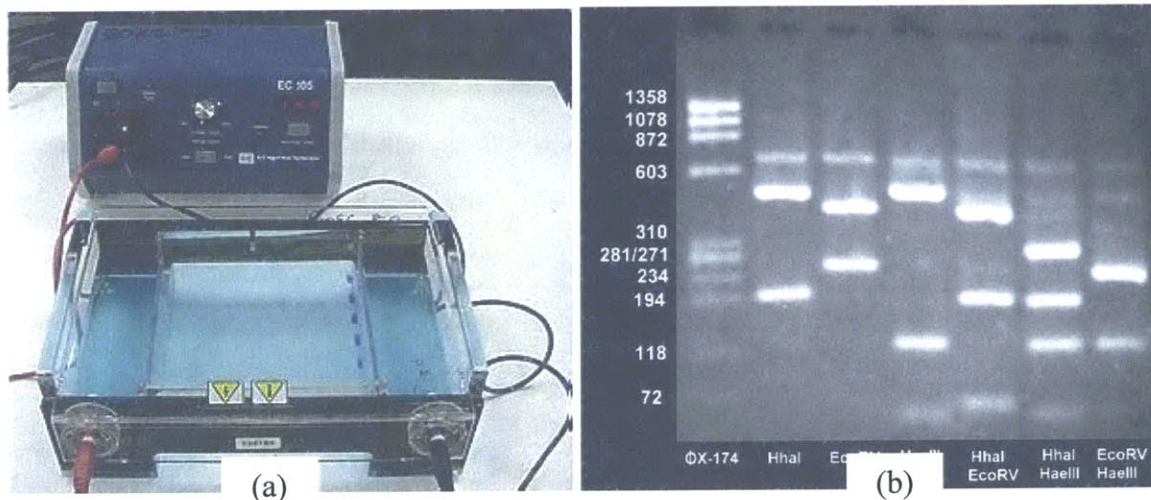
Figure 2-4: Gel Electrophoresis: (a) Experimental Setup, from Iowa [2006], and (b) result, from Carr [2006]. Note the kilo-base pair scale on the left of the results in (b), calibrated to the ladder that is shown in the left-most track.

In order to get sufficient resolution between the bands, the overall size of the gel makes this particular method not well suited to miniaturization. The procedure that does show promise

is called capillary electrophoresis. As the name suggests, the test is very similar to gel electrophoresis, but with a capillary tube in place of the gel. The capillary tube is merely a minuscule channel inside which the solution can flow. If the diameter is sufficiently small, on the order of tens of microns, a similar inhibition based on length will occur, leading to the same separation. The process will be discussed further in a subsequent section.

One other novel approach being taken by J. Han [1999] is to create nanofilters. These function by alternating the transverse depth of a fluid channel from wells on the order of microns deep to constrictions on the order of nanometers deep. In order to pass through the constrictions, the molecule is forced to pass single file, spreading out into a thread-like configuration. When it gets to the next well, it is free to ball up again. What Han has found is that this spreading/clumping process takes a different length of time for different strand-lengths, so given a constant flow rate across the nanofilter, the required separation also takes place.
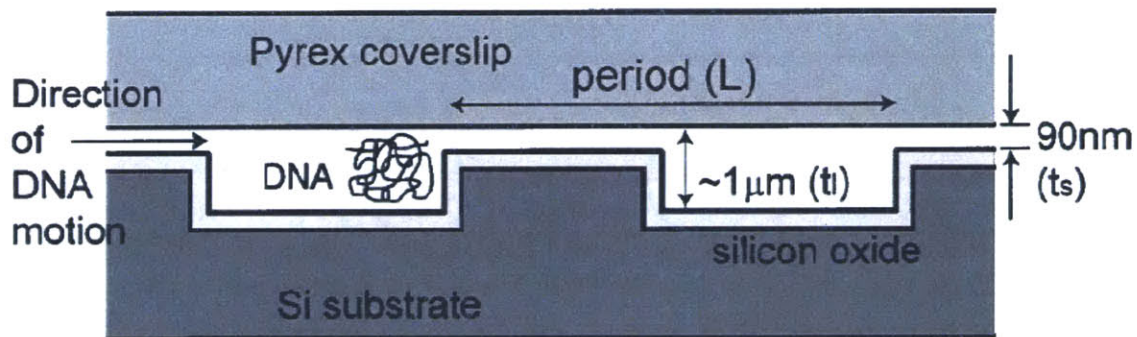
Figure 2-5: Diagram of Nano-Filtration, from Han [1999].

For proteins, in addition to the sequence of amino acid peptides that form the strands of the protein, there is a higher level of information about the protein: the physical shape of the molecule. Once a sequence of peptides has been strung together, they undergo a complex folding procedure based on the electrical interaction of the side-chains on the peptides, ultimately resulting in their finished shape. It is this shape that allows the proteins to have the functions that they do, so researchers are often interested in both the sequence and structure of the proteins. Thus, in addition to tests for determining the sequence of the amino acids, tests for determining the structure of the protein are also necessary. The former are similar in nature to the DNA tests described in this section, and a common method for examining the structure of the protein molecule is called protein crystallography, described in Section 2.3.3.

In the next sections, a few of the processes described above will be discussed in greater detail, and their functions delineated for adaptation to the micro-scale.

2.3.1 Polymerase Chain Reaction (PCR)

A graphical depiction of PCR is shown in Figure 2-6.
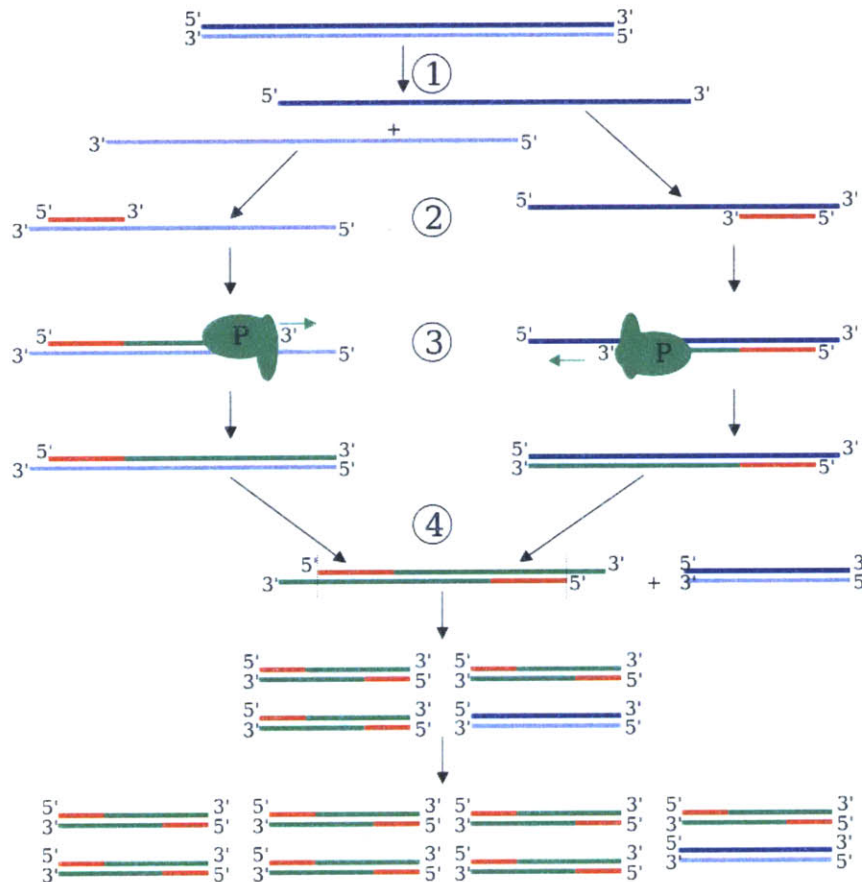
Figure 2-6: Polymerase Chain Reaction (PCR) Process Diagram, from Manske [2006].

DNA naturally occurs in matched strands. The four nucleotides discussed in Section 2.3, A, T, G, and C, each has a natural binding partner. A binds with T, and G binds with C. So while one segment of DNA might read GATTACA, its complement on the opposite strand would read CTAATGT. In Step 1, the two chains, which are normally bound together, must be detached so that the polymerases can get access to the nucleotides for the replication. This process is called denaturation, and takes place at a high temperature, normally 94° C to 96° C. Next, in Step 2, short strands of DNA known as primers are attached to the two denatured sides. The primers promote the activity of the polymerases, which take effect in the next step. The attachment of the primers is referred to as annealing, and the anneal occurs at 45° C to 60° C,

24

depending on the primer and the target strand. Once the primers are affixed, the polymerases go to work at replicating, at a temperature of 72° C.

This whole process, of denature-anneal-replicate, is repeated twenty to thirty times in a row, and if successful, the process leads to an exponential growth in the number of product strands. Care must be taken to prevent both evaporation of the mixture (given the high temperatures), as well contamination at any point in the process, since this could lead to erroneous duplication of unintended DNA strands.

The inputs to this process are the target DNA, the polymerase molecules, the primers, sufficient nucleotide bases to make up the final amount of DNA, and a buffer solution. The volume that usually is used for macro-versions of PCR is anywhere from 15-100 microliters. One restriction of PCR is that it is only useful for strands of DNA under 10 kilo-base pairs, and it is best suited in the 3-6 kilo-base pair regime. The reason for this is that errors in replication are more likely to crop up at the longer lengths.

Turning an eye to functionalities, the primary requirement of a PCR device is the very specific temperature control. Both time and temperature are constrained very tightly by the established processes. Beyond that, the material of the device must be able to withstand those temperatures, which rules out the common micro-material PMMA, and it must be impermeable to gas diffusion to prevent the evaporation of the solution. The device must be able to accept inputs and provide outputs, and if the components of the solution – DNA, primers, polymerase, nucleotides, and buffer – are to be combined on-chip, those ratios must also be carefully controlled. However, if the components were combined off-chip, the actual fluid network becomes very simple, in that it need do little more than give the solution a place to replicate.

One way of doing that is shown in Figure 2-7. In this scenario, the substrate below the microfluidic channels is what contains the heating elements, perhaps through a resistive electrical heater. Thus, as the fluid flows on top of the different heating sections, it would be heated to the proper temperatures. The time spent at each temperature is controlled by having different channel lengths on top of the different temperatures. Then, if the fluid is flowed through the channel at a known volume flow rate, the cross-sectional area can determine the mean velocity in the channel, which in turn can be used with the channel length to determine the time in a given region of the device. This approach is interesting, in that one of its functional requirements, which flows from the requirement of tight control of times at each temperature, is

thus similarly tight control of cross-sectional area along the channel, as gross variations would impact local velocity and from there, the heating times.
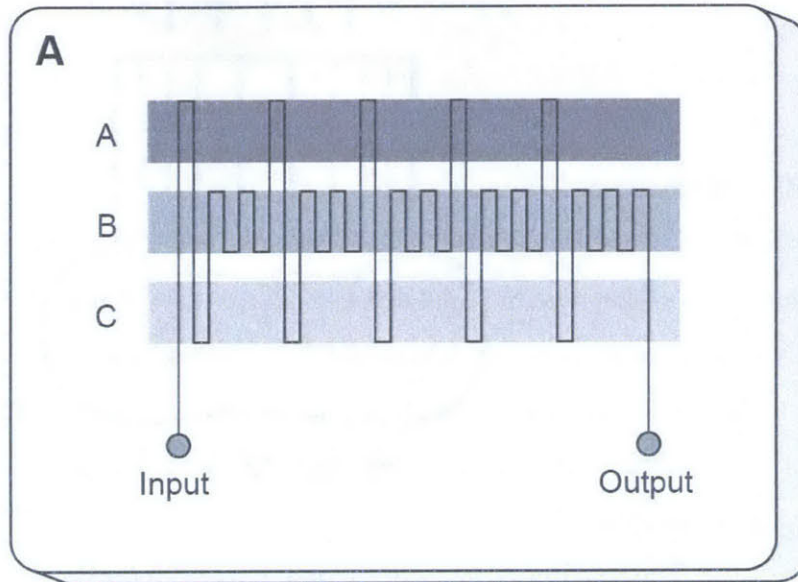
A   95°C - melting
B   77°C - extension
C   60°C - annealing

Figure 2-7: Microfluidic PCR Device, with heating controlled by the substrate and timing controlled by flow rate and channel length. From Kopp [1998].

$$t = \frac{L}{V} = \frac{L}{Q/A} \qquad (2\text{-}1)$$

where t is the time, L is the length of the channel, V is the mean velocity of the fluid, Q is the volumetric flow rate of the fluid, and A is the cross-sectional area of the channel.

2.3.2 Capillary Electrophoresis

As detailed in Section 2.3, capillary electrophoresis is one method of separating the different sizes of sub-chains within a solution. It uses the same motive force of an electrical potential field, or voltage drop, across its length, as gel electrophoresis. However, the flow-impedance is not the molecules of agarose gel, but instead the channel itself, which is very small. The width of typical capillary tubes used for capillary electrophoresis is 50 μm. The detection

method is also slightly different. Rather than observing the sample in all parts of the structure, as in gel electrophoresis to determine the relative positions, the detector is focused on the outlet, and the detection takes place on a time axis. The inputs are placed at the beginning of the capillary, the voltage is turned on, and then the detector waits until it sees the different chains come out in bursts. Plotted against time, these spikes give a relative measure of the charge of the sub-chains, again assuming that the rate of travel, and therefore total travel time along the channel, is proportional to the charge of the molecule.

As for requirements, beside the typical inputs and detector, the channel itself introduces some interesting issues. Specifically, the chemistry of the material of the channel may need to be designed or selected based on its ability to interact correctly with the DNA to provide adequate resistance to the flow. Also, the size of the channel can impact the final results, so the device must be able to have a fairly uniform along its length. However, it should be noted that detected results are always at best relative results, so the fabrication method used to make the devices need not necessarily have high repeatability of channel dimensions or uniformity.

2.3.3 Protein Crystallization

The shape of a folded protein molecule, which as discussed in Section 2.3 is often of interest to researchers, can be detected using a process known as x-ray crystallography. X-rays are passed through a crystal of the protein, and based on the scatter that results, the structure can be traced back to better understand the structure of the protein.

In order to perform the crystallography, a crystal of the protein must be grown. This is not an insurmountable task, as given the right conditions, the protein molecules will naturally self-align into the periodic lattice that forms a crystal. The challenge of the microfluidic designer is to re-create those conditions at the micro-scale that will lead to crystal growth. Typically, the method of growing the crystal is to carefully precipitate the protein molecules out of solution. When the molecules are singular and floating around in solution, they have the mobility necessary to grow in the proper arrangement out from the lattice, and not be dominated by other effects, such as gravity or inter-molecular forces leading to random clumping. The key, therefore, is to identify methods of very slowly decreasing the precipitation point of a solution containing the protein in a high concentration or identify methods of very slowly increasing the concentration of the protein near to the precipitation point, or both.

A solution with a high concentration of the protein is usually the starting point, and then specific reagents that lower the solubility to near the precipitation point are added. Finally, the concentration is slowly increased to foment the precipitation, by one of two methods. The first is vapor diffusion, in which a drop of solution containing the protein and reagents in high concentration is placed near a reservoir containing many of the same solutes with the exception of the protein. Then, due to diffusion, the solvent slowly diffuses out of the target drop. As the amount of solvent is reduced, the concentration of protein in the remaining drop correspondingly increases. The other method is known as dialysis, and is essentially a filtration method with a membrane permeable to the solvent but not the protein. As the solvent crosses the barrier, the remainder is again higher in concentration. In both of these methods, the protein will begin to precipitate, and the crystal will grow. Once a sufficiently large crystal has grown, the x-ray crystallography can commence.

From the functional side, the device must be able to input and convey the carefully balanced solution, or be able to balance the components on-chip. Then, the nucleation site must be accommodated, with either an embedded membrane or a method of containing both drop and reservoir for the vapor diffusion method. There must be sufficient volume on the chip to grow a crystal of the minimum usable size, and presuming the crystal will not be moved off the device before the detection, the device must be permeable to x-rays. Almost every candidate material is indeed permeable, so that requirement is easily fulfilled.

2.4 Cytology and Biotechnology

Cytology is the study of cells, their processes and functions. Cells can also be used as micro-laboratory themselves, where other processes can be implanted and examined. Biotechnology is a term that has come to mean many different things to many different people, but it is used in this context to indicate the use of biological processes to create some sort of useful product that is beneficial to humankind. This is the most general definition of biotechnology, using biology as a tool. Berthier [2006] contains a wealth of information related to microfluidic biotechnology. As discussed in Chapter 1, microfluidics are not well suited to mass production – micro being a possible antonym to massive – but it is conceivable that if only a trace amount of a particular substance were required, it might be possible to use a microfluidic device as the factory floor in which to create it.

28

There are many different procedures or techniques that could be used to examine the functioning or processes of cells, to explore the reaction of cells to various stimuli, or to grow a particular biotech product. Similar to the assays discussed in Section 2.1.2, this treatment will set aside the various specific applications, and instead focus on the issues important to the microfluidic engineer as this technology continues to moves forward.

A similar modular analysis to Figure 2-1, the general flow of an assay, is typically present in a microfluidic cytological application, for the examination of a cell can be viewed as an assay, in some respects. There are various inputs that are combined and then allowed to react, and finally, in order to know what happened during the reaction, it must be possible to detect some response. The areas where using cells as the target of interest might be more complex would be the incubation step, the detection step, and the output step.

In the detection step, cells are by their very nature quantized, unlike a fluid input, which can be more readily conceived of as continuous. If a particular gene was expressed in a cell, it would be expressed throughout that cell. However, there would be no way to know if the cell next to it had that particular gene. Thus, the method of detection needs to be able to both measure a cell once across the cell, and also be able to distinguish between different cells. This can also impact the output methods, as it might be desirable to sort the cells, based on the results of the detection. This issue was addressed by Chou [1998], leading to the device pictured in Figure 2-9. The requirements of a sorter and the method that was undertaken to address them will be explained in the next section.

The incubation step is another area that might require a more complicated approach. If the effects of the reagent or other non-cell input are immediate or are present after a few minutes, then the same methods of incubation from a regular assay may be sufficient – often, just a length of channel, and as the fluid flows along at a known flow rate, a specified length of time passes. But if the duration is to be longer, such as when a cell must continue growing before it expresses the gene, then a longer term of gestation is needed. The general terminology for the growing of cells is culturing them, usually referred to as a cell culture. A cell culture would also be used in biotechnology to support the cells that would be growing the product. Section 2.4.2 will discuss the general requirements for cell culture.

Functionally, any channel that a cell is to flow down must be able to fit that cell. Cell range in size from 1 μm to 100 μm, so there is a wide variation, but presumably the cell or cells

under examination would be known before building the device, so a nominal value would be easily enough to set. Thereafter, fluctuations in the size of the channel introduced by variations in the fabrication processes may not have a huge effect on the functioning of the device. The fluctuations must still be within the limits of too small to pass the cell and some arbitrary upper limit. One upper limit might be a channel where two cells could flow next to one another, in those cases where it is imperative that the cells flow one after another, such as in the sorter.

This is not to suggest that channel size and uniformity is never a key characteristic for cytology, since there are many different possible scenarios that could be envisioned where the particular application might require more specific control. For example, if it were necessary to squeeze a cell perpendicular to the direction of viewing, perhaps to better view the inside of the cell, it might be necessary to have the channel contract in depth to a much smaller value then when the cell is to flow normally. But the statement does imply that in the absence of other application-specific requirements like the example just explored, the demands on the channel size are indeed lax.

2.4.1   Cell Sorting

A block representation of the requirements for a cell sorter is shown in Figure 2-8.

After the bulk of cells are accepted, there must be some way of distinguishing among them. Very often, this has been done by separating the cell spatially in the flow, and having the channel narrow enough so only one cell at a time can pass along it. However, it could be done by some passive micro-well, or perhaps by a dynamic detector with resolution on the order of the cell size. Next, or perhaps simultaneously in the latter configuration, the detector must be able to interrogate the cell. This is probably best done with optical methods, similar to the assay, but could also be done with some other metric. Then, the detector feeds information to the structure that actually affects the sorting. In most cases, this will be multiple outputs with a valving arrangement. As will be discussed in Section 4.4.3.2, valving can take many forms, but still remains one of the outstanding challenges of microfluidics.

.

30
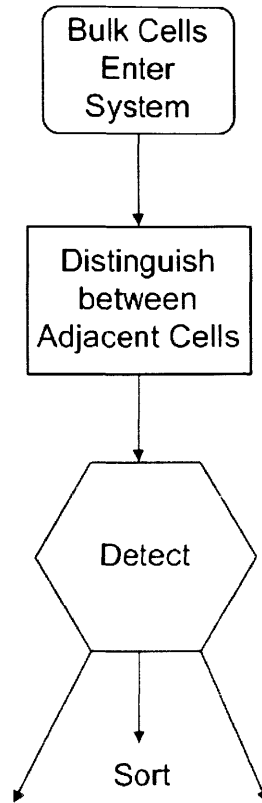
Figure 2-8: Block Diagram of a Cell Sorter.

A picture of the cell sorter developed Chou [1998] is shown in Figure 2-9. The general shape of the sorter was a T, with the bottom of the T the input, and the two outlets at the ends of the top of the T. The cells were separated from one another for detection by a constriction of the channel down to 5 μm, at which point they were forced to travel in single-file. The cells are detected via laser light and photo-detectors, with one of the cell-types fluorescing one color and the other a different color. In this way, it was possible to distinguish between which cells should go to one output and which to the other output. The actual valving was performed using relative pressures. The input was set at some constant feed pressure to push the cells down the channel. One of the outputs would have a neutral pressure, while the other output would have a much lower pressure. Thus, the flow would continue from the input to the low-pressure output. The measurement from the photo-detector would be able to switch which of the outputs was at neutral pressure and which was at low pressure. In this fashion, it was possible to send a green cell to the right, and a red cell to the left. As all of the functions and requirements of a cell sorter were met, the device was indeed a working cell sorter.
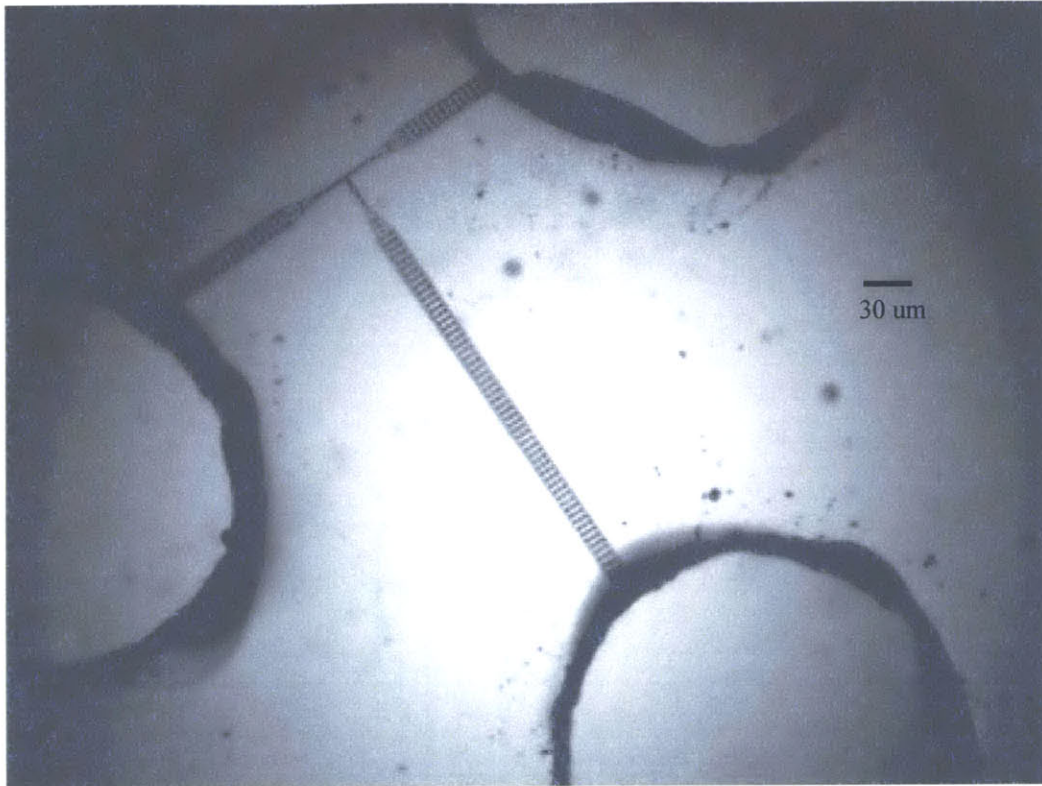
Figure 2-9: Cell Sorter, from Chou [1998].

2.4.2 Cell Cultures

The general requirement for any device performing a cell culture is that the cells have sufficient conditions to survive and thrive. More specific requirements than the general one are derived from the type of cell being cultured, but there are a few general categories. First, the cell needs some sort of food, such as nutrients and water, or in the case of chloroplasts (the organelle in plant cells that is responsible for photosynthesis), a source of ultraviolet light. Secondly, some cells may have an optimal temperature for growth, in which case providing this temperature becomes a functional requirement. Other than that, the cells just need some sort of container in which to grow.

Some cells might grow while floating around in a solution, while others might need to bind to a substrate. For the latter, particular surface chemistry of the underlying material might be required, or a particular geometrical shape over which to grow. Beyond this very topical treatment, a specific type of cell would have to be posited to address the specific issues for that cell. Leclerc addresses a major area of interest to cell cultures: tissue engineering, where particular types of cells are grown which then aggrandize into artificially grown tissues.

32

2.5 Drug Delivery

Drug delivery can be applied to microfluidics in any situation where the typical methods of drug delivery - injection, ingestion, infusion, inhalation, inter-rectal insertion, or absorption through the skin - prove insufficient. Perhaps sterile needles are unavailable, or the time for a pill to dissolve is too short, and microfluidics provides a better solution.

There are two areas where microfluidics show promise for drug delivery. The first is micro-needles, and the second is micro-containers filled with medicines that are implantable or can be triggered to rupture at a given time, or both.

A microneedle is just that – a needle that has a small diameter and an even smaller fluid channel inside of it with an opening at or near the tip. The case in which the opening might not be exactly at the tip, similar to the typical macro-needle, is if the fabrication method limits this positioning. Microneedles have been created in silicon with the port slightly off to the side of the tip. The small size of the needles allows them to more easily penetrate the target and deliver the drug, and they could be used singly or possibly in an array, to provide multiple points of injection over a given area. The further advantage of a microneedle is that since it has such a small cross-sectional area, it could be injected with no more force than applying an adhesive patch. The microneedle or microneedle array could be applied externally or internally, depending on the application.

The functional requirements of a microneedle are the general geometrical descriptions of the needle - long and thin, with a channel down the inside [Nguyen 2002]. The material must be sufficiently rigid to withstand the insertion force without buckling, and the structure must be biocompatible in any parts that touch the body, be they exterior – just the needles themselves – or interior – the entire device including the packaging behind the reservoir. Finally, there must be some motive force to drive the fluid from the reservoir out through the needle. At small volumes, capillary action or diffusive forces could be sufficient. At larger volumes, some method of increasing the pressure in the reservoir, such as the same force of injection, might be required. This is not an unreasonable design parameter, as similar to macro-injections, all of the fluid could be delivered at once.

The other major area of drug delivery that shows promise for microfluidic devices are devices that store a drug and then release it at some later date. This element of delayed release sets this area apart from microneedles conceptually, although theoretically, the two could be

coupled into one device. Most commonly, these devices would be implanted into the body. The storage requirement is very simple: a micro-well or other small reservoir to contain the medication, presumably in fluid form. The release requirement is slightly more complicated. Stated most generally: at a desired time, remove the barrier between the reservoir and the surrounding fluid. The method chosen to affect the former requirement could be tied in to the latter, in the case of a barrier that degrades over a known length of time, or could be separate, in the case of an exterior control system that sends a signal to rupture a fragile membrane. This second approach was exactly the one taken by Langer [Santini 1999], in creating a silicon device with a thin gold membrane. Upon applying a voltage that exceeded the dielectric breakdown strength of the gold, the membrane would burst, releasing the contents of the small micro-well underneath the membrane. Interestingly, Langer also investigated a degradable material, but used one that was impregnated with the drug, not involving any fluid components.

2.6 Surface Patterning

Surface patterning is a technique that could be applied in different areas, and works much like a microfluidic stencil. A fluid or other substance is deposited in a specific arrangement or pattern on a substrate [Benn 2006]. Some of the terminology used in injection molding is borrowed for this discussion, as the device acts like a mold, into which the fluid is injected. The process is shown in Figure 2-10.
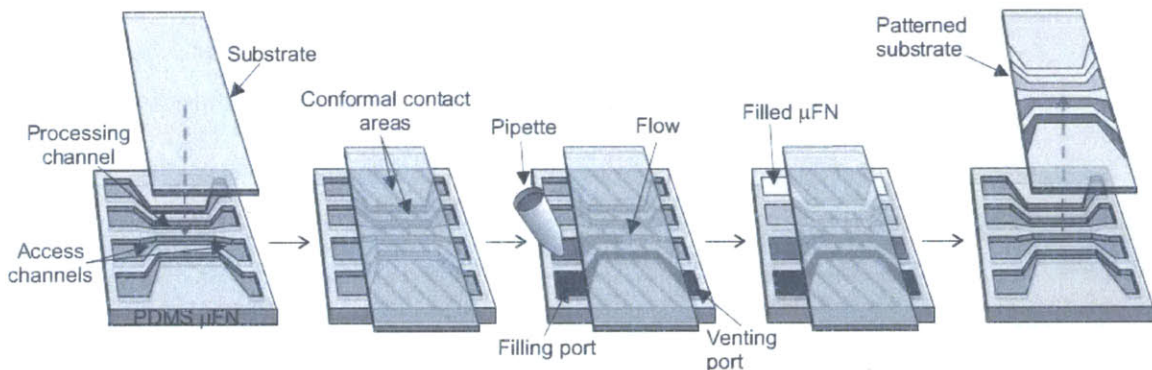
Figure 2-10: Surface Patterning, from Juncker [2001].

First, a compliant, open-channel device is attached to the target surface. The channels are open so that when they are filled with fluid, the target surface will form one of the walls of the channel, and thus the fluid will be in contact with the surface. The device is compliant to promote a good seal, as the surface might have some roughness or not be perfectly flat. If a rigid

device (such as one fabricated from glass) was used, unless the target substrate could be guaranteed to be as flat as the device, the seal would not be good, and the channels would leak, leading to a reduction in the resolution of the image duplicated. Another piece of glass would probably fulfill this requirement, but any other substrate would require another approach. A compliant material, like PDMS, would work much better. Also, PDMS is fairly sticky to many common substrates, which would also help with adhesion and sealing. In the absence of a chemical affinity, some other adhesive would have to be used, again to prevent leaks as the channels are filled. If there is some existing patterning or other location-specific features, alignment of the device to the substrate could become an issue.

Next, the channel is filled with the desired fluid, or a solution bearing the desired solute. In order to do so, there must be an escape mechanism for the air that was trapped in the channels during the fixation of the device to the substrate. This could be accomplished with a vent at the far end of the channel, allowing the air but not the fluid to escape. It could also be accomplished with a material that is gas permeable, such as PDMS [Randall 2005], and which could be backfilled, applying additional pressure as the fluid flows in to force the gas out of the channel and into the material.

At this point, the entire assembly, substrate, fluid, and device, can be baked to remove some of the solute. The goal would be to increase the viscosity of the fluid that is in the channel, so that when the device is peeled off of the substrate, the fluid will not flow elsewhere on the substrate, outside of the bounds of the desired area. Alternatively, the device could contain a heater, but this would introduce much more complexity into the device. A further alternative would be if the material were gas permeable, so some of the solvent could evaporate through the bulk, leaving the solute. Finally, if the potential energy of the fluid on the surface was sufficiently low, and the contact angle was less than 90° as a result, the fluid would be unlikely to flow. This scenario, which requires a specific choice of fluid and substrate, would require a greater pressure on the fluid to force it to flow into the channels. The same reluctance to flow in the uncontrolled post-removal regime would be a reluctance to flow in the force filling of the fluid into the channels.

Finally, the device is removed from the substrate, leaving the fluid or solute on the surface of the substrate. If the device is formed from a compliant mechanism, this will be a peeling operation; otherwise, it will be a prying operation to overcome the force of whatever

adhesive was used. In no circumstance would it be desirable to shift the device in the plane that it shares with the substrate, as this would likely mar the pattern.

Many of the functionalities were discussed in the explanation of the process earlier in this section. Among them is a sealing method, which could be accomplished with a sticky, compliant material, as well as possibly needing to align the device to the substrate. A mechanism of venting the gas trapped in the device is also required, as is a process of preventing post-removal spreading. In addition to these, the two dimensional dimensions of the device at the weld line, the plane where the device and substrate are in contact, can be important, as dictated by the particular application. Also important is the depth of the channel at any given point, because the depth of the channel could control the amount of fluid or solute in the channel above the surface of the substrate, and in turn, the amount that gets deposited onto the surface.

Benn [2006] has also addressed this type of microfluidic device, actually using surface patterning as a method of performing an array of assays. The arrangement uses two surface-patterning devices, each creating a pattern of parallel lines of multiple reagents on the substrate. First, one device is applied, and the first group of reagents is flowed into the channels. The first device is peeled off, and the second is applied perpendicular to the orientation of the first. The second group of reagents is flowed in, and then the second device is peeled off. What remains on the surface of the substrate is a hatched pattern, two sets of parallel lines perpendicular to one another. Each place a line crosses, a tiny assay is created, so in general if the first and second devices are identical and each has N inputs, there are N^2 combinations present on the substrate. Detection again becomes an issue, but if fluorescent markers are included and the substrate is a glass microscope slide, it becomes as simple as viewing the array under a fluorescent microscope.

Work done by Goluch [2005] took the compliance of the PDMS device to the next level, showing that surface patterning could be done on cylindrical surfaces, as well.

2.7 Summary of Applications

The information contained in this section is recapitulated in Table 2-1.

36

Table 2-1: Microfluidic Applications and Functional Requirements

Application	Functional Requirements
Assay	• Inputs • Combine • Incubate • Measure
ELISA	• Purification • Input Sequence • Washes • Surface Chemistry • Transparent
High-Throughput Screening	• Pre-fill Library • Distribute Targets • Transparent • Selective Output
Polymerase Chain Reaction	• Temperature/Time Control • Input Ratios • Gas Impermeable
Capillary Electrophoresis	• Surface Chemistry • Capillary Width (50 μm)
Protein Crystallization	• Input Ratios • Nucleation Site • X-ray Permeable.
Cell Sorting	• Input • Distinguish Cells • Detect • Sort
Cell Cultures	• Control Environment • Feed
Drug Delivery	• Store Drug • Release as Required
Surface Patterning	• Seal to Surface • Vent Air • Input Patterning Material • Prevent Post-Removal Spreading • Detach from Surface • Pattern Reproduction.

3 Survey of Polymer Microfluidic Techniques

In the majority of polymer microfluidic devices, the polymer is first shaped by a mold, and then sealed to create a final device. The mold carries the microfluidic features in negative, and the polymer is then formed around the mold, to create the finished device. In this respect, the creation of the polymer parts is parallel processes, where the entire face of the device can be fabricated simultaneously. The other alternative, a serial process like milling, is less preferred due to the potential for poor performance of the polymers if they were subjected to point processing, particularly if plastic yielding was non-localized on the device, leading to hysteresis or magnification of errors.

In the sections that follow, an overview of the processes in use to create microfluidic devices will be presented, with a focus on fabrication and manufacturing concerns, where appropriate.

3.1 Mold Creation

All of the polymer fabrication methods start with a mold. Fabricating the mold itself can be another entire process, sometimes more complex than the forming of the plastic from the mold. However, this additional time or cost is typically seen as justified if the mold can be used in the fabrication of many polymer parts.

Mold life is also dependent not on the number of cycles until failure of the mold itself, but the number of cycles until the design is obsolete. That is, in a research environment, a mold may only be required to produce a few devices before the design can be evaluated and improved upon. In that scenario, the balance of input resources to output usefulness again comes into play.

38

This leads to molds that would not have the capability to enter a production run, but would be relatively easy to fabricate.

Many of the techniques in mold formation are borrowed from microelectronics fabrication. Conventional machining, discussed in the next section, is size-limited beyond the scale of typical microfluidic devices. The microelectronics techniques, on the other hand, are designed to operate at that length-scale and below. At times, the perceived resolution of microelectronics, currently at tens of nanometers and shrinking, may seem like overkill. However that precision takes place only in the most tightly of controlled processes at precision electronics manufacturers or researchers. In the day-to-day world of microfluidics, where resolution is known only to be necessary down to a micron or so, shortcuts are introduced into the process to save on time and capital, and the practical resolution decreases accordingly. The usage of photolithographic masks serves as an example.

Photolithography is a technique whereby a two dimensional pattern can be transferred into two and a half dimensions, through the use of a chemical known as a photoresist [Plummer 2000]. The photoresist starts out in liquid form, enabling it to coat a given substrate. Typically, the thickness and uniformity of the photoresist layer is controlled by spin-coating, where balancing the viscosity of the liquid with the angular speed – and centrifugal forces as a result – allows for predictable control. The photoresist is then heated to bake out some of the solvent, making it tackier and resistant to further flow.

The primary characteristic of a photoresist is its sensitivity to ultraviolet light: exposing the resist leads to a chemical change in the resist. There are two categories of resist, positive and negative; in the former, the resist is chemically weakened by the ultraviolet light, whereas the latter is cross-linked by the ultraviolet, and thereby strengthened. Following exposure, the resist is developed with a wet chemical etch, and the photoresist is selectively removed based on which parts were exposed or not exposed. Once the resist has been patterned, that pattern can be employed to further differentially affect certain areas of the substrate, such as by etching away the substrate, implanting a species into the substrate, or depositing other materials on top of the substrate.

The photolithographic mask is what determines the pattern that is transferred. Parts of the mask are transparent, and parts are opaque. The mask is placed between the ultraviolet light source and the photoresist. Where the mask is clear, the ultraviolet light is able to pass through

the mask and enter the photoresist. Where the mask is opaque, the light is blocked. Thus, it is a key component in the photolithography process. For high precision operations in the microelectronics fabrication, the mask is usually fabricated from quartz glass with a layer of chrome, which serves as the medium of the pattern. But for microfluidics, where the design process is often too rapid to justify the creation of chrome masks, and where similar precision is not required, a different mask is employed. Instead of chrome on quartz, very high quality printers create a pattern of ink on a sheet of plastic transparency. The lifetime of the transparency mask is typically less than that of the chrome, and the resolution is limited, with a minimum line width of 10 μm. But for most microfluidics applications at the present state of the technology, it is sufficient.

3.1.1 Conventional Machining

If the microfluidic features are sufficiently large, conventional machining could be relied upon to fabricate the mold. However, the feature size is limited by the tooling and the control system. Ehmann [2005] reports end mill sizes down to 500 μm. The smallest channel an end mill can cut has the width of the diameter of the tool. However, the majority of molds are negative molds, so the channel would not be milled out as a pocket, as much as the material around an island would be removed with the dimensions of the final channel. This finite width would still limit the spacing of the channels on the chip. In addition, the resolution of the actuators in the computer numerical controlled (CNC) milling machine affects the resolution of the device that can be produced on that platform, in both the in-plane cuts (x, y) and out-of-plane cuts (z). Also, machining tends to leave a noticeable pattern from the cutting, with roughness on the order of a few microns. While this is smaller than most microfluidic channels, it can still be noticeable.

The benefits of a mold created with conventional machining are that the initial material used is well suited as a mold. That is, most machining happens in metals, like copper, aluminum, or steel. Whereas silicon tooling suffers from brittleness, and photoresist molds are short-lived, a metal tool can sustain many process cycles without failure. Unlike an electro-plating process, the metal tool is created in the first step in conventional machining. In addition, for hot embossing, the thermal properties of metal are preferable to those of silicon. A copper tool used for hot embossing is shown in Figure 3-1.

40

1 cm
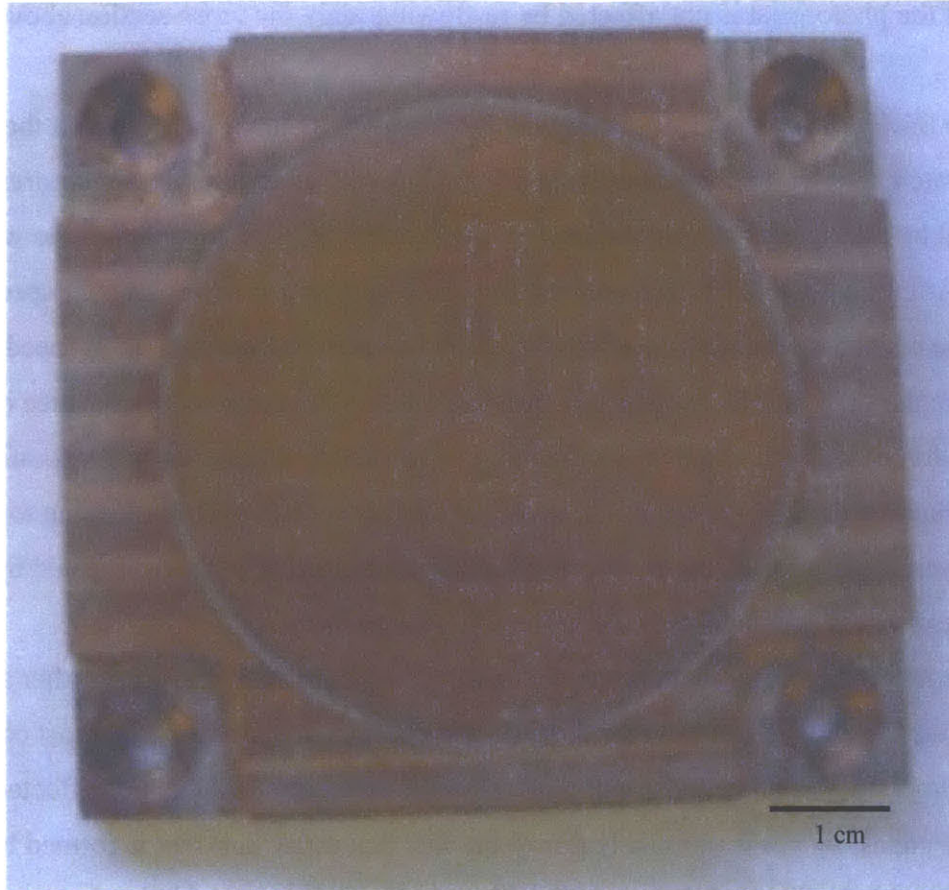
Figure 3-1: Copper mold for microfluidics. From Wang [2006].

3.1.2 Photoresist Mold

Photoresist, as discussed in Section 3.1, is a substance that is designed for use with photolithography to transfer patterns from a flat mask to patterns with some depth at, above, or below the wafer surface. Photoresist can be used as a mask to selectively etch only some areas of a wafer, leaving a pattern within the silicon, but in the simplest example, the patterned photoresist can be used itself as the mold for forming the polymer. If the photoresist is indeed intended to be used as a mold, the adhesion to the wafer substrate is of prime importance, requiring a thorough cleaning as well as a dehydrating bake of the wafer before applying the photoresist. Besides the advantage of rapid prototyping, certain types of positive photoresist can be re-flowed after patterning. Re-flowing heats the photoresist until it begins to melt and can be deformed. At this point, the surface tension is able to exert a rounding force on the cross-section of the photoresist, causing the features to have a more semi-circular profile. In general, the

footprint of the photoresist is not affected by re-flowing, only the cross-section above the wafer surface.

The thickness of a layer of photoresist is controlled by the speed at which the spin coater operates. Interestingly, the thickness is not affected by the initial amount of photoresist and is not affected by the amount of photoresist deposited (assuming full coverage of the wafer can be assured). After the photoresist is deposited, the wafer is spun at a lower angular speed to dispense the resist over the surface of the wafer, and then finally ramped up in speed to the final speed where the thickness is determined. The thickness is determined by a balance of the centrifugal forces with the viscosity of the resist. The other major factor is evaporation of the solvent during the handling or spinning, as this can increase the viscosity, leading to a less uniform layer of photoresist, but S. Han [2001] has shown that this can be negated by operating in an ambient that is saturated with the solvent in gaseous form.

The major drawback to a photoresist mold has already been discussed; after a certain length of time – usually tens of cycles or less – the photoresist will fail. The most common failure mode is that the photoresist will peel off of the substrate. This can be affected by insufficient adhesion, but is ultimately due to the fact that every part that is formed by the mold must be de-molded. The molding process will typically create some friction between the mold and the part, so de-molding will exert a force that tends to pull the photoresist off of the substrate.

The ease of creation, particularly when coupled with a low-cost transparency mask, makes photoresist molds ideally suited to low-part-count runs, which is virtually any prototyping design cycle. But photoresists are simultaneously unsuited to any sort of manufacturing scenario. PDMS and SU-8 photoresist molds often failed after the creation of one part.

3.1.3 Silicon Mold

Photoresist can also be used in its designed function, which is to mask a substrate during a subsequent etching operation. In this section, silicon is taken to mean not only the silicon material itself, but derivatives that can be grown on top, like silicon nitride or silicon oxide, that are functionally similar to silicon in terms of adhesion to the bulk and elastic modulus.

After the photoresist is patterned by ultraviolet light through the mask and then developed, the wafer with photoresist applied is etched. Etches are categorized as isotropic or

42

anisotropic, referring to the directionality or lack thereof of the etch. Figure 3-2 illustrates the etch patterns characteristic of each type appe
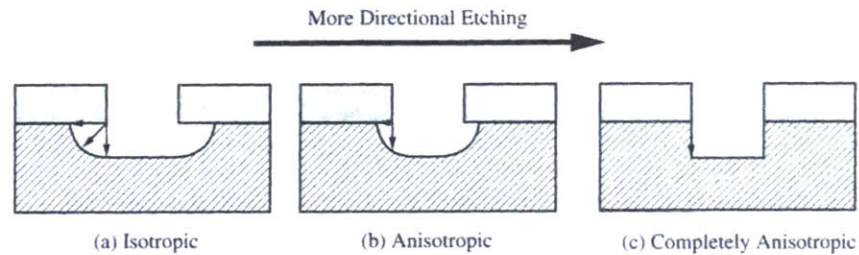
Figure 3-2: Etch Type - Isotropic, Partially Anisotropic, and Perfectly Anisotropic. From Plummer [2000].

The classic isotropic etch, shown in Figure 3-2(a), is a wet etch, where the wafer is submersed in a bath of chemicals. The chemicals are keyed to eat away at the wafer, but usually not the photoresist. The liquid etchant eats away equally in any direction at the silicon that it is exposed to. This will tend to create rounded features that undercut the photoresist, requiring the designer to create the mask with different dimensions than the desired feature size. The processes are well characterized and documented, so this is a straightforward procedure.

A perfectly anisotropic etch, as shown in Figure 3-2(c), etches straight down from the surface. Typically, this will take place in a dry etch, which often use a plasma or other charged reagent that is directed to bombard the surface by an electrical field. Here too, the etch rates and chemistries of the plasma are well understood. Though the ideal anisotropic etch could etch perfectly vertically, in reality, there is always some element of horizontal etch, due to variations in the field and wafer. A partially anisotropic etch is shown in Figure 3-2(b). As the height scales of microfluidic features are often much larger than those required by microelectronic fabrications, even a relatively small horizontal etch will build up over the depth. Thus there is a desire to create features in silicon that are deep and straight. One anisotropic etch that shows promise for creating silicon molds with microfluidic depths is the deep reactive ion etch, or DRIE. This process is sometimes known by its German acronym, LIGA. A diagram of the process is shown in Figure 3-3.

43

After etch and passivation	2 x etch and passivation	Final product, after cleaning
Mask	**Mask**	**Mask**
Polymer lining	Polymer lining	
Silicon	Silicon	Silicon
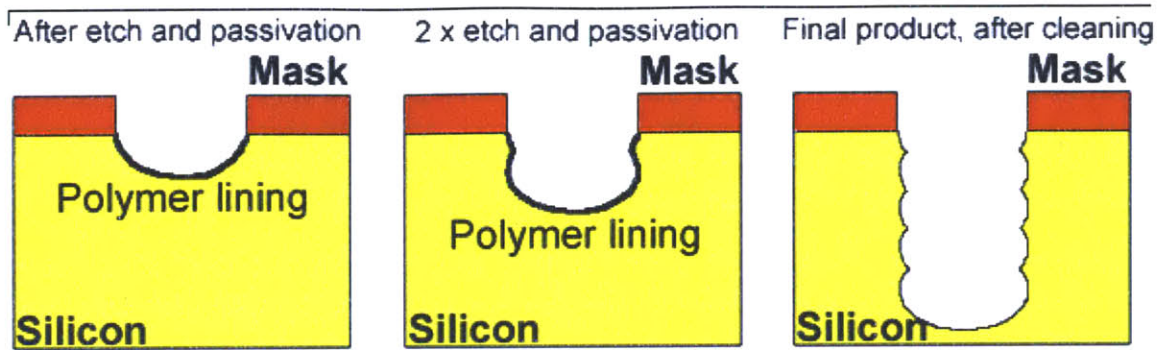
Figure 3-3: Deep Reactive Ion Etch, from Micromoulding [2006].

In the process, reactive ions are bombarded to perform the etch, which already have a good anisotropy, and then, after a short while of etching, a polymer, typically Teflon, is introduced in gaseous form to coat the wafer. The coating process is highly isotropic, so the Teflon coats the sides and bottom of the etch surface equally. Then the reactive ions are restarted. They quickly etch through the polymer at the bottom of the channel and continue etching the silicon where they left off. But the side-etch proceeds more slowly, taking longer to etch off the Teflon from the sidewalls. Just as the side-Teflon is etched off, the ions are halted, and the Teflon gas flowed in again. In this way, the side of the channel is only etched once at each segment, when the ions first expose it. The drawback of DRIE is that the sidewalls tend to become scalloped as a result of the process, and those small ridges act as so many friction enhancers when a polymer is formed onto them, preventing easy demolding. This has been demonstrated to be particularly problematic in hot embossing, where Wang [2006] found that for devices with a size of greater than a few square centimeters in area, demolding is virtually impossible. The size of the scallops is dependent on the relative times of ions and polymer application, and enters into the art of DRIE where an experienced operator has greater knowledge of the process. There has been some suggestion that after the DRIE is complete, a layer of silicon oxide could be grown on the surfaces, hopefully providing some smoothing.

The challenge is to the silicon-fabrication designer to pick a process that fits the needs for the final device, using depositions and etches in a carefully selected sequence through appropriate masks. Once done, the photoresist has to be removed, as DRIE did not remove it. This is commonly done in an oxygen plasma asher, and what remains, in silicon, forms the tool. Silicon is hard, and will not peel off from itself like a photoresist, so it shows promise as a long-run tool. However, it is a brittle material. Combined with the effects of friction from the

demolding, and particularly if DRIE scallops are present, the aspect ratio of features in the silicon is limited. A common rule of thumb is to limit the aspect ration to two. Another drawback to silicon is that it is thermally less conductive than metal, which can present minor problems in hot embossing.

3.1.4 Electroplating

If greater strength is desired from a mold, the next level of durability, as well as complexity of forming, is electroplating. A diagram of the process is shown in Figure 3-4.
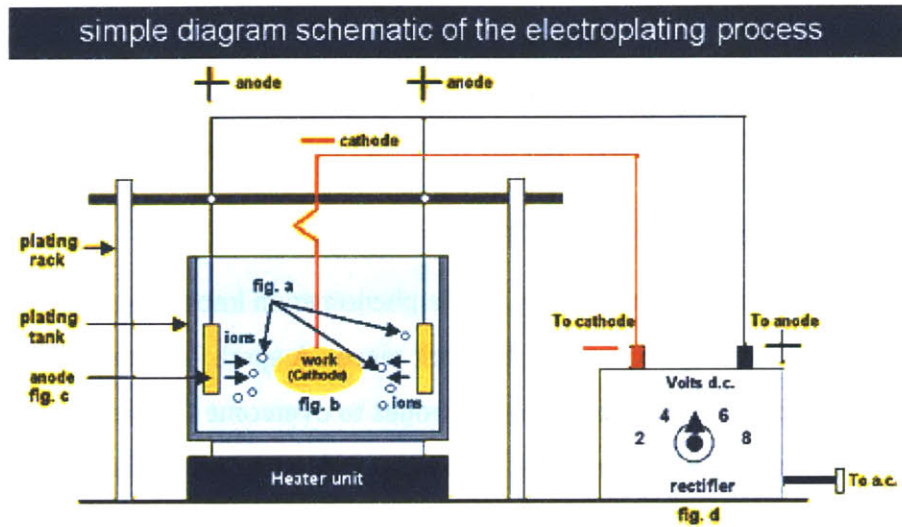
Figure 3-4: Diagram of Electroplating Process, from Artisan [2006].

The metal part is intended to form as the final mold for the polymer, therefore it carries a negative image of the channels. The metal is deposited on top of the silicon substrate, so the silicon initiator carries a positive image of the channels; the surface of the silicon has recessed channels that will eventually become the microfluidic channels. To begin the electroplating process, a seed layer of metal is sputtered onto the silicon wafer, containing the positive image of the device. Sputtering is a process that takes place in a high vacuum, where a sample of the element to be sputtered is hit with beam of charged particles, causing some of the molecules of the material to sputter off, into the vacuum, where they eventually make their way to the target that is being coated, located at the other end of the potential field. The sputtering process is fairly slow, and is only used to grow the initial layer of the material, to create a conductive layer on the surface. Once that conductive surface is in place, the electroplating can commence in earnest. The wafer is attached to an electrode, and submersed in an electrically conductive

solution containing the material that is to be deposited. Then another non-reactive electrode is submersed into the solution, and a voltage is applied across the electrodes. As the current flows through the solution, it will carry the plating material with it, depositing it on the surface. In this way, the thickness of the metal layer can be built up more rapidly. Common materials for electroplating include nickel and copper, but any conductive material will work. Once a sufficiently thick layer has been built up, the silicon is stripped off, typically in a wet etch. What remains is a metal part bearing a negative of the microfluidic features, also known as a mold.

Drawbacks to electroplating are primarily time and expense, and since it faithfully duplicates the silicon that it is deposited on, is subject to the same DRIE or anisotropy issues that confront silicon tools. But just as it virtually assured that production runs will never be done with photoresist tools, it is very likely that the tools that enter production will be metallic.

3.1.5 Electro-Discharge Machining (EDM)

EDM, unlike traditional machining, uses a phenomenon known as spark erosion to remove metal without actually contacting the work piece. A spark is formed when a sufficiently large voltage difference exists between two electrodes to overcome the dielectric breakdown strength of the medium that separates them. When a spark occurs, there is a small amount of the conductor that is eroded. While one spark will only remove a small amount of material, repeating the sparks, at high frequency and voltage, can be used as a means of material removal machining. The process is typically conducted submerged in a dielectric fluid, which helps with chip removal and cooling.

The earliest form of EDM was master-matching, where a tool representing the desired cavity in the final part was slowly advanced into a block of material, as the sparks are simultaneously occurring and removing material. However, a small tool can be used in conjunction with a CNC three-axis positioning system to provide greater flexibility in part creation. Often, a graphite tool is used, as it is conductive. Much less graphite is consumed in each spark than metal, allowing the tip to be used to remove a correspondingly much larger volume of the working material.

In theory, EDM could be used to create a mold for polymer microfluidic forming, as well, and recent work at the Technical University of Denmark [Theilade 2004] has been undertaken to

push the limits of resolution of EDM to bring it into the microfluidic regime. While current EDM is reliable down to 5 μm, there are attempts to further reduce that size [F. Han 2006].

3.2 Polymer Formation

Once a mold has been created, the next step is to form the polymer that will actually constitute the device. The sections that follow will describe the current methods for doing so.

There are four major tasks in mold replication in a polymer. They are:

- Fluidize the polymer.
- Fill the mold.
- Solidify the polymer
- Separate from mold (demold).

In the discussions that follow, this list will be referred back to periodically to emphasize the parallels between these otherwise different methods [Kalpakjian 2001].

3.2.1 Micro-Casting

This is the general heading given to processes in which the polymer is chemically solidified, and not merely cooled to below its glassy transition temperature. That is, though heat is sometimes used in polymerizing, it is the application of heat that leads to a chemical cure. In thermal methods, the heat must be removed to solidify the polymer.

Other methods of curing include exposing the polymer to ultraviolet light and the addition of chemical agents to promote the cross-linking of the polymer chains. Presumable, prior to the cure, the precursors are sufficiently fluid to fill the mold of their own accord. This is a major draw, as the precursors do not need to be fluidized, and filling the mold requires no additional force or encouragement. Solidifying the polymer means subjecting the mold and pre-polymer to the curing conditions, presuming molds that are compatible with the curing conditions. Removal from the mold would differ based on the material, but can be as simple as peeling the completed polymer off.

The polymer that has risen to prominence and widespread usage is polydimethylsiloxane (PDMS) for its rapid prototyping ability, good feature replication, and perhaps most importantly, ease of adoption. The beneficial characteristics of PDMS are its optical transparency, its ease of use, and its sealing abilities. By using an oxygen plasma asher, the seal can be made nearly

irreversible, which is to say the failure strength of the bond created after ashing is greater than the failure strength of the material itself. Attempting to peel a device apart after ashing will thus result in the device ripping before it delaminates. The drawbacks of PDMS are that its material properties, particularly physical properties and curing properties, are not very well understood. This may be due to the fact that prior applications have not demanded the same level of information about the material that microfluidics might.

The two main suppliers of PDMS are Dow Corning, which sells it under the name Sylgard 184, and GE Silicones, which sells it under the name RTV-615. In either case, the PDMS comes as two separate components, the monomer base and the curing agent. The user combines them in a ten-to-one ratio by weight, often pouring them one after the other into a disposable container, such as a plastic cup, atop an electronic scale. Then the two are thoroughly mixed, which unfortunately entrains many air bubbles in the fluid, requiring a degassing step under vacuum. The degassing goes very slowly if left undisturbed, as the air bubbles very slowly coalesce and pop. In fact, some jolts can be helpful to accelerate the degassing, as well as cycling vacuum and release of vacuum. This is very helpful in popping the bubbles that have formed at the top of the fluid. The ideal would be to be mixing the fluid simultaneously while degassing, and the Thinky Corporation, of Japan, has built a machine to do just that.

Once the PDMS is mixed and bubbles have been sucked out, it can be poured on top of the mold, prepared in one of the methods described in Section 3.1. The mold is often coated with a release agent, such as hexamethyldisilizane (HMDS), to facilitate the demolding after the PDMS has been cast. After pouring, it will then spread to fill the mold. If there are any areas where there is concern that a bubble might be trapped, such as a deep well, leading to incomplete penetration of the polymer and subsequently inaccuracies in replicating the mold, the mold and pre-polymer can be further vacuumed. Then, the whole assembly is baked. The temperature and time for the PDMS cure are inversely related. Temperatures that are too high will scorch the PDMS, so 95° Celsius for an hour set the working upper limit and lower limit for temperature and time, respectively.

Once the PDMS has been set, it is peeled off of the mold. It is still very flexible, and relatively soft; it can be cut with a razor blade or punched with a syringe needle with no more than hand pressure. This is another desirable feature of PDMS. Then, to finally seal the

channels, the PDMS part can be exposed to oxygen plasma for a short time to activate the surface and then inverted onto a piece of glass or another piece of PDMS.

Taken together, this process is often called soft lithography [Zhoa 1997].

The drawbacks of working with PDMS primarily that its mechanical properties are not well understood. Cheung [2005] has done some work to better characterize it, but parameters like shrinkage, elastic modulus, proper time of curing, and the effects of long-term cure can vary from batch to batch, and are likely interrelated. That is, under seemingly similar processing conditions, one PDMS part might be very rigid, while its subsequent mate is very soft. Another factor at work might be the relative ratios of base and curing agent that are used. The ratios are regularly tweaked from 5:1 up to 20:1 [Urbanski 2004], which they use to create relative hardness difference between their layers, but the influence of the ratio is not well understood beyond that simple rule of thumb. These issues spring primarily from the use of PDMS in an area for which it was not originally intended.
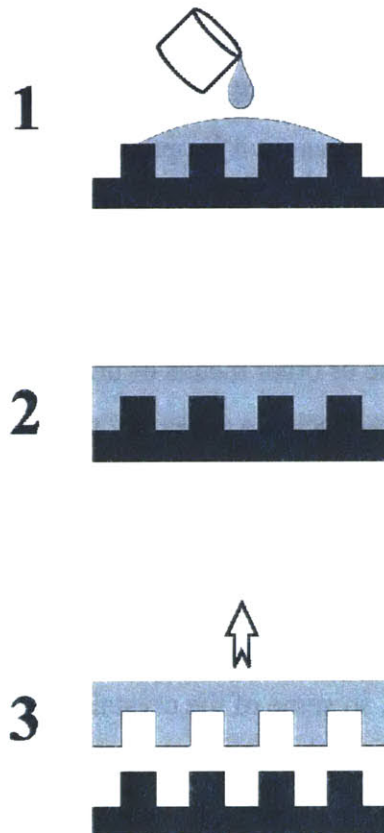
Figure 3-5: Diagram of the Soft Lithography Process, from Dirckx [2005].

3.2.2 Micro-Forging

While micro-forging is typically used to refer to this second major area of polymer microfluidic forming, technically, this taxonomy is a slight misnomer. In the micro-scale, a shaped tool is used in conjunction with a large force to create the finished part, but there is only one impact. Any more than that would be unnecessary and would risk slight misalignments that could create shadows of the features. This process is usually combined with a thermal input to slightly melt the polymer, leading to its more common name, hot embossing.

Following the general outline presented in Section 3.2, the method of fluidizing the polymer is, as just mentioned, thermal. The working material is some sort of thermoplastic, commonly polymethyl methacrylate (PMMA). Thermopolymers can be melted and flowed, but below the melting point, there is another important temperature, the glassy transition temperature. Above this temperature, the material has a lowered yield strength, but is not fully melted to the point where it will flow under its own body forces. That is, if a force is applied, the material can be easily deformed, but it will not form a puddle by itself. This regime is typically where the temperature of the work piece will be raised during the first step of the procedure.

PMMA is typically chosen because it is optically transparent, because its glassy transition temperature of 95° C is high enough to use in most applications, and because it is fairly easy to work with.

To have the polymer fill the mold, the mold pushed into the glassy polymer by some mechanism, typically a load frame or other means of uniformly applying a high but prolonged force. Force and displacement feedback are necessary to monitor how much the mold is filled, as when the mold is fully filled with polymer, the force will raise steeply for a given displacement as the transition is made from deforming areas locally on the surface to attempting to compress the bulk of the material.

Once the mold is fully filled, the temperature of the part is lowered to take the part below the glassy transition temperature, so some of the crystallinity that was lost in the heating is regained, giving the part greater rigidity. Finally, the part is separated from the mold. This requires greater force than in soft lithography, since while shrinkage is present in both, the part is much more rigid in hot embossing, so a local deformation and peeling are harder to achieve. This large force makes tooling on a silicon substrate all but impractical, as any attempt to clamp a silicon tool at its edge and remove along the inverse direction as the embossing was performed

50

would lead the tool to snap under the bending moment as the center of the tool de-embosses. Vacuum chucks have been proposed to apply an evenly distributed removal force, but they cannot apply the necessary de-embossing force. Therefore, metal tools are seen as the only reasonable production-volume tooling.
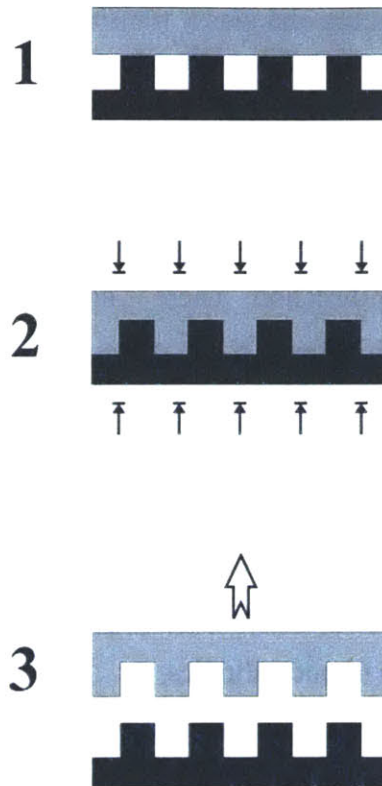
Figure 3-6: Diagram of Hot Embossing Process, from Dirckx [2005].

In order to correctly control the temperature of the work piece during the process, there are two main approaches. The first is to have the contact surfaces on the load frame, known as the platens, have temperature control elements embedded within them. This is the approach taken by Dirckx [2005]. The second is to create an environmental chamber around the work piece and tool, and heat or cool within the chamber. In either scheme, both the work piece and the mold have to be heated prior to embossing, or the relative temperature difference of a cooler tool could cause rapid re-solidification, or mold freezing, which would halt the forming before it begins. In addition, the part must be cooled while the force is still being applied, to ensure that the dimensions of the mold are faithfully recreated in the polymer. If the mold was withdrawn prior to sinking below the glassy transition temperature, the unconstrained shrinkage that would then occur would likely distort the features in unpredictable manners.

While the hot embossing typically starts with a thin, flat sheet of polymer, another variant of this process takes small pellets of a polymer, scatters them over the work area, and then heats the polymer up beyond the melting temperature, while applying pressure between the platens to compress the fluid polymer into shape around the mold. Then the platens and work piece are cooled below the melting temperature and glassy transition temperature, and the polymer is de-molded.

While the two methods presented differ in the temperature they take the polymer, and subsequently whether the polymer flows into position or is merely embossed, they share to distinct similarities. They use heat to control the polymer's resistance or propensity to deform, and they apply force in one linear direction. There is no constraint on the outside edges of the polymer, and while friction could induce a shear stress, the polymer is technically free to flow outwards.

3.2.3 Micro-Injection Molding

Microinjection molding is an adaptation of the macro-scale process of injection molding to the microfluidic device fabrication. This makes implementation a bit simpler, but also introduces some issues particular to microfluidics.

The general process of injection molding is shown in Figure 3-7. First, pellets of a thermoplastic, similar to those used in the molten method of hot embossing, are melted in a reservoir beyond both the glass melting point and melting point, to where they are fully fluid. The mold starts out as a hollow cavity that fully defines the shape of the finished part. The mold is typically divided into two halves, known as the core and cavity, respectively. Similar to molds used for other areas of microfluidics, they are limited in that each mold-half can only be two and a half dimensions by itself, as the finished, rigid part has to be removed from the mold along a straight exit vector. The one exception to this could be if the part was unscrewed from the mold, but this would require a part with helical symmetry, which is unpractical for microfluidic applications. The other major option, used frequently in macro-injection molding to introduce further complexity into finished parts, is to use a multi-part mold, with three or more different sections that come together during the part creation, but then pull apart to reveal the finished part. However, each of the mold sub-sections is still constrained itself by the two and a half dimensions restriction. Also, for microfluidics, where the slides – the name for the smaller mold

parts besides the main two mold parts – would need to be on the order of a microfluidic channel, less than a square millimeter in area. Additional problems would then be introduced in terms of creating a robust slide that could be used repeatedly without breaking and in terms of positioning and alignment of the slide. Therefore, at present, microfluidic injection molding is currently restricted to two mold-halves.
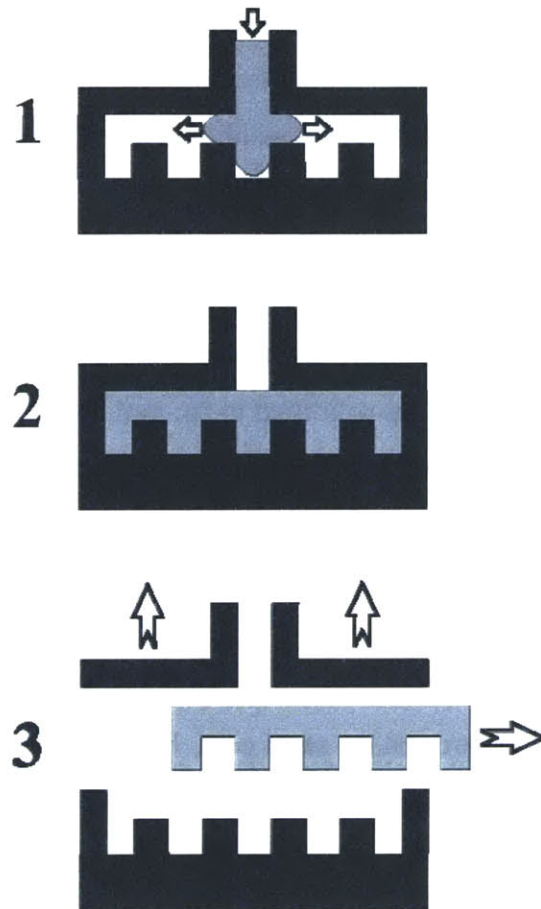
Figure 3-7: Diagram of Injection Molding Process, from Dirckx [2005].

In addition to the features themselves, the molds usually carry a few other features. The cavity typically is the site of the sprue, the inlet that connects to the reservoir to allow the melted plastic to flow into the mold. Either half might have small holes to allow air to escape as the mold is filled, known as vents or risers. Finally, the core could be outfitted with ejector pins. Even in the macro-case, shrinkage of the cooling plastic will cause the part to shrink onto the mold, requiring additional force to remove the part from the mold. Rather than pull each part off with a pair of pliers, ejector pins were developed. After the part is finished and the mold is opened, the ejector pins extend through the core to push the part off the mold. This is an

additional benefit to injection molding, as it provides an easy way to assist de-molding, since injection-molding machines are already equipped with piston and other linear actuators.

Once the mold is assembled and affixed with sprue to reservoir, the molten plastic is forced into the mold. Usually this happens via a piston, a screw thread, or some combination thereof. The mold is not typically heated, relying on the heat capacity of the plastic beyond its melting point to keep the plastic from solidifying before it fully fills the mold. Just like in hot embossing where pressure is maintained during the solidification, pressure will usually be applied at the reservoir during the cooling and solidification of the part in the mold. Then, once the part is sufficiently solidified, the mold is opened.

This is when the distinction between the core and cavity is evident: the core is the side where the part should stick when the halves are separated. The shrinkage due to the cooling is what causes the part to grab onto the mold, and the core is the side it should grab. The reason for this is that the part of the sprue that has solidified in the mold is then simultaneously torn free from the reservoir and the mold. At that point, ejector pins can be employed, or the part can be pulled from the mold by an end effecter that can pull the part off, like pliers or a robot hand. Care is taken during the demolding to exert demolding forces that are sufficiently gentle as to not deform the still-warm plastic part.

One of the benefits of injection molding is that it has the potential of creating parts that have both macro and micro features on the same part. For hot embossing, where the initial work piece is a thin piece of plastic, the height of the final features is limited to a fraction of that initial thickness, and it is possible that if high profile features were incorporated next to microfluidic features, the deformation of the plastic during the embossing of the large features could have an adverse affect on the micro-features. But for injection molding, the volume of the mold is limited only by the size of the reservoir and the cross-sectional area of the part normal to the injection direction. This area is limited as the force the machine can exert in holding the mold closed divided by the pressure of the injector. The mold might be a composite, with the macro features formed by conventional machining, and a small insert that carries the microfluidic features affixed to the larger part of the mold. If alignment of the microfluidic features to the macro-features is in any way critical, however, additional issues could be introduced.

54

Like hot embossing, metal molds are the only practical option for a production run, given the forces involved during mold filling and demolding, as well as the fragility of silicon or the low failure point of photoresist.

3.3 Device Fabrication

The microfluidic device is not yet complete after the channels have been formed. All of the methods presented, given their limitations as two and a half dimensional processes, will produce devices with open channels. Thus, the first step is to seal the devices to create internalized channels. Exceptions to this case might include those devices which are only needed to be run as open channels, such as the surface patterning devices discussed in Section 2.6, or those devices where the structure they are to be used with will provide the sealing, as in the functional testing platform constructed by Thaker [2006]. Finally, for the vast majority of device in which the input or output is not fabricated in parallel with the channels, those ports need to be created or affixed. The one exception might be a device with an open well inlet fabricated into the device, which has sufficient reservoir space to negate the necessity of an outlet.

3.3.1 Sealing the Channels

The simplest cover for the open channels is a flat piece of material, as then positioning is not an issue, and the cover need merely stick and not stick in a particular location. The other alternative would be a part that has features itself, either other microfluidic elements, or macro-features, that need to be referenced to the part being sealed. The techniques for properly referencing related layers, as well as some associated issues, will be discussed in Section 5.2, and thus for the purposes of this section, only the sealing itself will be discussed.

The easiest method of sealing would be to have two haves that are inherently attracted to one another and therefore bond merely on being brought into contact. PDMS bonded to another piece of PDMS or a piece of glass, after a brief treatment in the oxygen plasma asher, has this property, which increases the attractiveness of PDMS for prototyping.

A second method is to use two pieces that can be subtly altered to affix to one another. Typically, the two halves will be brought into contact, and then the bonding performed. Thermal bonding and ultrasonic welding are two methods that take this arrangement. Thermal bonding

takes its strength from the large number of thermoplastics that are used in microfluidic fabrication, such as those used in hot embossing or injection molding. Once the halves are brought into contact, usually under pressure, the whole assembly is heated, with the goal of using the heat and pressure to cause the top and bottom to fuse. The risk is that the same conditions that are introduced to induce what is a fundamental alteration of the polymers might also affect the channels themselves and the dimensional tolerance that was achieved with the forming of the part prior to the thermal bonding. In particular, there is a possibility of the channels being collapsed by the bonding, but D. Kim [2005] has demonstrated a method to exert pressure on the parts during bonding only in the areas where they will bond between the layers, conveniently a negative of the mold used to form the channels to begin with. Ultrasonic welding replaces heat with low-amplitude ultrasonic vibration that causes local melting at the interface between two parts. The advantages are that the bond formed by ultrasonic welding is very strong, but the downside is that the process is relatively expensive, particularly for a low-cost disposable plastic part.

The final major area of sealing would be to use an adhesive. An adhesive is a tertiary substance applied at the interface between the parts that sticks to both top and bottom, creating a seal. Often, the adhesive dries out or cures after being applied, setting the seal more permanently. The drawback of an adhesive is that there would be a high probability of the adhesive being present within the finished channels, via either migration or direct application to the cover-side. The adhesive would then interact with the fluid flowing through the channel, possibly having negative effects on the operation of the device. There are many different types of adhesives, however, so it is possible that one could be found to be chemically compatible with both the device and the fluid operations. Finally, if the layer of the adhesive was too thick, that could also negatively impact the device.

3.3.2 Inputs/Outputs

The current approaches to inputs and outputs can be classified as either open to the surroundings or closed. The latter implies that some sort of tube or pipe carries the fluid to and from the device, whereas the former has a well or other reservoir stationed at the inlet and outlet that is open to the environment. For a tube that is connected to the device, there must be some way of adequately sealing the tube to the device. If the material is compliant, it is possible to

56

take advantage of the flexibility of the material in creating a seal. A hole is created in the material to receive the tube, but it is made smaller than the tube that will be inserted. Then, the tube forces the material into compression as it is inserted, which forms a decent seal. Chon [2005] addresses these issues related to ports. Another option is to adhere the tube to the device, using some sort of adhesive. Here too, alignment to the micro-port is an issue but could be performed with a recess, that is oversized instead of undersized. Finally, a pressure fitting and gasket method could be employed, where a cap block, with holes to match those on the device below, is positioned on top of the device. Then, a gasket material, either the device itself in the case of a compliant device, or a separate layer in the case of a rigid device, is compressed between the cap and device, using some sort of external clamping mechanism. This approach has been taken by both Thaker [2006] and Fluidigm [2005], in their TOPAZ FID Crystallizer.

A device with open wells is shown in Figure 3-8.
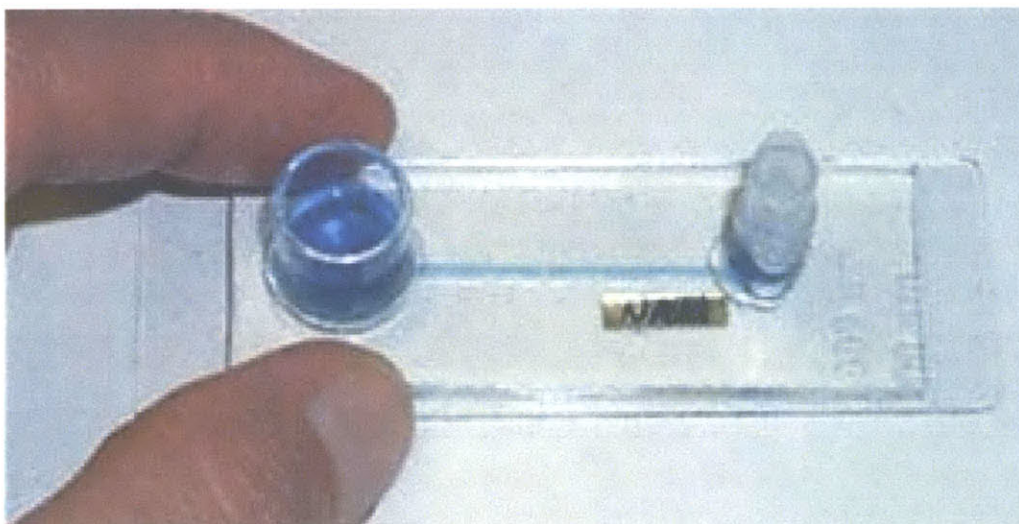
Figure 3-8: Microfluidic Device with Open Inlet and Outlet, from Vitae [2006].

Any time the end users of the device is required to insert the working fluid by themselves, without the aid of any sort of other equipment or fixtures, as will likely be the case in many of the in-field assays that are envisioned, an open inlet is a likely option. They are well suited to prototype applications, similar to the one shown in Figure 3-8. The well can be the high profile example displayed, or could be a lower profile well on the size scale of flow channels. One advantage of a high profile device is that the gravitation potential energy could build up a pressure head, as a potential challenge is creating a motive force in these devices, since an open input forfeits the ability to increase the pressure at the input beyond atmospheric. The remaining

options will be discussed in Section 4.4.3.2, including providing a lower pressure at the outlet to suck the fluid into the device. Two examples of existing devices that use user-applied fluids in open inlets are the Element, by Pria Diagnostics [2006], and cholesterol sensors used in medical screening. In both, a fluid sample to be analyzed is placed on a well above the device, and no other input force is required.

If the wells are not fabricated as part of the device, they have to be affixed as well. If the interface at the end of the well is tiny, alignment will become an issue. If instead the well is a large tube, and the port is a small hole on the surface below, the port must merely be somewhere within the footprint of the well (which is easier to achieve). The well can then be glued around its outside diameter, which is in contact with the substrate.

4 Elements of a Microfluidic Test Device

As can be seen in the previous section, there are many different choices to be made at every step in the process of creating a microfluidic device. The plethora of options makes choosing one particular method daunting.

In an attempt to provide a metric against which different platforms can be evaluated, we propose the creation of a microfluidic test device. A test device provides a means of systematically examining the capabilities of a given process, by methodically interrogating each process as to its capability in fabricating the building blocks of any microfluidic structure. Just as a standardized test-mass can be used to evaluate the capabilities of many different scales, the test device can be used as a metric, if not in determining which process is the best, at least in determining which process is best suited to a particular application and the functional requirements that flow from that application, as have begun to be delineated in Chapter 2.

4.1 Chemical-Mechanical Polishing Precedent

Appendix A gives an overview of the test wafer developed by Noh [2005] to assess process capabilities of concurrent methods of chemical-mechanical polishing (CMP). The idea is to identify the key input parameters and systematically vary them and examine the process capability of different processes simultaneously in fabricating those desired features. We hope this concepct can be applied to the microfluidic world. That is, we would like to determine the basic characteristic or building blocks of microfluidics, the features that will most likely exist in any microfluidic device in the future. Then, we will create a design for the test device that will incorporate variations of these building blocks across a desirable spectrum, to assess the limitations of the various technologies as well as their capabilities and uniformities within their operating windows. Next, the test device can be fabricated using any one of the various processing options discussed in Chapter 3, and ideally all of them and any new processes that

may come forward at a later date. Finally, the parts that are produced by the various methods should be measured to determine their adherence to the nominal desired values. For the CMP example, the wafer was measured using a profilometer to find the height of the post-polished structures. In this way, it should be possible to compare the various fabrication methods.

The focus with the various parameters listed below is to assess the minimum, maximum, uniformity, and repeatability of the parameters.

An additional benefit of creating this test device might be in pushing forward the technology of microfluidic fabrication. If limitations are found in fulfilling a particular functional requirement required by an application in all of the existing techniques, it would help to identify the necessity that would drive the creation of new methods.

4.2   Limitations of a Test Device

The major limitation of the test device is metrology. A measurement, in this case the uniformity and other parameters of interest, is only as good as the measuring device. Micro devices are between macro and nano-metrology methods. Macro-measuring devices, like calipers and micrometers, have a resolution of approximately 25 μm. This is too large to adequately measure the 1 μm variations in microfluidic devices, not to mention that the forces they apply at the measurement surface could easily deform the polymer devices or photoresist molds that are being worked with. Nano-measuring devices, like Scanning Probe/Tunneling Microscopy or Scanning Electron Microscopy, though they have resolutions on the order of nanometers, very often lack the range necessary to encompass a single channel [Thaker 2006]. The methods that are currently most beneficial to microfluidics are optical comparison, optical interferometry and some stylus profilometry for smaller molds. Optical interferometry is best suited to depth measurements, and is limited in resolution of in-plane measurements. Optical comparison is performed through the lens of a microscope, comparing the micro-image with tick marks of known length. Here too, the trade-off between range and resolution comes into play, in that a higher magnification objective would provide more resolution, but is less likely to contain the entire image in the field of view.

Another drawback of the features in this chapter is that by and large, they exist in two-and-a-half dimensions, not in the full three. This is to say, since the molds have to be built up from the flat surface of a wafer or machined down from a block of material in most of the

60

existing mold technologies, features have to rest on top of other features, and overhanging structures are not possible. This is an obvious problem, as we fall into the same paradigm that we are struggling to escape, of the existing technology limiting the realm of possibilities that we explore or conceive of. But all of these structures proposed to go into a test device are basic right now, and the test device should by necessity adapt as time goes by or duplicability of less complex structures is shown to be standard among the processes. At the very least, adaptations or updates will be necessary to address new functional requirements that come forward as new applications are identified, and if more standardized solutions to some the issues that remain open at the moment, like valving, come forward. The intention at the moment is to categorize those basic capabilities that are universal, and that all processes must be able to accomplish, so that none of the basics slip through the cracks as we increasingly turn our attention to the technological leading edge of microfluidics. In addition, the first step in overcoming a challenge is acknowledging its existence, which is what we have done here. Finally, as can be seen in Chapter 5, some issues that are involved in creating multilayer devices, the first step toward a fully 3D structure, are discussed.

In the same vein, some capabilities are only possible in a subset of the processes available. Multilayer valving [Urbanski 2004], for example: the material used is PDMS, and by filling a top channel with a high pressure fluid, the membrane between the top and bottom channels deflects down to seal the bottom channel. Using the flexibility of the material the device is fabricated in to affect a valving schema is not possible in any of the rigid material used in hot embossing or injection molding. But again, right now, we are trying to establish the basics before we move further forward, not necessarily account for every different possible structure. New features are created every day as researchers explore near areas and solutions to problems. Also, when this multilayer approach is decomposed, we see that what is required from the fabrication process itself, and not the material, are the same fluid channel dimensions required in any device and the same alignment issues that will affect multilayer devices in any material.

In the next sections, the common elements to any microfluidic device, the building blocks, will be reviewed, and their key input characteristics discussed. Similar to how the Thorsen multilayer technique was decomposed into a network of in-plane channels and an alignment schema between the levels, any component of any device that is generated should be

able to be divided into one or more of these categories, or new categories are needed to more fully describe the range of possibilities of design elements.

4.3 Definitive Features

In considering features for a test device, there are two categories of candidates. The first is definitive features, where there exists a clear idea of the geometry of the feature, and a few definitive parameters that fully describe the feature. The second are more complex features, but the former group is presented first.

4.3.1 Single Channel

This is the simplest example of a microfluidic element. It is simply a straight canal along which fluid can flow. Figure 4-1 depicts a diagram of this channel, which is no more than a cross section extruded along its length.
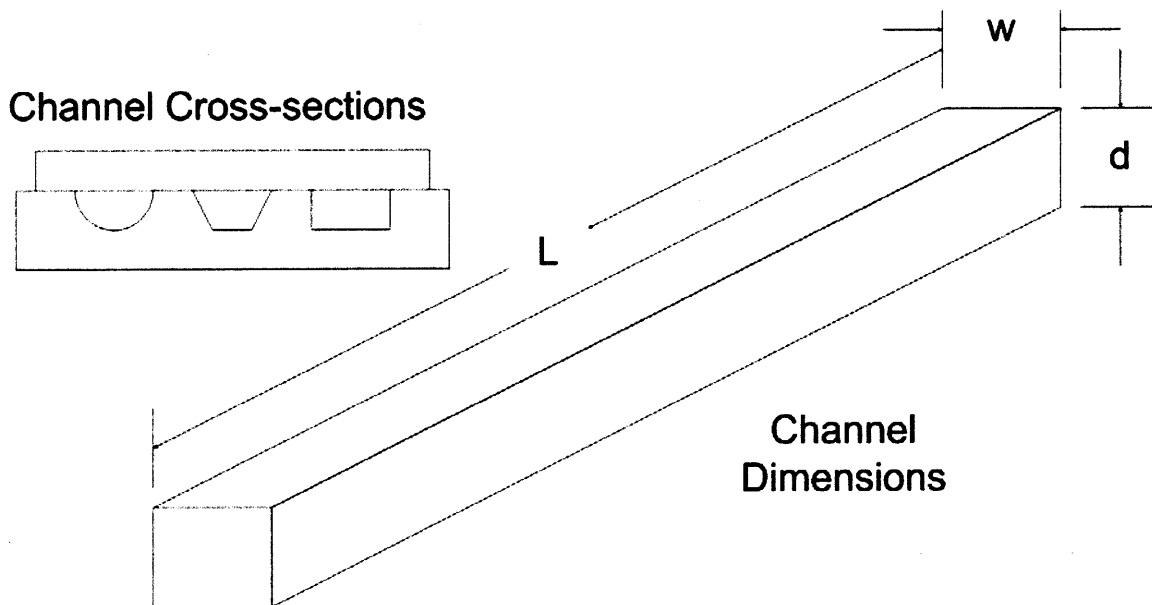
Figure 4-1: Diagram of a Single Channel.

As can be seen, the most obvious characteristic of the channel is its length, L. Secondarily, the cross section along the length could be one of a few different shapes, or possibly others. Temporarily constraining the possibilities to existing technologies, three possible cross-sections are a semi-circular cross section, as would be created from an isotropic wet etch, a trapezoidal cross section as would be expected from a preferential etch like a potassium hydroxide (KOH) etch, or a rectangular cross section. Highly anisotropic dry etches and

62

photoresists are usually assumed to be rectangular in cross section. For rectangular channels, there are two parameters that define the cross section. They can be considered as width w and depth d, or alternatively the aspect ratio and one of the other dimensions as the characteristic, usually the width, given the planar nature of many of the processes. The aspect ratio is the ratio of the depth to the width, and gives an idea of the relative tallness or squatness of the channel. In either case, there are two variables that define the channel. It may be that viewing the variables in one way may give a better feeling for the limits than the other may, but it might be hard to determine this before running the experiments. For example, suppose a test device looking only at single channels was constructed, with discrete variations in the width and depth of the channel. The results have been plotted in Figure 4-2, with a green mark indicating a successful and reliable duplication of the features, and a red mark indicating a failure to achieve the dimensions.
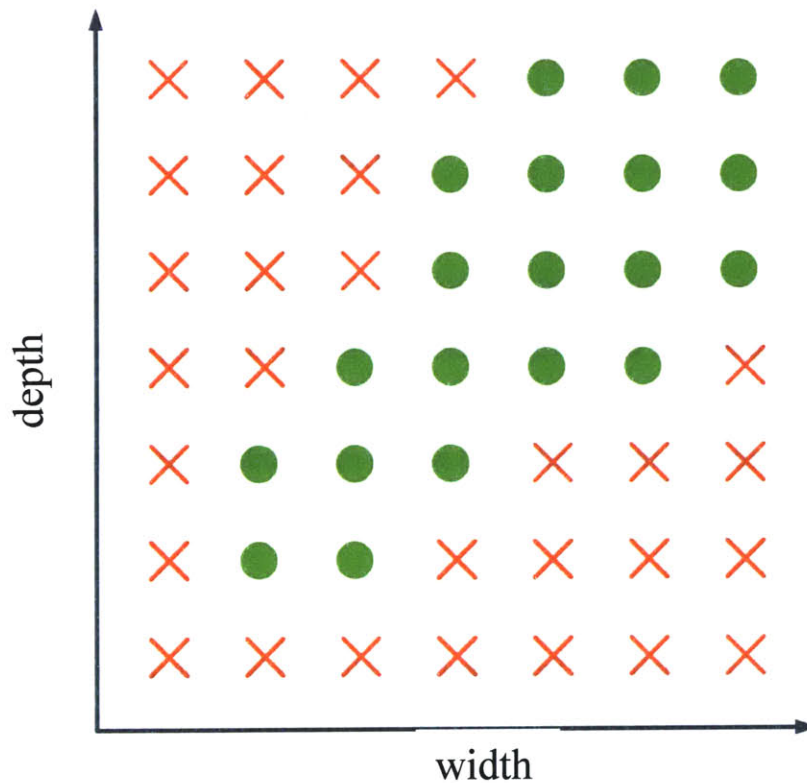
Figure 4-2: Hypothetical Results of Channel Fabrication, Height v. Width.

If the same data are considered as Aspect Ratio and Characteristic Dimension, say the width, and plotted again, it might look like Figure 4-3.
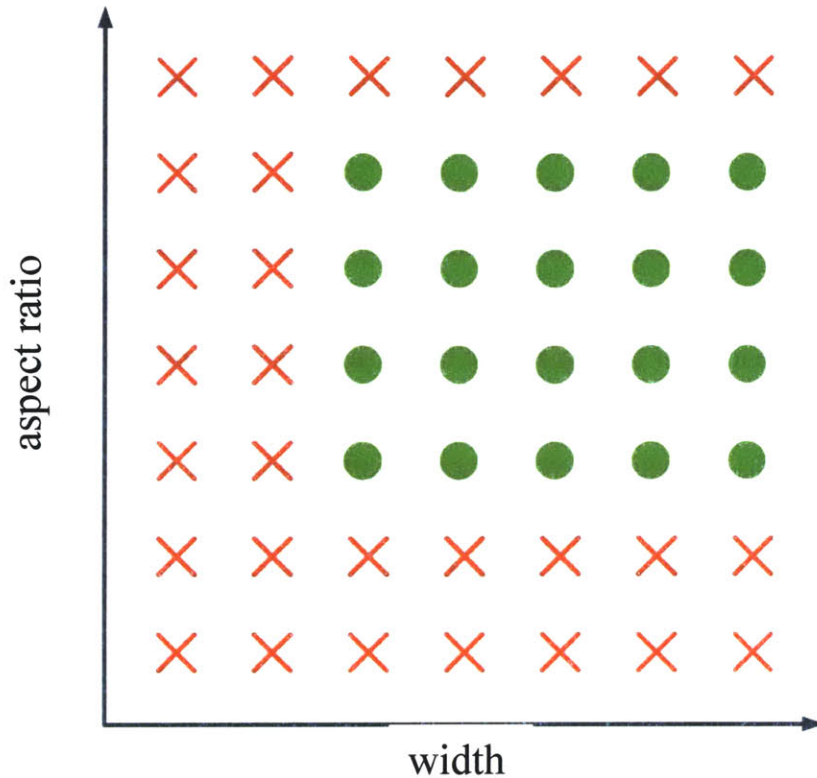
Figure 4-3: Hypothetical Results of Channel Fabrication, Aspect Ratio v. Width.

As can be seen, conceiving of the data in a slightly different manner gives a more clear-cut view of the limitations of the device. That is, it seems in this hypothetical case that the limiting factor is not merely the height, but a combination of the height and width, so it is simpler to quote the limitation on width and aspect ratio, rather than trying to fit a curve to the height and width data.

4.3.2 Multiple Channels

One level of complexity up from the basic channel is an arrangement of channels running next to one another. A typical device involving multiple channels in a device next to one another is shown in Figure 4-4. It should be noted that while the figure displayed a snaking channel, where all of the multiple straight lengths are connected, this concept of multiple channels could be applied equally well for disconnected channels that travel alongside one another. A diagram of the key characteristics is shown in Figure 4-5.
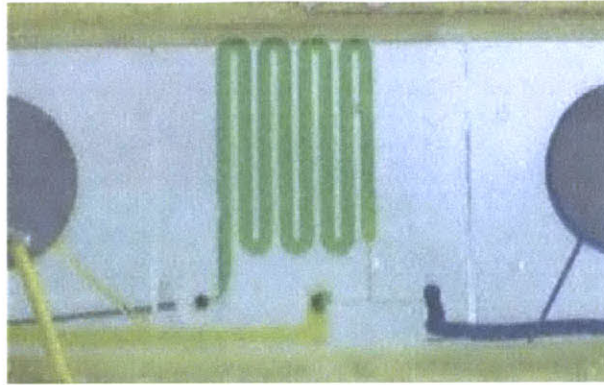
Figure 4-4: Microfluidic Device with Multiple Channels, from Kaye [2006].
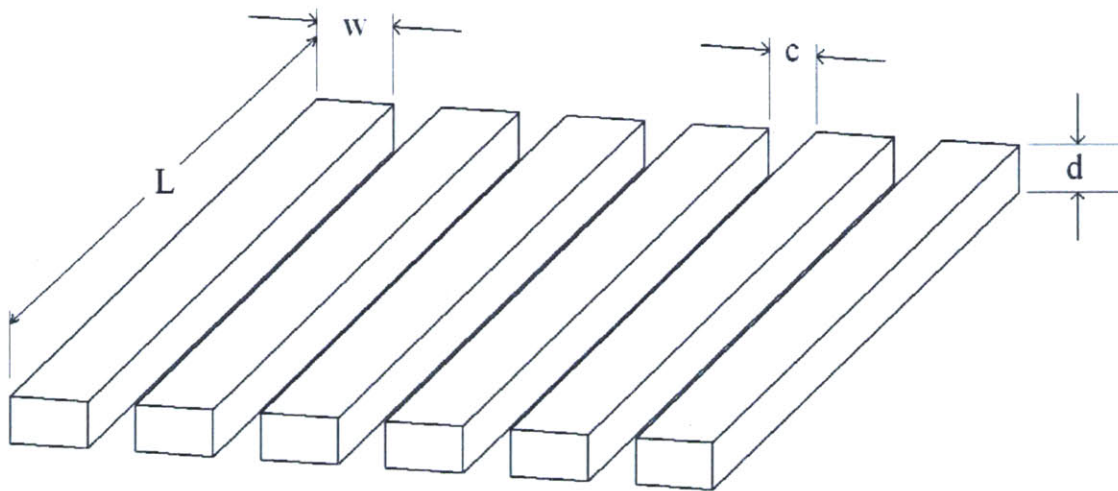
Figure 4-5: Diagram of Key Characteristics of Multiple Channels

Just as if the single channel, width and depth are two keys, but an added parameter, c, defines the thickness of the wall between adjacent channels. Similar to the single channel as well, there are various other parameters that can be assembled from these most basic interpretations. For example, in addition to the same aspect ratio of the channels themselves, a pitch of the channel array can be formed by adding the width of the channel and the wall. Or, similar to the Test Wafer, the density of features can be calculated by dividing the channel width by the pitch. Regardless of how the dimensions are presented, there will be three of them as there are always three degrees of freedom in the description.

4.3.3 Turn

Besides going in straight lines, channels can alter direction, and to do so, a turn is required. A diagram of the key elements of a turn is illustrated in Figure 4-6.
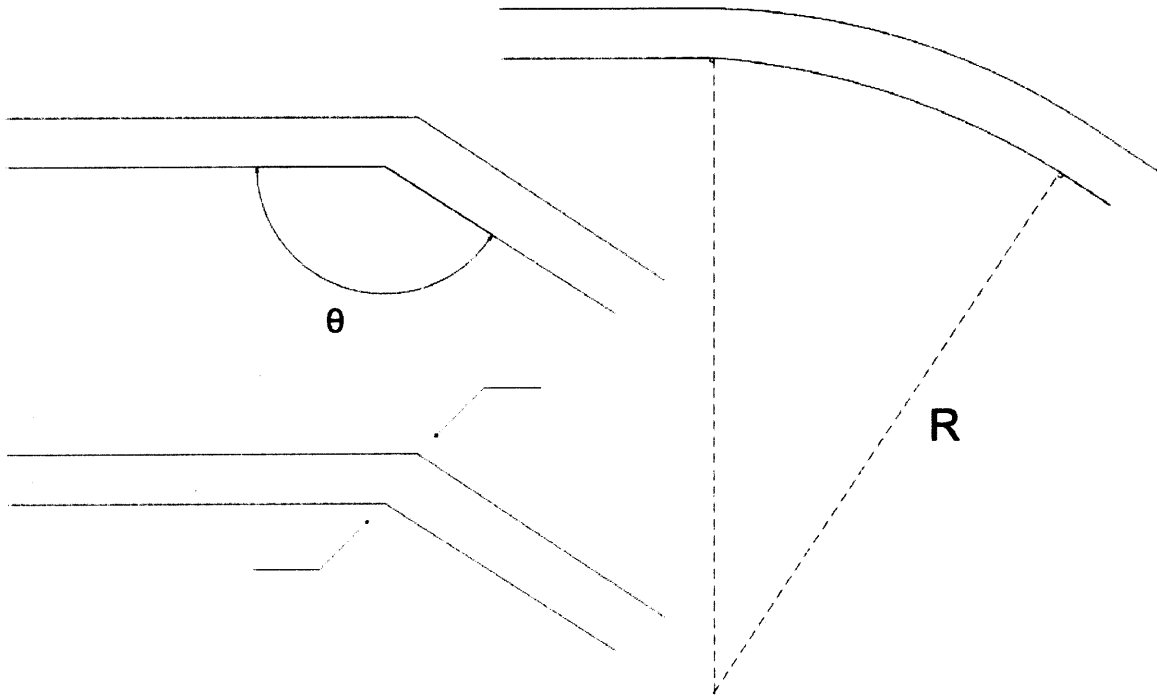
Figure 4-6: Diagram of the Key Characteristics of a Turn.

The most basic information that can be stated about a turn is the size of the angle formed by a continuation of a tangent to the inlet and a tangent to the outlet. That is, how much it redirects the stream of flow. This is shown as θ in Figure 4-6. Beyond that, the turn can be either sharp or smooth. If the turn is sharp, the sidewalls are straight going into and coming out of the turn, right up to the moment of turning. If the turn is smooth, the sidewalls are curved. In the former case, a sharp turn, the profiles of the inside corner and outside corner are probably not exactly sharp, and it would be of interest to investigate their deviations from that ideal at the points indicated by the arrows in the diagram. For the smooth case, the major parameter of interest is the radius of curvature, R. A small radius of curvature means a tight turn, and a larger radius means a more gradual change of direction.

4.3.4 Intersection

The next level of complexity is when multiple channels interact with each other, at intersections. Two typical intersections are shown in Figure 4-7.

66
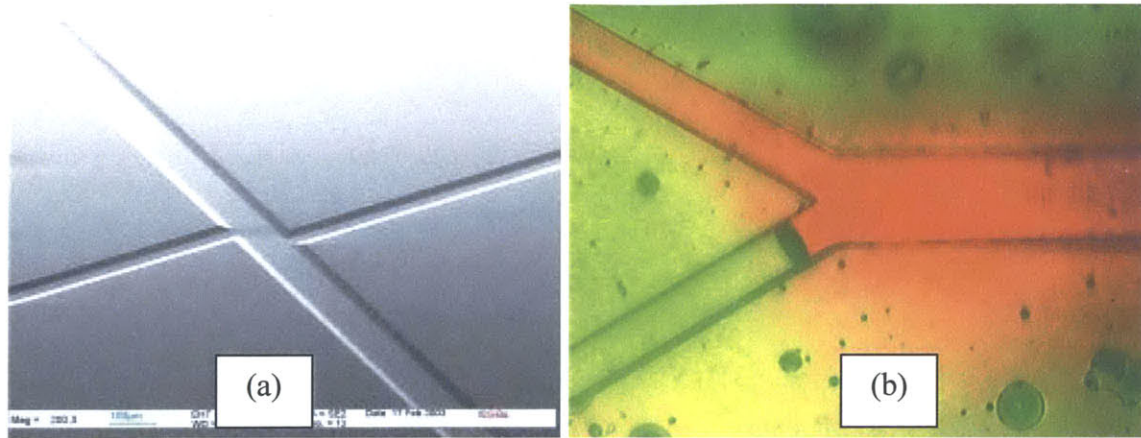
Figure 4-7: Microfluidic Intersections, left from Pfohl [2006] and right from Coventor [2006].

As can be seen, there can be many different types of intersections, but there are three fundamental parameters that describe an intersection. First is the number of channels that are involved in the intersection that form the inputs and outputs. This has a minimum value of three, else the intersection is actually just a straight channel or turn. Second are the angles of intersection between the channels, and third are the relative sizes of the various channels. The cross sections of the inputs could add to the cross section of the outlet, as shown in the diagram of the "Y" intersection in Figure 4-7(b), or any other combination of sizes.

For the purposes of a test device, it would probably be sufficient to limit the number of intersecting channels to three and four, respectively. Going much beyond that is less likely to be seen in one individual intersection on a microfluidic device, and should more streams need to be combined, a series of three- or four-branched intersections could be strung together. For example, consider the illustration in Figure 4-8 of the laminar properties of fluids in the microfluidic regime developed by the Whitesides group [Kenis 1999]:
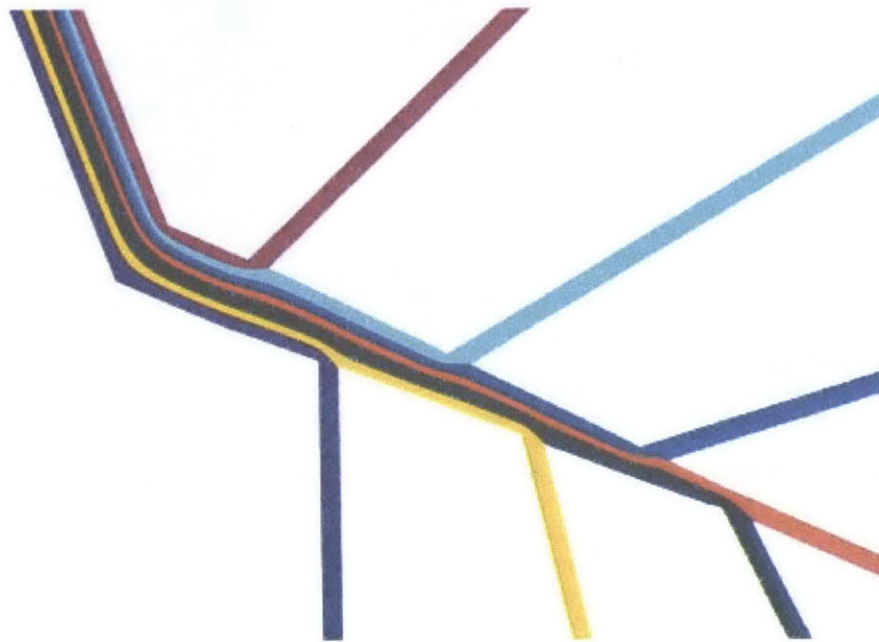
Figure 4-8: A multi-entranced microfluidic channel, demonstrating the laminar nature of fluids at the micro-scale. From Kenis [1999].

4.4 Complex Features

The second category are more open-ended features, where there are still many different possibilities for how to accomplish a particular function due to the infancy of the field or different strengths of different fabrication methods. These are also good candidates for inclusion in an emerging test device, but unlike the simpler features described in Section 4.3, where a channel can be described by its width, length, and depth and subsequently testing functionality of a fabrication method is a simple matter of varying those quantities arbitrarily, these features are not so easily described.

4.4.1 Posts

The laminar nature of most fluids in micro-scaled devices demonstrated in the preceding picture can be undesirable if two different inputs are designed not to merely travel side by side, but mix together. At sufficiently long length scales of this parallel flow, diffusion will act to introduce some mixing, but in applications where the time or distance is undesirable, structures have been created to promote mixing at a greater rate, often by creating a turbulent flow within the device. However, structures like those shown in Figure 4-9 do not qualify as novel mixers.
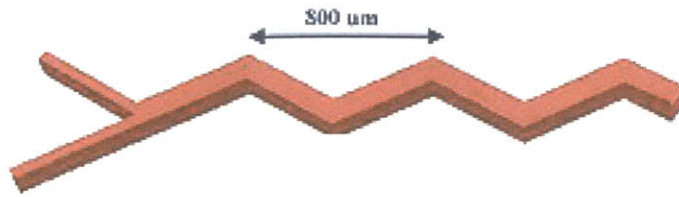
Figure 4-9: A Non-novel Mixer.

The mixer pictured in Figure 4-9 is no more than a continuous straight channel with a series of turns along its length and an intersection at the input. All of these components have been described already, and this arrangement does not add significantly in a new way. Thus, the purpose of this section is not to provide a repository of different design tips for inducing mixing in a microfluidic channel, but rather to catalog those features that are sufficiently different from the structures listed above to justify further exploration of the element in a test device.

There are two sub-categories of mixers currently in use: obstacle-induced-turbulence mixers, and non-obstacle turbulence-inducing structures mixers. A picture of two types of obstacle mixers is shown in Figure 4-10.
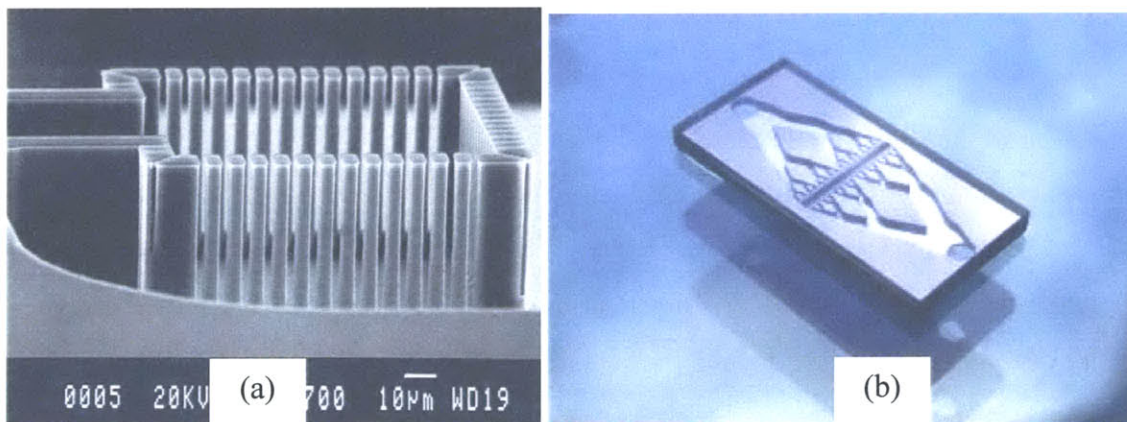
Figure 4-10: Microfluidic Mixers, (a) from Electrum [2006], (b) from Protron [2006].

Figure 4-10(a) is characteristic of in-channel obstructions, like the posts that appear here, that cause the fluid to go around them in many divergent and convergent streamlines, and thus mix very rapidly. This element is characterized by introducing the obstacles into the inside of the existing channel width. These posts or other obstructions can also be used as a filter, if the fluid has any relatively large objects suspended in it, like a cell. The picture shows the posts arrayed in three rows, but they could also be deployed densely within a channel. Obviously, if the channel size is at or near the lower limit of what can be fabricated, it will be difficult to

create structures that are smaller than that within the channel, but with larger channels, this element becomes a possibility. However, this level of intricacy of features could introduce difficulties for most polymer techniques, particularly in the de-molding step: the posts and the surrounding material will have a high degree of interdigitation, increasing the friction force between the mold and the part, possibly to the point of severing the posts. For a test device, a parameter akin to the density seen earlier in the multiple channels might be a good one to investigate, in addition to the more obvious depth and shape of the obstacles.

Figure 4-10(b) shows a different type of mixer, where a channel rapidly divides and divides again into a large number of sub-channels, which then reconvene back into a single output. Very often, the splits will divide into two, and then four, then eight, et cetera, so this structure can be referred to as an exponential differentiator. One could attempt to re-classify this type of structure as a series of multiple channels and intersections, but it seems clear that the density of features and the multiple intersections in a short length-scale sets this structure apart from those two simpler cases. Whereas the posts were characterized by being contained within a channel, this fluid element is characterized by the channel itself dividing and dividing again. Here too, the interdigitation around the islands that are created by the channel multiplications could be a problem for demolding, and a Test incarnation should focus on the density of channels, as well as the minimum size capillary that can be achieved in the midst of the complexities of this structure.

Both of these prior two methods involve creating posts inside the flow channel. In one case, the posts are explicit, and in the other, the posts are the small islands that divide the branches of the flow network. Unlike the walls that divide the channels in Section 4.3.2, which have small width but large length, the posts have very small length. Whereas the former is a one-dimensional high aspect ratio, the latter is two-dimensional high aspect ratio. This is the key characteristic that must be measured by a test device. And in addition to merely creating one structure with high aspect ratio in two dimensions, a closely packed array of these structures must be created.

A different scheme for promoting mixing is depicted in Figure 4-11:
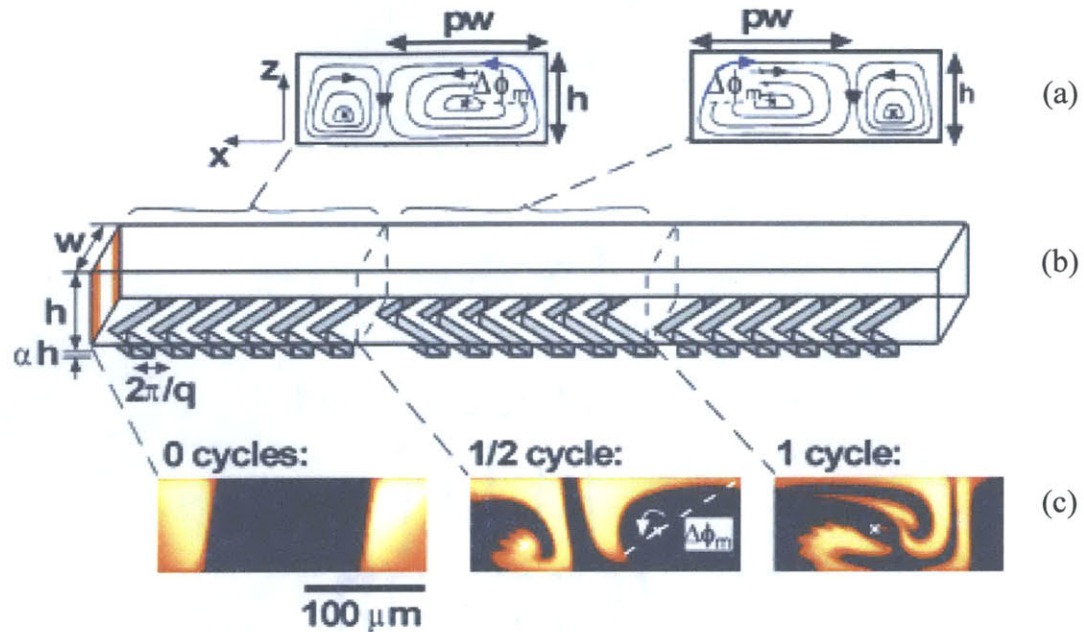
Figure 4-11: Herringbone Mixer, from Whitesides [2006].

This type of structure, which induces turbulence without introducing obstacles into the flow, employs a feature known as a herringbone pattern, referring to the offset chevrons, a reference to a bricklaying pattern. This structure is a good example of a two-and-a-half dimensional element: in an additive process, the channel would be deposited first, followed by the herringbone structures atop the channel. As shown in Figure 4-11(a) and Figure 4-11(c), respectively, the herringbone structures promote rotational flow of the fluid, in two flow cells. By altering the position of the chevrons along the length of the channel, the cells will collide and mix. The key characteristics here are the alignment of the second layer to the first, as well as similar metrics of features size and density as from the multiple channel model.

4.4.2 Alignment

Alignment will be discussed at much greater length in Section 5.2. As devices move to greater complexity beyond simple channels, issues of alignment and positioning the various parts that make up the device become more pressing. The two key areas where alignment arises are inputs/outputs and multilayer devices.

4.4.2.1 Inputs and Outputs

An example device is displayed in Figure 4-12.
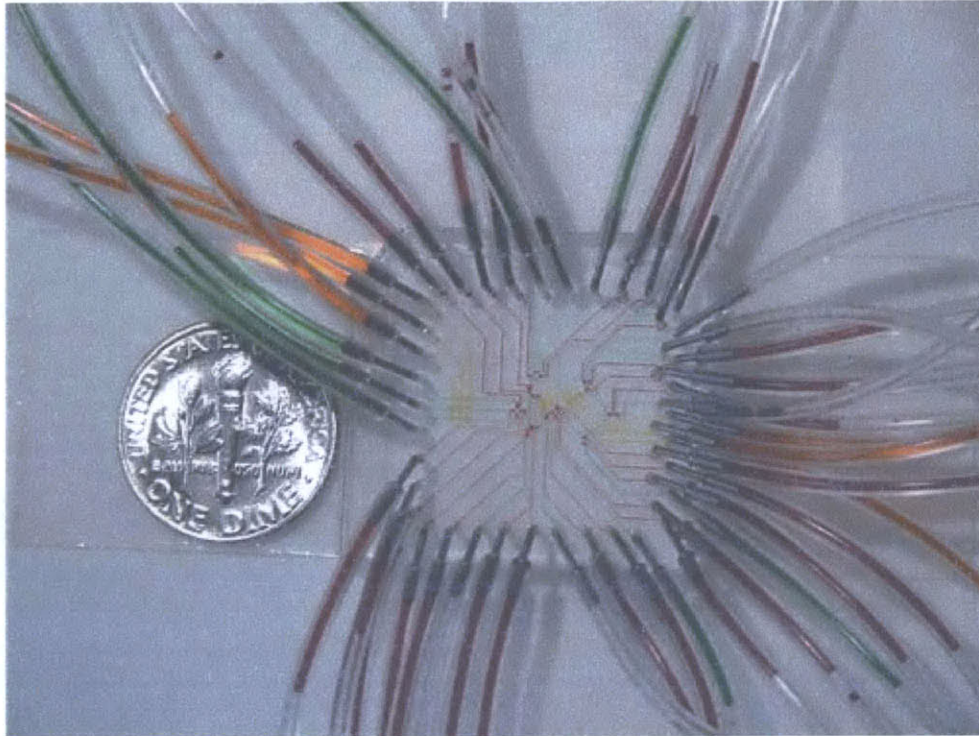
Figure 4-12: Microfluidic Device with Many Inlets and Outlets, from Tseng [2006].

While this is an extreme example, it underscores the importance of the inputs and outputs to and from the microfluidic devices. While the device shown is about the size of a dime, the tubes leading to the inputs and outputs take up a much larger area. This case addresses a larger issue with microfluidics, namely balancing the fluid channels themselves, which are unequivocally micro, with the rest of the device, including ports, fluid control, detection, and packaging, which are often not. The question then becomes one of, if the majority of the device is much larger than the microchannels, what is the advantage of going to microfluidics? There are valid responses to this question, namely that some of the flows present on the chip would make a macro-incarnation that much larger, that the chip remains disposable, and others, but the general perception needs to be addressed nonetheless.

As discussed in Section 3.3.2, there are two major approaches to inlets and outlets: closed, and open. Figure 4-12 is an example of the former, and Figure 3-8 is an example of the latter.

In terms of functionalities for a test device to recreate, alignment is again at the top of the list, though in a different way than its other uses in the device. Instead of needing to align to layers of a microfluidic device together, now the inlet punch or drill must align with the

corresponding well or inlet channel on the device. Refraction could make optical alignment of a punch from off-axis unpredictable through a thick block of material, but in general, oversizing has worked to minimize the difficulty of this operation. But while it is not currently pressing, every microfluidic device needs to have some way of interfacing with other devices, so ports cannot be overlooked.

4.4.2.2 Multilayer Flow

As will be explored in greater detail in Chapter 5, multilayer devices are an important next step for microfluidic devices. Two examples of multilayer devices are shown in Figure 4-13.
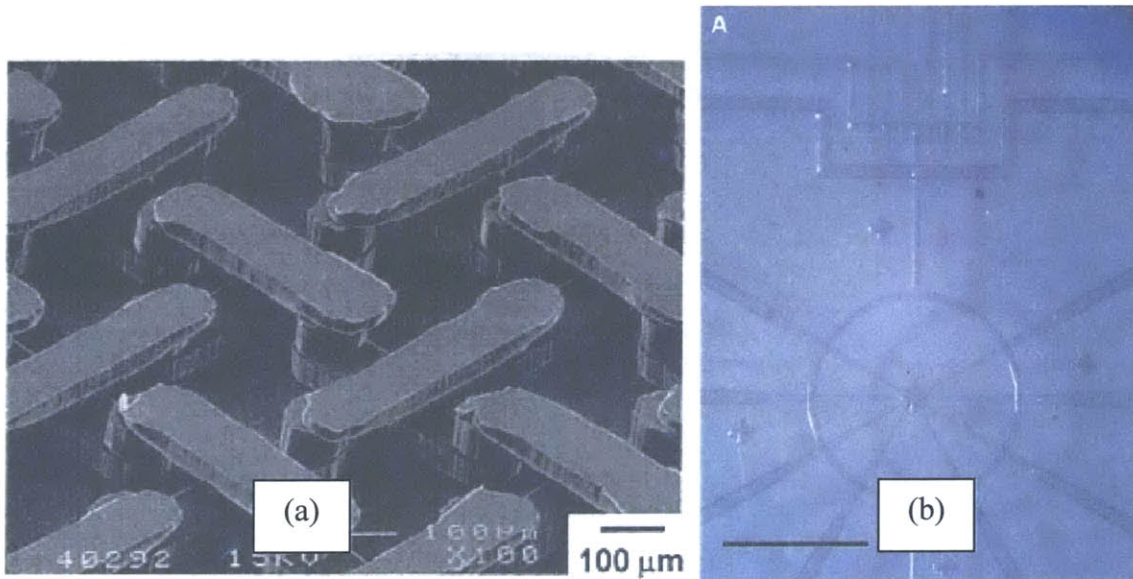
Figure 4-13: Multilayer Microfluidic Devices. (a) from Andreson [2000], (b) from Chou [2001].

Figure 4-13(a) is of the multilayer technique developed by Anderson [2000], which will also be discussed in Section 5.3 in greater detail. What are actually pictured are not the channels themselves, but rather a urethane that was injected into the channels and then cured. The PDMS bulk was then stripped away, leaving the urethane, to create the picture. Using the technique developed, the complex weave structures shown were created via casting of PDMS.

Figure 4-13(b) is a pump developed by Quake [Chou 2001] that uses the multilevel soft lithography technique. The circular channel is the flow layer, where the fluid of interest travels, and the radial lines are the control layer. The control layer is pressurized to defect down and into the fluid flow layer, sealing it off.

The major issue when fabricating a multi-layer device is alignment of one layer to the next. That is, once the bottom layer has been fabricated, and it is time to fabricate the next layer, the two must be properly positioned relative to one another. For Anderson [2000], this is during casting of the flow layers, and relies on mechanical contact between structures on the top mold and the bottom mold. For Quake [Chou 2001], the two layers are fabricated independently, and then aligned manually, by optical features on the two layers. For hot embossing, it is relatively easy to press the polymer with two molds on each side, but aligning the molds relative to one another, which is necessary in all non-trivial multilayer devices, can be problematic, as the molds need to be properly positioned relative to the wafer that carries them. Then the wafers need to be properly positioned relative to the platens that they sit on, and then finally the platens need to be both properly positioned in plane and coplanar as they contract and smash into the plastic. A trivial case, in this treatment, refers to a device that has two layers of devices on its two faces, but where the layers do not interact, and thus do not need to be referenced to one another at all.

Interestingly, though it has not enjoyed the popularity of hot embossing or soft lithography in common microfluidic usage, injection molding might be the best of the three for creating multilayer devices. At the macro scale, almost every injection mold is two-sided, so schemes already exist for reliably positioning the two halves of the mold, known as the core and cavity. While they would have to be improved in order to achieve micrometer-level repeatability, the work by Culpepper [2000] with kinematic couplings could be applied to reliably position the molds relative to one another. This assumes that the multilayer molds could be fabricated in metal (which thanks to electroplating they can) and that the micro-features of the mold could be aligned to the macro-features or that the micro-features would incorporate the kinematic couplings.

Related to alignment, but technically an additional requirement, are through-holes between layers. The multilayer soft lithography technique does not require holes that travel between the layers, as the fluid flow layer does not communicate with the control layer. The Anderson method [2000], on the other hand, was created for exactly that purpose. By providing a means of connecting channels at different layers, the topologically complex microstructures they created become possible. These holes are similar to the via-plugs described in Section 4.1 that are used in VLSI systems, with the in-plane fluid channels becoming the interconnects. Rather than carrying electrons, though, the channels carry fluid.

74

Adding via plugs between layers of the mold puts an additional requirement on the alignment between the two layers, as well as requiring a method of actually connecting the layers. The additional requirement on the alignment is that now there is a very definite position that the layers need to be in, and smaller deviations will appear to create proportionally larger problems. For example, examine Figure 4-13(a). There is a noticeable step resulting from the slight mismatch of the top layer from the ones below it. As for piercing the layers, the easiest way is to make certain that one of the molds has two and a half dimensions. The taller features form the via-plugs, while the shorter features form the interconnects.

Even these methods are not yet a true three-dimensional structure, as long as the processes that are used for polymer processes require a mold. The mold fabrication methods and the requirement that after molding the mold and the polymer be able to separate, or demold, imply that the only places the two molds, themselves each only two and a half dimensions, can touch and create the via connections, is at the weld line. Thereafter, once the multilayer part is created, it could be built up with other layers, similar to the multilayer soft lithography technique. Thus we see that there are actually two different types of alignment in creating a multilayer device: mold to mold, and layer to layer.

While creating matching kinematic couplings would address mold-to-mold alignment during forming, layer-to-layer alignment could be limited by optical methods. In addition, once alignment is achieved between two layers, sealing the layers of the device to one another is also necessary. For PDMS, which is formed by combining a curing agent with the monomer base, by tweaking the ratios in the different layers – e.g., deviating from the 10:1 target by having the top layer at 20:1 and the bottom layer at 5:1 – it is possible to exploit the material to fuse across the boundary between the layers. However, the same stickiness that the layers have for one another can serve as a detriment to the alignment, as the layers sticking together makes fine adjustments that much more difficult. D. Kim [2005] at Dankook University in South Korea took one approach to solve this problem. They devised a method where a thin layer of methanol can be used in between the two layers of PDMS during positioning and alignment, but can then be baked off, bringing the two layers into contact in the correct alignment. For non-sticky rigid materials, no such system is necessary, but it is still imperative to affix the layers after alignment without disturbing the alignment.

With a test device approach to multilayer methods, the accuracy of inter-layer alignment would be the key characteristic to be evaluated.

4.4.3   Encapsulation

Ultimately, there are limits to what the bulk polymer is capable of, and as seen in Chapter 2, many applications require greater functionality on the device. In these cases, it may become necessary to encapsulate another material or device within the greater microfluidic device. Two cases where this might be necessary would be in detecting the results of a test and controlling the fluid flow. Encapsulation is almost always dependent upon alignment, but represents a step up in complexity beyond the alignment discussed in Section 4.4.2.

4.4.3.1   On-Chip Sensing

Two examples of detection schemes are shown in Figure 4-14.
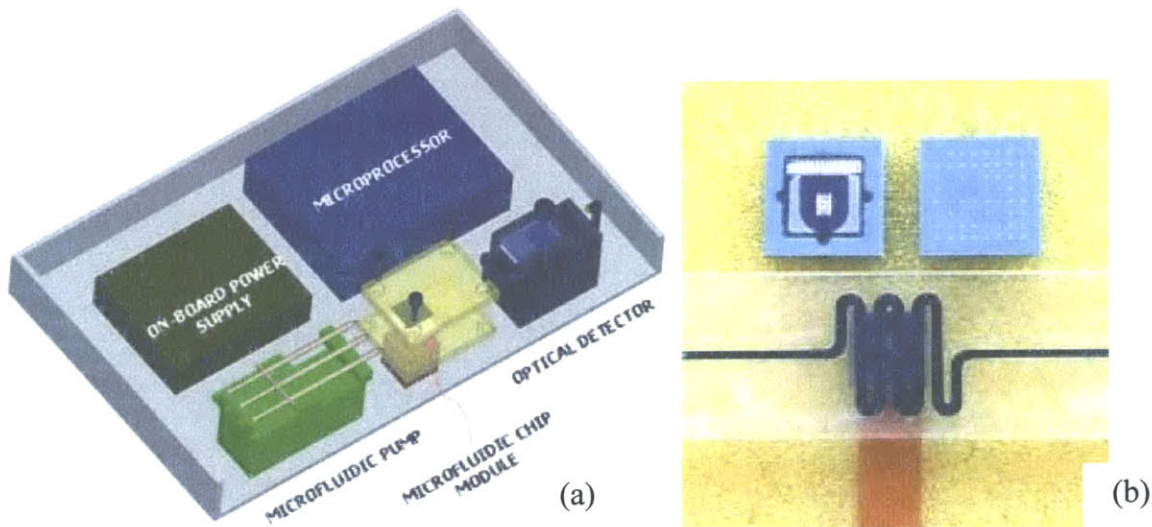
Figure 4-14: Microfluidic Detection Schemes. (a) from Batt [2006], (b) from Cismst [2006].

Detection is another area where the relative size of the microfluidic device itself and whatever devices are necessary to accomplish the detection come into play. As can be seen in Figure 4-14(a), the microfluidic chip takes up relatively little space compared with the detection components. Figure 4-14(b) addresses this issue elegantly: a light source and photodetector that are on the same size scale as the chip are used to measure the color of the fluid within the channel.

Most of the proposed detection is optical. When coupled with a clear material of the device, detection can be done outside of the chip. There are many fluorescent markers or means of changing the color of a fluid under certain conditions that can be employed by the application designer. This section, pertaining to the possibilities for a test device, focuses on the on-chip variants, as those are the areas of concern for a process engineer.

The two possibilities that appear in the literature are an encapsulated optical fiber, which could route the impinging light or the reflected or filtered output light, and a micro-avalanche photodiode. Both of these possibilities, if they are to be incorporated into a device, must be somehow encapsulated or potted into the device, in the proper arrangement.

The other possibility for detection is to use the substrate underneath the device as the detector. An electronic detector, such as a microelectronic device, is fabricated into a flat surface, and then an open-channel polymer device is attached to the top, so that the detector surface serves as one of the walls of the channel. This opens up the list of possible detectable properties beyond optical, into electrical or magnetic. As demonstrated by Gadish [2005], the electronic device could also be used as an electro magnetic filter, attracting suspended particles in the fluid with a sufficient electrical charge. For this approach, the alignment of the channels to the substrate could be a key parameter, depending on the size of the detector and channel. Killeen [2003] describes adapting liquid chromatography to microchips.

In a test device, the ability either to encapsulate the sensor in a reliable position relative to the flow stream would need to be demonstrated by each candidate process.

4.4.3.2 Fluid Control Elements

Moving fluid around on microfluidic chips in desired directions is another issue of importance to microfluidics that remains wide open to potential solutions. One approach was show in Figure 4-13, and another example of a valve is shown in Figure 4-15.
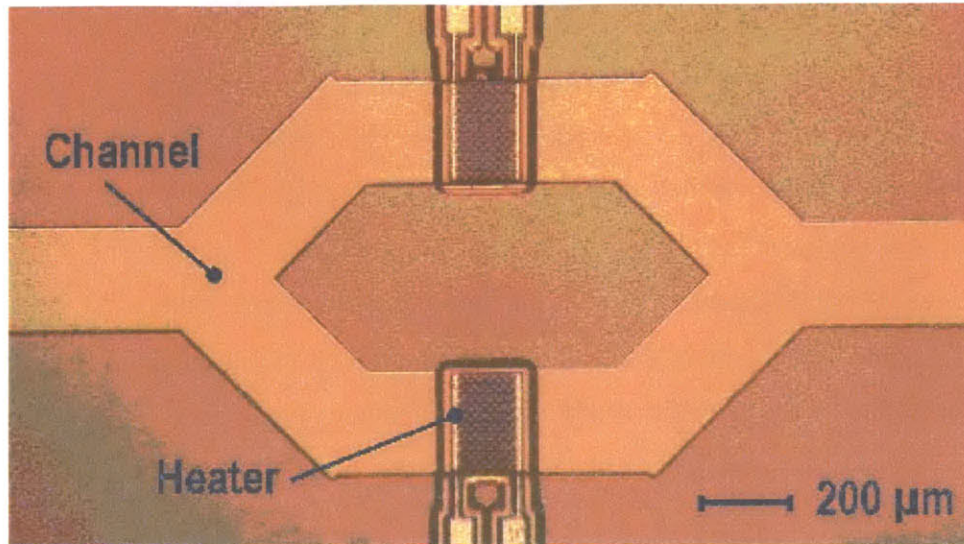
Figure 4-15: Microfluidic Valving via Micro-heater. From Stoeber [2006].

The device in Figure 4-15, created by Stoeber [2006], works by using a special fluid that contains a triblock copolymer. This additive causes the fluid to become a gel when the temperature is increased by the heaters, effectively sealing the channel. When the heat input is removed, the flow returns to liquid within 33ms, the blockage is removed, and the valve has been opened. A similar approach has been attempted with local coolers to create ice, but the response time is much slower. In both of these thermal methods, the heat-control element must be encapsulated within the device.

The two major categories of fluid control elements are pumps and valves. Similar to the discussion about sensing elements in Section 4.4.3.1, this treatment will focus on the on-chip solutions to these problems. That is, it is very easy to hook a microfluidic device up to a syringe pump, but in that case there is no process-related issue in the fabrication of the device that must be addressed, beyond connecting the ports in the device to tubing.

Ultimately, valving and pumping boil down to relative pressures. A pressure differential drives a flow or halts it, and it is the fundamental goal of any fluid control element to create a pressure difference on the device. For pumps, this conception is obvious: the purpose of a pump is to increase the pressure head necessary to drive the fluid. For a valve, the concept also holds: a flow-stopping valve creates a barrier that has a high failure pressure, and a flow-directing valve in an intersection creates a higher-pressure resistance in the channel where flow is undesired than in the desired escape branch. The combined effects of how hard the inlet pushes, how hard the

valve is pushing, and how hard the other routes of escape are pushing will determine the resultant flow.

Any catalog of pumps or valves for microfluidic devices ends in an ellipsis, as there are numerous approaches to both of these issues, and new ones are being created or refined continually. With that caveat, the following will portray a number of different approaches to provide an overview of the existing spectrum.

Pumps can be mechanical, gravitational, electro-osmotic, or passive. Mechanical pumps typically have rigid moving parts, which covers a wide range of possibilities. Using mechanical pumps introduces additional complications into the fabrication, such as the insertion of micro impellers in forming the compressors, and providing a force to drive the mechanical elements. Gravitational pumps use wells similar to those described in Section 4.4.2, with the input well containing a greater height of fluid than the output well. Then the pressure differential will be relative to the difference in heights, causing the liquid to flow. Electro-osmotic methods utilize a fluid that has some electrical charge in combination with a voltage field. The voltage field can be applied via electrodes that are implanted into the device. The attraction of the fluid to one of the electrodes will cause it to flow from the repulsive electrode toward the opposite polarity. Electro-osmosis is commonly used in the electrophoresis processes that were described in section 2.3.2. Electro-osmosis only provides a motive fluid force perpendicular to the voltage gradient, so it is best suited for simple devices with little more than a straight channel. Passive pumps need no input for the fluid to flow through the device with sufficient penetration for device functionality. For passive pumps, the fluid either is pulled along by other phenomena or pushes itself forward. The former refers mainly to capillary action. When the fluid is sufficiently attracted to the surface, and the cross-sectional area is sufficiently small, surface tension will pull the fluid through the channel. The latter, where the fluid pushes itself forward, is only found in special cases. One application that used a fluid that propelled itself was a male home-fertility tester. The user deposits a sample of semen into the device inlet, and if the sperm are functioning normally, they swim along the microfluidic channel toward the detector. No other force is necessary to power the fluid moving through the device. A picture of the device is shown in Figure 4-16.

Figure 4-16: eleMENt Male Fertility Tester, an open-well microfluidic device. From Pria Diagnostic [2006].

As for valving, it is first necessary to observe that many of the valving solutions could also be used as pumps by having a number of valves in series. By closing them in succession, the fluid is pushed along by a peristaltic mechanism. Different types of valves include mechanical, pressure-differential, deformation-based, and temperature altering valves. Mechanical valves are similar to mechanical pumps, in that they involve some rigid component that has been ingeniously buried within the device. The component shifts position to open or seal various channels. Similar actuation issues arise in valves as in mechanical pumps. However, a linear actuator would suffice for a valve whereas rotational actuation may be required by many of the pumps.

Pressure-differential valves refer to fluid control similar to the fluid control described in Section 4.3.4. The fluid flows down the channel with the least resistance. The limitation of this method is that there is usually some leakage since the channels are never fully closed off, and diffusion potentially occurs at the site of the intersection.

There are two types of deformation-based valves: multilayer valves, and in-plane valves. Multilayer valves are shown in Figure 4-13. In-plane valves also take advantage of the flexibility of some materials, like PDMS, to create check valves. In one direction of flow, there is little resistance to the flow. But in the other direction of flow, the resistance is great enough to prohibit flow. There is a fluid check valve that relies on deformation present in the body of the reader, and that is a lymph valve. Whitesides pioneered the adaptation of the lymph valve to microfluidics [McDonald 2002], and a picture is shown in Figure 4-17. In addition, Jeon [2002] proposed a multilayer built-up check valve where the fluid flow in the check valve is temporarily normal to the overall flow direction.

FLOW

NO FLOW

250 μm
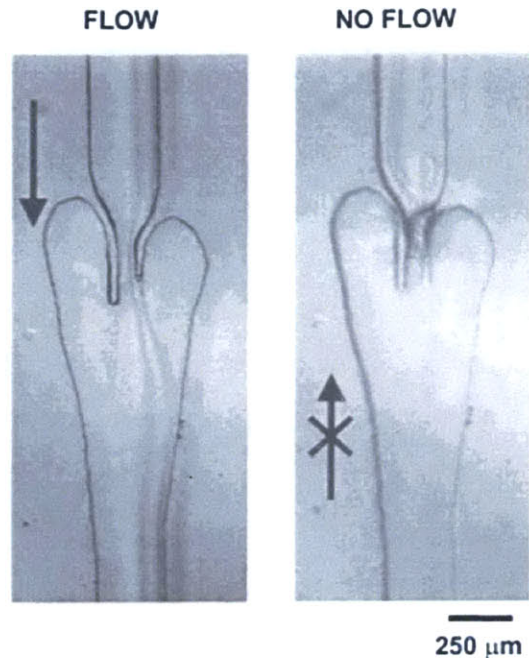
Figure 4-17: Check valve working off of lymph node valving principal, developed by Whitesides. From McDonald [2002].

Fluid can easily flow from left to right, as the thin lips are deformed outward by the fluid flowing through. But if the fluid has reason to reverse in direction, pressure will be built up around the outside of the flaps, sealing them off, preventing flow in the other direction. These two deformation methods are limited to microfluidic devices formed from compliant materials. Rigid materials are likely unable to deform sufficiently to cut off the channels. The functionality here is no more than the thickness of the flaps that have to be deflected.

Temperature control is an innovate approach to valving. By locally heating or cooling a segment of the channel, the phase of the fluid can be changed to solid, either by gel formation or by creation of a small plug of ice. The solid plug seals the channel, creating an effective valve. The literature suggests that the major drawback to this method is response time; once activating or deactivating the valve, the time to seal and then unseal the channel is longer than desirable.

4.5 Moving Forward with the Test Device

This chapter has described the many different candidate features for inclusion into a test device, as well as their key characteristics that a test device would highlight. These features or areas of functionality are:

- Single channel (width, length, aspect ratio)

- Multiple channels (density of channels)
- Turn (degrees of turn, radius of curvature)
- Intersection
- Posts
- Alignment
- Encapsulation

Future directions for the test device will be discussed in Section 9.1. Any proposed test device must include a demonstration not only of the simpler features like the single channel, but ideally will include a holistic view of the functionality of a microfluidic device, including the methods of inputs/outputs, fluid control, and sensing.

5 Multilayer Flow: A Next Direction

5.1 Background

In the vast majority of devices created to date, the on-chip flow, as distinguished from flow to the chip through the inlets or outlets, is contained within one plane. Using the two and a half dimensional techniques offered by silicon-wafer processing in creating a mold, channels can vary in depth across the device. On the other hand, the channels rarely directly flow from one layer to layers at different levels. Even the multilayer soft lithography technique developed by the Chou [2001] has two isolated layers, one designated as the flow layer and one as the control layer, that do not communicate with one another on the device. A likely reason that there has not been a focus on multilayer flow, to date, is that there has been no need. The devices in use are free to spread in-plane without greatly increasing the overall size of the device. But as devices grow in complexity, in order to avoid devices that spread significantly out in-plane, creating devices that are perhaps tens of centimeters in length and width but still no more than 100 microns in channel depth, the research must move in the direction of multilayer devices. In some ways, this is another area where microfluidics may mimic microelectronics. For example, the rudimentary metal-oxide-silicon field-effect transistors (MOSFET) devices had no more than one or two active regions on a silicon wafer. As the number of transistors, resistors, and capacitors steadily grew, so too did the importance of back-end technology: metal connections above the surface of the wafer that connect the devices together. The difference, and where the analogy falls apart, is that in microelectronic devices, all of the alterations of the signal, the functional components of the circuit, appears on the surface of the wafer, and the metal wires, known as interconnects within a layer and via plugs between layers, merely convey the signal. There are some occasions where an inductor coil could be built up by a series of layers, and any device must be checked to see that its interconnects do not inadvertently act as capacitors, but for the most part, the device functionality takes place at the wafer level. For microfluidic devices, the

situation is a bit different. The channels themselves are often the site of the functionality, which could take place on any level. In that way, microfluidics could prove more flexible in terms of design than microelectronics. Given that multilayer devices are a likely next direction for the field of microfluidics, that not too much work has been done on developing them to date, and that they requires innovation that micro-electronics does not require, multilayer flow is a desirable area for focusing.

Ultimately, the fabrication of multilayer devices can be devolved into a problem of alignment. There are two types of alignment – mold to mold, and layer to layer. Both of these scenarios raise one question: how is it possible to position correctly the two components relative to one another so the features that are designed to interact between them do so properly?

The reason for asking this question is that lack of correct alignment will negatively impact the performance of the device, as in general, a misalignment will tend to reduce the cross-sectional area of the multilayer joint. A reduction in area for the fluid to flow between layers will increase the pressure drop across the port, and this is what is meant by negatively impacting performance: an unanticipated increase in pressure drop could reduce the effectiveness of the other components in the system. As the complexity of the devices increases hand in hand with the number of multilayer joint, misalignment between the layers will cause greater and greater problems.

A large part of the problem is that the particular scenario introduced by a multilayer microfluidic channel is not well understood at present. While various analytical fluid flow models exist for simplified scenarios where the fundamental governing equations can be solved definitively, scenarios that are more complex are not so easily solved. To compensate, empirical models have been derived to elucidate common areas of interest in fluids. A good example is the transition from laminar flow to turbulent flow. This transition occurs when the Reynolds number, shown in Equation 5-1, of the flow exceeds 2000 [White 1999]. The basis for this parameter is empirical, not analytical. Reynolds measured many different pipes and fluids under different flow rates to determine the transition to turbulence:

$$\mathrm{Re} = \frac{\rho V D}{\mu}, \tag{5-1}$$

where ρ is the density of the fluid, D is the pipe diameter, and μ is the viscosity of the fluid, for Newtonian flow.

84

Section 6.3 on the theoretical model will discuss this in further depth, but any non-straight portion of a channel can be treated as a pressure head loss. The data that exist for pressure losses are primarily developed for devices of interest to macro-scale engineering, such as creating plumbing designs for a building or large pipelines. In these cases, the pump must be correctly sized for the rest of the network, so correctly assessing the impact of the various components on the pressure drop is essential to proper design. Therefore, components like a globe valve or a 45° elbow are well characterized, even down to different manufacturers of these components. But when searching for a fluid model for the pressure drop across a multilayer joint in a microfluidic device, there is little data. This is mainly because no one has required the information previously. Most of what does exist is for the turbulent regime, because for a low viscosity fluid, like water, traveling in the size range of common pipes at flow rates typical of engineering use, the fluids exceed the critical Reynolds value of around 2000. In microfluidics, flow is almost universally laminar, and if turbulence is desired, it must be specially designed into the system.

The models developed in Chapters 6 and 7, both theoretical and experimental, will investigate the very area that we believe will become of greater importance but where no prior data exists: assessing the pressure loss across a multilayer joint in a microfluidic device. In particular, the effects of misalignment on the pressure drop will be interrogated. As the complexity and density of micro-fluidic devices increases, this understanding of the impact of multilayer joints on fluid flow will enable designers of microfluidic devices to factor the effects into the design.

To that end, one interesting piece of information to be sought is in the special case where misalignment actually promotes greater overlap, increasing the cross section of the joint, and reducing the pressure drop across the joint. In this work, overlap area is meant to refer to the cross sectional area between the two layers that the fluid flows through, the area of the multilayer joint. An important question is raised; is there an amount of overlap area that could be deliberately induced so that the multilayer channel over the length is indistinguishable from a flat channel, with regards to pressure drop? That is, how big does the hole between layers have to be in order to provide a joint with no additional resistance? Is that even possible, or is it inevitable that any joint, no matter the size, will create a pressure loss? This model will seek to find out.

In the simplest case, a microfluidic multilayer joint, viewed from the side, would look like Figure 5-1.
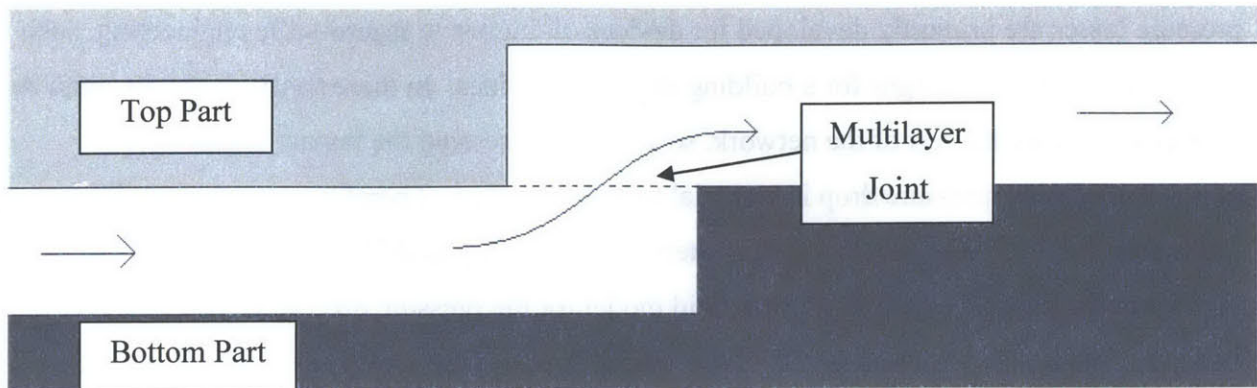
Figure 5-1: Simple Multilayer Fluid Flow, side view.

There is an inlet on one layer, and then fluid flows through the joint up to the second layer. The fluid executes two right angle turns in rapid succession. While these could theoretically be treated separately, each one as a minor pressure loss, their proximity suggests that they probably interact and affect one another in ways that two right angle turns separated by 10 diameter-lengths might not.

From the point of view of the page that Figure 5-1 is printed on, misalignment between the top and bottom layers would act a left-to-right direction or a direction perpendicular to the page. Figure 6-3 through Figure 6-8 will show these misalignments in greater detail.

For a first model, a slightly modified design was developed to simplify some fabrication concerns. It is shown in Figure 5-2.
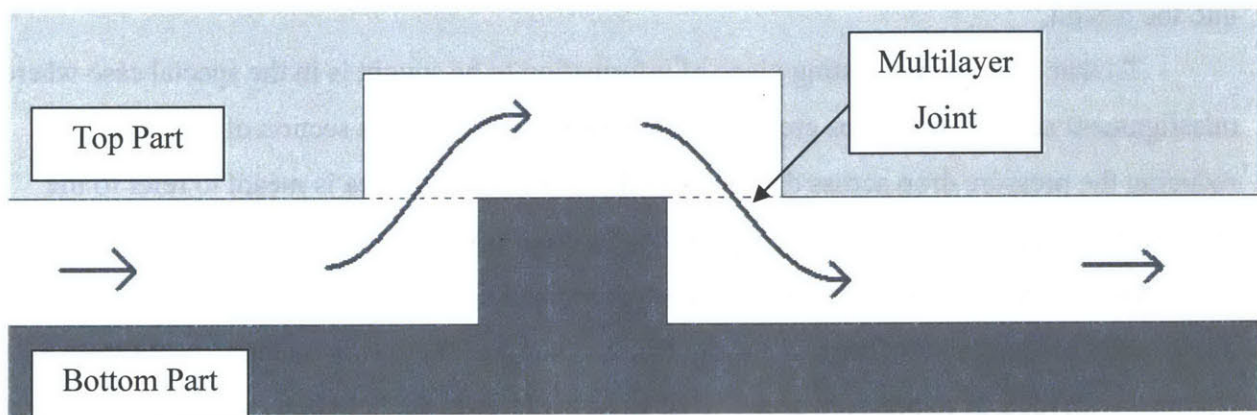
Figure 5-2: Multilayer Fluid Flow with Two Joints, side view.

This is nearly identical to the first simple case, but with two of those, one up and one down, coupled together. This means that fluid will flow into and out of these channels from the

same level on the device, rather than worrying about fluid ports at different levels. The design is symmetric about its centerline, giving the fabrication additional flexibility. From the top, the second layer will look like a connector between the two sides of the bottom layer, assisting alignment. Also, a slight shift along the axis of the channels could potentially be self-compensating, if the multilayer joint on one side is opened the same amount as the other is closed, as shown in Figure 5-3. Here, the top layer has been shifted to the right due to misalignment. The multilayer joint on the left is made smaller, but the multilayer joint on the right is made larger.
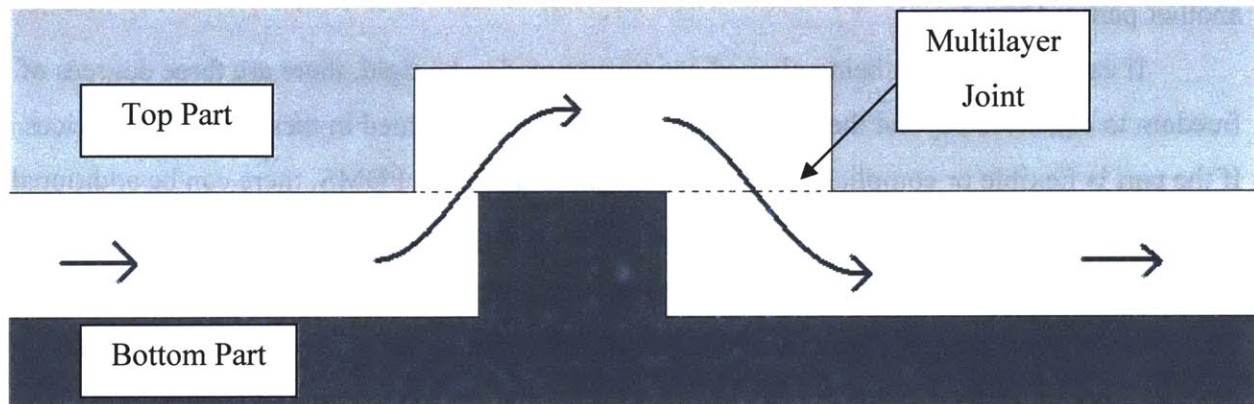
Figure 5-3: Multilayer Fluid Flow with misalignment of the layers.

Finally, if the channel is centered over the bottom two channels, it will be in the correct position, whereas a realization of the first incarnation would require features to assist with correct alignment overlap area, particularly when it is intentionally shifted to assess the pressure drop at different values of the overlap area. This is the design for the models.

5.2 Alignment

There are two primary methods of alignment: mechanical, and optical. These two methods can be applied to the two places where alignment is required in the fabrication of microfluidic devices: mold-to-mold alignment, and part-to-part alignment. Mold-to-mold occurs during or immediately prior to the forming of the polymer, whereas part-to-part occurs after the polymer has been formed. The separated layers of the part that were formed independently are brought together in a stack to build up the multilayer device.

Optical methods require at least one of the two sides being aligned be transparent. Since many of the applications require transparent materials, and most of the molds under

consideration are opaque, it is likely that optical methods will be better suited for part-to-part alignment. Mold-to-mold alignment will therefore typically require mechanical methods.

5.2.1 Mechanical Alignment

Whitney's book [2004] is an instructive resource on mechanical alignment. To align any part properly, all of its degrees of freedom must be constrained without creating over-constraint where two references compete for control of one of the positions or degrees of freedom. Constraints are achieved through mates, places where the part to be aligned is in contact with another part or fixture.

If each mold or part being aligned can be assumed to be rigid, there are three degrees of freedom to constrain beyond the face-to-face contact that is assumed in these flat-layer devices. If the part is flexible or compliant, such as a thin part made from PDMS, there can be additional degrees of freedom that need to be constrained. The six degrees of freedom are the three orthogonal directions in three-dimensional space, in addition to rotation about each of those axes. The plane-to-plane contact characteristic of joining different layers constrains three of those degrees automatically: rotation about each of the axes that are in the plane of contact, and linear motion normal to the plane of contact. The structures that interact on the layers must then constrain the other three degrees of freedom: rotation about the normal to the plane, and linear movement in the plane. Tying back to Figure 5-2, the directions described that would tend to lead to misalignment are those in-plane directions.

A further implication of bulk planar contact augmented by further constraint to align the other three degrees of freedom is that at least one of the sides must be multi-tiered itself, in the two and a half dimensions sense of at least two different heights of features on the one side. That is, if each side only had one layer to itself, there would either be no way to constrain the parts in-plane, assuming the multiple layers were maintained (Figure 5-4(a)), or there would be a collapsing of the multiple layers into one layer (Figure 5-4(b)). This would violate the postulate that it be a multilayer device (Figure 5-4(c)),

Two Single-Layer Molds Halves

Two Flow Layers   (a)   No In-Plane Constraint   In-Plane Constraint   (b)   Only One Flow Layer
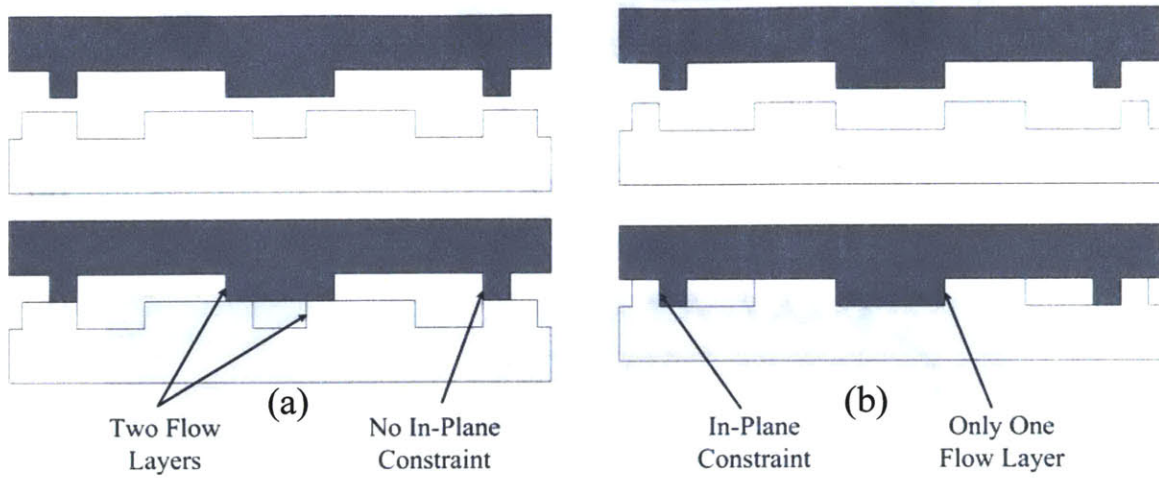
One Single-Layer, One Double-Layer

Two Flow Layers   In-Plane Constraint   (c)
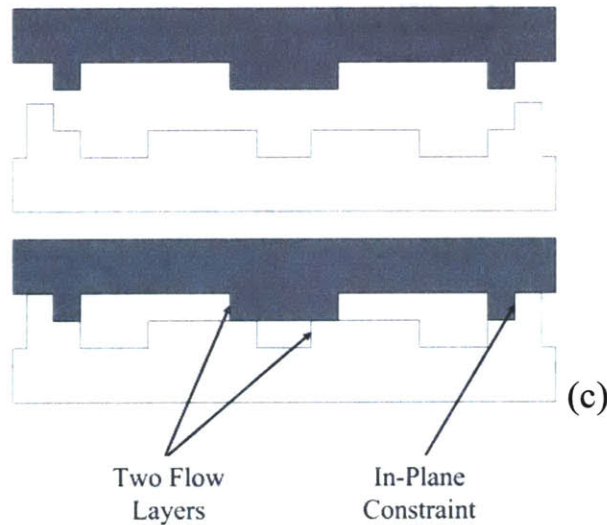
Figure 5-4: Mechanical Alignment of Multilayer Microfluidic Devices.

Interestingly, if photolithography is used to create the stepped profile necessary for one of the mold halves, the mechanical alignment chain of alignment will actually entail an optical link. That is, the features that interact with the other side of the mold are connected to the channel features on the same side by the photolithography step, and the only way of aligning a photolithographic mask is optically, if a reduction mask is not employed. As reduction masks are designed more for much smaller features, their use for microfluidics would be unnecessary. Then, the flow chain is as shown in Figure 5-5(b):
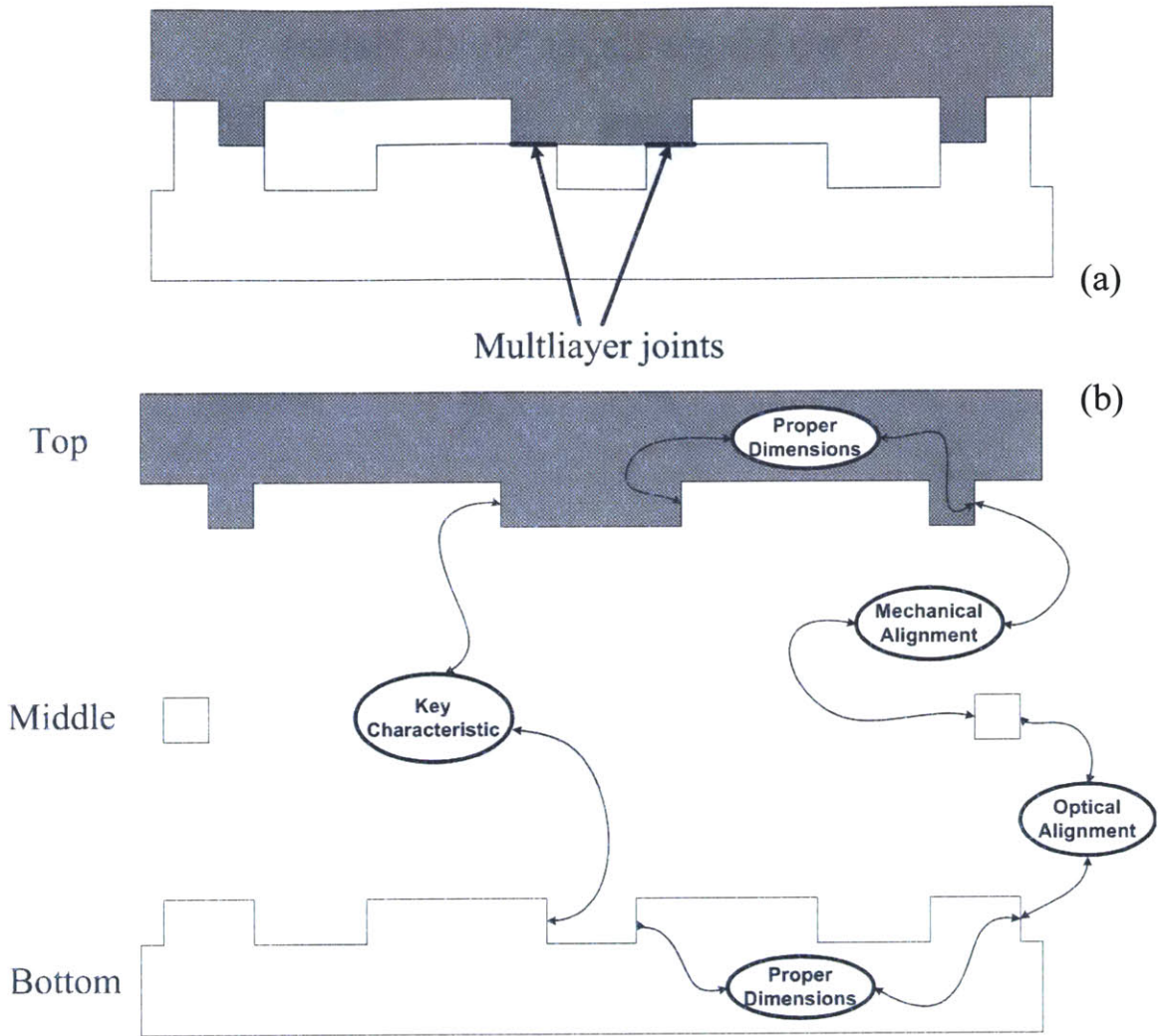
Figure 5-5: Datum Flow Chain through the Multilayer Device.

A picture of a pedagogically correct way to constrain two perfectly rigid devices is shown in Figure 5-6. The figure focuses on the alignment features, and does not show the channels or other fluid features.

Each of the three cylinders has one point of contact. The two that contact the same wall constrain motion in one direction as well as rotation, and the third contact constrains the other direction of movement. In reality, however, it may not be so easy. The forces at work may exceed the deformation limits if so much force is put on three tiny areas of contact in attempting to achieve and maintain the correct alignment. Also, since these features will have a very low aspect ratio, implying that they are very shallow, it will be easy for them to act like seismic plates and slip over one another.
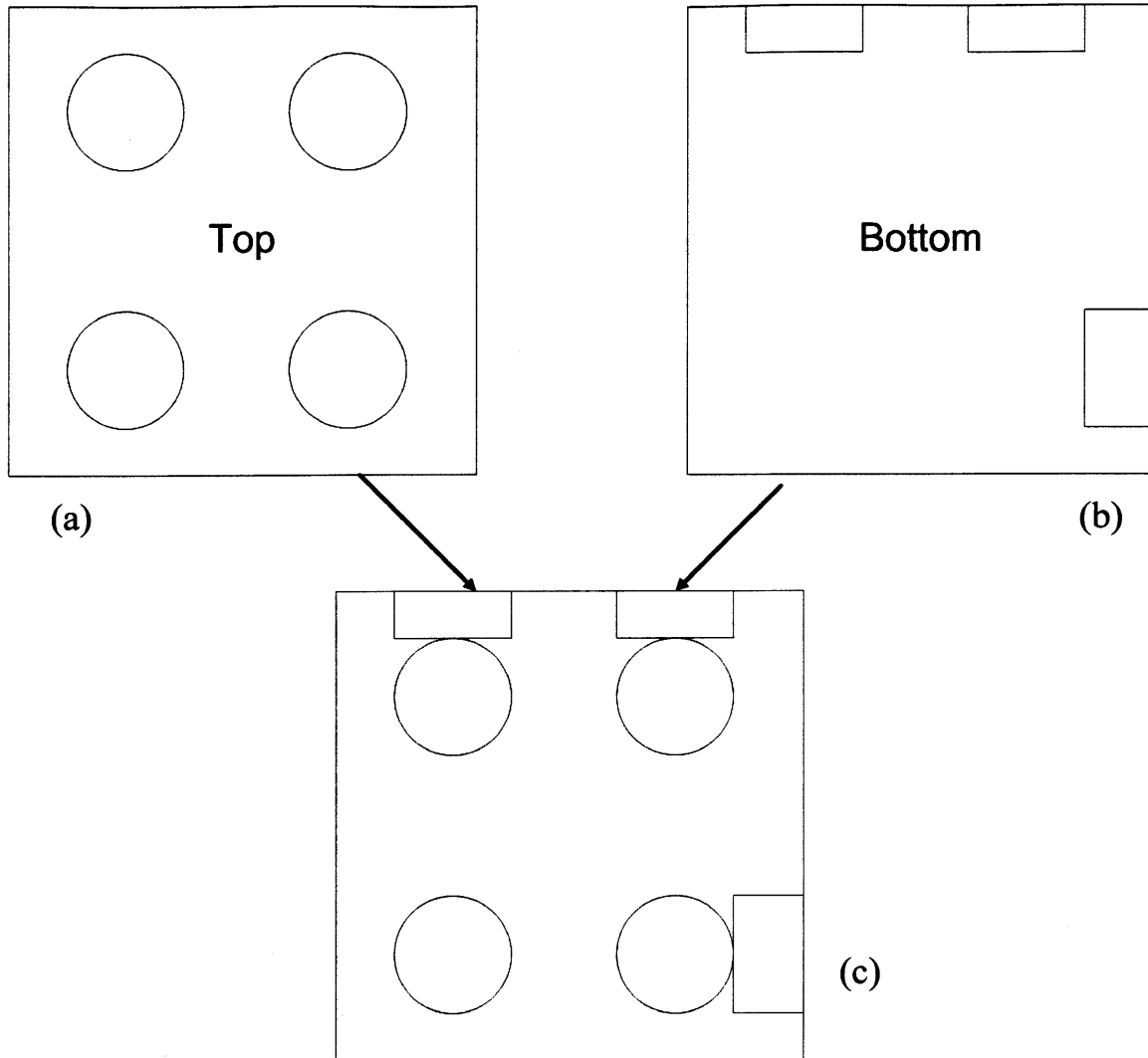
Figure 5-6: Properly Constrained Alignment Scheme. The protruding cylinders in the top (a) align to the protruding rectangles in the bottom (b), forming the completed mate (c).

Even the method proposed by Anderson [2000], which will be discussed in greater detail in the next section, used four ridge-in-slot contacts. These ostensibly over-constrained each linear dimension once and over-constrained the rotation three times. But they found it to work properly to bring their features into alignment. They may have been aided by the fact that one mold half was made out of PDMS, so it could have deformed to fit the over-constraints.

Areas deserving of more attention might be the other macro-mates that could be adapted to microfluidic fabrication: pin-in-hole, cylinder-in-vee, box-in-box, or others. In order to observe good design practice, the alignment scheme that involves the least over-constraint but still reliably aligns the parts should be used. In addition to the deformation of the parts or molds, another issue to be tackled is the balance of the forces needed to form the polymer versus

establish the alignment. That is, for a multilayer device to be formed from two mold-halves, there will likely be through-holes, places where the mold halves touch, excluding the polymer in those areas. In the final part, there will be a void extending through the part. If the polymer is placed between the mold halves before the molds are brought together, such as when working with PDMS or PMMA in the hot embossing case, the polymer must be forced out of those locations. If it is not, the forming is incomplete. Even in injection molding, where the molds can be touching before the polymer is injected, the force closing the two molds together must be great enough to prevent the pressurized molten polymer from flowing into the crack between the molds. If the machine fails to do this, the thin layer of plastic is called flashing, or simply flash. Flash is particularly worrisome for multilayer microfluidic devices, for it threatens to seal off a channel where there was supposed to be an inter-layer through-hole. For PDMS, an additional phenomenon has been observed: since it is in the liquid phase at room temperature before curing, and it is fairly viscous, it tends to further resist compression that would lead to exclusion between the through-hole mold elements. For these reasons, it is necessary to apply a large amount of pressure between the mold halves. But at the same time, it is necessary to allow a certain measure of freedom in the directions normal to the mold-parting plane, in order to allow the mates to be established via contact between the matching parts on each side of the mold. Friction induced by the compression could fight against that movement, and the low profile of the features would mean that there would be very a very small resistance force when contact is made before the features would prove insufficient to prevent further displacement. That is, the features jump over one another instead of resisting the in-plane alignment shear force. Thus, what is required is a contraption capable of providing high pressure in the molding direction but that is able to apply a much smaller force with high sensitivity to force feedback in the plane of the molds.

For injection molding, the sequence is different, in that alignment occurs before the filling of the mold. Thus, the alignment step could be performed at very low force levels, and once the mate is established, the high pressure necessary for the injection can be applied. This system would require some compliance in the mold halves to allow the mate to be established before pressure is applied, and then subsequently the ability to clamp tightly. As discussed in Section 3.2.3, it is easy enough to attach a micro-mold, such as would be produced by

electroplating, to a macro-mold or macro-aligner, but designing the mates is problematic, as the natural matching mate for the micro-features is itself a micro-feature.

Hot embossing bodes the worst of both worlds. Alignment cannot be made until pressure is being applied and the polymer is being deformed, and there is no luxury of in-plane movements after contact is made, as they would require a level of fluidity from the polymer not seen at the glassy transition point. The other possibility is that the in-plane movements would cause distortion of the features transferred. Hot embossing will require a scheme that could be deployed in the other two cases, where the mate is made before forming above the polymer, and then the layers are pressed together in exactly the right relative position. The datum flow chain, similar to the datum flow chain shown in Figure 5-5, would be required to go through at least one macro-scale part, be it the load frame or alignment rods. The introduction of these macro-features to assist with the alignment simultaneously introduces the alignment of the micro-features to the macro-features within each mold half. There are encouraging examples of well-controlled injection molding processes, such as those that create contact lenses. The dimensional tolerance of a contact lens is relatively tight, so it is possible to create well-matched molds that can be affixed to the load frame and then will repeatably position themselves through multiple cycles. The molds are aligned once at the beginning of the run, and thereafter the frame shafts maintain the positioning through the cycles.

5.2.2 Optical Alignment

The other major approach to alignment is optical. Optical methods require a clear material for one of the parts, in order to look through the part at the features on both sides while bringing them into alignment. The microfluidic features on both parts will be touching, and unless they are positioned specifically with regards to the edge of the part, it is otherwise impossible to detect via optical methods where the structures that need to be brought into alignment are relative to one another. In addition, a method of manipulating the parts relative to one another with very fine control is required. That is, it is not enough merely to be able to see the features if they cannot be adjusted to bring them into greater alignment. The positioning mechanism also requires resolution on the order of that desired by the device. Multi-layer photolithography relies on optical alignment, and the machine that exposes the photoresist through the mask regularly will have an alignment mechanism as an integral component, to the

point where the machine is referred to as the "aligner", even when it is used with simpler or single-layer designs that do not actually require alignment.

In those devices, the mask is uniformly chrome on quartz; a transparency mask lacks the rigidity necessary to perform optical alignment. The wafer, with the optical marks already patterned on it, is brought into contact with the mask of the next layer. The two of them are viewed with a microscope to magnify the image, and then the wafer is dropped slightly into separation. The wafer and mask are thereby decoupled, but still very close together to the point that the alignment marks on the wafer can be seen through the mask. The wafer is attached to a stage that can be actuated in three degrees of freedom: two linear directions in the plane of the mask, and one rotational direction about the normal to the plane of the mask. Often, there are multiple alignment marks across the wafer or at the extents, as a rotational mismatch is hard to detect by only one tiny alignment mark. By aligning two or more features at different sides of the wafer, the features in between are more likely to also be correctly aligned. Once aligned, the wafer and mask are brought back into contact, and the assembly is exposed. The positioning is maintained by the friction of the contact force, which itself is brought to bear by springs, compressed air, or both.

This last point illustrates another key feature of any optical alignment system, in which it must have a way of rigidly fixing the two sides together, or maintaining the alignment temporarily until another method can be employed to finalize the attachment.

To do so, an aligner and sealing mechanism could be combined in the style of the photolithographic exposure machine, where the bond is created in place directly after the alignment is complete. Examples of this approach might be an aligner with an integrated heater, to induce thermal bonding of the part in place. Alternatively, a temporary connection could be made at the aligner to allow the aligned parts to be transferred to a bonder. In these cases, clamping the two together with a temporary clamp could suffice while the parts were transported to the ultrasonic welder. Clamping is not practical for a production scale or for any device that needs to be used outside of a controlled laboratory environment, as it contributes very greatly to the size of the device, and clamping depends on friction to maintain alignment. Any relaxation of the clamping force or disturbance with sufficient amplitude sufficient to disturb the position of the device would likely misalign the device.

5.2.3 Design Approaches

Finally, there is one other approach that could be employed, though it is a design approach instead of a tooling approach: abandon accurate alignment, and design around what rough alignment is easily achievable. This concept permeates the world of alignment, including the very notion of a "loose fit" for a screw through a part: a hole that is intentionally bigger than it needs to be in recognition of the fact that not all of the different holes are probably going to match between the two parts being joined by the screw. Even a properly constrained part might require oversized holes if there are more attachment points required than degrees to be constrained, as discussed in Whitney [2004]. In the microfluidics case, this could mean having the multilayer joint terminate in a large reservoir, so a tight control of the position is not necessary.

As can be seen from this discussion, alignment is a major issue that will arise as multilayer devices are developed.

5.3 Review of Existing Approaches

To date, most of the focus on multilayer devices has been on the most flexible platform for microfluidics, flexible both in ease of altering processing and in elastic modulus, soft lithography in PDMS. Hot embossing and injection molding have issues related to the heavy tooling both of those processes require, and a separate micro-to-macro alignment scheme for hot embossing.

In their method, described in Anderson [2000], two molds are brought together with a thin layer of pre-polymer in between. Sufficient force is applied to prevent the PDMS from forming flash in the through-hole areas, and the whole stack is cured. After the oven bake, the thin layer is removed from between the two molds and affixed carefully to other thicker layers, preserving the possibility of attaching it to another similar layer to create a larger stack of layers. The innovation of Anderson [2000] was to use PDMS to create the top mold in this sandwich molding process. The PDMS mold is created from a further removed mold, typically fabricated out of photoresist. The use of a PDMS top mold allows optical rough alignment, though they turned to mechanical alignment for the final step. This is likely due to the fact that the features on the PDMS upper mold virtually disappear when in contact with the pre-polymer on the wafer.

Using this method, they were able to create the intricate structures shown in Figure 4-13(a) and Figure 5-7.

Figure 5-7: Three Dimensional Structures Created via Soft Lithography. From Anderson [2000].

The features shown in Figure 4-13(a) are actually not in PDMS, but an ultraviolet-cured urethane that was flowed into the channels and then cured. The PDMS was then dissolved, leaving the structures shown to remain on the device and make a good SEM picture. The features in Figure 5-7 are still within the PDMS block, and this picture has been taken through the top of the block. Though it is hard to see in this top view, the straight channel in the middle is actually circled by the other channels in helical fashion. This example extends the process one step further, taking one two-layer device and combining it layer-to-layer with a three-layer device.

Beyond this method, Ooe [2005] devised a method to create a multilayer device via imprint lithography. By tightly controlling the bonding conditions, a PDMS layer with a thin structures thicker regions can be deposited and then peeled off, leaving only the thin regions. The area where the features were thicker peels off with the top mold, leaving a through-hole in the thin layer. These layers, which are patterned merely by the existence of through-holes, can be laid up one after the other to form a multi-layer device. This method takes advantage of one

of the benefits of PDMS that makes it an attractive option for these prototypes: due to general stickiness and the ability to be activated via oxygen plasma ash to create a secure bond, sealing layers together is very easy.

Alignment has also been addressed in PDMS. The same stickiness that makes PDMS attractive tends to work against fine-tuned alignment. That is, PDMS will stick to another layer of PDMS, creating a temporary seal, so detaching the layers in order to move them around often jostles the alignment. That is, if two pieces of PDMS were being aligned, and the positioning was off, gently pushing it toward proper alignment would do nothing, as the parts would be stuck together. Pushing hard enough to overcome the stiction would cause the parts to jump, likely not landing any closer to alignment than before the push. A potential solution to this problem was first published by Jo [2000], but the reference cited is listed as "G. M. Whitesides, private communication, 1998." In the proposition, methyl alcohol, methanol, is used as a surfactant between the layers, to allow them to slide smoothly. They can then be aligned properly, and the methanol can be baked out in place, gently bringing the layers into contact in the correct location. J. Kim [2005] extended this approach to include a positioning stage and a computer controller to assist with alignment.

Fluidigm, perhaps the only company in the world to market packaged devices created from PDMS, also relies on manual assembly of its multilayer devices, as reported by Frederickson [2003].

.

6   Theoretical Model

In this chapter, a mathematical model will be created to duplicate the proposed device presented in Figure 5-2. Much of this discussion is adapted from White [1999] and Hetsroni [2005].

6.1   Creeping Flow

The flow in microfluidic channels, as mentioned in Section 5.1, is in the laminar regime. In fact, it is so highly laminar that it can be described as a creeping flow. The creeping regime is when the Reynolds number is less than one. As discussed in Section 4.3.1, the cross sectional shape is rarely circular, so the Reynolds number shown in Equation 5-1 is changed slightly to reflect the non-circular profile.

$$\text{Re}_H = \frac{\rho V D_H}{\mu} \qquad\qquad (6\text{-}1)$$

where D, the characteristic dimension that was the diameter in a round pipe, has been slightly altered by the addition of a subscript H. The H stands for hydraulic, and the hydraulic diameter is given as:

$$D_H = 4\frac{A}{\wp} \qquad\qquad (6\text{-}2)$$

where $\wp$ is the perimeter of the channel. When the hydraulic Reynolds number is less than one, the flow is in the creeping regime. This value is assured by the small channel dimensions, and the correspondingly small velocity in the channel. Another implication of the creeping flow regime, which is a subset of the laminar flow regime, is that the flow is not dependent on the roughness of the channel. This has fortuitous implications in that the surface quality reproduced in the device need not be high.

6.2 Momentum Approach

Another express of the Reynolds transport theorem is the linear momentum equation. This relates the change in momentum, itself the product of mass and velocity, to the forces impingent on a given fluid volume. This is an ideal next step in this case, for the velocity is constant, and thus momentum is also conserved along the length. The control volume is the fluid within the channels. The pressures at each end of the control volume act as force exacters at the boundaries. The only other force exerted on the fluid volume is the shear stress at the boundary around the edge of the pipe. These can be written as:

$$\Delta p \, A - \overline{\tau}_w \, \wp \, L = \dot{m} \, \Delta V = 0 \qquad (6\text{-}3)$$

where Δ is the difference operator, p is the pressure at each point in the fluid, τ_w is the average shear stress at the wall of the channel and $\dot{m}$ is the mass flow rate. Finding τ_w is the key to solving this problem, and it is done using dimensional analysis on the various parameters that could affect the wall shear, namely fluid density, fluid velocity, channel size, and fluid viscosity. Dimensional analysis [White 1999] finds that

$$\overline{\tau}_w = \frac{\rho V^2 f}{8} \qquad (6\text{-}4)$$

where f is the correction factor, called the Darcy friction factor. The Darcy friction factor is determined empirically, and for non-circular cross-section ducts, is a function of the geometry of the channel divided by the Reynolds number for the flow.

$$f = fcn\left(geometry, \mathrm{Re}_H\right) = \frac{C}{\mathrm{Re}_H} \qquad (6\text{-}5)$$

where C is the experimental constant, and for rectangular channels, it is a function of the aspect ratio of the channel.

Combining Equations 6-2, 6-3, and 6-4,

$$\Delta p = \rho \, f \, \frac{L}{D_H} \frac{V^2}{2}. \qquad (6\text{-}6)$$

This is inline with Foster [1970]. By substituting f with Equation 6-5,

$$\Delta p = \rho \, \frac{C}{\mathrm{Re}_H} \frac{L}{D_H} \frac{V^2}{2} \,. \tag{6-7}$$

By substituting the Reynolds number with its components:

$$\Delta p = \mu \, C \, \frac{L}{D_H^2} \frac{V}{2} \,. \tag{6-8}$$

Finally,

$$\Delta p = \mu \, \frac{C}{32} \left(\frac{\wp}{A} \right)^2 L \, V \,. \tag{6-9}$$

6.3   Minor Head Losses

The treatment of the multilayer joint is as a minor pressure head loss in the system. Mathematically, this introduces another pressure drop that scales by the density of the fluid and the square of the mean velocity in the channel. Each particular valve, gate, or other fitting has its own constant, but most existing data are for macro-flow in the turbulent regime. The value of this constant, K, is usually determined empirically, and is defined as

$$K = \frac{h_m}{V^2 \big/ 2g} = \frac{\Delta p}{\frac{1}{2}\rho V^2} \,, \tag{6-10}$$

where h term is the minor head loss in the fitting. Head is the energy in the fluid expressed as an equivalent height of a fluid column with equal potential energy. It is this K value that we seek to determine for a particular amount of area in the microfluidic multilayer joint.

The only reference that touched upon situations similar to those in the model was Idelchik [1994]. There are two cases presented. In the first, there is a sudden expansion in one direction of a channel, as shown in Figure 6-1.

This situation could be applied to this model for situations of great overlap area, in which case a K value of 0.24 is suggested. However, it is unclear if this applies to the laminar case, and the opposite scenario of sudden contraction in one direction is not well addressed.
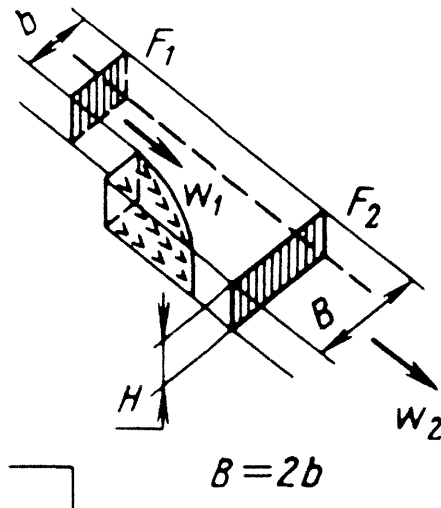
100

Figure 6-1: Sudden expansion in one dimension of a channel [Idelchik 1994].

The other situation in Idelchik [1994] that could potentially be applicable is a "Z" fitting, of two 90° elbows used in series.
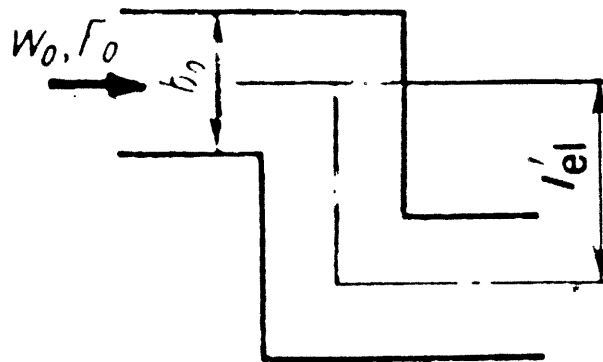

Figure 6-2: "Z" fitting in a fluid channel [Idelchik 1994].

For the no-mismatch case that we have used, the data suggest a K of 2.89, but this is clearly intended for the turbulent case. The data is also focused on the length of the intervening section, which could be helpful in the extended via-plug case, but is less so in this research. What is interesting about the Idelchik description of the "Z" fitting is that an acknowledgement is made in the text that it is not merely two elbows in series, but rather that the proximity of the two fittings has an additional effect.

6.4 Experimental Design

In order to find the value of the loss coefficient K, a series of devices with different misalignments will be tested to determine their fluid flow rate to pressure drop curve, with a

minimum of four steady-state data points for each device. The total pressure drop in the device is the sum of the pressure drop in the channel plus the pressure drops at the two multilayer joints:

$$\Delta p_{total} = \Delta p_{channel} + \Delta p_A + \Delta p_B + H \tag{6-11}$$

where H is inherent head in the system, independent of fluid flow rate. Using Equations 6-9 and 6-10, this equation can be rewritten as

$$\Delta p_{total} = \frac{1}{32} \mu C \left(\frac{\wp}{A}\right)^2 L V + \frac{1}{2}\left(K_A + K_B\right)\rho V^2 + H. \tag{6-12}$$

The velocity can be calculated in the channel based on the volumetric flow rate divided by the cross-sectional area of the device. Using the data points for each device, a quadratic equation can be fit statistically to the data to approximate the coefficients for Equation 6-12, which is itself a quadratic equation in fluid velocity. Using the second-order coefficient, the loss coefficient K can be derived.

6.5 In-plane Mismatch to Overlap Area Relationship

In order to test the hypothesis that the loss coefficient is related to the area of the multilayer joint, it is first necessary to develop a better understanding of how the in-plane mismatch of the two layers affects the cross-sectional overlap area between the layers, the area that constitutes the multilayer joint through which the fluid flows.

6.5.1 No Mismatch

In this simplest of cases, the misalignment is zero, and the centers of the semicircular tips of the top and bottom channel are in the same location. This is shown in Figure 6-3.

102
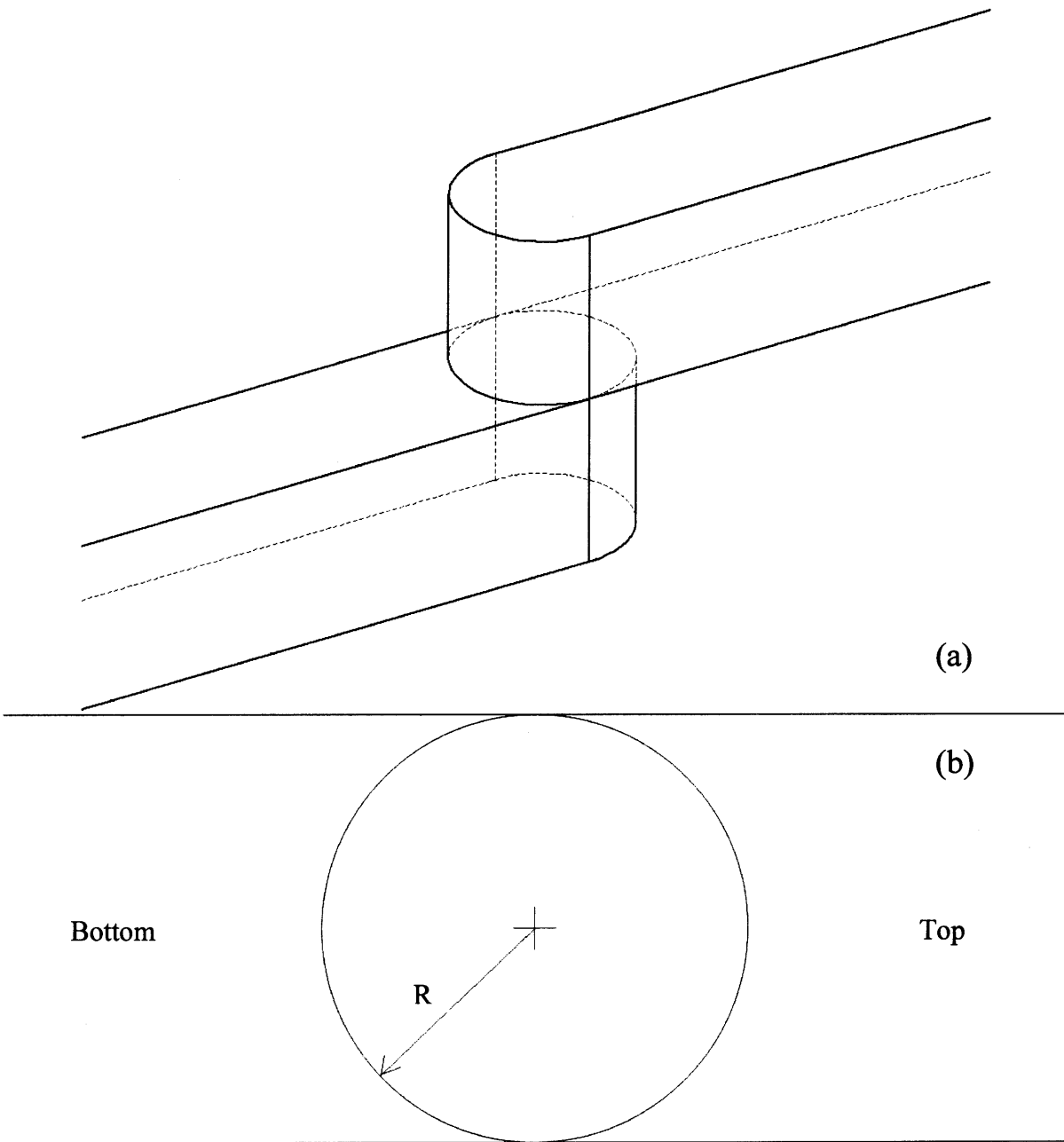
Figure 6-3: Multilayer Joint, with no misalignment. (a) perspective view, (b) diagram of top view.

Here,

$$u = 0$$
$$v = 0 \qquad , \qquad \textbf{(6-13)}$$
$$A_{overlap} = \pi R^2$$

where R is the radius of the circle, and it is also half of the width of the channels.

6.5.2 Horizontal Additive Mismatch

In this case, there is still no vertical mismatch, and the mismatch is within the plane that joins the two parts, along the axis of the channel is in the positive direction. This direction of mismatch is referred to as horizontal, and is represented by u.

Figure 6-4: Positive horizontal mismatch, zero vertical mismatch. (a) perspective view, (b) diagram of top view.

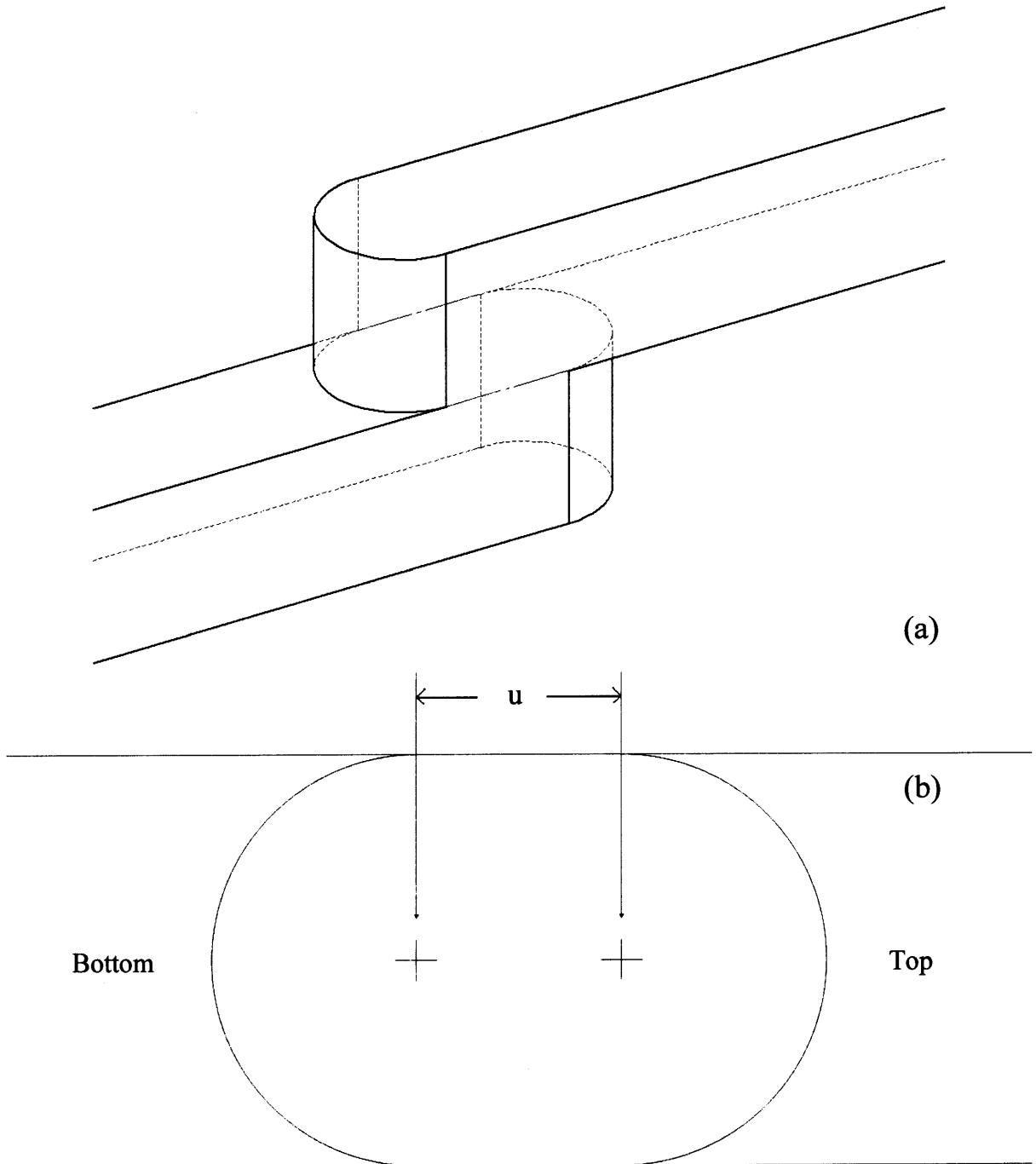The rectangular segment between the semi circles adds another term:

$$u > 0$$
$$v = 0$$
$$A_{overlap} = \pi R^2 + 2Ru$$

(6-14)

6.5.3 Horizontal Subtractive Mismatch

This gets slightly more complicated, as the overlap area is now a bounded by two circular arcs that are not mutually tangent.

The area is calculated by calculating the area in one-half of the shape and doubling it. Each half is the area in the circular segment created by the two radii from the points of intersection that is not within the chord defined by the intersection points. The distance from the chord to the centers is half of the absolute value of u, and that the half-length of the chord can be related to u and the radius via the Pythagorean theorem:

$$u < 0$$
$$v = 0$$
$$A_{overlap} = 2A_{crescent}$$
$$A_{overlap} = 2\left(A_{segment} - A_{triangle} \right)$$
$$A_{overlap} = 2\left[\left(\frac{2\theta}{2\pi} \pi R^2 \right) - 2\left(\frac{1}{2} bh \right) \right]$$
$$b = \frac{|u|}{2}$$
$$h = \sqrt{R^2 - \frac{u^2}{4}}$$
$$\theta = \cos^{-1}\left(\frac{|u|}{2R} \right)$$
$$A_{overlap} = 2\cos^{-1}\left(\frac{|u|}{2R} \right) R^2 - |u|\sqrt{R^2 - \frac{u^2}{4}}$$

(6-15)

(a)

(b)

$A_{segment}$

Bottom

Top

$A_{crescent}$ $A_{triangle}$

u
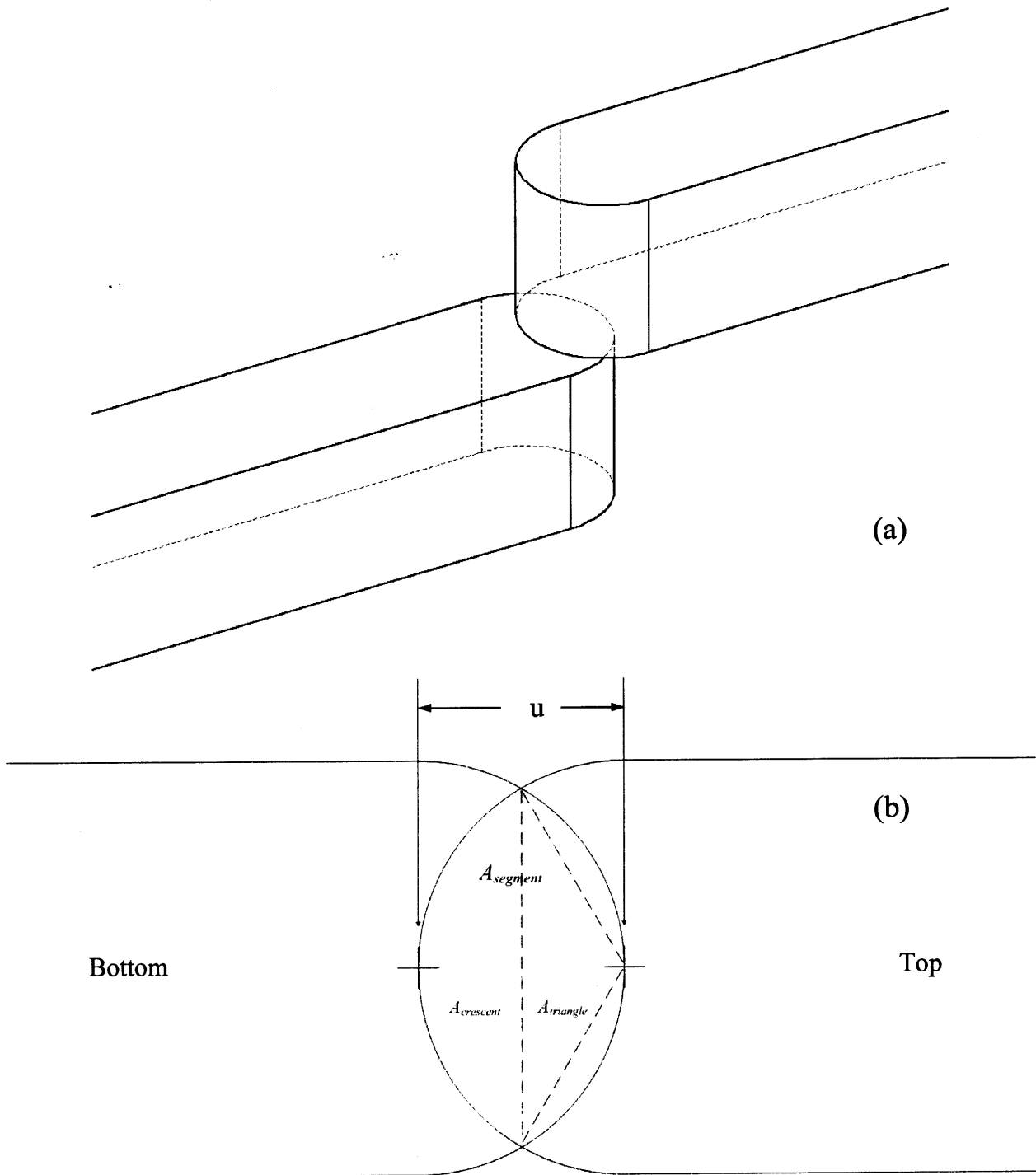
Figure 6-5: Negative horizontal mismatch, zero vertical mismatch. (a) perspective view, (b) diagram of top view.

6.5.4 Vertical Mismatch

Now that horizontal mismatch in the absence of vertical mismatch has been dealt with, the opposite situation is analyzed: vertical mismatch in the absence of horizontal mismatch. Vertical mismatch is taken here to mean in-plane mismatch perpendicular to the axis of the channel, and it is represented by v. The situation is as shown in Figure 6-6.
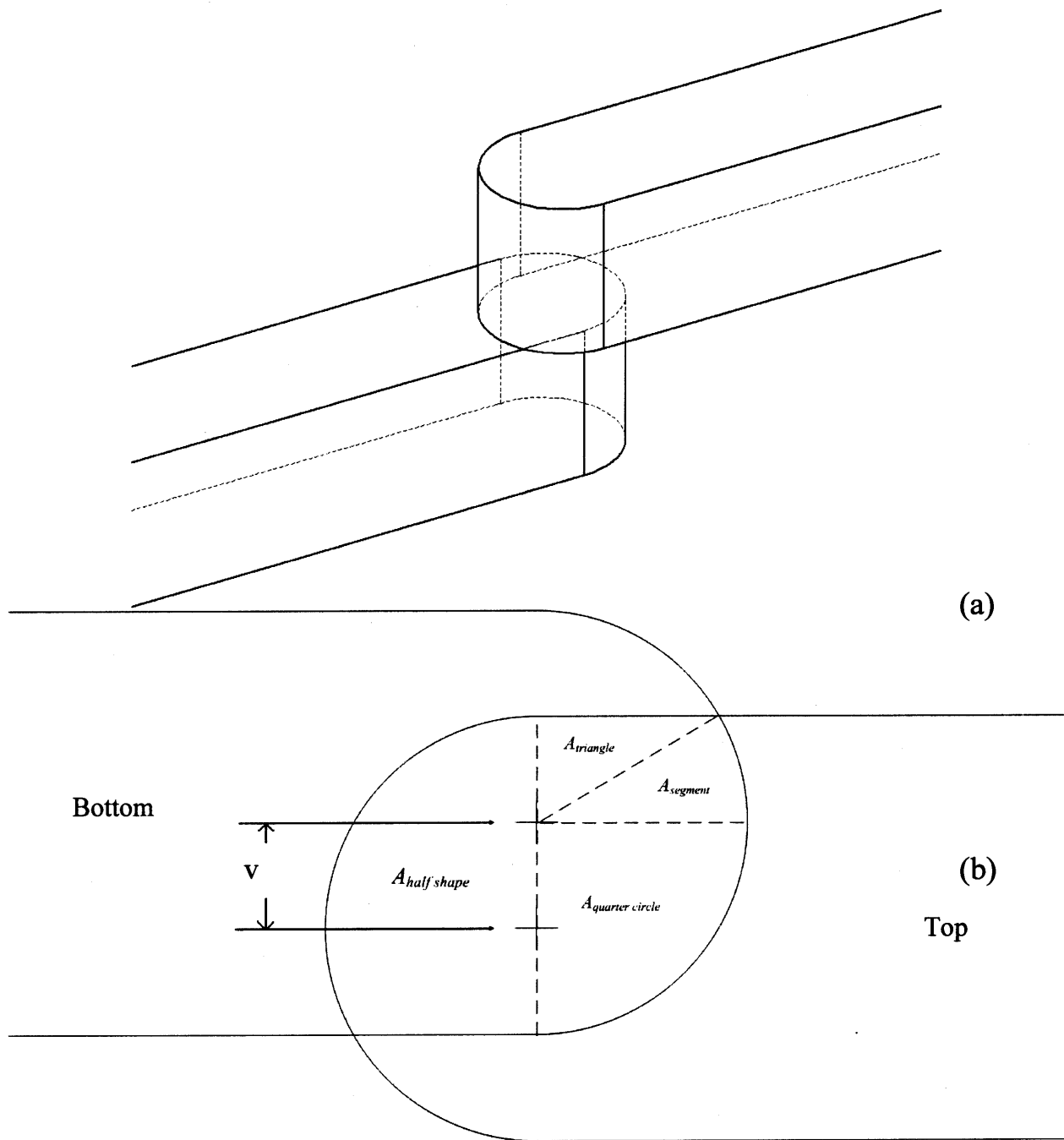
Figure 6-6: Negative vertical mismatch, zero horizontal mismatch. **(a) perspective view, (b) diagram of top view.**

This also creates an abnormal shape of overlap area, but as before, trigonometry is our guide. This approach also takes the approach of dividing the area up into first halves and then smaller regions of a circle:

$$u = 0$$

$$v \neq 0$$

$$A_{overlap} = 2A_{half\_shape}$$

$$A_{overlap} = 2\left(A_{quarter\_circle} + A_{segment} + A_{triangle} \right)$$

$$A_{overlap} = 2\left[\frac{\pi R^2}{4} + \frac{\theta}{2\pi}\pi R^2 + \frac{1}{2}bh \right]$$

$$h = R - |v|$$

$$b = \sqrt{R^2 - \left(R - |v|\right)^2} = \sqrt{R^2 - R^2 + 2R|v| - v^2} = \sqrt{2R|v| - v^2}$$

$$\theta = \sin^{-1}\left(\frac{R - |v|}{R} \right)$$

$$A_{overlap} = \frac{\pi R^2}{2} + \sin^{-1}\left(1 - \frac{|v|}{R} \right)R^2 + \left(R - |v|\right)\sqrt{2R|v| - v^2} \qquad . \qquad (6\text{-}16)$$

6.5.5   Dual Mismatch, Non-arc Intersecting

Finally, we arrive at one part of the general case, in which there is some vertical mismatch, and the horizontal mismatch is either positive or small enough in negative so that the corner of the tip, where the straight edge is tangentially connected to the semicircle, is still part of the overlap area. Beyond that point, the situation is similar to that in Section 6.5.3, where the overlap area is a symmetric area bounded by the semi-circular line segments. This will be discussed further in the next section. A diagram of this dual mismatch, non-arc intersecting case is shown in Figure 6-7.
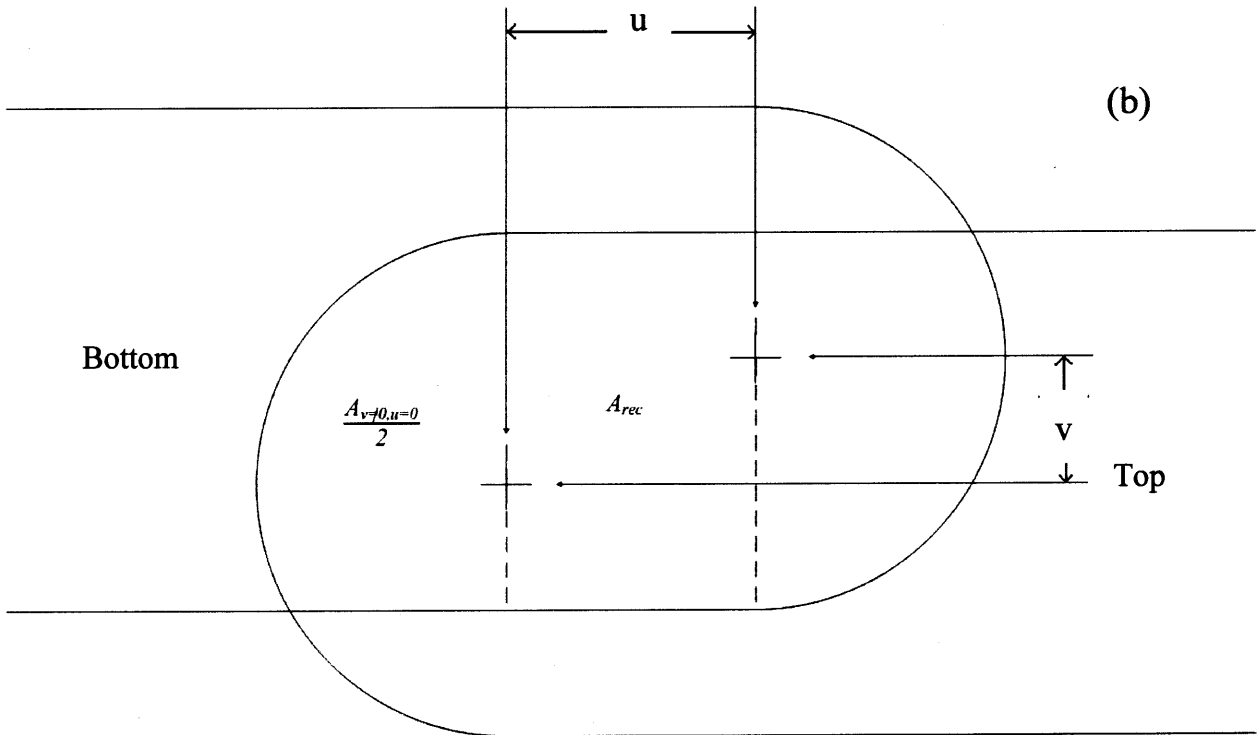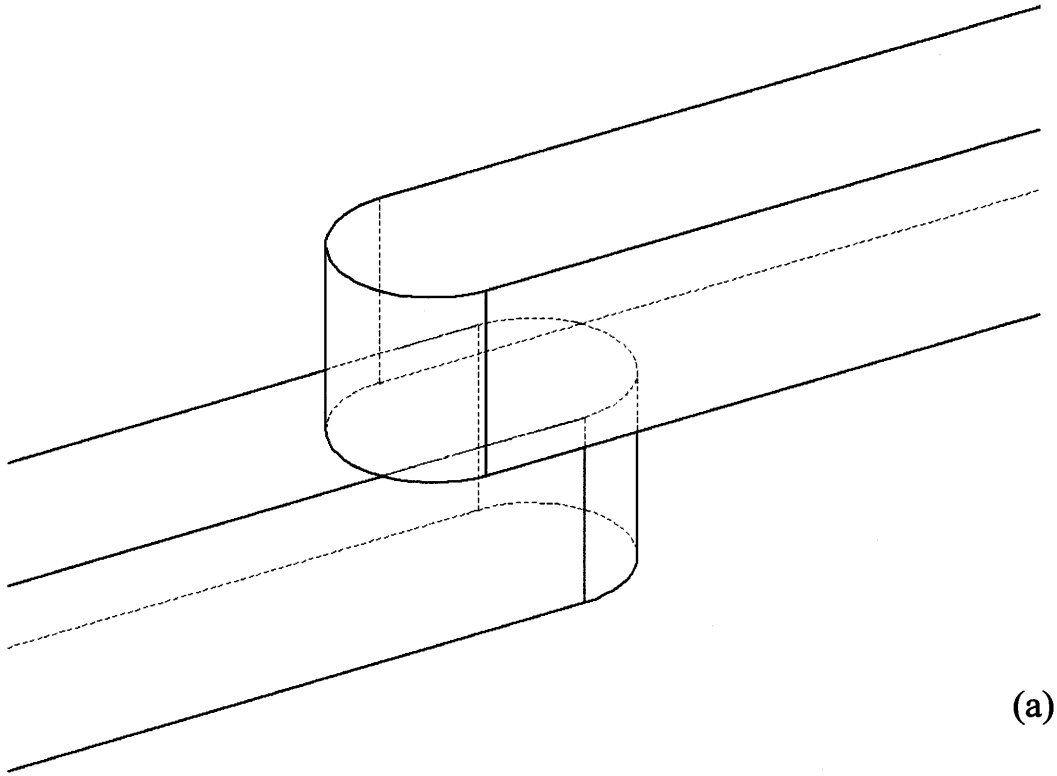
Figure 6-7: Positive vertical mismatch, positive horizontal mismatch. (a) perspective view, (b) diagram of top view.

The extension from the case in the preceding section to this case is similar to the extension of the simplest case of no mismatch to the positive overlap area. That is, the results from the previous section merely have an additional term added to them to account for the rectangular overlap area:

$$u \neq 0$$
$$v \neq 0$$
$$A_{overlap} = A_{v \neq 0, u=0} + A_{rec} \qquad . \qquad \text{(6-17)}$$
$$A_{overlap} = \frac{\pi R^2}{2} + \sin^{-1}\left(1 - \frac{|v|}{R}\right) R^2 + \left(R - |v|\right)\sqrt{2R|v| - v^2} + u\left(2R - |v|\right)$$

This case is only valid up to the point when the corners of the tips are part of the perimeter of the overlap area. This is true when

$$R^2 - u^2 \geq \left(R - |v|\right)^2 . \qquad \text{6-18)}$$

6.5.6 Dual Mismatch, Arc Intersecting

This case is merely a transposition of the case covered in Section 6.5.3, where there is an overlap area that is sufficiently small so that only the two circular segments form the boundaries of the region of overlap area. In this case, shown in Figure 6-8, the overlap area can be expressed as:

(a)

(b)
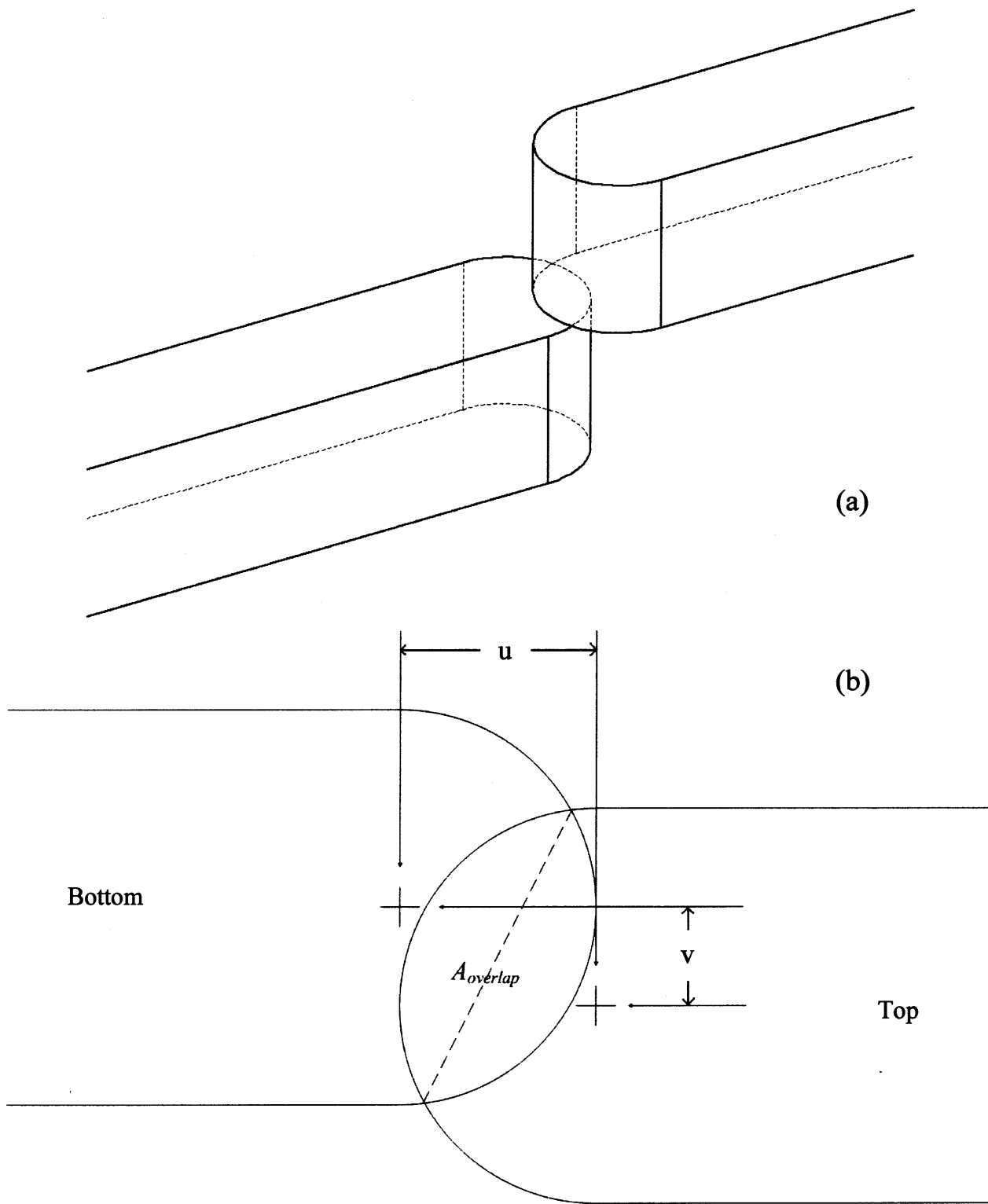
Figure 6-8: Negative horizontal mismatch, negative vertical mismatch. (a) perspective view, (b) diagram of top view.

$$u < 0$$

$$v \neq 0$$

$$R^2 - u^2 < \left(R - |v|\right)^2 \qquad \qquad . \qquad \qquad \text{(6-19)}$$

$$A_{overlap} = A_{u<0,v=0}\left(\sqrt{u^2 + v^2} \rightarrow u\right)$$

$$A_{overlap} = 2\cos^{-1}\left(\frac{\sqrt{u^2 + v^2}}{2R}\right)R^2 - \sqrt{u^2 + v^2}\sqrt{R^2 - \frac{u^2 + v^2}{4}}$$

6.5.7   Graphical Representation of Area as a Function of Mismatch

Taken together, Sections 6.5.5 and 6.5.6 provide the general case in the two regimes, one with the arcs intersecting, and one without. These are shown in Figure 6-9. Unsurprisingly, the graph is zero beyond the following boundaries:

$$|v| > 2R, \quad u > 0$$
$$\sqrt{u^2 + v^2} > 2R, \quad u < 0 \qquad \qquad \text{(6-20)}$$

Figure 6-9: Overlap area in a Multilayer in a Joint as a function of linear mismatch.

113

7 Experimental Model

Given the theoretical basis discussed in Chapter 6, the charge of the experiment was to produce the structure shown in Figure 5-2. As this was a preliminary study, the choices made in creating the device were guided in large part by ease of implementation. The reason for this was to allow the focus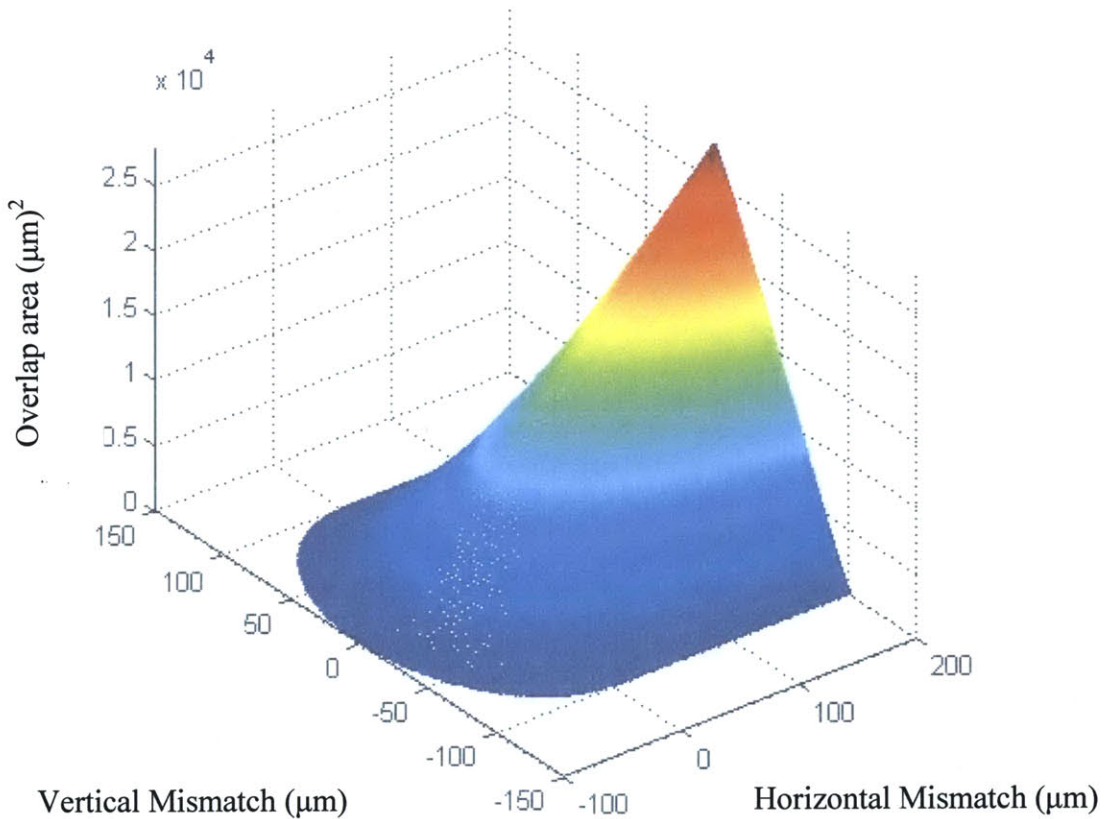 to be more on the fluid model, and less on the fabrication methods. The long-term intent would be along the lines of the test device model, where the same structure is fabricated via different fabrication technologies, and the model is verified across platforms. In addition, the focus of this research was not on minimizing variation, but rather in gaining a better understanding of the effect of the variation on the performance of the device. Thus, variation was systematically introduced into the design, as will be described in Section 7.1.2, so the additional reduction in accuracy introduced by a less-than-precise method was not a problem. This is true as long as the variations could be properly quantified.

7.1 Preliminary Decisions

Figure 7-1 shows a perspective view of the microfluidic channel. In order to build a device containing this channel, certain further choices were necessary.

7.1.1 Layout and Dimensions

One design consideration was how to get the fluid to and from the microfluidic channel, which as discussed in Section 4.4.2 is always a key decision. In order to so, reservoirs were incorporated into the design at the ends. These were large circular areas with a filleted joint to the channels, as shown in Figure 7-2.

114
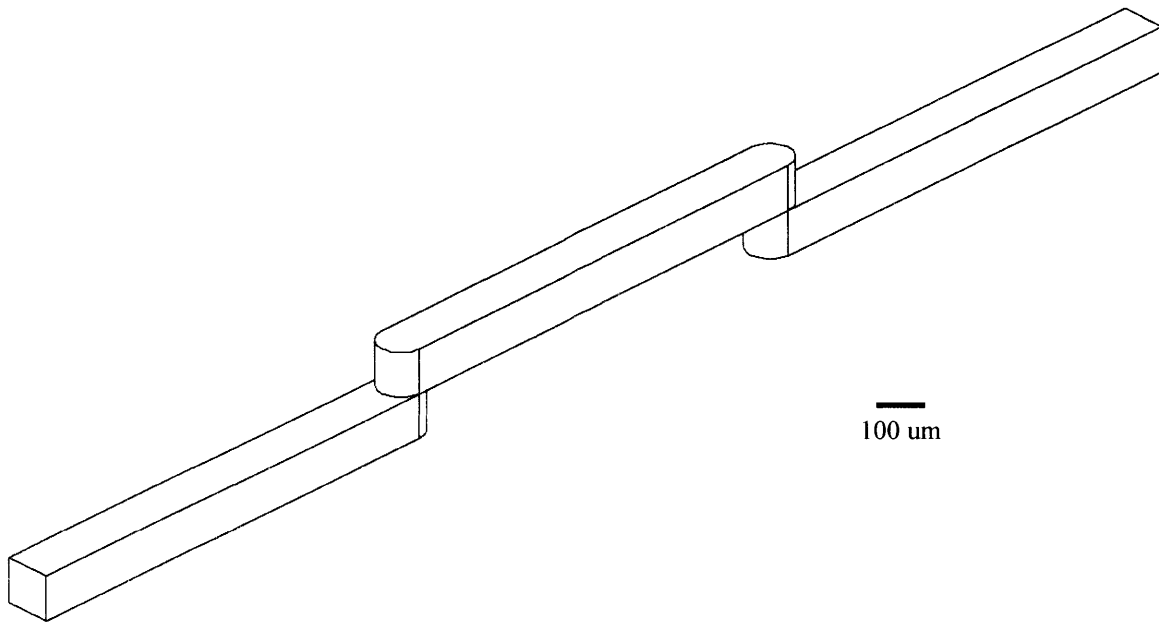
Figure 7-1: Basic Channel Model Theory is built around.

The purpose of the reservoirs was to serve as an over-sized target for the macro-tube that would ultimately be used to connect between the microfluidic device and the fluid supply and outlet. There would always be some misalignment in this step, given the limitations of the macro-positioning of the ports, and in order to minimize the amount of variation passed on to the pressure drop as a result, a large reservoir, 2 mm in diameter and the same 100 μm in height, was employed. The final fluid channel, including the beginning of the tubes leading off of the reservoirs, is shown in Figure 7-3.
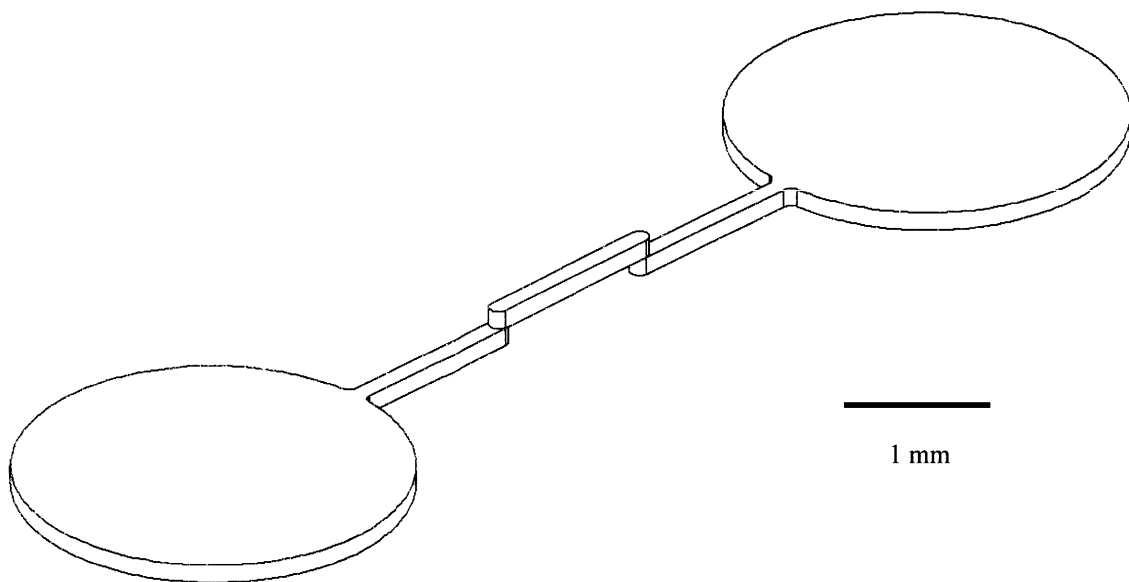
Figure 7-2: Microfluidic Design, showing reservoirs.
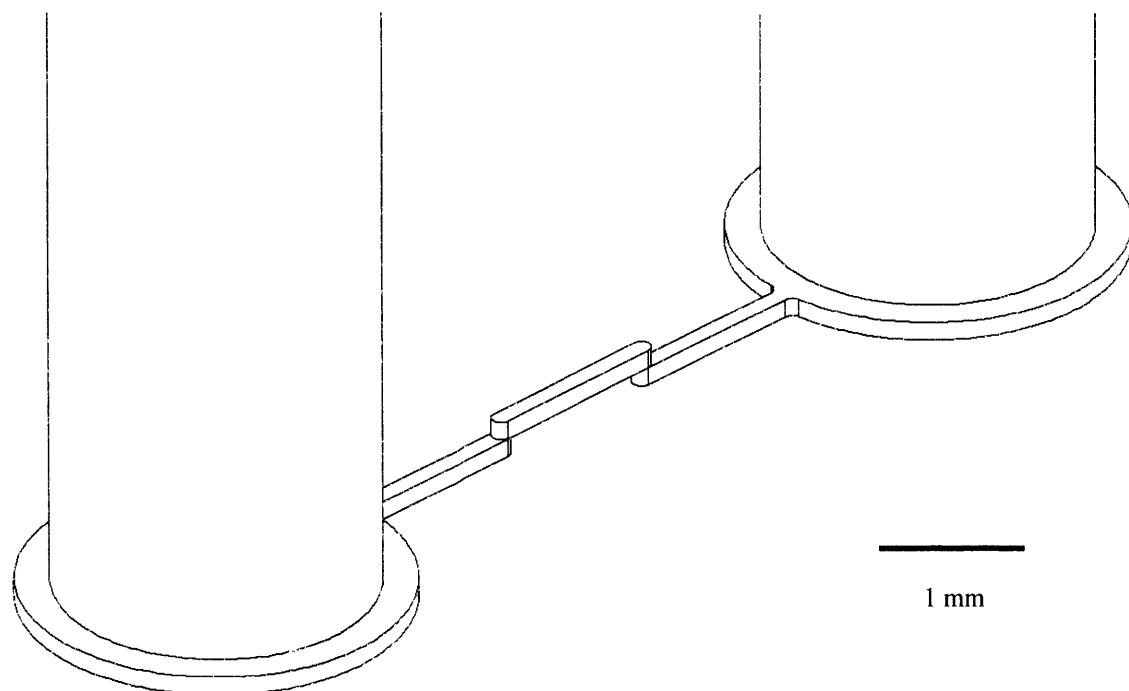
Figure 7-3: Microfluidic Design, showing inlet and outlet.

116

The next consideration was the dimensional selection for the various parts of the device design. Equation 6-11 shows that the majority of the pressure drop in the device is due to the channels themselves, and less to the microfluidic multilayer joint. Thus it was desirable to amplify the effect of joint, and to that end the aspect ratio for the channels that provides the smallest pressure drop for a given cross-sectional area is 1, or a square. Existing capabilities drove the selection of the particular dimensions. As will be discussed in the next section, a fabrication method was selected to produce molds from photoresist, specifically SU-8. The SU-8 series consists of a number of products with successively higher viscosity, for targeting different thickness. In order to coat a substrate with a layer of photoresist, an appropriate amount on the order of 5 mL of photoresist is deposited on the substrate, and then the substrate is rotated rapidly in a spin-coater to distribute the photoresist across the surface and then eject enough to come to the target thickness. The manufacturers of photoresist publish guidelines that relate the spin speed to the final thickness of their products. An example of a Spin Chart is shown in Figure 7-4.

Figure 7-4: Spin Chart for SU-8 2000 Series, from Appendix B.

117

Figure 7-4 shows that the thickness versus spin speed curves are steeper at lower revolutions-per-minute (rpm), and flatter at higher speeds. Since the thickness is less sensitive to variations in the speed out at 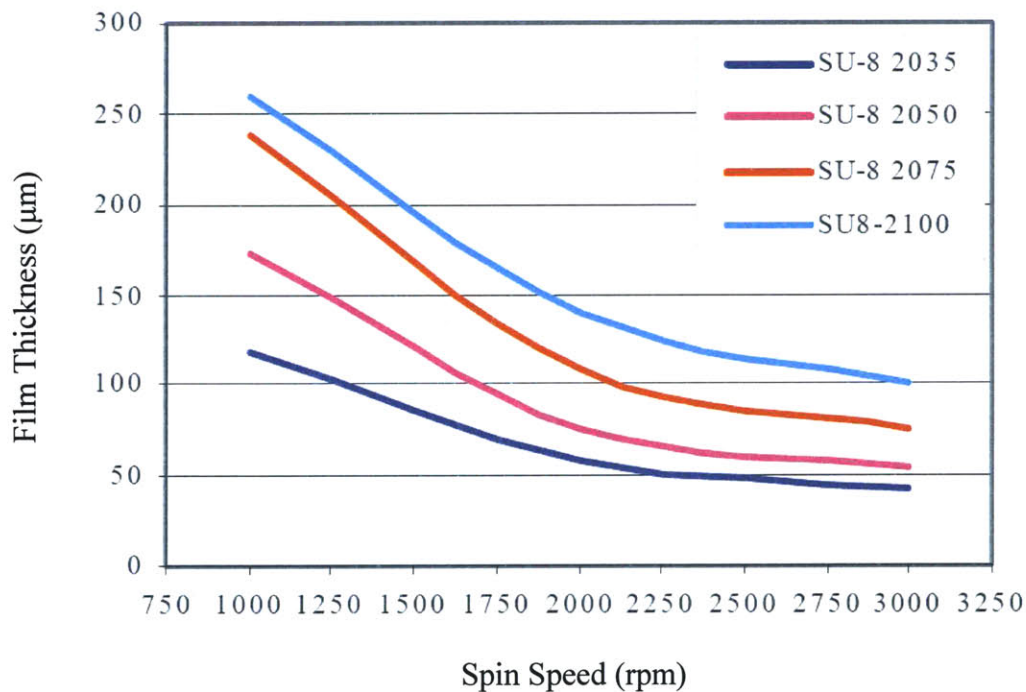that end of the curve, it was decided to choose a value at the end of the curve. This reduced the selection of depths of the channel to a quantized list: 35 μm, 50 μm, 75 μm, and 100 μm. Of those, 100 μm was chosen to assist the alignment methods in creating continuity of the channels. Larger features are easier to align than much smaller features.

Therefore, given the selection of mask processing and knowledge about the most desirable aspect ratio, the main fluid channels were chosen to be 100 μm in depth and 100 μm in width. The lengths of the channels were chosen to be 10 times the width and depth in an attempt to further minimize entrance affects [Idelchik 1994]. Thus the channel segments were chosen to be 1 mm long each, for a total channel length of 3 mm. The tube bringing fluid to the channel is 1.6 mm in outer diameter, so in order to comfortably oversize the reservoirs, they were made to be 2 mm in diameter.

7.1.2 Design of Mismatches

The other major design consideration was the method of generating sufficient data to evaluate the effect of misalignment on pressure drop. It was necessary to introduce different amounts of misalignment into the device. A two-joint device was selected in an attempt to correct for some of the horizontal mismatch in the molding process used for this study. Thus in order to overcome this corrective mechanism and effectively vary the misalignment, it was necessary to create different molds. To facilitate the selection, a design grid was created, which, in addition to a number-line visualization of the mismatches u divided by the channel width that would be produced, allowed a good density of final devices. A secondary goal was to create as wide an experimental range as possible with the fewest masks, in order to reduce the tooling necessary to create the series. Vertical mismatch v has a much tighter range of allowable values before there will be no overlap area, since vertical mismatch beyond an absolute value of one width of the channels will create no connection between the two layers. Therefore, the experiment-introduced misalignment was determined to be sufficient in creating enough data points, and the mold-introduced misalignment was the only for horizontal mismatch u.
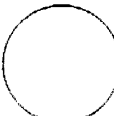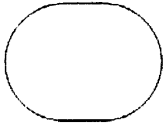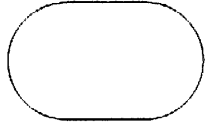
The treatment of overlap area described above is one in which two channels are visualized, each with the same width and a semi-circular tip. The neutral condition is one in

118

which the centers of the semi-circles overlap, and a perfect circle is created as the multilayer joint, as shown in Figure 6-3. Misalignment introduces a horizontal mismatch u and a vertical mismatch v between the two centers, as shown in Figure 6-8. The horizontal mismatch is considered positive in the direction of increased overlap area and negative in the direction of reduced overlap area. The vertical mismatch is symmetric in its effects, and thus is arbitrarily positive or negative. Also, the convention has been to view this schematic as the first of the two multilayer joints, with the inlet to the left and the second joint and subsequently the outlet to the right. In this orientation, the bottom layer is the one on the left that connects to the inlet, and the top layer is the one on the right that joins the two multilayer joints.

Since merely changing the relative positions is not an option, given the two-sided nature of the design, the molds must be lengthened or shortened to vary the mismatch. To create greater overlap area, either the top or bottom could be lengthened, and similarly, to create lesser overlap area, either could be shortened. However, it was decided to uniformly increase the overlap area by lengthening the top, as illustrated in Figure 6-4, and decrease the overlap area by shortening the bottom, as illustrated in Figure 6-5.

From there, the design matrix was created in order to facilitate the choice of which molds to fabricate. Each top mold can be combined with each bottom mold in building different devices, so there is a full matrix of combinations possible. The design matrix lists the possibilities that are created from a given selection of mold sizes. The length units and overlap areas are normalized by the width of the channels. Thus, a mismatch of "+1" will be taken to mean that the centers of the two semicircles have a distance of one width between them and that it is an increased overlap area, as indicated by the positive sign. The width of the channel is also t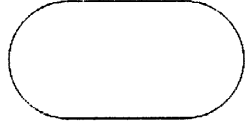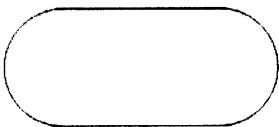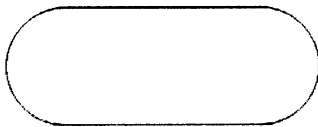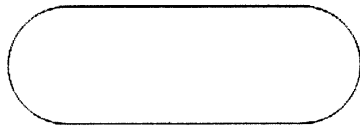he same as the diameter of the semi-circles, so these two terms are used interchangeably. Given the decision to only increase the tops and only decrease the bottoms, the values for the top molds will be either zero (neutral) or positive, and the values for the bottom molds will either be zero (neutral) or negative. The combined effect of the top and bottom is also expressed in this manner, and it is the sum of the two values from the top and bottom.

To generate nine different combinations using three tops and three bottoms, the choices were as displayed in the design matrix in Figure 7-5. The design choices taken to arrive at these sizes appears in Appendix C.

	-2/3	-1/3	Neu
Neu	-2/3	-1/3	0
+1	+1/3	+2/3	+1
+2	+1 1/3	+1 2/3	+2

$$\longrightarrow \quad \times \quad \times \quad \ast \quad \times \quad \times \quad \ast \quad \times \quad \times \quad \ast \longrightarrow \frac{u}{2R}$$

$$-1 \qquad 0 \qquad +1 \qquad +2$$
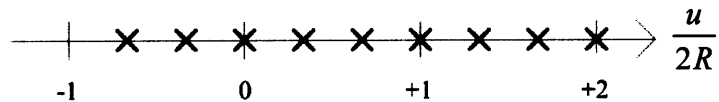
Figure 7-5: Design Matrix and Number Line, Final Selection.

These were the sizes of masks printed in order for the corresponding molds to be created.

The final device configuration that was added to the list was a control device, one with a simple straight channel in the same dimensions as the other channels – depth, width, length, and reservoirs – but with only a single layer and thus no multilayer joints. This was created in order to assess the affects of specifically the joints as opposed to the general device affects, be they in the channel or elsewhere, like inlets and outlets or elsewhere in the complete fluid system.

Given the selection of these seven layers – three tops, three bottoms, and one control – the ten devices were then advanced toward creation.

7.1.3 Choice of Working Materials

In order to build the devices, a fabrication method had to be selected from those described in Chapter 3. The guiding principle was simplicity.

For that reason, the natural choice of material was PDMS. PDMS was selected for all of the reasons given in Section 3.2.1, but primarily because it is very easy to prototype with. And as described more specifically in Section 5.3, it is currently one of the few technologies where multilayer technology is possible without inordinately complex tooling. In addition to

120

addressing alignment and bonding, this also simplified the inlets and outlets, as they could be the simple compression fits described in Section 3.3.2.

Mold fabrication method selection was similarly as straightforward: a photoresist mold provided the quickest and easiest solution. No etching of the silicon wafer nor sputtering and electroplating was necessary. Negative resists provided a taller profile, whereas positive resists are limited to 30-50 μm in a single layer. SU-8 is a common negative photoresist, and as shown in Figure 7-4, can be coated at a thickness of 100 μm. There are two common classes of SU-8; the original, and the 2000 series. The 2000 series has a faster processing time, requiring significantly less dehydration baking, but has a tendency to incorporate more bubbles as a result. However, since the devices being designed required only a tiny percentage of the photoresist to remain when they were used as molds, this tendency was acceptable. The mask was positioned in such a way on each mold as to avoid the deformations.

The remaining issue for using photoresists was assessing their actual as-spun thickness. And as stated in the preamble to this chapter, the focus was not on tightly-toleranced devices as much as quantifying the effects of one particular variation. Since the height of the photoresist layer could be measured optically to one micron in variation, the fluctuations were acceptable.

7.2 Mold Creation

The process used to create photoresist masks was straightforward and standard for photoresist processing. The guidelines for the SU-8 processing appear in Appendix B.

Silicon wafers 100mm in diameter were used in creating the molds. As all of the processing that followed happened above the surface of the wafer, it was possible to use low-quality or recycled wafers, as long as they had been sufficiently cleaned as to not interfere with the adhesion of the photoresist.

The photoresist processing followed the guidelines provided by the manufacturer, Microchem. After a dehydration bake, the wafer was inserted into the spin-coater, shown in Figure 7-6. The picture is yellow as ultraviolet light is filtered out in photolithography room to prevent premature exposure of photoresists.

121
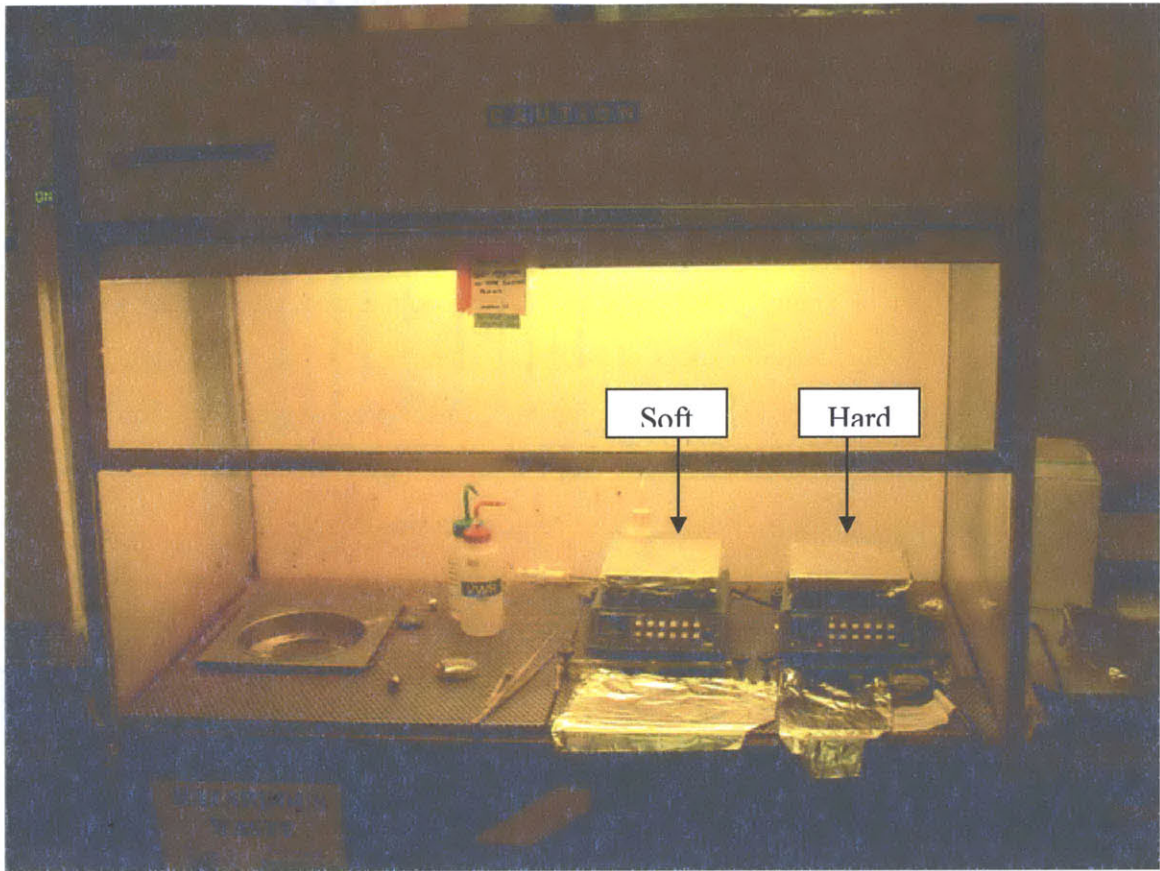
Figure 7-6: Spin coater and hot plates for soft/hard bakes.

After a nitrogen dust, a final cleaning was performed while spinning at approximately 1000 rpm, with acetone to clean and then isopropanol to displace the acetone, followed by a spin-evaporate. This procedure left the wafer dry and clean. Next, an appropriate amount of SU-8 2100 was applied to the center of the wafer. Then, the spin-coater is activated. The photoresist is spread across the wafer at 500 rpm for 10 seconds and then ramped up to 3000 rpm for 30 seconds for the final spin to achieve the desired thickness.

The coated wafer is moved to a hotplate for the soft bake, prior to exposure, where it is baked at 65° C for 5 minutes and then 20 minutes at 95° C.

The next step is the photolithography itself. This required the creation of the masks for the photolithography. As described in Chapter 3, the easiest method of creating a mask is to use a high-precision printer on a plastic film transparency. Given that the dimensions were well above the submicron regime in this design, this was an acceptable method. This facilitated the usage of contact lithography. In contact lithography, the mask is placed in direct contact with the photoresist during the exposure. The one lithographic issue inherent in SU-8s is a tendency to

scatter the lower wavelengths of light present in the typical mercury lamps in use. Thus the features can appear mushroomed, with the top of the feature wider due to the scattering at the top of the photoresist under the mask edges. This obstacle is easily overcome by filtering out the shorter wavelength light during the exposure. The photolithographic exposure machine is shown in Figure 7-7. The microscope viewer can be used in conjunction with the knobs shown in the figure to perform alignment between layers, or the exposure can just be allowed to occur without precise alignment, as in a single-layer process. The 200W mercury lamp (wavelengths of 365-405 nm) slides forward during the exposure to cover the wafer. Timing is controlled by the buttons shown in the figure.

The mask was placed atop the photoresist-coated wafer, with the emulsion-side toward the wafer, to further reduce the possibility of diffraction affecting the features. The two were inserted into the exposure machine, and the low-wavelength filter was installed. Then the wafer was exposed for 120 seconds; this exposure length was also based on the photoresist manufacturer recommendation. Following exposure, the mask was removed, and the wafer was hard baked, for one minute at 65° C and then ten minutes at 95° C, to bake out the last of the solvent. Then the wafer was returned to the spin-coater, where it was spin-developed. Polymono acetate (PMA) was used to remove the unexposed photoresist by dissolving it off the wafer. This was done until the wafer appeared clean of unexposed resist. Then isopropanol was again used to displace the PMA and rinse the wafer. The isopropanol was evaporated off of the wafer will spinning at approximately 1000 rpm.

At that point, the wafer was fully transformed into a microfluidic device mold.

A necessary caution with the photoresist was that it not be baked or exposed for too long. Both of those processes tended to cause the photoresist to contract, removing further solvent by over-baking, and promoting greater cross-linking of the photoresist by over-exposing. The slight contraction due to shrinking would introduce tensile stresses into the photoresist layer, which, particularly at the thick 100-μm level, could lead to greater tendency for the photoresist to peel off the wafer under normal molding operations. This meant a reduced lifetime of the molds.
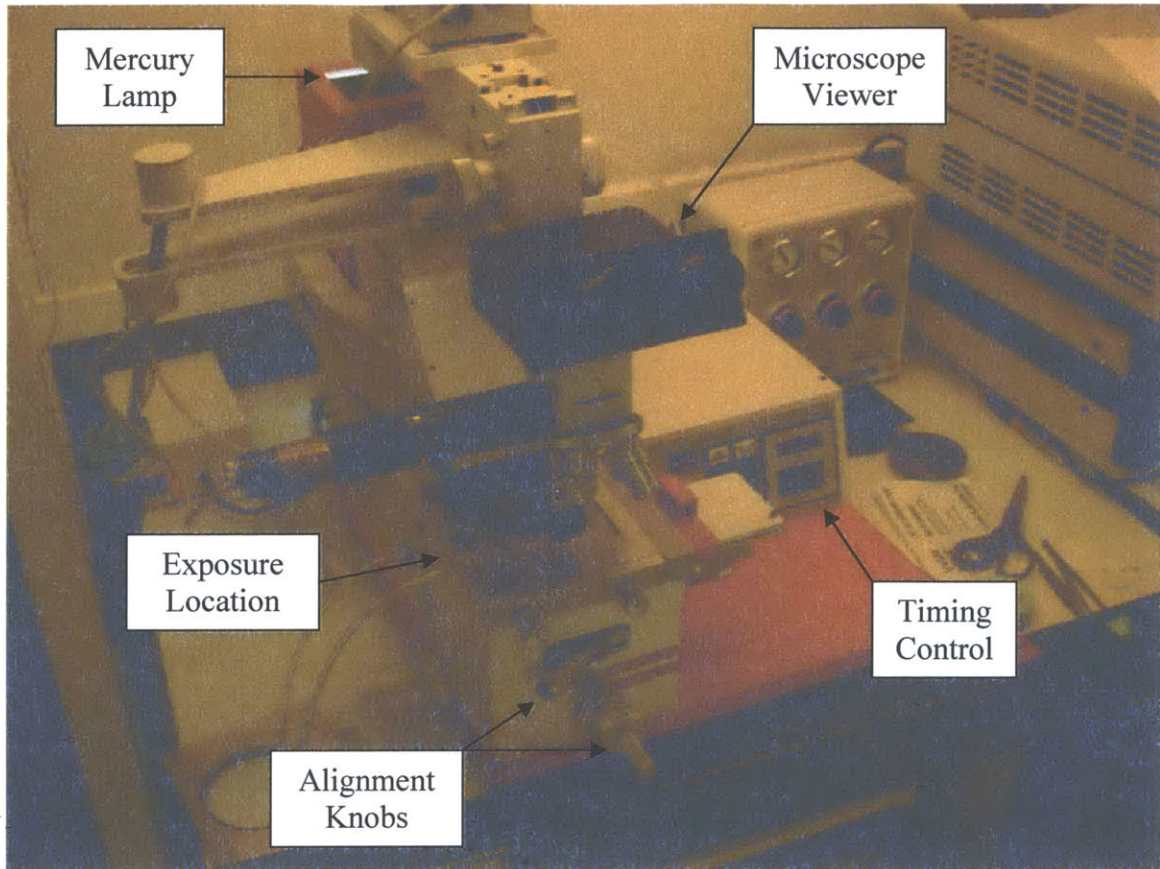
Figure 7-7: Karl Suss Aligner.

The final step in fabrication of the molds was to treat them with a release agent, in this case HMDS. The molds are placed inside a vacuum chamber, as shown in Figure 7-8, accompanied by a few drops of HMDS in liquid form on a non-corrosive substrate, like a glass slide. The vacuum then removes the bulk of the air from the chamber, allowing the HMDS to evaporate into a silane gas, which then coats the molds with a monolayer of silane. The formed polymer part is much easier to de-mold when the mold has been treated with HMDS.

7.3 Microfluidic Device Fabrication

The first approach employed in the research to produce the microfluidic device was to use the sandwich layer developed by Anderson [2000], which was described in Section 5.3. This became known as G1, for Generation One. The details of how this approach faired, as well as the reason that it was passed over, are found in Appendix D. The next approach was to try more-closely to duplicate the sandwich layer method, using the wall-in-slot mates. This was the second generation device, or G2. This also failed to work, and is also discussed in Appendix D.

124

Figure 7-8: Vacuum chamber used for HMDS treatment. A wafer is shown undergoing treatment, which usually lasted for at least half an hour.

A simpler two-mask process was employed to create the third generation device.

Rather than continue to attempt the mechanical positioning with the pre-polymer PDMS fighting against the positioning, mold-to-mold alignment was passed over in favor of layer-to-layer alignment. Both the top and bottom layers were created with open channels, which were then inverted, optically aligned, and thermally bonded. A process flow is shown in Figure 7-9.

Start: Bare Wafer

Coat Wafer with
SU-8

Expose and
Develop SU-8

Pour PDMS

Pre-Cure PDMS
and Peel

Punch Ports in
Bottom

Rough Align

Final Align and
Contact

Final Cure PDMS
and Install Tubing
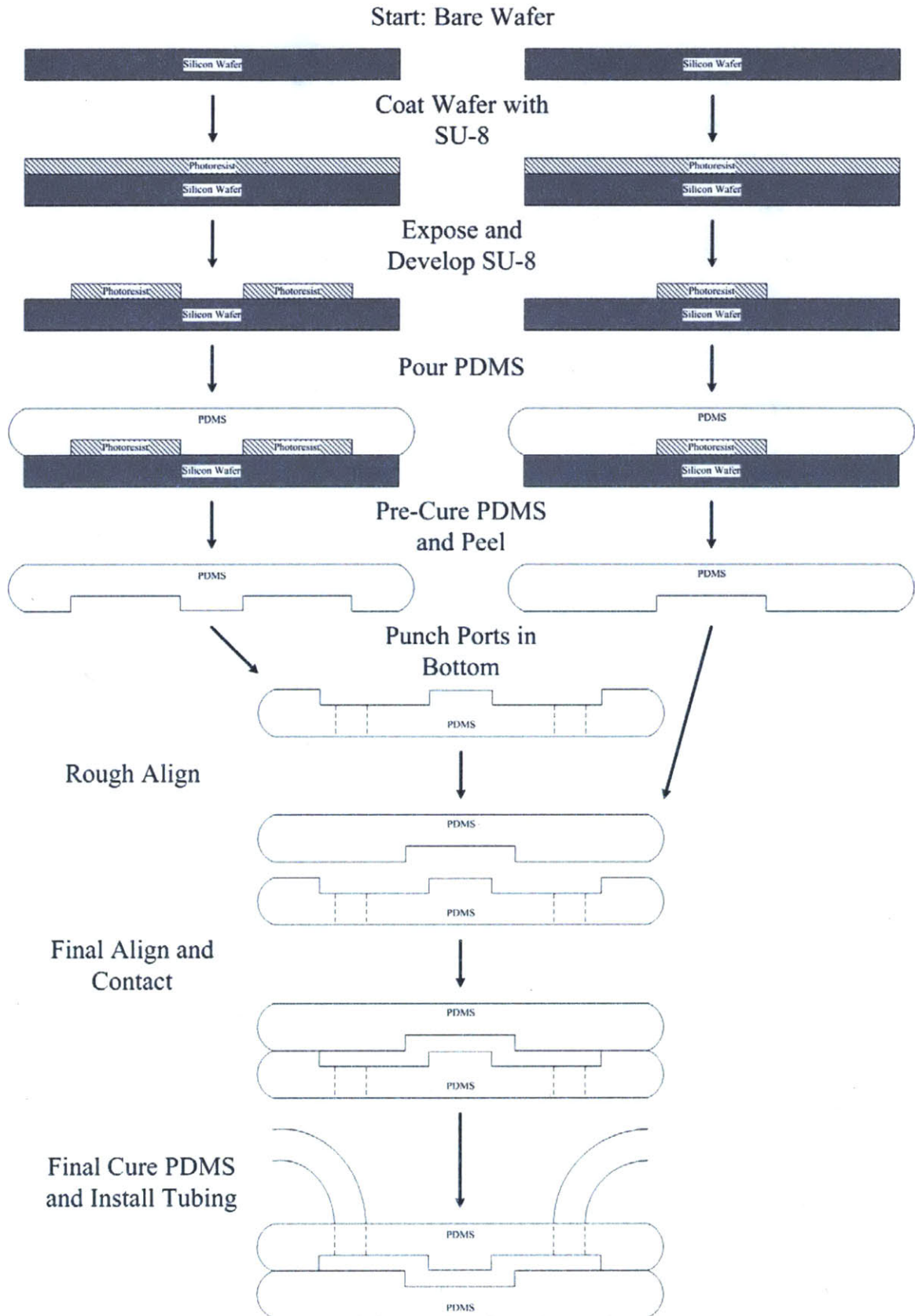
Figure 7-9: Schematic of Microfluidic Device Fabrication Process.

The mold with the reservoirs remains unchanged from earlier generations. But the non-reservoir mold changes, in that rather than a photoresist positive and PDMS negative molds, there is only one mold, a photoresist negative. This will also address the lip affect seen in G2 leading to poor channel fidelity. The new mask is shown in Figure 7-10.
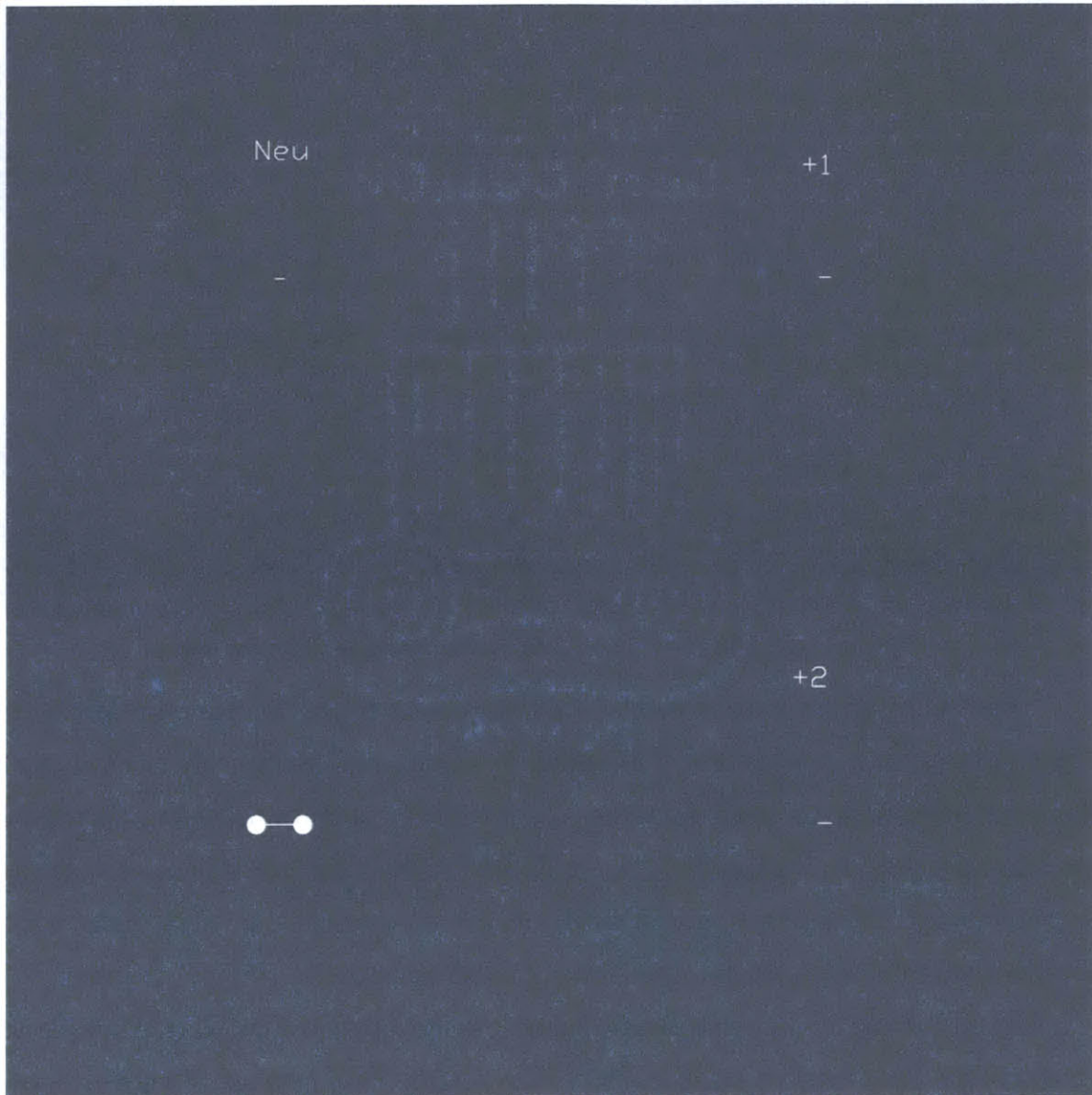
Figure 7-10: Transparency Mask, G3.

PDMS device fabrication begins with weighing of the components, both the base and curing agent, at a mean ratio of 10:1 by weight. The guidelines for processing both the Dow Corning Sylgard 184 PDMS employed in the fabrication appear in Appendix B. The mass scale used to perform this metering is shown in Figure 7-11.
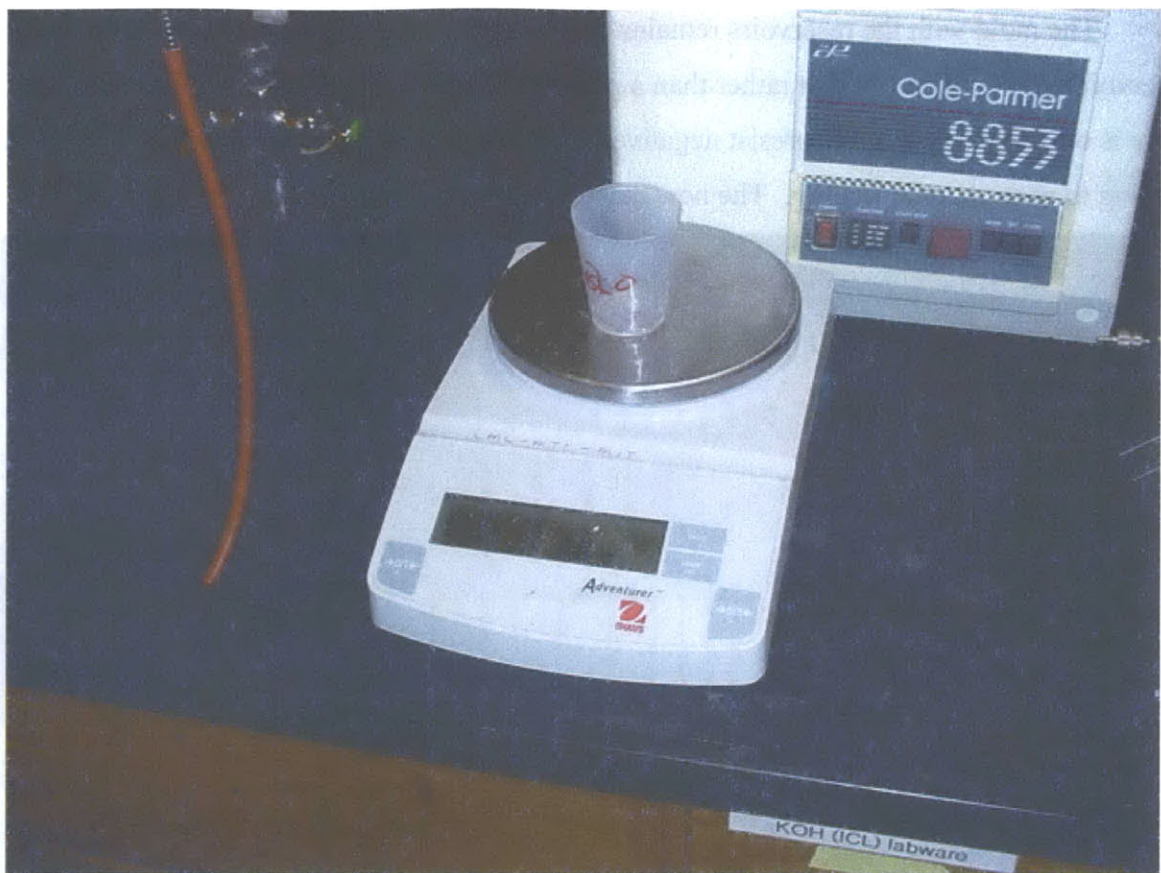
Figure 7-11: Massing PDMS to obtain the proper ratio for the mix.

After weighing, the two components were vigorously stirred for approximately five minutes, and then the pre-polymer was degassed. Degassing took place in another vacuum bell, similar to the HMDS vacuum bell, shown in Figure 7-12. To promote the degassing, the bell was periodically vented. The inrushing air would tend to break the largest bubbles on the surface of the prepolymer. Degassing depended heavily on the volume of PDMS being mixed and the ratio of base to monomer, but was on the order of 30-45 minutes.

The optical alignment was conducted similar to that presented in J. Kim [2005], where the bottom layer is set out on a substrate that can be heated, like a hotplate. Then a layer of methanol is dropped onto the surface, after which the top layer of PDMS is laid on the methanol. The methanol acts a surfactant preventing premature sticking of the PDMS, which would make alignment very difficult to achieve. Then the two layers are viewed through a microscope at the alignment features, in this case the channels themselves, and the top PDMS layer is manipulated until it comes into proper position. The heater is then activated, quickly boiling off the methanol. This method was adapted slightly to create a better bond between the layers, using a

technique developed by the Thorsen group [Urbanski 2004]. It is referred to as the thermal bonding method.
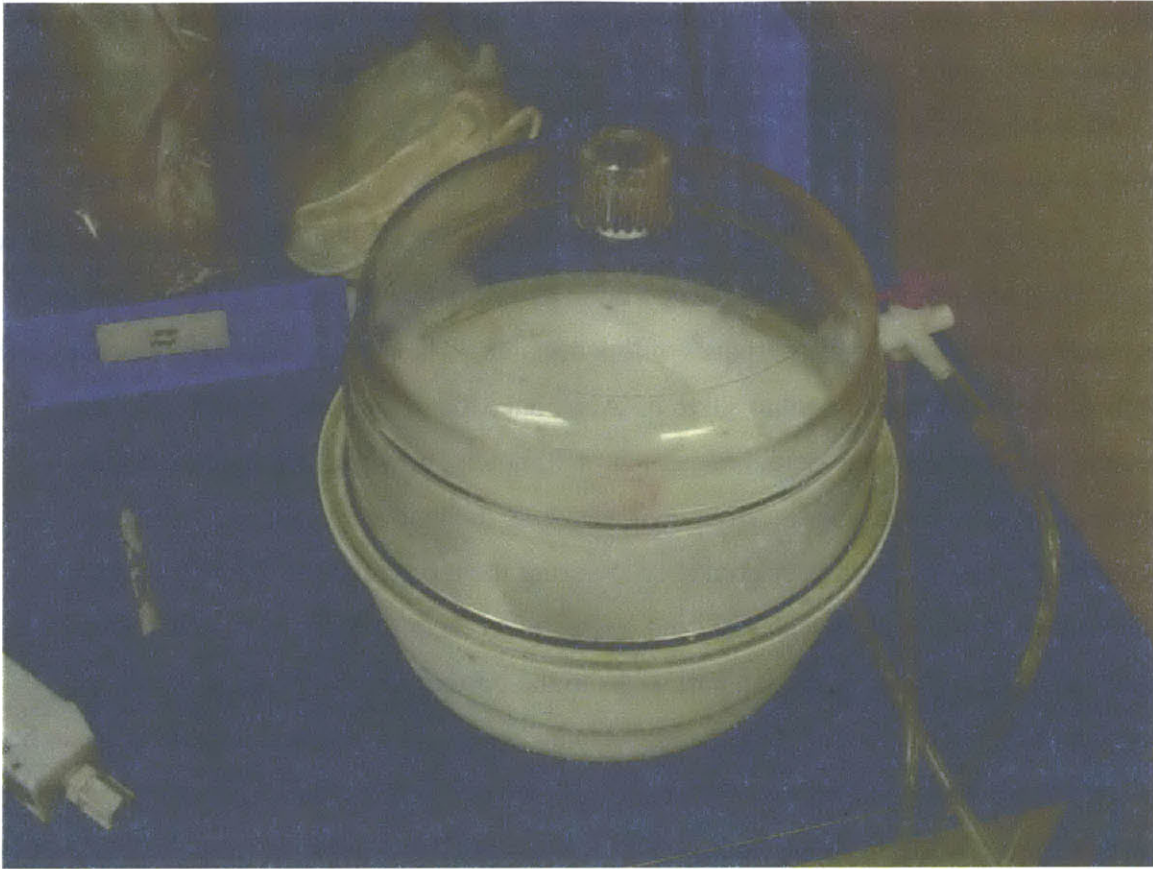
Figure 7-12: Degassing of PDMS under vacuum.

In the thermal bonding method, two separate batches of PDMS are prepared. Instead of the usual 10:1 base to curing agent ratio, one of them has a 1:20 ratio, and the other has a 1:5 ratio. Both of them then follow the typical PDMS protocol of extensive mixing to insure proper combination of the base and curing agent and degassing under vacuum to remove the air that the mixing introduced into the pre-polymer in order to reduce the inclusion of bubbles in the finished device. Then, the PDMS is poured carefully onto the molds, again attempting to minimize the formation of bubbles. When the layers are cast on top of the molds through an oven bake, they are only cured for long enough so that the pre-polymer loses enough of its fluidity that the features will be maintained, but the polymer is still not fully cured and is still quite sticky. The layers are de-molded and this is the point at which they are aligned, again optically. Finally, the two layers are further cured, still in proper alignment. As the curing continues, the excess of base in the bottom and the excess of curing agent in the top are able to diffuse across the

boundary between the layers, effectively increasing the bond between the two layers of polymer. In order to achieve this, the 20:1 layer is baked for 18-20 minutes at 90° C, and the 5:1 layer is baked for 10-12 minutes at the same temperature. Then the two are baked for a further two hours once in contact. Prior to alignment, the access ports are punched in the bottom device for the inlet and outlet tube with a 16-gauge luer-stub syringe needle, and the plug of punched-out PDMS removed.

As stated in the beginning of this chapter, though the manual alignment does not have the highest precision, particularly as the evaporation of the methanol appears to introduce small movements, it suffices for the purposes of this research. The purpose here is to investigate the effects of the misalignment, not to solve it. Also, once the devices are created, they are measured to determine their actual mismatch. Ultimately, however, the methanol was abandoned as unreliable, and the alignment was done by hand in the absence of methanol. The alignment process involved very gradually lowering the top part down onto the bottom, observing the position of the channels and trying to get them as close as possible to their desired locations. Once a corner of the top part sticks to the bottom part, there is still some maneuverability of the layer before the bulk bonds in the region of the device, which can be exploited to perform a last-second correction. A picture of an alignment being performed is shown in Figure 7-13. Looking through the microscope, it was possible to see the channels in both layers, and then they were gently manually lowered into contact. The alignment took place directly on top of a hotplate, so the final cure could be conducted without further movement of the samples following initial alignment.

Finally, once the device is assembled, it can be bonded to a glass microscope slide for support using the plasma ashing technique.

7.4   Failure Pressures

In order to determine the operating pressure range, the burst strength of a number of samples was ascertained. During the testing, the flow rate was gradually increased in steps to detect the pressure at each flow rate at the entrance to the microfluidic device. Eventually, increasing pressure lead to the failure of the device. Using the Hi/Lo recorder on the pressure sensor discussed in Section 8.2, the maximum pressure the device withstood without failing could be retrieved even after the pressure returned to zero. The data are presented in Table 7-1.

The rows are the sizes of the top mold used in creating each device, and the columns are the sizes of the bottom mold used, similar to the presentation shown in Figure 7-5.

Figure 7-13: Optical alignment being preformed.

Table 7-1: Failure Pressures (kPa)

Device	Failure Pressure (kPa)
a	154
b	103
c	154
d	157
e	111
f	151
g	152
h	181
i	163
Control	192

The failure mode was that the device delaminated under the pressure in the channels, and the two halves of the device split back apart. The failure pressure can be seen as a measure of the bonding process; a stronger bond will resist a higher pressure without splitting apart, and this could be another metric to take back to the test device idea for evaluating different bonding schemes. To be safe, most of the data were taken in the range of 0-140 kPa.

8 Experimental Study

The purpose of the experimental study, as discussed in Chapter 6, to evaluate the loss coefficient K as a function of the overlap area, A, between the two layers.

8.1 Requirements

In order to fulfill that purpose, there were four basic requirements for the experimental study.

The first was a working fluid. Distilled water was chosen as a sufficient and readily available fluid.

The second was to provide fluid flow at a range of flow rates. The failure pressure of the devices ultimately limited the range of flow rates, which as shown in Section 7.4, was on the order of 140 kPa. A range of 0 to 10 mL/min was more than sufficient to accommodate that maximum pressure in the devices. The resolution should be at least 0.01 mL/min, with accuracy of at least 1%.

The third was to measure pressure drop in the system. Here, the range should be at least 0 to 300 kPa, with resolution of at least 0.1 kPa and accuracy of at least 1%.

The final requirement was the microfluidic device itself, also referred to as the test section, with layout and various overlap positions as described in Section 7.1.

8.2 Apparatus

Given those requirements, components were selected to fulfill them and then assembled. Figure 8-1 shows a schematic of the platform, and the components shown in Figure 8-2 will be detailed in the sections that follow. Much of this work was performed by Thaker [2006].
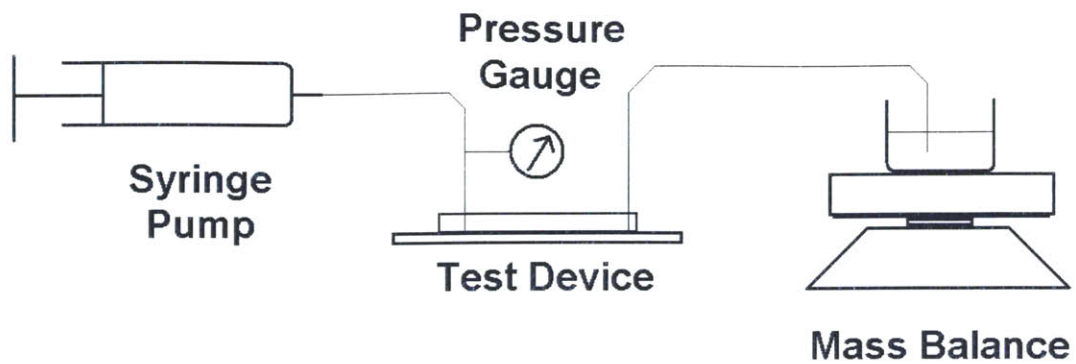
Figure 8-1: Experimental Setup in abstract form.

Figure 8-2: Experimental Setup, in realized form.

The pump selected to meet the requirements of a flow-rate source was a Harvard Apparatus PHD 2000 Infusion Pump, shown in Figure 8-3. A syringe pump pairs a linear actuator with a syringe to push fluid out at a known flow rate. By varying the size of syringe, a large variety of flow rates and pressures can be achieved.
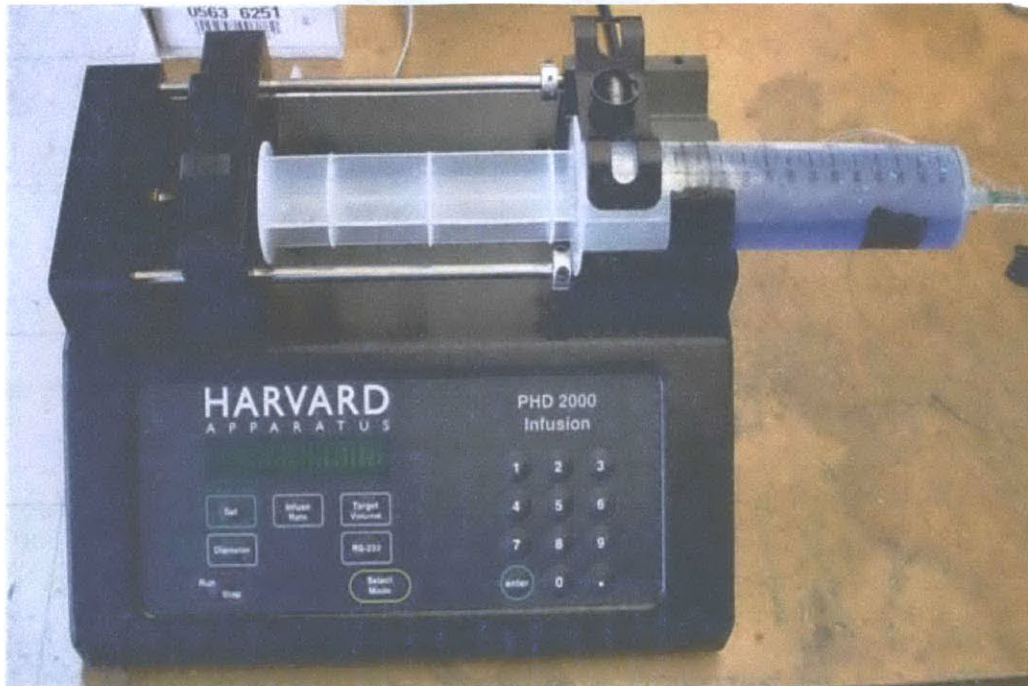
Figure 8-3: The syringe pump used to create fluid flow through the system.

The specifications for this pump appear Appendix E. The resolution can be altered by varying the size of syringe used with the system at a chosen scale. As shown in Appendix E, in addition to range, both resolution and accuracy exceed the requirements stated in Section 8.1.

Since the pump only accurately knows the speed that its linear actuator moves, it was necessary to calibrate the flow rate for a given syringe diameter. In order to do this, a mass scale was incorporated into the system. The user can select a given flow rate for the syringe pump, but in order to do so, they syringe diameter must be entered. It was this parameter of syringe diameter that was used to calibrate the commanded flow rate to the actual flow rate through the system. The pump was run at a given speed for the chosen syringe, with the manufacturer-recommended syringe diameter, and the scale collected the fluid expelled by the syringe. By running the pump for a long enough period of time, the mass scale could be relied upon to give a measure of the actual flow rate at that commanded flow rate. The deviation was found to be one of scaling, so the inputted syringe diameter was scaled by the same ratio. The calibration curves are shown in Figure 8-4.
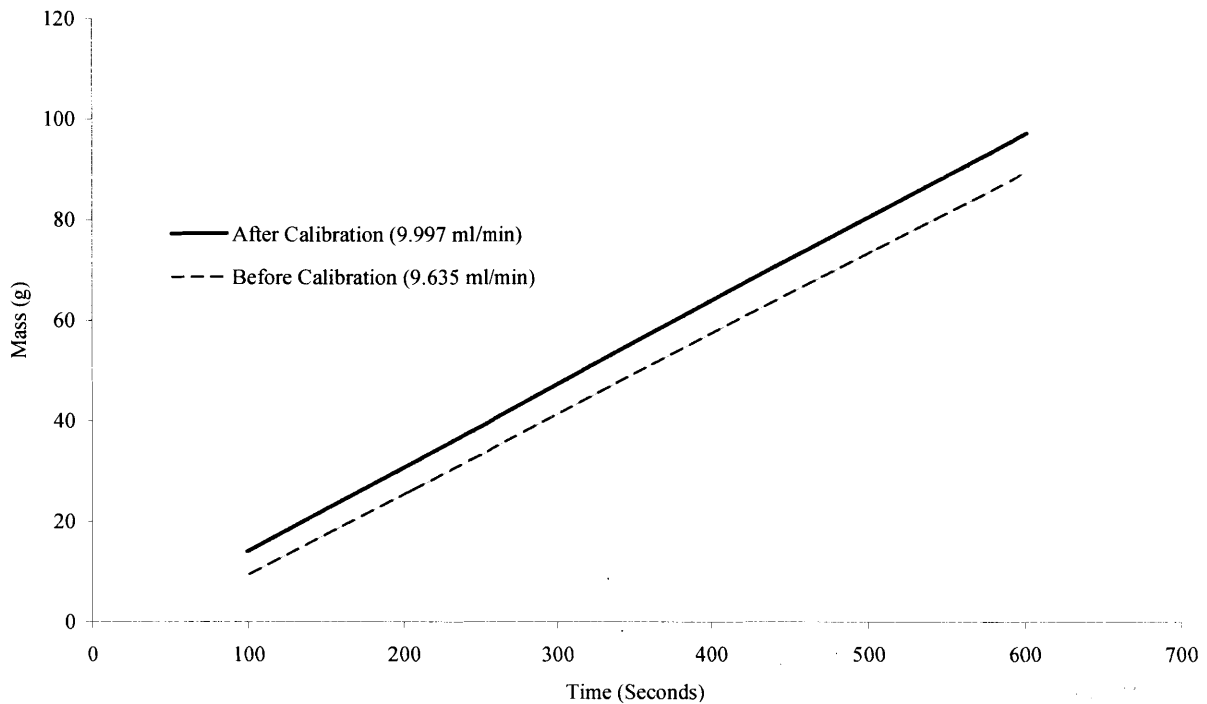
Figure 8-4: Calibration curves used to set proper syringe diameter for the syringe pump [Thaker 2006].

As shown in Figure 8-3, the primary working syringe was one of the largest compatible with the pump, 140 milliliters. This size was chosen to address one of the limiting issues when using a syringe pump, namely that once the syringe is completely compressed, the entire system must be shut down to refill the syringe. However, by using a large-volume syringe, testing could continue for longer times between refills. The pump also has the ability to pump two syringes simultaneously, increasing the maximum capacity to 280 milliliters.

Due to the relative sizes of the tubes that bring the fluid to and from the microfluidic device and the micro-channels on the device, a simple gauge pressure sensor sufficed in measuring the pressure drop across the test section. The tubing is 1/16" in interior diameter, or 1.4mm, and the microfluidic channel is 100 μm in diameter. Equation 6-8 shows that the pressure drop in a channel is relative to its volume over the hydraulic diameter squared. But the fluid velocity is also affected by size, for a given volume flow rate in the system, as the flow rate over the cross-sectional area, which itself is the square of the radius. Thus the pressure drop is inversely proportional to the fourth power of the diameter, so for a tube that is almost 15 times as

136

large as the microfluidic channel, the pressure drop in the tubing is four and a half orders of magnitude greater than the drop in the channel for a given length. Effectively, the entire pressure drop in the system, which terminates in a collector at the mass scale at atmospheric pressure, happens across the microfluidic channels in the device. Thus the pressure gauge is simply connected anywhere upstream of the channel, and provides an accurate measure of the pressure drop across the channel. The pressure gauge that was selected is shown in Figure 8-5. The gauge is a 3D Instruments Digital Test Gauge, and its specifications are listed in Appendix E. Of note are the range, 0-700 kPa, the resolution, 0.05 kPa, and the accuracy, 1% below 150 kPa, which fulfill the requirements stated in Section 8.1. The pressure sensor was calibrated by the manufacturer, but was tared to zero gauge pressure with nothing connected to the system.

Figure 8-5: Pressure Gauge used to measure pressure drop across the device.

The mass scale needs merely to have good resolution in the regime of fluid that might be outputted from the syringe pump. 140 milliliters is the maximum volume that could come out of

the syringe, and at the density of water, this equals 140 grams. The mass scale that was selected, shown in Figure 8-6, has a capacity of 300 grams, more than sufficient, even if both cylinders are run at maximum capacity. The mass scale is calibrated using two test masses provided by the manufacturer, following the standard protocol in the manual.

The fluid flows in from the top into the beaker placed on the scale. The enclosure and additional sensor were added to address the potential of evaporation from the beaker for a very low flow rate test over a long duration. However, since the scale was used primarily for calibration of the pump, and the channels were on the larger end of the micro-regime, this concern was not realized. However, the addition of these two components does extend the capability of the machine for future tests. The specifications for the Mass Scale and Humidity Sensor appear in Appendix E.

Figure 8-6: Mass Balance Used to Confirm the Accuracy of the Syringe Pump, and Humidity Sensor.

Along with the usage of PDMS comes its flexibility. The flexibility of the material can be used to create a pressure coupling. A hole is punched through the PDMS using a luer stub, and then a metal tube of slightly larger diameter than the punch is inserted into the hole to act as the port. The PDMS will have to deform outwards to accept the tube, and as it does so, it will

138

exert a compressive force on the tube, effectively sealing it. This connection has been shown to resist at least 140 kPa, depending also on depth of insertion. Since the focus throughout was on creating the experimental model in the simplest method possible, this method was chosen. The metal pipes are then inserted into the plastic tubing that carries the fluid from the pump and to the mass scale. The same mechanism is at work in resisting leakage on that joint, too. A picture of the inlets and outlets is shown in Figure 8-7.
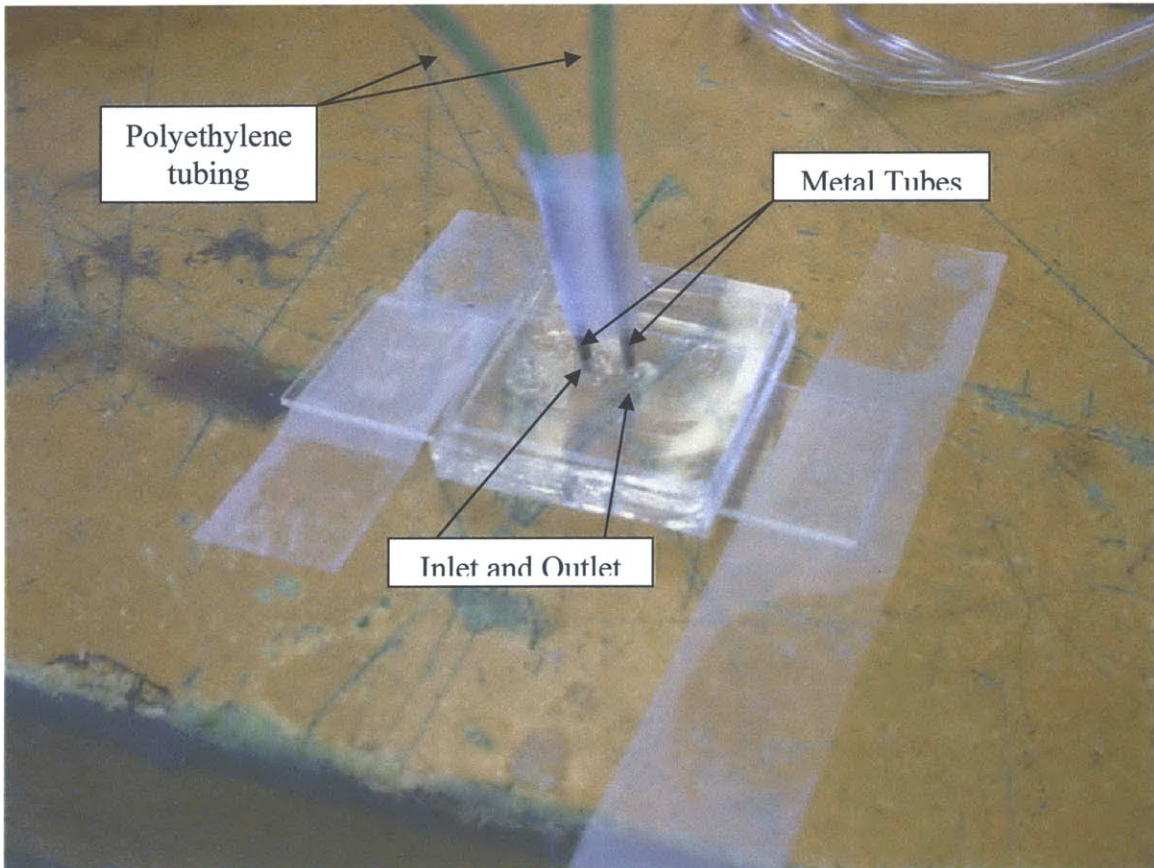
Figure 8-7: The microfluidic device, showing inlet and outlet via metal tube attached to polyethylene tubing.

The test section was assembled using the processes described in Sections 7.2 and 7.3. In order to determine the K value, as shown in Equation 6-12, the input of flow rate from the syringe pump must be converted to average fluid velocity in the channel. The link between these two was the cross-sectional area of the microfluidic channel. To find the cross-sectional area, each of the molds was measured to determine width and depth. The in-plane measurements – the width of the channels – were performed using a calibrated optical measurement with the aid of the microscope. The out-of-plane measurements, specifically the heights of the channel-features, were also performed optically, but using a focal-plane measurement. That is, the focal length of

139

a microscope objective is a fixed distance away from that objective. To focus on different heights of the part being examined, the objective is moved up and down, so that the plane of interest is brought into the focal plane, which remains the exact same distance from the objective. A linear displacement sensor can be attached to measure the changing distance between the stage and objective head, and can be used to determine the height of features by first focusing on the bottom of the feature, zeroing the sensor, and then focusing on the top of the feature. A picture of the microscope that was used to perform the measurements is shown in Figure 8-8. The micrometer that measures displacement of the stage appears on the main back column of the microscope, and its digital display and zeroing buttons are visible. The computer in the background is running the software that was used to take the bulk of the micrographs that appear in this work.

Figure 8-8: Microscope employed to perform optical measurements.

PDMS has been shown to reliably reproduce various mold features down to resolutions far below the microfluidic scale, so it is assumed to take the dimensions of the mold, except when catastrophic affects are seen during de-molding, specifically a tearing of the PDMS for

various reasons. Barring failure, the features are those of the mold. The other issue to take into account is shrinkage: the polymer shrinks slightly during setting, causing a slight reduction in sizes. GE Silicones' RTV 615 has a published shrinkage of 1.6%, and the common working value for the shrinkage in Dow Corning's Sylgard 184 is 1.7%. These are both very small percentages, and are below the limits of detection for this scheme. However, to be safe, the original masks used to create the devices were scaled up by that percentage, as well. The data are presented in Table 8-1.

Table 8-1: Mold Sizes

Mold Name	Configuration	Channel Width (μm)	Channel Height (μm)
Bottom	Neutral	105	95
Bottom	-1/3	112	99
Bottom	-2/3	114	136
Top	Neutral	117	101
Top	+1	117	96
Top	+2	112	109
Control		112	108
	Mean	113	106
	Standard Dev	4	14

As can be seen, the variation in these results, particularly height, was considerable. The nominal value for each of these dimensions was 100 μm. The variations were likely due to the highly manual control of the system: the photoresist was poured onto the wafer by hand in an approximate volume, and then the spin speed was also controlled by manual input during the spin coat. All of these factors contributed to the variation which showed low repeatability in forming the molds, but, since they were measured, they can be accounted for. The purpose was not to reduce variation but rather quantify its effects. The offset mean of the channel widths suggests effects from the photolithography, such as oversizing of the mask features, or some other factor that would have added to the area that was cross-linked, such as scattering of the light. The height has a mean closer to the nominal, but does show those large variations as a result of the manually-introduced variation.

In an automated process, it would be possible to more tightly control all of these factors: a dispenser would deposit the correct amount of photoresist in the same position each time within much tighter tolerances and the spin profile would be uniform from part to part.

8.3 Procedure

Each device that was created was tested to collect the data for evaluating the pressure drop at the microfluidic interface. Before connection to the testing platform, the overlap area and mismatch are evaluated, also using the optical comparison method. In order to generate the value of the misalignment, the distance between the top channel tip and bottom channel tips are measured on both sides, as well as the vertical misalignment. Under the manual manipulation method employed, rotational misalignment about the axis perpendicular to the plane of the channels was minimized, but linear mismatch was harder to control. This is likely due to the Abbe sine error being performed in reverse, as the block of material containing the channel was much larger than just the channel. Thus while a small linear movement at the edge of the part would result in exactly similar linear movement of the channel being aligned, a rotational movement of the same displacement at the edge would result in a much smaller change in angle at the channel.

The testing then shifted to the use of the testing platform. The device was connected to the pump on one end and the mass scale at the other, and fluid flow was commenced. The method of testing was to set the pump to a series of constant flow rates, and then observe the steady-state pressure value at those flow rates. The system showed some dynamic response even after the pump came quickly to a set flow rate. It is unclear what exactly was the source of the delayed response, as the microfluidic channel was relatively short. Two possible sources would be a reservoir capacitance of the plastic tubes in front of the device that takes time to be charged up with pressure, or potentially the droplets being formed at the end of the enclosed channel above the mass scale. A separation was maintained between the tube and the beaker in order to decouple the mass that exited the pipe from the pipe itself, but it may have added a tendency to fluctuate the pressure within the device. In any event, during testing, the pressure measurement was allowed to settle after changing the flow rate before the data point was taken. Using this input of a step change in flow rate and a steady-state observation of pressure drop, four or five data points were taken from each device. With the failure pressure on the order of 140 kPa, each of the data points was targeted for a flow rate that would not cause the device to exceed that failure pressure. These values were used to fit the data to a quadratic model in order to correlate

142

a value for the loss coefficient K at the multilayer joints. In order to evaluate the repeatability of each data point and reduce any affects of hysteresis, each point was evaluated by arriving at the pressure drop from a lower pressure and also from a higher pressure. That is, the test was first performed by raising the flow rate from a lower value, and observing when the pressure came to steady state. Then the test was again performed by starting at a higher pressure and flow rate, lowering the flow rate to the target value, and observing the flow rate come down to a steady state.

Then, a final test was performed by continually raising the pressure until the device failed. This measure of the failure pressure of the device was done to determine upper limits for testing, to characterize the failure pressure of the bond, and to gain a better understanding of the failure mechanisms under high pressure of the device.

8.4 Results

The following chart displays micrographs of the fabricated devices. They are presented in a grid, corresponding to the molds used to create each one. The molds used in created in each of the microfluidic devices shown in Figure 8-9 are listed in Table 8-2. Using the optical methods described in Section 8.2, the misalignment between the layers was measured, as evidenced by the misalignment of the channels. The measurements, as well as the target values for each mold-combination, are presented in Table 8-2. The target vertical mismatch in all cases was zero, so that is omitted. As can be seen from the table, the optical detection method had a practical resolution of 10 μm, which for measurements on the order of a mismatch of down to 20 μm, was sizable. Using this information as well as the equations presented in Section 6.5, it was possible to calculate the overlap area between the channel layers. That overlap area for both the right and left multilayer joints, as well as the target value for each microfluidic device, is presented in Table 8-2.
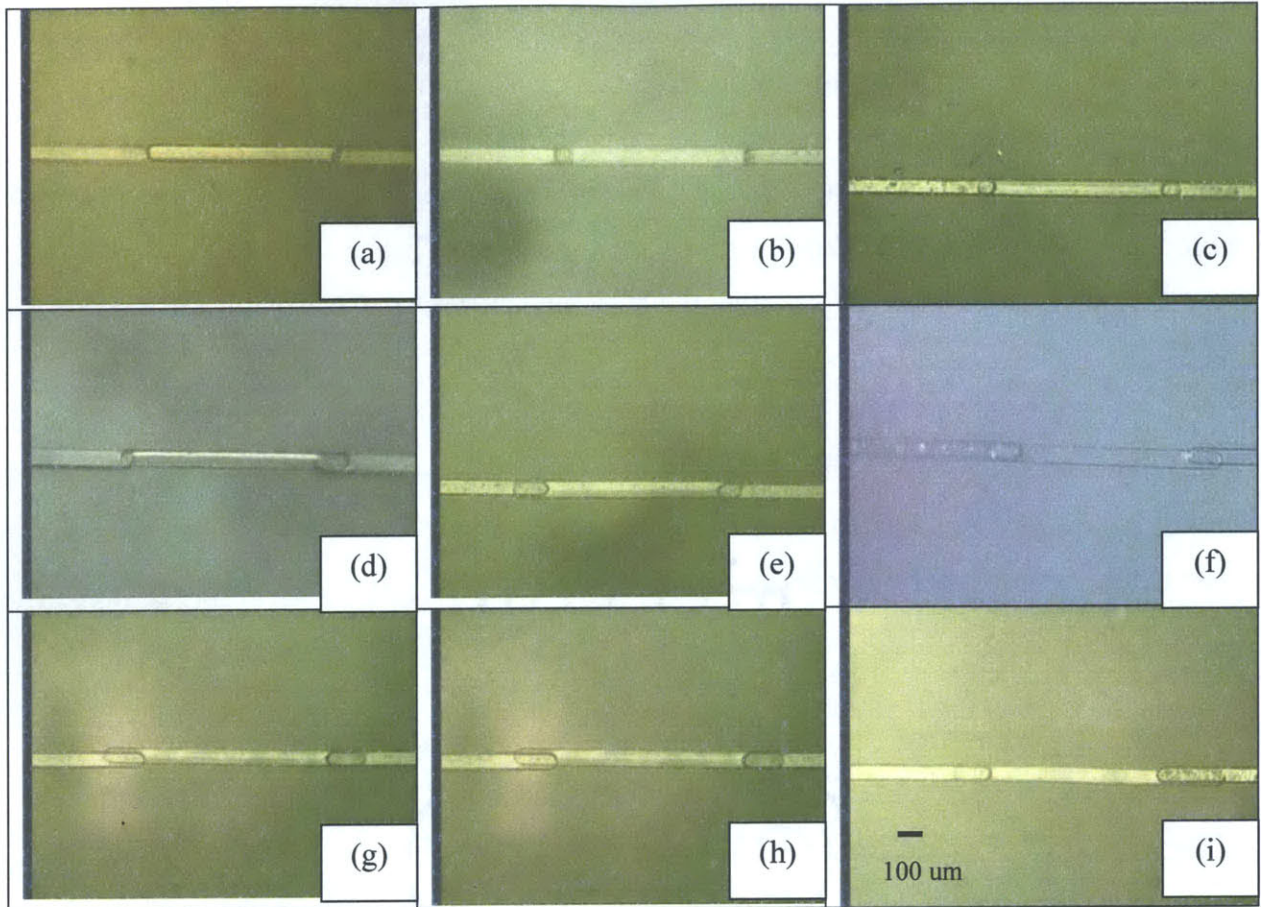
Figure 8-9: Multilayer Microfluidic Devices, displaying misalignments in various configurations.

Table 8-2: Mold Sizes, Mismatch, and Overlap Area in the Fabricated Devices

Molds		Picture	Linear Mismatch (µm)				Overlap Area (µm²)		
Top	Bottom	Figure 8-9	Target u	Left u	Right u	Vertical v	Target	Left Joint	Right Joint
-2/3	Neu	(a)	-67	-80	-40	20	1700	674	3540
-1/3	Neu	(b)	-33	0	-80	0	4610	7850	818
Neu	Neu	(c)	0	0	0	0	7850	7850	7850
-2/3	+1	(d)	33	-20	80	20	11200	5140	13100
-1/3	+1	(e)	67	100	40	0	14600	17900	11900
Neu	+1	(f)	100	100	100	20	17900	17900	14700
-2/3	+2	(g)	133	140	120	20	21200	13300	19900
-1/3	+2	(h)	167	180	160	0	24600	25900	23900
Neu	+2	(i)	200	120	280	10	27900	19900	29100

144

With the overlap area calculated, the devices were installed in the testing platform, inlets and outlets connected, and the pump was activated to begin flowing fluid through the device. The pump was set to a series of flow rates, and the pressure was measured at those flow rates. The steady-state pressure drop at each of those flow rates was recorded, both manually and via use of the computer recorder.

A plot of one of the device's flow-rate/pressure diagram is shown in Figure 8-10. The pressure sensor had a resolved display down to 0.05 kPa, though there was usually some fluctuation around the mean value at each pressure reading, on the order of 1%.
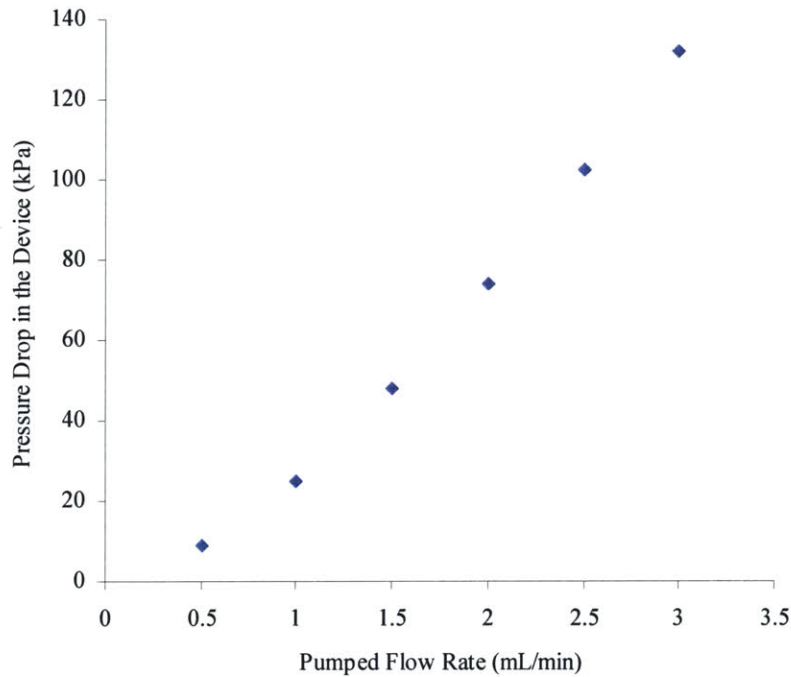
Figure 8-10: Flow Rate to Pressure Relationship, Figure 8-9(d) device.

Using the dimensions of the channels measured from the molds, it was possible to calculate the average velocity in the channels, as follows:

$$V_{av} = \frac{Q}{\frac{2}{3} w_{bottom} d_{bottom} + \frac{1}{3} w_{top} d_{top}} \tag{8-1}$$

where Q is the volumetric flow rate, and w and d are the width and depth of the channels, respectively. The graphs were then slightly adjusted to portray velocity in the channel, instead of overall flow rate. The pressure was also converted from the imperial units to SI.

Using these data, it was possible to use least-squares regression to create a polynomial approximation that most closely fit the data. In this case, the data were fit to quadratic equations in order to bring them in line with the theoretical model presented in Equation 6-12. The combined velocity-pressure drop data are shown in Figure 8-12, and the individual plots, both raw data and with trend lines and mean volumes, appear in Appendix F.
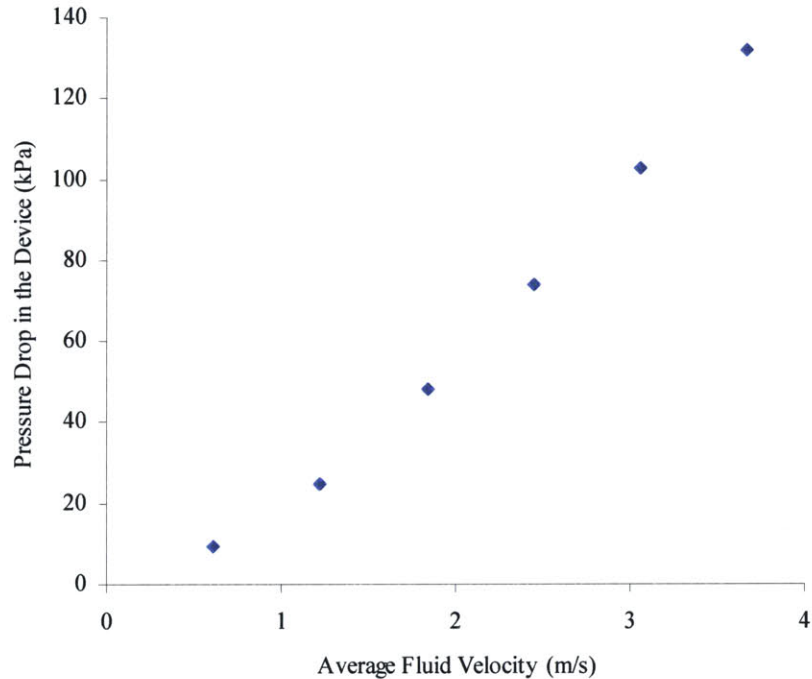
Figure 8-11: Velocity to Pressure Relationship, Figure 8-9(d) device.
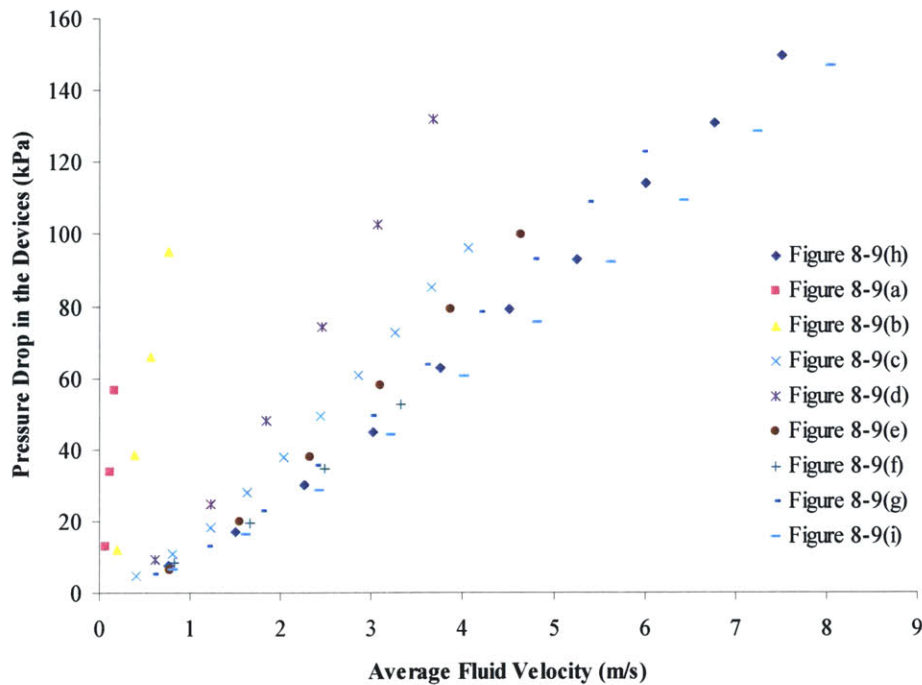
Figure 8-12: Velocity and Pressure Drop for all Devices.

The coefficient of the quadratic term in the polynomial that is fit to each set of data is the useful part, for as shown in Equation 6-12, this value is equal to one half of the sum of the loss coefficients at each of the joints, multiplied by the density of the fluid.

For this experimental setup, it is regrettably impossible to determine the relative effects of each of the two joints, as the pressure of the flow in between the joints cannot be measured to evaluate the relative contributions of each joint to the pressure drop. This is the major drawback that was found to this experimental model. Thus, though the area through each joint may be different within a single device, and the pressure drop across each is correspondingly different, it is not possible to distinguish exactly the values of K_a and K_b, the values of the loss coefficient at the right joint and the left joint, respectively. Thus an average value K_{ave} is used, and a corresponding area term A_{ave} for the device must be assembled. This represents a loss of precision of the experimental model, and as will be discussed in the conclusion, this will be the major recommendation for future work in this area.

The coefficients from the quadratic fit and the corresponding average K values are shown in Table 8-3. The quadratic coefficient has density units, kg/m^3, while loss coefficients are dimensionless.

Table 8-3: Quadratic Coefficients (kg/m^3) and Associated Average Loss Coefficients

Picture	Quadratic Coefficient (kg/m^3)	K_{ave}
Figure 8-9(a)	1.42×10^6	1430
Figure 8-9(b)	2.05×10^4	20.6
Figure 8-9(c)	2.17×10^3	2.17
Figure 8-9(d)	4.28×10^3	4.29
Figure 8-9(e)	1.51×10^3	1.51
Figure 8-9(f)	2.44×10^3	2.44
Figure 8-9(g)	1.09×10^3	1.09
Figure 8-9(h)	7.64×10^2	0.77
Figure 8-9(i)	7.12×10^2	0.71

The loss coefficient data from Table 8-3 are combined with average area data from Table 8-2 in Figure 8-13.

The data have been plotted on a semi-logarithmic scale, as the K value increases drastically at the very small overlap areas. As was expected, there is a clear inverse relationship between the overlap area and the loss coefficient. The hypothesis of overlap area having an inverse effect on the loss coefficient was borne out by the experimentation. The data is asymptotic in its behavior. There is a clear asymptote at zero overlap area, where the loss coefficient is infinite, but there also appears to be an asymptote of a minimum K value, where further overlap area does not further decrease the loss coefficient. This seems to be on the order of 0.7.

Between these outer regions on the graph, there is the section in the middle, where the overlap area is on the order of a circle like that shown in Figure 6-3 with the same width as the channels themselves. These data points have loss coefficients of approximately 3. As discussed in Section 6.3, for a turbulent "Z" macro-fitting, 2.89 is given in the literature. White [1999] suggests a value of .5 to 1 for a single, turbulent, macro-scale 90° elbow. Two in succession, as presented here, would likely have the combined loss coefficient of 1 to 2. Thus at least preliminarily, these data are in line with the literature for the macro-scale equivalents.
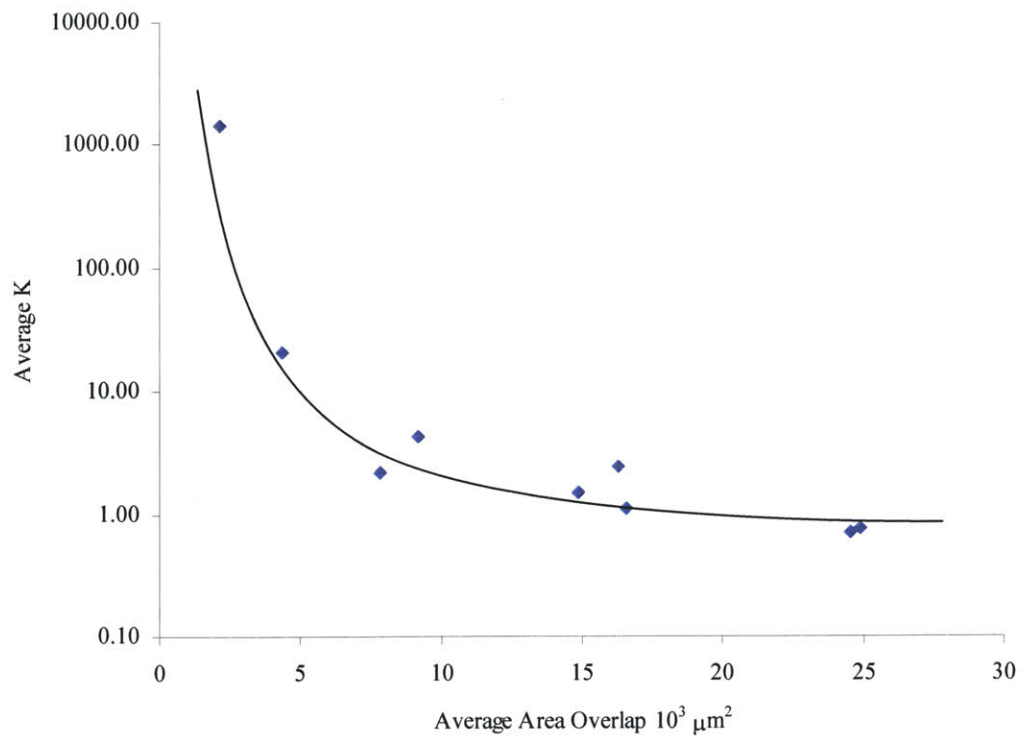
148

Figure 8-13: Coefficient of Pressure Loss as a Function of Overlap Area in the Devices.

9 Conclusion

The background research presented in Chapter 2 reveals a number of potential applications for microfluidic devices. Those applications were surveyed for their functionalities, as presented in Table 2-1. From there, a number of common features were cataloged in Sections 4.3 and 4.4.

The various processing methods currently available for creating microfluidic devices, and their advantages and disadvantages, were presented in Chapter 3. It became apparent that there is a need to evaluate the relative strengths of the different methods as well as any new processes that may come forward in the future to fulfill the requirements of the functionalities of the applications. For this reason the idea of a test device was advanced.

One outstanding issue was multilayer devices. As the complexity of microfluidic devices advances, with more functionality in a small area, the pressure to create multilayer devices will increase. As discussed in Section 5.2, the major challenge in achieving reliable multilayer devices is alignment between the layers. This was our area of focus, and in order to study alignment, a functional test was performed as described in Chapters 7 and 8.

9.1 Test Device Design

Based on the background research, it was found that there were three common features seen in multiple applications. The features were analyzed for their basic key characteristics. There is the single, straight channel, for which there is only its height, width, and length. Multiple channels also have the concept of density of channels in addition to the ones for the single channel. Turns have the angle of turn and the radius of curvature, as well as the basic single-channel parameters. There were other features discovered, but they were not common to all applications.

Given this concrete list of the universal features, the concept of a test device is validated. That is, as all microfluidic devices can be described by some combination of these simple features, a test device with these features over a range of sizes represents the spectrum of applications in the abstract. And by knowing the key features, the test device can indeed be created.

9.2 Alignment Method

Another area that was raised in the survey of applications was that of multilayer devices. We wanted to discover how important the alignment of the layers in a multilayer microfluidic device was on the device performance. As detailed in Chapter 5, Chapter 7, and Appendix D, alignment is of central importance to the fabrication of multilayer devices.

In order to do so, we developed a methodology of understanding the effects of misalignment on overlap area between the fluid channels in different layers, of conceptualizing the effects of the multilayer joint on the fluid flow, and of choosing proper design sizes. To evaluate this methodology, the functional test in the experimental study was conducted. Pressure drop was employed to evaluate the impact of misalignment. Additionally, ways of achieving alignment were examined to see if they were suitable candidates for multilayer microfluidic device fabrication. Ultimately, finding reliable solutions to the problem of accurate alignment will be what is necessary to implement multilayer microfluidic devices.

9.3 Experimental Study

When the devices were tested for pressure and flow rate relationship, they did indeed display the quadratic behavior predicted by Equation 6-12. Another conclusion was clear: misalignment can indeed have a large impact on the device performance. The data presented in Figure 8-13 show that for a misalignment of only 2/3 of the width of a microfluidic channel, there is an increase in the loss coefficient K by three orders of magnitude. This is a drastic increase for a relatively small misalignment. And as shown in Figure 6-9, even if overlap area is intentionally increased in an attempt to reduce the loss coefficient, the overlap area falls off steeply for any misalignment perpendicular to the designed overlap area.

9.4 Future Directions

As with any research, particularly the initial exploration of a new research area, many ideas and suggestions for future work were raised. Three points stood out.

- Pursue mechanical alignment
- Restructure experimental design for single-joint multilayer device
- Expand to three-layer designs

As detailed in Appendix D, mechanical alignment was originally attempted in this research, but was ultimately passed over in favor of the less-problematic optical alignment. However, optical alignment requires optical observation, manipulation, and in-situ fixation of the layers being aligned. A relatively simple mechanical self-alignment mechanism, perhaps employing the work of Whitney [2004], would reduce the complexity required to align each device that is fabricated. Addressing the issues of alignment not only in PDMS processes but also in hot embossing and microfluidics is the long-term direction of this research. For those latter two processes, though existing molds can create features with good tolerances, as discussed in Section 5.2.1, the features are created with conventional machining. Moving to micro-scale features may require silicon-wafer-derived inserts, for which alignment is again brought to the fore.

Second, the choice to go to a two-joint device, which was taken to introduce some simplification in assembly and alignment of the device as well as anticipated reduction of errors due to inlet and outlet similarity, now seems to have been wrong. The lack of specificity in addressing what pressure drop was due to which of the two joints on the device only introduced greater uncertainty into the results. One joint introduces issues of alignment of the two layers, as the gap between the bottom channels that was used for alignment of the two-joint devices no longer exists. These could be overcome with alignment structures both locally near the joint to confirm the location, and globally for the two layers, which will assist in the macro-alignment before the fine adjustment near the channels is performed. This reduction in the number of joints will remove the requirement to average both the loss coefficient and the overlap area from the two devices. A complimentary goal would be to see if there is sufficient repeatability of the data that some of the results can be generalized or non-dimensionalized. Identifying a dependence on some generalized parameter, perhaps overlap area divided by the square of channel width, would aid the applicability of the results to other scenarios.

152

Once the two-layer joint is well understood, the next direction is clear: three-layer joints. The design of a via-plug in microelectronics manufacturing is not merely an overlapping area between two layers, but a plug that exists in its own layer between the top layer and bottom layer. This is topologically required to pass over another channel, and was evident in the devices developed premiering the multilayer technology. The via-plug involves a quick pair of two-layer joints, so the understanding gained from researching the dual-layer joint will be invaluable, but just as the multilayer flow is more complex than a single right-angle turn, it is likely that the three-layer joint will show additional complexity beyond a series of two-layer joints.

Bibliography

Anderson, J.R., et al. "Fabrication of Topologically Complex Three-Dimensional Microfluidic Systems in PDMS by Rapid Prototyping," in Analytical Chemistry, vol. 72, pp. 3158-3164, 2000.

Artisan Plating, Metal Arts Specialties. (May 2006), available http://www.artisanplating.com/articles/platingbasics.html .

Batt Research Group, Cornell University. (May 2006), available http://foodmicro.foodsci.cornell.edu/fmlab/sensors.html .

Benn, J.A., J. Hu, et al. "Comparative modeling and analysis of microfluidic and conventional DNA microarrays," in Analytical Biochemistry, vol. 348, no. 2, pp. 284-293, January 2006.

Berthier, J., P. Silberzan, Microfluidics for Biotechnology. Boston, MA: Artech House, 2006.

Carr, S.M. Personal Website, Department of Biology, Memorial University of Newfoundland. (2006 May), available: http://www.mun.ca/biology/scarr/Lab_5_gel_1999.gif

Cheung, R.C. Private interview, 18 November 2005.

Chon, S. C., et al. "Disposable Polydimethylsiloxane Package for 'Bio-Microfluidic System'," Proceedings IEEE Electronic Components and Technology Conference, pp. 617-621, 2005.

Chou, H.-P., et al. "Microfabricated Devices for Sizing DNA and Sorting Cells," in Micro- and Nanofabricated Structures for Biomedical Environmental Applications, vol. 3258, pp. 181-187, 1998.

Chou, H.-P., et al. "A Microfabricated Rotary Pump," in Biomedical Microdevices, vol. 3, no. 4, pp. 323-330, 2001.

CIS Institute for Micro Sensors. (May 2006) available: http://www.cismst.de/english/infocenter/presse/2005-04.htm .

Coventor, Inc. (May 2006), available: http://www.coventor.com/microfluidics/ .

Culpepper, M. "Design and Application of Compliant Quasi-kinematic Couplings," Ph.D. Thesis, Department of Mechanical Engineering, Massachusetts Institute of Technology, Cambridge, MA, 2000.

Daub, M., et al. "Microfluidics and Beyond: Devices of Applications in Biotechnology," in
Materials Research Society Symposium Proceedings, vol. 820, pp. R6.6.1 – R6.6.11,
April 2004.

Derksen, J.S. "A New Coating Method for Semiconductor Lithography: Fluid Overlap in
Extrusion-Spin Coating," S.M. Thesis, Department of Mechanical Engineering,
Massachusetts Institute of Technology, Cambridge, MA, 1997.

Dirckx, M. "Design of a Fast Cycle Time Hot Micro-Embossing Machine," S.M. Thesis,
Department of Mechanical Engineering, Massachusetts Institute of Technology,
Cambridge, MA, 2005.

Ehmann, K.F., et al. World Technology Evaluation Center Panel Report on International
Assessment of Research and Development in Micromanufacturing. October 2005.

Electrum Laboratory, Royal Institute of Technology in Stockholm. (2006 May), available:
http://www.electrumlab.se/artikel/908/047002/en .

Eteshola, E., D. Leckband. "Development and characterization of an ELISA assay in PDMS
microfluidic channels," in Sensors and Actuators B, vol. 72, pp. 129-133, 2001.

Fiorini, G. S., D. T. Chiu. "Disposable microfluidic devices: fabrication, function, and
application," BioTechniques, vol. 38, no. 3, pp. 429-446, March 2005.

Fluidigm Corporation. "The TOPAZ FID Crystallizer," in Screen-To-Beam Protein
Crystallization, South San Francisco, CA: 2005.

Foster, K., G. A. Parker, Fluidics: Components and Circuits. London: Wiley-Interscience, 1970.

Frederickson, R., "Bringing Integrated Circuits to Life," Bio-IT World, February 2003.

Gadish, N. " A Combined Microfluidic/Dielectrophoretic Mircoorganism Concentrator," M.Eng.
Thesis, Department of Electrical Engineering and Computer Science, Massachusetts
Institute of Technology, Cambridge, MA, 2005.

Goluch, E.D., et al. "Deposition and Patterning of Thin-Film Materials on Curved Surfaces using
Microfluidic Methods," in Proceedings of 9th International Conference on Miniaturized
Systems for Chemistry and Life Sciences, vol. 2, pp. 948-950, October 2005.

Han, F., et al. "Experimental attempts of sub-micrometer order size machining using micro-
EDM," in Precision Engineering, vol. 30, pp. 123-131, 2006.

Han, J., S.W. Turner, H.G. Craighead. "Entropic Trapping and Escape of Long DNA Molecules
at Submicron Size Constriction," in Physical Review Letters, vol. 83, no. 8, pp. 1688-
1691, August 1999.

Han, S. "Modeling and Analysis of Extrusion-Spin Coating: An Efficient and Deterministic
Photoresist Coating Method in Microlithography," S.M. Thesis, Department of
Mechanical Engineering, Massachusetts Institute of Technology, Cambridge, MA, 2001.

Hetsroni, G., A. Mosyak, E. Pogrebnyak, L. P. Yarin. "Fluid Flow in micro-channels,"
International Journal of Heat and Mass Transfer, vol. 48, pp. 1982-1998, 2005.

Human Genome Project, National Human Genome Research Institute, National Institutes of
Health. (May 2006), available: http://www.genome.gov/10001772

Hutchinson, J. B., et al. "Robust polymer microfluidic device fabrication via contact liquid photolithographic polymerization (CLiPP)," Lab on a Chip, vol. 4, pp. 658-662, 2004.

Idelchik, I. E., Handbook of Hydraulic Resistance. Third Edition. Boca Raton, FL: CRC Press, 1994.

Iowa State University Biotechnology Program. (May 2006), available: http://www.biotech.iastate.edu/publications/ppt_presentations/html/Fingerprinting/Studen tInstruction-gel/05.html

Jeon, N.L., et al. "Design and Fabrication of Integrated Passive Valves and Pumps" in Biomedical Microdevices, vol. 4, pp. 117-121, 2002.

Jo, B.-H., et al. "Three-Dimensional Micro-Channel Fabrication in Polydimethylsiloxane (PDMS) Elastomer," in Journal of Microelectromechanical Systems, vol. 9, no. 1, pp. 76-81, March 2000.

Jourdan, D., "Special Report: Microfluidics and bio Polymer microcomponents," Micronews: The Yole Developpement magazine for Semiconductors, MEMS, Nanotechnology, Bio & Microfluidic Chips and Optics, vol. 29, pp. 3-4, October 2004.

Juncker, D., et al. "Soft and rigid two-level microfluidic networks for patterning surfaces," in Journal of Micromechanics and Microengineering, vol. 11, pp. 532-541, 2001.

Kalpakjian, S., and S.R. Schmid. Manufacturing Engineering and Technology. 4th ed. Upper Saddle River, NJ: Prentice Hall, 2001.

Kaye, P. Microfluidic & Microengineering Group, University of Hertfordshire. (May 2006), available: http://strc.herts.ac.uk/mm/micromixers.html .

Kenis, P., R.F. Ismailov, G.M. Whitesides. "Microfabrication Inside Capillaries Using Multiphase Laminar Flow Patterning," in Science, vol. 285, pp. 83-85, July 2, 1999.

Killeen, K., et al. "Chip-LC/MS: HPLC-MS Using Polymer Microfluidics," in Proceedings of the 7th International Conference on Miniaturized Chemical and Biochemical Analysis Systems, Squaw Valley, CA, 2003, pp. 481-484.

Kim, D.S., et al. "A Collapse-Free Thermal Bonding Technique for Plastic Microfluidic Systems with Large Area Microchambers," in Proceedings of 9th International Conference on Miniaturized Systems for Chemistry and Life Sciences, vol. 1, pp. 684-686, October 2005.

Kim, J. Y., et al. "Automatic aligning and bonding system of PDMS layer for the fabrication of 3d microfluidic channels," in Sensor and Actuators A, vol. 119, pp. 593-598, 2005.

Kimball, J. K. (May 2006) "ELISA," Kimball's Biology Pages [online]. Available: http://users.rcn.com/jkimball.ma.ultranet/ .

Kopp, M.U., A. J. de Mello, A. Manz. "Chemical amplification: continuous-flow PCR on a chip," in Science vol. 280, pp. 1046–1048, 1998.

Kulite Semiconductor Products, Inc. (May 2006) Available: http://www.kulite.com

Langer, R. "Drug Delivery and Targeting," in Nature, vol. 392. pp. 5-10, 1998.

156

Leclerc, E., Y. Sakai, T. Fujii. "A Multi-Layer PDMS Microfluidic Device for Tissue Engineering Applications," in Proceedings IEEE Sixteenth Annual International Conference on Micro Electro Mechanical Systems, Kyoto, Japan, January 2003, pp. 415-418.

Manske, M. (2006 May), covered by the GNU FDL, available: http://en.wikipedia.org/wiki/Image:Pcr.png

McDonald, J.C., G.M. Whitesides. "Poly(dimethylsiloxane) as a Material for Fabricating Microfluidic Devices," in Accounts of Chemical Research, vol. 35, no. 7, pp. 491-499, July 2002.

Michigan High-Throughput Screening Center. (May 2006) "Services," Available: http://mhtsc.kvcc.edu/Services.htm

Micromoulding Interest Group. (May 2006) available: http://wombat.irc.brad.ac.uk/ben/page.php?id=14

Nguyen, N.-T., S. T. Wereley, Fundamentals and Applications of Microfluidics. Boston, MA: Artech House, 2002.

Nilsson, D., S. Balslev, A. Kristensen. "A microfluidic dye laser fabricated by nanoimprint lithography in a highly transparent and chemically resistant cyclo-olefin copolymer (COC)," Journal of Micromechanics and Microengineering, vol. 15, pp. 296-300, October 2004.

Noh, Kyungyoon. "Modeling of Dielectric Erosion and Copper Dishing in Copper Chemical-Mechanical Polishing," Ph.D. Thesis, Department of Mechanical Engineering, Massachusetts Institute of Technology, Cambridge, MA, 2005.

Ooe, H., et al. "Three-dimensional multilayered microstructure fabricated by imprint lithography," in Journal of Vacuum Science Technology B. vol. 23, no. 2, pp. 375-379, March/April 2005.

Pfohl, T. Biomaterialien und Mikrofluidik, University of Ulm. (May 2006), available: http://www.uni-ulm.de/uni/fak/natwis/angphys/english/projektgruppen/pfohl/pfohlgebiet.html

Plummer, J.D., M. D. Deal, P. B. Griffin, Silicon VLSI Technology: Fundamentals, Practice and Modeling. Upper Saddle River, NJ: Prentice Hall, 2000.

Pria Diagnostics LLC. (May 2006), available: http://www.priadiagnostics.com.

Proton Mikrotechnik. (May 2006), available: http://www.protron-mikrotechnik.de/protron_home_e.htm .

Randall, G. C., P. S. Doyle. "Permeation flow in poly(dimethylsiloxane) microfluidic devices," Proceedings of the National Academy of Sciences, vol. 102, no. 31, pp. 10813-10818, August 2005.

Sanger Institute. "About Frederick Sanger" (May 2006), available: http://www.sanger.ac.uk/Info/Intro/sanger.shtml

Santini, J., M. Cima, R. Langer. "A Controlled-release Microchip," in Nature, vol. 397, pp. 335-338, 1999.

Stoeber, B. Personal Webpage (May 2006), available
http://www.cchem.berkeley.edu/~sjmgrp/people/boris/boris.htm .

Suh, N. P. Axiomatic Design: Advances and Applications. New York, NY: Oxford University Press, 2001.

Texas Instruments Incorporated. "Digital Light Processing Technology," (May 2006) available: http://dlp.com .

Thaker, K. "Design of a Micro-Fluidic Functional Testing System for Process Characterization of a Hot Micro-Embossing Machine," S.M. Thesis, Department of Mechanical Engineering, Massachusetts Institute of Technology, Cambridge, MA, 2006.

Theilade, U.R.A. "Surface micro topography replication in injection moulding," Ph.D. Thesis, Department of Manufacturing Engineering and Management, Technical University of Denmark, Lyngby, Denmark, 2004.

Townsend, R. J., et al. "Fluid modeling of microfluidic separator channels," Sensors and Actuators B, vol. 111-112, pp. 455-462, 2005.

Tseng Research Group, Department of Molecular & Medical Pharmacology, University of California, Los Angeles. (May 2006), available: http://labs.pharmacology.ucla.edu/tsenglab/labtour/microfluidics.htm.

Urbanski, J.P. Private interview, 24 September 2004.

Verpoorte, E., N. F. De Rooij. "Microfluidics Meets MEMS," Proceedings of the IEEE, vol. 91, no. 6, pp. 930-953, June 2003.

Vitae LLC. (May 2006), available: http://www.vitaellc.com/pages/technology.htm .

Voldman, J., M. L. Gray, M. A. Schmidt. "Microfabrication in Biology and Medicine," Annual Review of Biomedical Engineering, vol. 1, pp. 401-425, 1999.

Wang, Q. " Process Window and Variation Characterization of Micro-Embossing Process," S.M. Thesis, Department of Mechanical Engineering, Massachusetts Institute of Technology, Cambridge, MA, 2006.

White, F. M. Fluid Mechanics. Fourth Edition. Boston, MA: McGraw-Hill, 1999.

Whitesides, G.M. (May 2006), available gmwgroup.harvard.edu . Figure 4-11: http://gmwgroup.harvard.edu/research_microfluidics/figure4.html

Whitney, D. E. Mechanical Assemblies: Their Design, Manufacture, and Role in Product Development. New York, NY: Oxford University Press, 2004.

Zhao, X.-M., Y. Xia, G.M. Whitesides. "Soft lithographic methods for nano-fabrication," in Journal of Materials Chemistry, vol. 7, no. 7, pp. 1069-1074, 1997.

Appendix A: Chemical-Mechanical Polishing Test Wafer

Chemical-mechanical polishing is a step in the fabrication of modern micro-electronic devices, most commonly in very-large scale integrated (VLSI) devices. This is a general heading that encompasses many different types of devices that are similar in little more than their complexity and that work with the same tools and materials. These devices start with a bare silicon wafer, and build from there into the complex chips that are the heart and memory of any modern electronic device. The wafer is processed at or near its surface to form the tiny transistors, resistors, capacitors, inductors, and other tiny incarnations of electronic circuitry. Thereafter, all of the circuit components have to be connected to one another, and this is done in successive layers on top of the wafer, known as interconnects, which transverse each layer, and via plugs, which penetrate from one layer to the next.

In Figure A-1, the typical process of creating a layer of interconnects is shown. Employing photolithography, the bulk material is patterned and selectively etched away, creating the holes into which the metallic via and interconnect material will be deposited. Next, the metal is deposited, filling the holes and creating a layer on top of the substrate, as well. The desired final state is one in which the excess metal has been removed, down to the insulator, so that another layer of insulator can be uniformly deposited across the wafer. This will then be selectively etched, leading to the next repetition of the process. The process used to remove the excess metal is called chemical-mechanical polishing, or CMP.

CMP, as the name implies, uses a simultaneous assault of chemical and mechanical methods to grind down the deposited material atop the wafer. An example of what a CMP machine looks like is shown in Figure A-2.
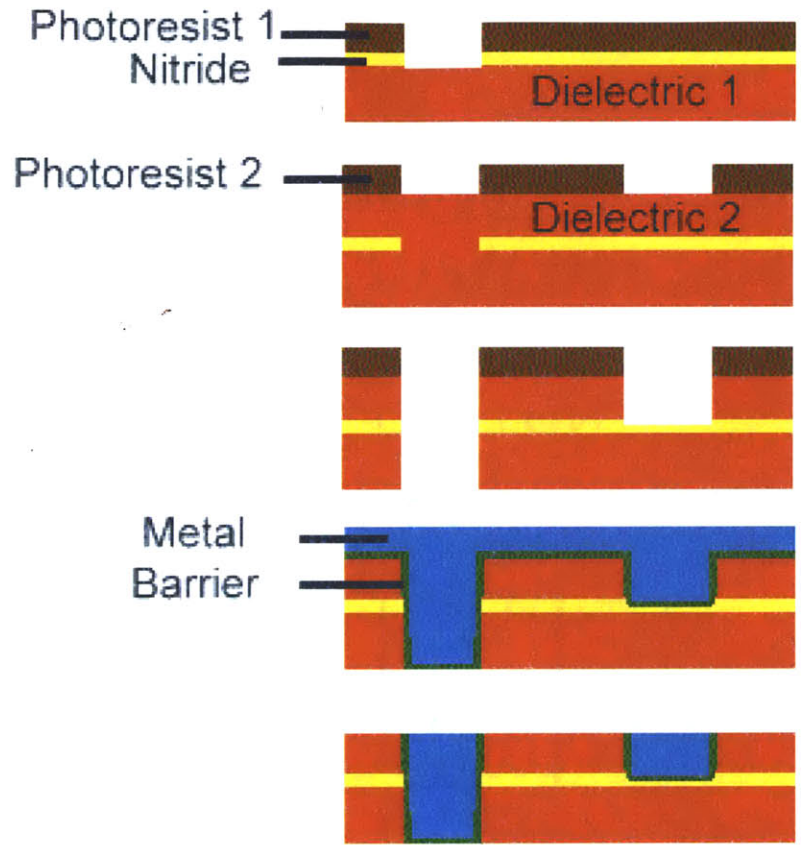
Figure A-1: Diagram of Silicon Wafer Processing, showing the CMP step.

The wafer is placed face down on a special pad. A specially constituted slurry that consists of an abrasive and a corrosive chemical is eluted into the interface between the pad and wafer. Then, the wafer and polishing pad are simultaneously rotated at the same angular speed. The pad is more than twice the diameter of the wafer, and where the axes of the pad rotation and wafer rotation are parallel but non-collinear, the magnitude of the relative velocity between the pad and the wafer is conveniently uniform across the wafer, insuring a nominally uniform rate of polishing.

The reason CMP is used as opposed to more conventional methods of etching, is due in large part to the chemical properties of the common metallic interconnect material employed: copper. For an etch to be successful, there needs to be a chemical compatibility between the etchant and the bulk where the etchant is very effective at dissolving or otherwise removing the bulk. For the common insulators of silicon nitride and silicon oxide, such relationships exist. But for copper, it makes more sense to use CMP.
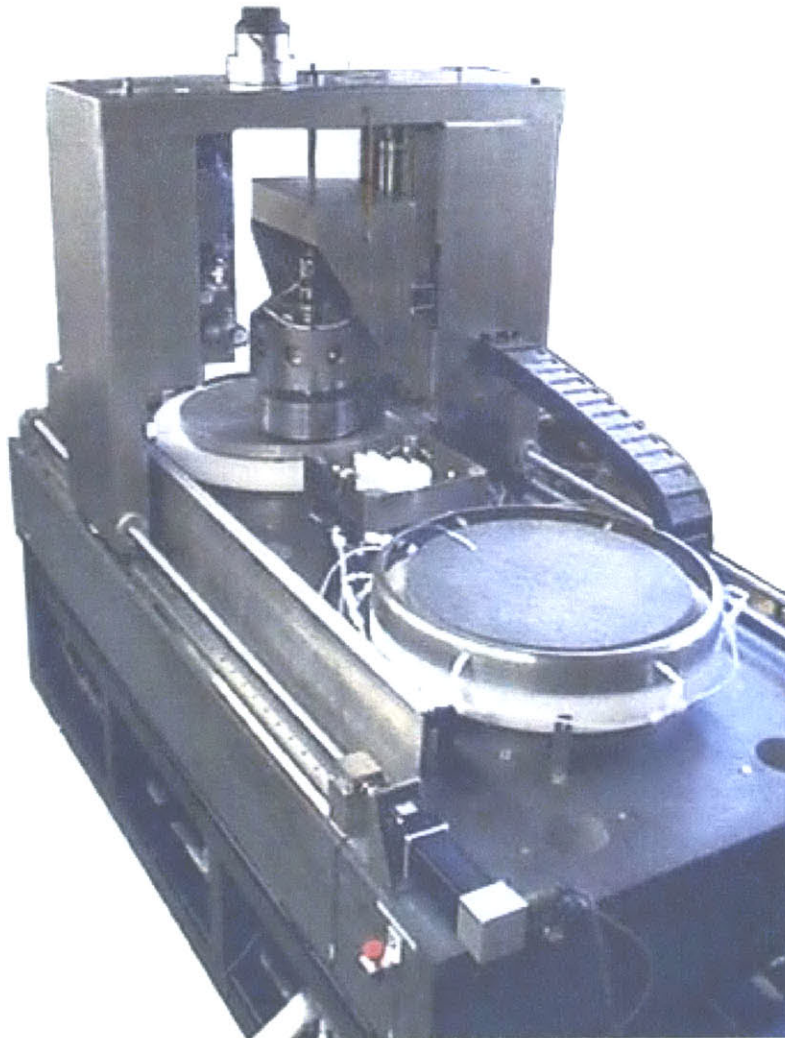
Figure A-2: A Chemical-Mechanical Polishing Machine.

The nominally uniform rate of polishing across the wafer is unfortunately only nominal. There are many factors that can lead to non-uniformity in the polishing rate, and entire research groups have been devoted to examining and improving CMP. Among these might be incomplete penetration of the slurry in between the pad and wafer, uneven pressure across the wafer, as well as variations in the patterns that are present on the surface of the wafer. In order to evaluate different machines against each other as to which performs CMP better, the test wafer was developed.

The singular key characteristic of interest after CMP is performed is planarity. A polish that creates a very flat wafer after the process is successful, and one that does not is unsuccessful. Variations can be between features that are next to one another, between different areas within a

die, or across the area of the wafer. Dies arose as the size of wafer employed in microelectronics processing grew larger than the size of the chips that ultimately get used in the devices. Thus, a given wafer will have the same pattern of chip repeated over an over across its area. The pattern is known as a die.

The singularity of planarity as the output parameter of importance makes distinguishing between the processes easier, if the input parameters can be justifiably representative of the diversity of inputs that CMP might be required to deal with.

In his work with CMP, Noh [2005] identified two parameters to represent the general variations that might be represented on a microelectronic chip. These are shown in Figure A-3, along with a representation of the variations across the wafer, across a die, and at the feature level.

The two parameters he chose to represent the general input variables were line width, shown as w in Figure A-3, and spatial frequency, shown as λ. The die he constructed featured line width and spatial frequency systematically varied from appropriate minimums to maximums. By using this test wafer in different machines, it would be possible to see which machine was able to polish to the greatest uniformity across the widest variation of feature sizes and arrangements, over the size of the entire wafer.
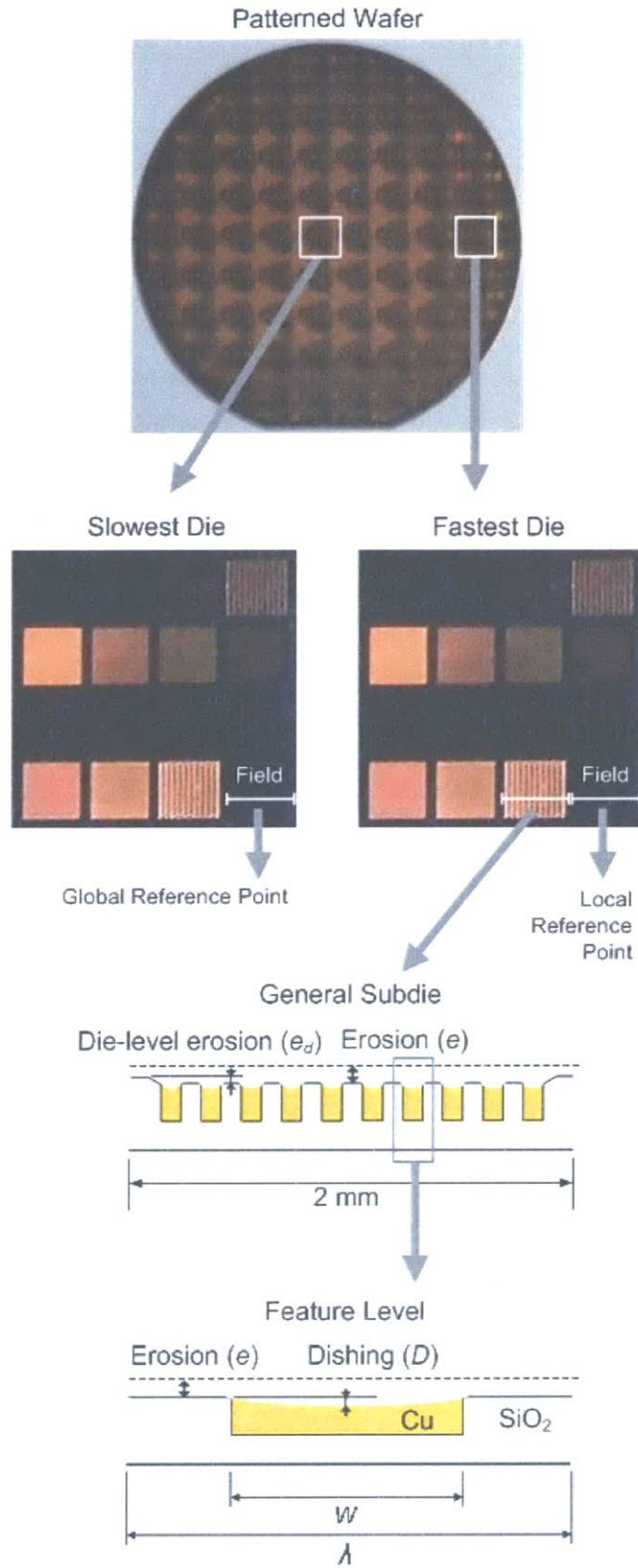
Figure A-3: Variation Across a Test Wafer. From Noh [2005].

Appendix B: Material Data Sheets

(from Dow Corning)

Information about *Dow Corning*® brand Silicone Encapsulants

Silicones and Electronics

Long-term, reliable protection of sensitive circuits and components is becoming more important in many of today's delicate and demanding electronic applications. Silicones function as durable dielectric insulation, as barriers against environmental contaminants and as stress-relieving shock and vibration absorbers over a wide temperature and humidity range.

In addition to sustaining their physical and electrical properties over a broad range of operating conditions, silicones are resistant to ozone and ultraviolet degradation, have good chemical stability and are available in a variety of useful forms as conformal coatings, encapsulants and adhesives. Dow Corning's broad range of general purpose and specialty products offers you a choice of materials for your application needs.

DESCRIPTION

Dow Corning® silicone encapsulants are supplied as two-part liquid component kits comprised of:

Mix Ratio (by weight or volume)	Components (as supplied)
1:1	Part A/Part B
10:1	Base/Curing agent

When liquid components are thoroughly mixed, the mixture cures to a flexible elastomer, which is suited for the protection of electrical/electronic applications. *Dow Corning* silicone encapsulants cure without exotherm at a constant rate regardless of sectional thickness or degree of confinement. *Dow Corning* silicone elastomers require no post cure and can be placed in service immediately following the completion of the cure schedule with an operating temperature range of –45 to 200°C (–49 to 392°F). Select materials have been classified by Underwriters Laboratories and/or meet military specifications. Standard silicone encapsulants require a surface treatment with a primer in addition to good cleaning for adhesion while primerless silicone encapsulants require only good cleaning.

Two-Part Silicone Elastomers

Type
Elastomers

Physical Form
Two-part silicone elastomers

Special Properties
Flowable liquid; cures to flexible elastomer; constant cure rate, regardless of sectional thickness or degree of confinement; service range of –45 to 200°C (–49 to 392°F); no post cure required

Potential Uses
Protection of electrical/electronic devices

DOW CORNING

164

PRODUCT INFORMATION

Product	Description	Features
Silicone Encapsulants		
Sylgard 182 Silicone Elastomer	Transparent; long pot life; heat cure	Two part; 10:1 mix; minimal shrinkage; no exotherm during cure; no solvents or cure byproducts; deep section cure; repairable; good dielectric properties; flexible elastomer
Sylgard 184 Silicone Elastomer	Transparent; RT/HA cure	

Product	Potential Uses	Application Methods	Cure[1,2]
Silicone Encapsulants			
Sylgard 182 Silicone Elastomer	General potting applications: power supplies, connectors, sensors, industrial controls, transformers, amplifiers, high voltage resistor packs, relays; adhesive/encapsulant for solar cells; adhesive handling beam lead integrated circuits during processing	Supplied as two-part liquid component kits comprised of Base/Curing Agent to be mixed in a 10:1 ratio by weight or volume; automated mixing and dispensing; manual mixing	45 minutes at 100°C (212°F) 20 minutes at 125°C (257°F) 10 minutes at 150°C (302°F)
Sylgard 184 Silicone Elastomer			~48 hours at room temp 45 minutes at 100°C (212°F) 20 minutes at 125°C (257°F) 10 minutes at 150°C (302°F)

TYPICAL PROPERTIES

Specification Writers: Please contact your local Dow Corning sales office or your Global Dow Corning Connection before writing specifications on this product.

Product	Mix Ratio	Color	Viscosity, centipoise or mPa·s	Durometer, Shore A	Specific Gravity	Working Time at RT	Unprimed Adhesion, Lap Shear			Thermal Conductivity		Linear Coefficient of Thermal Expansion, µm/m·°C or ppm	Shelf Life from Date of Manufacture at Room Temp, months
							psi	MPa	kgf/cm²	Watt/meter·°K	cal/cm·sec·°C		
Silicone Encapsulants													
Sylgard 184 Silicone Elastomer	10:1	Clear	3900	50	1.03	>2 hours	NA	NA	NA	0.18	4.3 x 10⁻⁴	310	24

Product	UL Listing		Military Specification		Dielectric Strength		Dielectric Constant at 100 Hz	Dielectric Constant at 100 kHz	Volume Resistivity, ohm-cm	Dissipation Factor at 100 Hz	Dissipation Factor at 100 kHz
	Flammability Classification	UL Temperature Index, Electrical/Mechnical, °C	Specification	Type, Class, Group	volts/mil	kV/mm					
Silicone Encapsulants											
Sylgard® 184 Silicone Elastomer	94 V-1	130/130	MIL-I-81550C	Type I, QPL	540	21.2	2.65	2.65	1.2×10^{14}	0.0005	<0.001

MIXING – 1:1/PART A:PART B

Dow Corning silicone 1:1 encapsulants are supplied in two parts that do not require lot matching. The 1:1 mix ratio, by weight or volume, simplifies the proportioning process. To ensure uniform distribution of filler, Parts A and B must each be thoroughly mixed prior to their combination in a 1:1 ratio. When thoroughly blended, the Part A and B liquid mixture should have a uniform appearance. The presence of light-colored streaks or marbling indicates inadequate mixing and will result in incomplete cure.

Due to the fast-curing characteristics of some encapsulants included in this data sheet, automated mix and dispense equipment should be utilized. In applications sensitive to air entrapment, deairing with 28 to 30 inches Hg vacuum is required.

MIXING – 10:1/BASE:CURING AGENT

Dow Corning silicone 10:1 encapsulants are supplied in two parts as lot-matched base and curing agent that are mixed in a ratio of 10 parts base to one part curing agent, by weight. After thoroughly mixing base and curing agent, agitate gently to reduce the amount of air introduced. Allowing the mixture to set for 30 minutes before pouring may be adequate for removal of the air introduced during mixing. If air bubbles are still present, vacuum deairing may be required. Deair in a container with at least four times the liquid volume to allow for expansion of material. Air entrapped in the mixture can be removed by using a vacuum of 28 to 30 inches Hg. Continue

the vacuum until the liquid expands and settles to its original volume and bubbling subsides. This may take 15 minutes to 2 hours depending on the amount of air introduced during stirring. For best curing results, glassware and glass or metal stirring implements should be used. Mix with a smooth action that does not introduce excess air.

POT LIFE/WORKING TIME

Cure reaction begins with the mixing process. Initially, cure is evidenced by a gradual increase in viscosity, followed by gelation and conversion to a solid elastomer. Pot life is defined as the time required for viscosity to double after Parts A and B (base and curing agent) are mixed. Please refer to individual pot life for each silicone encapsulant.

PROCESSING AND CURING

Thoroughly mixed *Dow Corning* silicone encapsulant may be poured/dispensed directly into the container in which it is to be cured. Care should be taken to minimize air entrapment. When practical, pouring/dispensing should be done under vacuum, particularly if the component being potted or encapsulated has many small voids. If this technique cannot be used, the unit should be evacuated after the silicone encapsulant has been poured/dispensed.

Dow Corning silicone encapsulants may be either room temperature (25°C/77°F) or heat cured. Room temperature cure encapsulants may also be heat accelerated for faster cure. Ideal

166

cure conditions for each product are given in the product selection table. Two-part condensation cure encapsulants should not be heat accelerated above 60°C (140°F).

Dow Corning® 255 Curing Agent should be stirred prior to use because some settling may occur during shipping and storage. The curing agent is reactive with atmospheric moisture so care should be exercised to limit exposure to air prior to use.

PREPARING SURFACES

In applications requiring adhesion, priming will be required for the silicone encapsulants. See the Primer Selection Guide for the correct primer to use with a given product. For best results, the primer should be applied in a very thin, uniform coating and then wiped off after application. After application, it should be thoroughly air dried prior to application of the silicone elastomer. Additional instructions for primer usage can be found in the Dow Corning literature, "How To Use Dow Corning Primers and Adhesion Promoters" (Form No. 10-366) and in the information sheets specific to the individual primers.

USEFUL TEMPERATURE RANGES

For most uses, silicone elastomers should be operational over a temperature range of -45 to 200°C (-49 to 392°F) for long periods of time. However, at both the low and high temperature ends of the spectrum, behavior of the materials and performance in particular applications can become more complex and require additional considerations.

For low-temperature performance, thermal cycling to conditions such as -55°C (-67°F) may be possible, but performance should be verified for your parts or assemblies. Factors that may influence performance are configuration and stress sensitivity of components, cooling rates and hold times, and prior temperature history. There are specialized products including Dow Corning® 3-6121 Encapsulating Elastomer that can perform at -65°C (-85°F) and below.

At the high-temperature end, the durability of the cured silicone elastomer is time and temperature dependent. As expected, the higher the temperature, the shorter the time the material will remain usable.

COMPATIBILITY

Certain materials, chemicals, curing agents and plasticizers can inhibit the cure of Dow Corning silicone encapsulants. Most notable of these include:
- Organotin and other organometallic compounds
- Silicone rubber containing organotin catalyst
- Sulfur, polysulfides, polysulfones or other sulfur-containing materials
- Amines, urethanes or amine-containing materials
- Unsaturated hydrocarbon plasticizers
- Some solder flux residues

If a substrate or material is questionable with respect to potentially causing inhibition of cure, it is recommended that a small scale compatibility test be run to ascertain suitability in a given application. The presence of liquid or uncured product at the interface between the questionable substrate and the cured gel indicates incompatibility and inhibition of cure.

Dow Corning 255 Elastomer is not subject to these inhibition concerns but may experience reversion in sealed applications at high temperature and pressure.

REPAIRABILITY

In the manufacture of electrical/electronic devices it is often desirable to salvage or reclaim damaged or defective units. With most non-silicone rigid potting/encapsulating materials, removal or entry is difficult or impossible without causing excessive damage to internal circuitry. Dow Corning silicone encapsulants can be selectively removed with relative ease, any repairs or changes accomplished, and the repaired area repotted in place with additional product.

To remove silicone elastomers, simply cut with a sharp blade or knife and tear and remove unwanted material from the area to be repaired. Sections of the adhered elastomer are best removed from substrates and circuitry by mechanical action such as scraping or rubbing and can be assisted by applying Dow Corning® brand OS Fluids.

Before applying additional encapsulant to a repaired device, roughen the exposed surfaces of the cured encapsulant with an abrasive paper and rinse with a suitable solvent. This will enhance adhesion and permit the repaired material to become an integral matrix with the existing encapsulant. Silicone prime coats are not recommended for adhering products to themselves.

HANDLING PRECAUTIONS

Dow Corning 255 Elastomer curing agent and uncured catalyzed material will burn skin and eyes upon prolonged contact. In case of eye contact, flush with copious amounts of water for at least 15 minutes and seek medical attention at once. Skin contact areas should be washed with soap and water. Persistent irritation should receive medical attention. Use only with adequate ventilation; if not available, use respiratory protection.

PRODUCT SAFETY INFORMATION REQUIRED FOR SAFE USE IS NOT INCLUDED IN THIS DOCUMENT. BEFORE HANDLING, READ PRODUCT AND MATERIAL SAFETY DATA SHEETS AND CONTAINER LABELS FOR SAFE USE, PHYSICAL AND HEALTH HAZARD INFORMATION. THE MATERIAL SAFETY DATA SHEET IS AVAILABLE ON THE DOW CORNING WEBSITE AT WWW.DOWCORNING.COM, OR FROM YOUR DOW CORNING REPRESENTATIVE, OR DISTRIBUTOR, OR BY CALLING YOUR GLOBAL DOW CORNING CONNECTION.

USABLE LIFE AND STORAGE

Shelf life is indicated by the "Use By" date found on the product label.

For best results, Dow Corning silicone encapsulants should be stored at or below 25°C (77°F). Special precautions must be taken to prevent moisture from contacting these materials. Containers should be kept tightly closed and head or air space minimized. Partially filled containers should be purged with dry air or other gases, such as nitrogen.

Dow Corning 255 Elastomer should be kept refrigerated (10°C/50°F) until use. Any special storage and handling instructions will be printed on the product containers.

PACKAGING

In general, *Dow Corning* silicone 1:1 mix ratio encapsulants are supplied in nominal 0.45-, 3.6-, 18- and 200-kg (1-, 8-, 40- and 440-lb) containers, net weight. *Dow Corning* silicone 10:1 mix ratio encapsulants are supplied in nominal 0.5-, 5-, 25- and 225-kg (1.1-, 11-, 55- and 495-lb) containers, net weight. Packaging options may vary by product. Consult Dow Corning Customer Service at (989) 496-6000 for additional packaging options.

LIMITATIONS

These products are neither tested nor represented as suitable for medical or pharmaceutical uses.

HEALTH AND ENVIRONMENTAL INFORMATION

To support customers in their product safety needs, Dow Corning has an extensive Product Stewardship organization and a team of Product Safety and Regulatory Compliance (PS&RC) specialists available in each area.

For further information, please see our website, www.dowcorning.com, or consult your local Dow Corning representative.

LIMITED WARRANTY INFORMATION – PLEASE READ CAREFULLY

The information contained herein is offered in good faith and is believed to be accurate. However, because conditions and methods of use of our products are beyond our control, this information should not be used in substitution for customer's tests to ensure that Dow Corning's products are safe, effective, and fully satisfactory for the intended end use. Suggestions of use shall not be taken as inducements to infringe any patent.

Dow Corning's sole warranty is that the product will meet the Dow Corning sales specifications in effect at the time of shipment.

Your exclusive remedy for breach of such warranty is limited to refund of purchase price or replacement of any product shown to be other than as warranted.

DOW CORNING SPECIFICALLY DISCLAIMS ANY OTHER EXPRESS OR IMPLIED WARRANTY OF FITNESS FOR A PARTICULAR PURPOSE OR MERCHANTABILITY.

DOW CORNING DISCLAIMS LIABILITY FOR ANY INCIDENTAL OR CONSEQUENTIAL DAMAGES.

(from GE Silicones)

GE Silicones

RTV655

Product Description RTV615, RTV655 and RTV656 silicone rubber compounds are clear liquids which cure at room temperature to high strength silicone rubber with the addition of curing agents. These two-component products are supplied with curing agent in matched kits which are designed for use at a convenient 10:1 ratio by weight.

These compounds are clear and colorless but differ in low temperature flexibility. All three are low viscosity, easily pourable liquids with nominal viscosities ranging between 3000 and 7000 cps. RTV655 and RTV656 silicone rubber compounds have the capability of remaining flexible at temperatures -115°C (-175°F).

RTV615, RTV655 and RTV656 silicone rubber compounds have been used for protection of electronic components and assemblies against shock, vibration, moisture, ozone, dust, chemicals, and other environmental hazards by potting or encapsulation of the components and assemblies.

The optical clarity of these silicone rubber compounds suggests evaluation for applications such as potting solar cells for maximum light transmission and electronic assemblies where component identification is necessary or desirable. RTV655 and RTV656 silicone rubber compound are preferred where flexibility at temperatures down to -115°C (-175°F) is required.

Key Performance Properties

- Convenient 10:1 mixing ratio for use in automatic dispensing or hand operations
- Low viscosity allows easy flow in and around complex parts, providing excellent electrical insulation and shock resistance
- Cure rate can be accelerated by heat
- Will cure in deep sections or enclosed assemblies without exotherm and with low shrinkage
- Chemical composition contains no solvents for ease of use on production lines
- Reversion resistance and hydrolytic stability permit use in high humidity environments at elevated temperatures

- Clarity permits visual inspection for easy identification and repair of encapsulated parts
- Retention of elastomeric properties at temperatures up to 204°C (400°F)

UNCURED PROPERTIES	RTV615A	RTV615B	RTV655A	RTV655B	RTV656A	RTV656B
Color	Clear Colorless	Clear Colorless	Clear Colorless	Clear Colorless	Clear Colorless	Clear Colorless
Consistency	Easily Pourable	Easily Pourable	Easily Pourable	Easily Pourable	Easily Pourable	Easily Pourable
Viscosity, cps	4300	—	5700	—	5000	—
Specific Gravity	1.02	—	1.04	—	1.03	—

UNCURED PROPERTIES WITH CURING AGENT ADDED	RTV615	RTV655	RTV656
Color	Clear, Colorless	Clear, Colorless	Clear, Colorless
Consistency	Easily Pourable	Easily Pourable	Easily Pourable
Viscosity, cps	4000	5200	5000
Work Time @ 25°C (77°F), hrs	4	4	4

CURED PROPERTIES (Cured 1 hr. @ 100C/212F)	RTV615	RTV655	RTV656
Mechanical			
Hardness, Shore A Durometer	44	45	44
Tensile Strength, kg/cm^2 (psi)	65 (920)	65 (920)	65/(920)
Elongation, %	120	120	100
Shrinkage, %	0.2	0.2	0.2
Refractive Index	1.406	1.430	1.430

Electrical			
Dielectric Strength, kv/mm (v/mil) (1.9 mm thick)	19.7 (500)	19.7 (500)	19.7 (500)
Dielectric Constant @ 1000 Hz	2.7	2.69	2.69
Dissipation Factor @ 1000 Hz	0.0006	0.0004	0.0004
Volume Resistivity, ohm-cm	1.8×10^{15}	1.2×10^{15}	1.2×10^{15}
Thermal			
Useful Temperature Range, °C (°F)	-60 to 204 (-75 to 400)	-115 to 204 (-175 to	-115 to 204 (-175 to

		400)	400)
Thermal Conductivity, gm-cal/sec, cm^2, °C/cm (Btu/hr, ft^2, °F/ft)	0.00045 (0.11)	0.00045 (0.11)	0.00045 (0.11)
Coefficient of Expansion, cm/cm, °C (in/in, °F)	27 x 10^{-5} (15.3 x 10^{-5})	33 x 10^{-5} (18.3 x 10$_{-5}$)	33 x 10^5 18.3 x 10^{-5})
Specific Heat, cal/gm, °C (Btu/lb, °F)	0.3 (0.3)	0.3 (0.3)	0.3 (0.3)

FDA STATUS

RTV615 silicone rubber compound and SS4120 silicone primer may be used in food contact applications where FDA regulations apply.

Compatibility

RTV615, RTV655 and RTV656 silicone rubber compounds will cure in contact with most clean, dry surfaces. However, certain materials, such as butyl and chlorinated rubber, sulfur-containing materials, amines, and certain metal soap-cured RTV silicone rubber compounds, can cause cure inhibition. Cure inhibition is characterized by a gummy appearance of the RTV silicone rubber compound at the interface between it and the substrate.

It is recommended that a sample patch test be performed with RTV615, RTV655 and RTV656 silicone rubber compounds to determine if a barrier coating or other inhibition-preventing measures are necessary before pouring the material.

Mixing

Select a mixing container 4-5 times larger than the volume of RTV silicone rubber compound to be used. Weigh out ten parts of the A component and one part of the B component. Since RTV615, RTV655 and RTV656 silicone rubber compounds are kit-matched, work time (or pot life), cure time, and final properties of the cured RTV silicone rubber compound can be assured only if the A component is used with the B component from the same kit.

With clean tools, thoroughly mix the A and B components together, scraping the sides and bottom of the container carefully to produce a homogeneous mixture. When using power mixers, avoid excessive speeds which could entrap large amounts of air or cause overheating of the mixture, resulting in shorter pot life.

Deaeration

Air entrapped during mixing should be removed to eliminate voids in the cured product. Expose the mixed material to a vacuum of about 25 mm (29 in.) of mercury. The material will expand, crest, and recede to approximately the original level as the bubbles break. Degassing is usually complete approximately two minutes after frothing ceases. When using the RTV silicone rubber compound for potting, a deaeration step may be necessary after pouring to avoid capturing air in complex assemblies.

Automatic equipment designed to meter, mix, deaerate, and dispense two-component RTV silicone rubber compounds will add convenience to continuous or large volume operations. For additional information refer to GE Silicones equipment guide (1758).

Curing

RTV615, RTV655 and RTV656 silicone rubber compounds will cure sufficiently in 24 hours at 25C (77F) to permit handling. To achieve optimum properties an elevated temperature cure or a cure time of 7 days at room temperature is required. The table below illustrates the effect of temperature on cure time:

Temperature, °C (°F)	Cure Time*
25 (77)	6-7 days
65 (149)	4 hrs.
100 (212)	1 hr.
125 (257)	45 min.
150 (302)	15 min.

* Cure times are only approximate. The actual time is affected by the mass of the unit and the time required to reach the desired temperature.

Bonding

These silicone rubber compounds require a primer to bond to non-silicone surfaces. RTV656 is tested for adhesion and will typically outperform RTV656 when a very low temperature adhesive/encapsulant is needed. All of these products do require a primer for bonding as stated herein.

Thoroughly clean the substrate with a non-oily solvent such as naphtha or methyl ethyl ketone and allow to dry. Then apply a uniform thin film of SS4155 silicone primer and allow the primer to air dry for one hour or more. Finally, apply freshly catalyzed RTV silicone rubber compound to the primed surface and cure as recommended. When dry, SS4155 silicone primer exhibits a white haze which will show through RTV615, RTV655 and RTV656 silicone rubber compounds. If the appearance of the surface to be bonded must be unchanged, SS4120 silicone primer (which dries to an invisible film) may be used. For more details on priming and adhesion, refer to GE Silicones data sheet on silicone primers (1873).

Handling and Safety Material Safety Data Sheets are available upon request from GE Silicones. Similar information for solvents and other chemicals used with GE products should be obtained from your suppliers. When solvents are used, proper safety precautions must be observed.

Caution

RTV615B, RTV655B and RTV656B curing agents can generate flammable hydrogen gas upon contact with acidic, basic, or oxidizing materials. Such contact should be avoided.

172

Storage and Warranty Period	The warranty period is 12 months from date of shipment from GE Silicones if stored in the original unopened container at a temperature of 27°C (80°F) or below.
Availability	RTV615, RTV655 and RTV656 silicone rubber compounds may be ordered from GE Silicones, Waterford, NY, 12188, the GE Silicones sales office nearest you or an authorized GE silicone product distributor.
Government Requirement	Prior to considering use of a GE Silicones product in fulfilling any Government requirement, please contact the Government and Trade Compliance office at 413-448-4624.

CDS1870

MICRO•CHEM

NANO™ SU-8 2000

Negative Tone Photoresist
Formulations 2035-2100

Square posts in thick SU-8 2000

- **High aspect ratio imaging**
  Near vertical side walls

- **Near UV (350-400nm) processing**

- **Improved coating properties**
  Uniformity (lower surface tension)
  Adhesion

- **Faster drying**
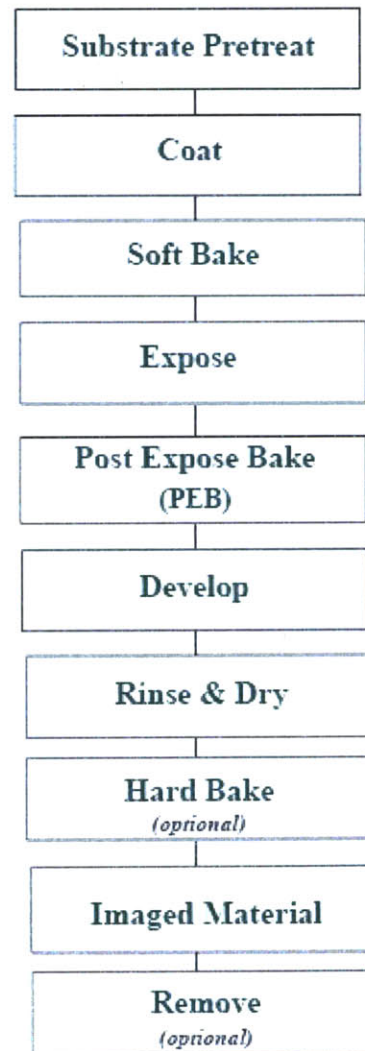 Improved throughput

SU-8 2000 is a high contrast, epoxy based photoresist designed for micromachining and other microelectronic applications, where a thick, chemically and thermally stable image is desired. SU-8 2000 is an improved formulation of SU-8, which has been widely used by MEMS producers for many years. By using a faster drying, more polar solvent system, improved coating properties and higher throughput are realized. Film thicknesses of 0.5 to >200mm can be achieved with a single coat process. The excellent imaging characteristics of SU-8 are maintained. The exposed and subsequently cross-linked portions of the film are rendered insoluble to liquid developers. SU-8 2000 has very high optical transparency above 360nm, which makes it ideally suited for imaging near vertical sidewalls in very thick films. SU-8 2000 is best suited for permanent applications where it is imaged, cured and left in place

Process Guidelines

SU-8 2000 is most commonly processed with conventional near UV (350-400nm) radiation, although it may be imaged with e-beam or x-ray. i-line (365nm) is recommended. Upon exposure, cross-linking proceeds in two steps (1) formation of a strong acid during the exposure process, followed by (2) acid-initiated, thermally driven epoxy cross-linking during the post exposure bake (PEB) step.

Substrate Pretreat
Coat
Soft Bake
Expose
Post Expose Bake (PEB)
Develop
Rinse & Dry
Hard Bake *(optional)*
Imaged Material
Remove *(optional)*

A normal process is: spin coat, soft bake, expose, post expose bake (PEB) followed by develop. A controlled hard bake is recommended to further cross-link the imaged SU-8 2000 structures when they will remain as part of the device. The entire process should be optimized for the specific application. A baseline process is given here to be used as a starting point.

Substrate Pretreat

To obtain maximum process reliability, substrates should be clean and dry prior to applying the SU-8 2000 resist. Start with a solvent cleaning, or a rinse with dilute acid, followed by a DI water rinse. Where applicable, substrates should be subjected to a piranha etch / clean (H_2SO_4 & H_2O_2). To dehydrate the surface, bake at 200°C for 5 minutes on a contact hot plate or 30 minutes in a convection oven. Adhesion promoters are typically not required. For applications that require electroplating and subsequent removal of SU-8 2000 apply MicroChem's OmniCoat prior to processing.

Coat

SU-8 2000 resists are designed to produce low defect coatings over a very broad range of film thickness. The film thickness versus spin speed data displayed in Table 1 and Figure 1 provide the information required to select the appropriate SU-8 2000 resist and spin conditions, to achieve the desired film thickness.

The recommended coating conditions are:

(1) STATIC Dispense: Approximately 1ml of SU-8 2000 per inch of substrate diameter.
(2) Spread Cycle: Ramp to 500 rpm at 100 rpm/second acceleration. Hold at this speed for 5-10 seconds to allow the resist to cover the entire surface.
(3) Spin Cycle: Ramp to final spin speed at an acceleration of 300 rpm/second and hold for a total of 30 seconds.
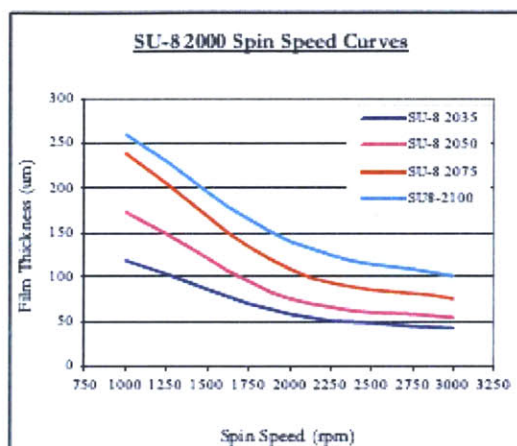

Figure 1. Spin speed vs. thickness curves for selected SU-8 2000 resists.

Soft Bake

After the resist has been applied to the substrate, it must be soft baked to evaporate the solvent and densify the film. SU-8 2000 is normally baked on a level hot plate, although convection ovens may be used. The following bake times are based on contact hot plate processes. Bake times should be optimized for proximity and convection oven bake processes since solvent evaporation rate is influenced by the rate of heat transfer and ventilation.

For best results, ramping or stepping the soft bake temperature is recommended. Lower initial bake temperatures allow the solvent to evaporate out of the film at a more controlled rate, which results in better coating fidelity, reduced edge bead and better resist-to-substrate adhesion. Refer to Table 2. for TWO STEP contact hot plate process recommendations.

Product Name	Viscosity (cSt)	Thickness (ums)	Spin Speed (rpm)
		35	3000
SU-8 2035	7000	55	2000
		110	1000
		50	3000
SU-8 2050	14000	75	2000
		165	1000
		75	3000
SU-8 2075	22000	110	2000
		225	1000
		100	3000
SU-8 2100	45000	140	2000
		260	1000

Product Name	Thickness (µms)	Pre-bake @ 65°C	Softbake @ 95°C
	35	2	5
SU-8 2035	55	3	6
	110	5	20
	50	3	6
SU-8 2050	75	3	9
	165	5	30
	75	3	9
SU-8 2075	110	5	20
	225	5	45
	100	5	20
SU-8 2100	140	5	35
	260	7	60

Table 1. Thickness vs. spin speed data for selected SU-8 2000 resists.
** Approximate

Table 2. Recommended soft bake parameters

Expose

SU-8 is optimized for near UV (350-400nm) exposure. i-line exposure tools are recommended. SU-8 is virtually transparent and insensitive above 400nm but has high actinic absorption below 350nm. This can be seen in Figure 2. Excessive dose below 350nm may, therefore, result in over exposure of the top portion of the resist film, resulting in exaggerated negative sidewall profiles or T-topping. The optimal exposure dose will depend on film thickness (thicker films require higher dosage) and process parameters. The exposure dose recommendations in Table 3. are based on source intensity measurements taken with an i-line (365nm) radiometer and probe.

Expose tip: When using a broad spectral output source, for best imaging results, i.e. straightest sidewalls, filter out excessive energy below 350nm.

Catastrophic adhesion failure, severely negative sidewalls and excessive cracking often indicate an under cross-linking condition. To correct the problem, increase the exposure dose and/or increase the post exposure bake (PEB) time.
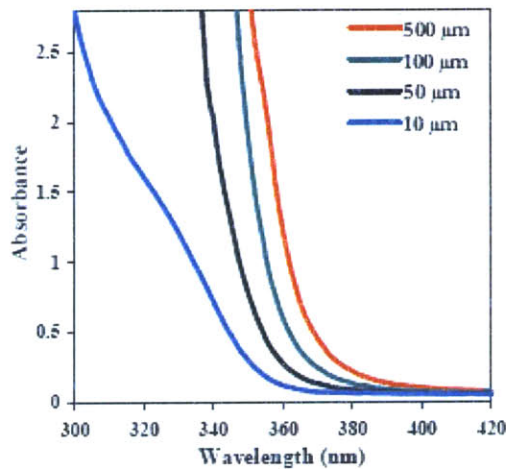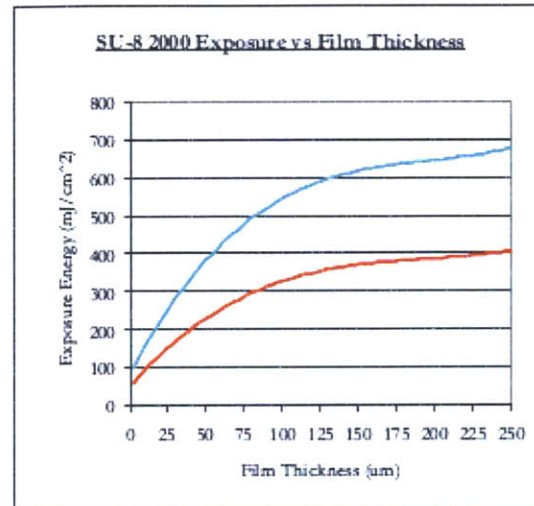

SU-8 2000 Exposure vs Film Thickness

Table 3. Recommended expose dose processes

Post Expose Bake

Following exposure, a post expose bake (PEB) must be performed to selectively cross-link the exposed portions of the film. This bake can be performed either on a hot plate or in a convection oven. Optimum cross-link density is obtained through careful adjustments of the exposure and PEB process conditions. The bake recommendations below are based on results obtained with a contact hot plate.

PEB tip: SU-8 is readily cross-linked and can result in a highly stressed film. To minimize stress, wafer bowing and resist cracking, a slow ramp or TWO STEP contact hot plate process, as shown in Table 4., is recommended. Rapid cooling after PEB should be avoided.

Figure 2. SU-8 absorbance vs. film thickness

Product Name	Thickness (μms)	PEB 1 @65°C	PEB 2 @95°C
	35	1	3
SU-8 2035	55	1	5
	110	1	10
	50	1	5
SU-8 2050	75	1	7
	165	1	12
	75	1	7
SU-8 2075	110	1	10
	225	1	15
	100	1	10
SU-8 2100	140	1	15
	260	1	15

Table 4. Recommended post expose bake parameters

176

Develop

SU-8 2000 resists have been optimized for use with MicroChem's SU-8 Developer. Immersion, spray or spray-puddle processes can be used. Other solvent based developers such as ethyl lactate and diacetone alcohol may also be used. Strong agitation is recommended for high aspect ratio and/or thick film structures. Recommended develop times are given in Table 5. for immersion processes. These proposed develop times are approximate, since actual dissolution rates can vary widely as a function of agitation rate, temperature and resist processing parameters.

Product Name	Thickness (urns)	Development (minutes)
	35	5
SU-8 2035	55	6
	110	10
	50	6
SU-8 2050	75	7
	165	12
	75	7
SU-8 2075	110	10
	225	12
	100	10
SU-8 2100	140	15
	260	20

Table 5. Recommended develop processes

Rinse and Dry

Following development, the substrate should be rinsed briefly with isopropyl alcohol (IPA), then dried with a gentle stream of air or nitrogen.

Rinse tip: If a white film is produced during rinse, this is an indication that the substrate has been under developed. Simply immerse or spray the substrate with SU-8 developer to remove the film and complete the development process. Repeat the rinse step.

Hard Bake (cure)

SU-8 2000 has good mechanical properties, therefore hard bakes are normally not required. For applications where the imaged resist is to be left as part of the final device, the resist may be ramp/step hard baked between 150-200°C on a hot plate or in a convection oven to further cross link the material. Bake times vary based on type of bake process and film thickness.

Removal

SU-8 2000, after expose and PEB, is a highly cross-linked epoxy, which makes it extremely difficult to remove with conventional solvent based resist strippers. MicroChem's Remover PG will swell and lift off minimally cross-linked SU-8 2000. However, if OmniCoat has been applied immersion in Remover PG should effect a clean and thorough Lift-Off of the SU-8 2000 Material. It will not remove fully cured or hard baked SU-8 2000 without the use of OmniCoat. Alternate removal processes include immersion in oxidizing acid solutions such as piranha etch / clean, plasma ash, RIE, laser ablation and pyrolosis.

To remove minimally cross-linked SU-8 2000, or if using Omnicoat, with Remover PG, heat the bath to 50-80°C and immerse the substrates for 30-90 minutes. Actual strip time will depend on resist thickness and cross-link density For more information on MicroChem Omnicoat and Remover PG please see the relevant product data sheets.

Storage

Store SU-8 2000 resists upright in tightly closed containers in a cool, dry environment away from direct sunlight at a temperature of 40-70°F(4-21°C). Store away from light, acids, heat and sources of ignition. Shelf life is twelve months from date of manufacture.

Disposal

SU-8 2000 resists may be included with other waste containing similar organic solvents to be discarded for destruction or reclaim in accordance with local state and federal regulations. It is the responsibility of the customer to ensure the disposal of SU-8 2000 resists and residues made in observance all federal, state, and local environmental regulations.

Environmental, Health and Safety

Consult product Material Safety Data Sheet before working with SU-8 2000 resists. Handle with care. Wear chemical goggles, chemical gloves and suitable protective clothing when handling SU-8 2000 resists. Do not get into eyes, or onto skin or clothing. Use with adequate ventilation to avoid breathing vapors or mist. In case of contact with skin, wash affected area with soap and water. In case of contact with eyes, rinse immediately with water and flush for 15 minutes lifting eyelids frequently. Get emergency medical assistance.

The information is based on our experience and is, we believe to be reliable, but may not be complete. We make no guarantee or warranty, expressed or implied, regarding the information, use, handling, storage, or possession of these products, or the application of any process described herein or the results desired, since the conditions of use and handling of these products are beyond our control.

Appendix C: Selecting Mold Sizes

In the simplest case, first consider the design matrix when only two molds are used, one each for top and bottom, and they both are neutral. The results are shown in Figure C-1.
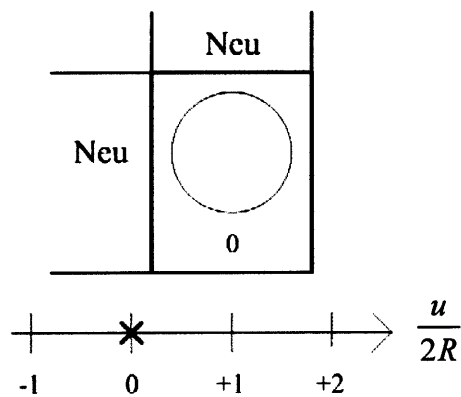

Figure C-1: Design Matrix and Number Line, Simple Case.

Adding one additional top mold, with a value of +1/2, adds one possible combination, and gives the design matrix in Figure C-2.
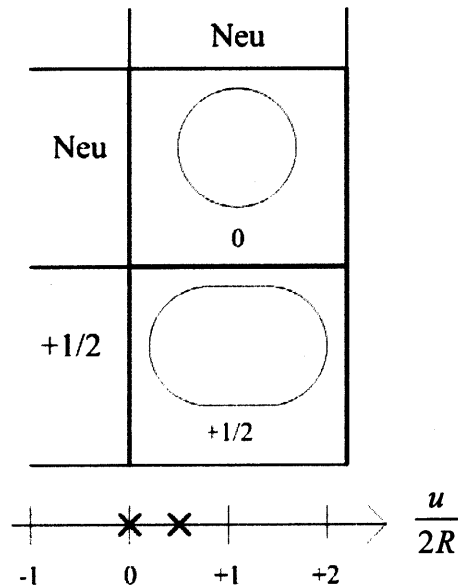

Figure C-2: Design Matrix and Number Line, with +1/2.

As can be seen, this adds the possibility of one other configuration, where the overlap area is half a diameter, and the area of the joint grows. Another point is added to the number line, at +1/2, which is the sum of 0 and +1/2. The next approach is to add another value to the bottom mold library, for instance -1/2, in an attempt to maintain the same density of points on the number line. The results are shown in Figure C-3.
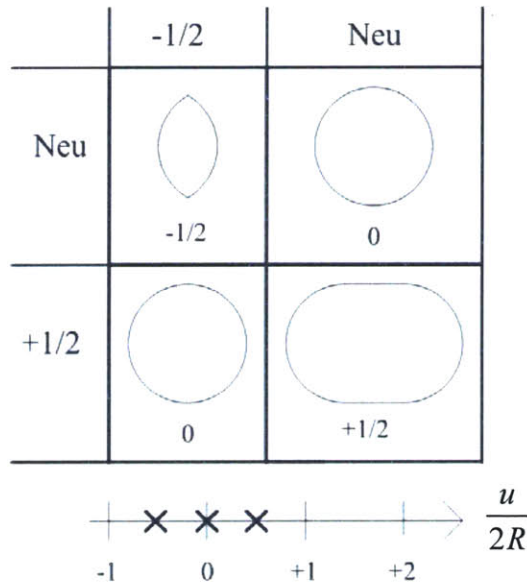

Figure C-3: Design Matrix and Number Line, with -1/2.

This arrangement indeed adds the addition point of -1/2, but unfortunately, it adds the redundant point of -1/2 and +1/2, which have a combined result that is the same as the two neutral values. This fails to make the best use of the molds, so it is rejected as a possibility. It seems the error was in selecting an increment between values for both bottom molds and top molds that was the same. That is, the mistake was in choosing a difference of 1/2 for both the top (0 and +1/2) and bottom (0 and -1/2).

With this observation in mind, the next set of possibilities was chosen with a different approach. The tops were chosen with values of 0, +1, and +2, while the bottoms were chosen with values of 0, -1/4, and -1/2, in an attempt to capture a 1/4 increment resolution. The results of the design matrix are shown in Figure C-4.

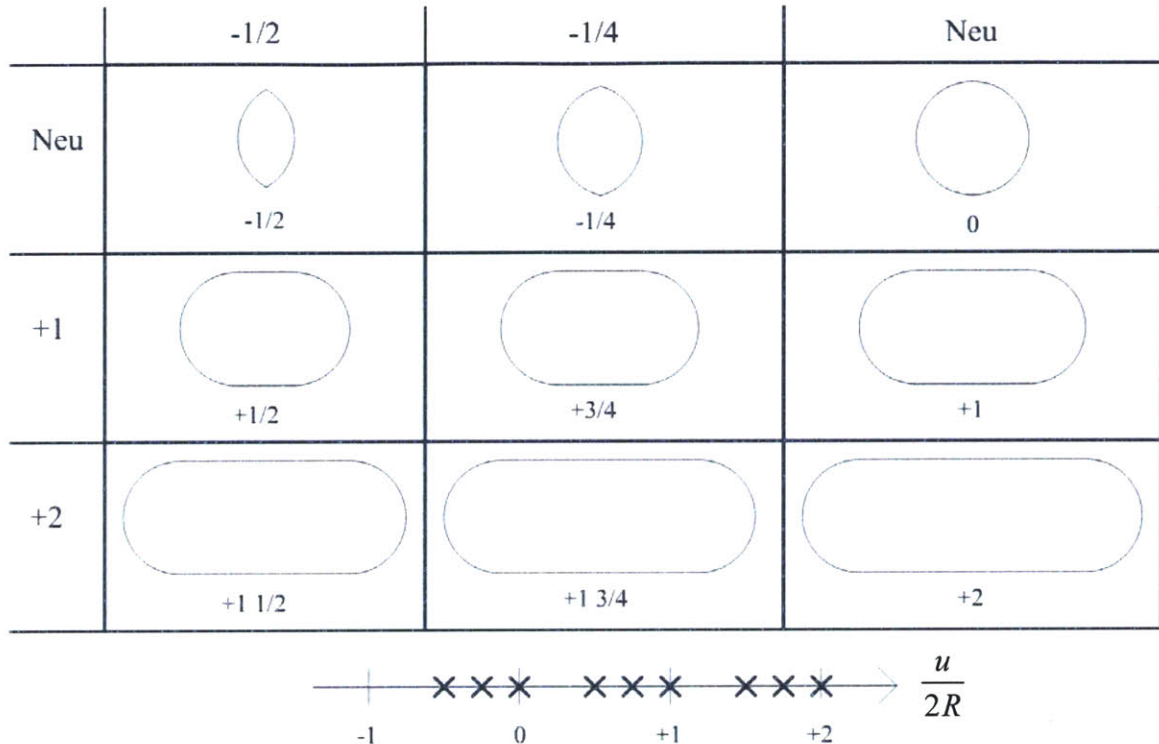|	-1/2	-1/4	Neu
Neu	-1/2	-1/4	0
+1	+1/2	+3/4	+1
+2	+1 1/2	+1 3/4	+2

$$\frac{u}{2R}$$

-1   0   +1   +2

Figure C-4: Design Matrix and Number Line, with three tops and three bottoms.

This is where the number line helps dramatically in visualizing the drawbacks of this selection. There is indeed a resolution of 1/4 between three subsequent values, but between the third of one set and the first of the next, there is a disparate jump of 1/2. It seems that the values that show up in the device are a superposition of the possibilities from the top and bottom. That is, the first group of three points on the left is the three bottoms combined with the neutral top, then the second group is the three bottoms combined with the +1 top, and finally the third group is the three bottoms combined with the +2 top. An alternate view, but equally valid, is of the three left-most dots in each set as the tops combined with the -1/2 bottom, the middle dots as the tops combined with -1/4 bottom, and the right-most dots as the tops combined with the neutral bottom. Regardless of either of these views, the implication of the superposition is that there must be some relationship between the choices for top and bottom increments if the goal is to ensure an even coverage of the range. Specifically, again assuming that the full range of bottoms is less than the minimum increment of tops, the increment of tops should be uniform, and the increment for the bottoms should be one increment of the top divided by the number of bottoms desired.

Appendix D: Mold Design Iterations

This appendix details the approaches attempted in fabricating the microfluidic devices prior to the arrival on the method described in Chapter 7.

D.1 Initial Approach (G1)

The first approach employed in the research was to use the sandwich layer developed by the Whitesides group [Anderson 2000], which was described in Section 5.3. Though the design developed in this research only required a two-layer device, and the capability of that method is for three or more layers, it was hoped that gaining experience in the method would prove a boon for future research. We could then explore three-level multilayer flow as a next step. This became known as G1, for Generation One.

D.1.1 Design

The Whitesides technique [Anderson 2000] is a mechanical mold-to-mold alignment method, and thus a third mask and photoresist layer was necessary to be created in order to facilitate the mechanical contact. The three masks used in the process are shown in the Figure D-1, Figure D-2, and Figure D-3.

The most obvious note is that the mask for the top layer is light-field, meaning that the majority of the mask is light, whereas the other two are dark-field. This is because the method actually requires a double-molding for the top channels, first PDMS cast onto the photoresist on the wafer. This PDMS forms the top mold for the final sandwich-molding step, as shown in Figure D-4.
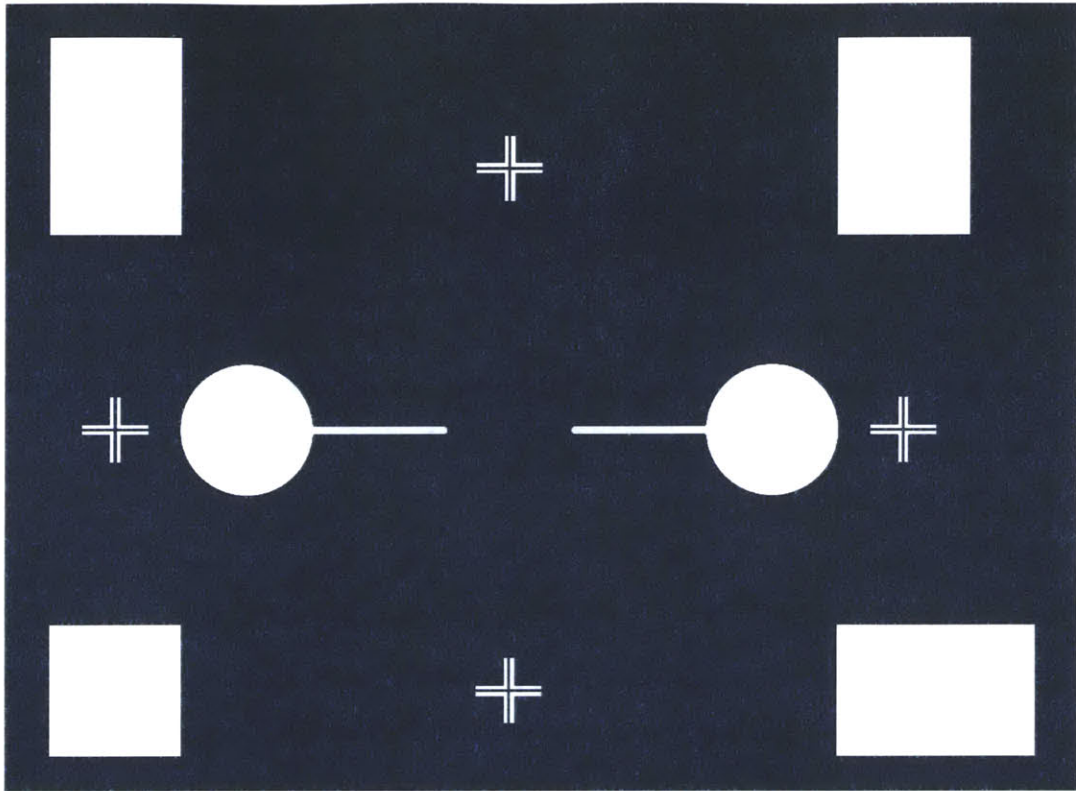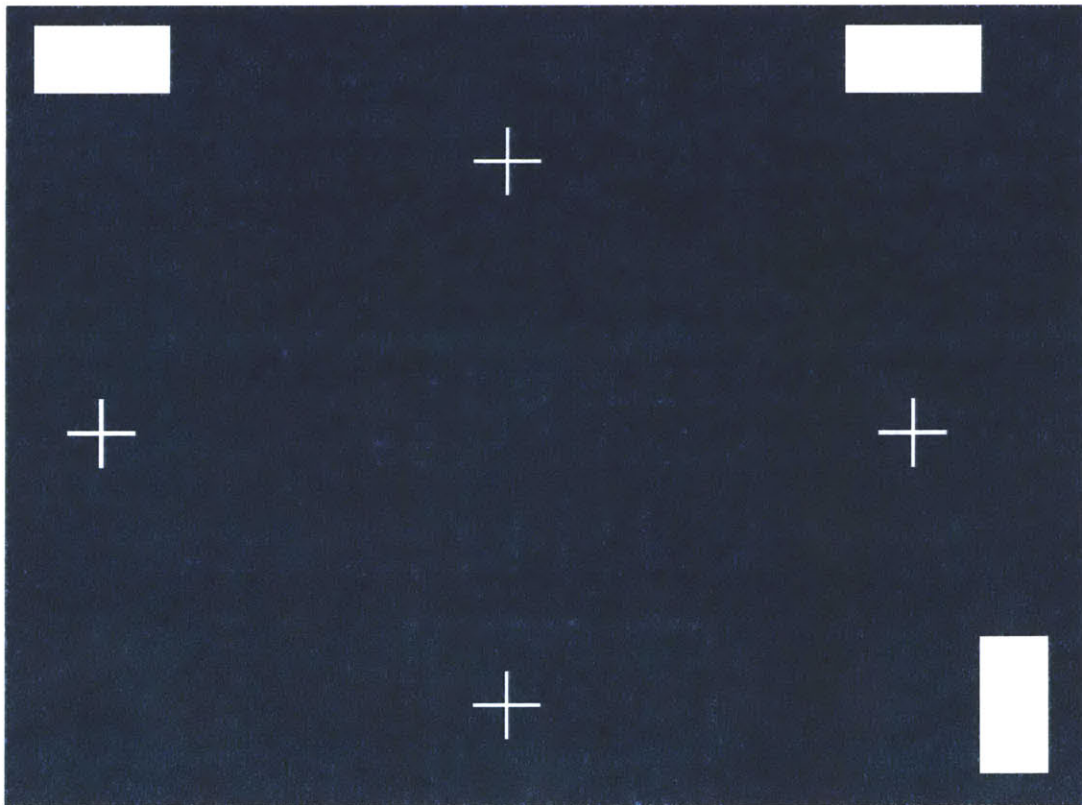
Figure D-1: Bottom Mask, G1.

Figure D-2: Middle Mask, G1.

Figure D-3: Top Mask, G1.

50 μm
negative photoresist
Si wafer

A Bake

high resolution transparency
(photomask) with pattern of
first level

B Expose, remove photomask, and bake;
spin-coat additional layer of photoresist

100 μm
unexposed photoresist
on exposed photoresist

C Align a second photomask
to crosslinked photoresist

photomask with pattern
of second level

D Expose, remove photomask, and bake

E Develop and silanize

two levels of
high-relief features
in photoresist

Bottom
Master

A Make pre-master by
two-level photolithography

cross-
section
100 μm

B Pour PDMS on top; cure

C Remove, trim, and silanize

cross-
section
100 μm

Top Master
Two levels of
high-relief features

PDMS master
drop of PDMS
prepolymer
Si master

A Align masters face-to-face
with features touching;
cure under pressure

interdigitated alignment
PDMS membrane
150 μm
two points of crossing

B Peel off membrane
and top master

C Seal bottom of membrane
to flat piece of PDMS

D Peel off top master

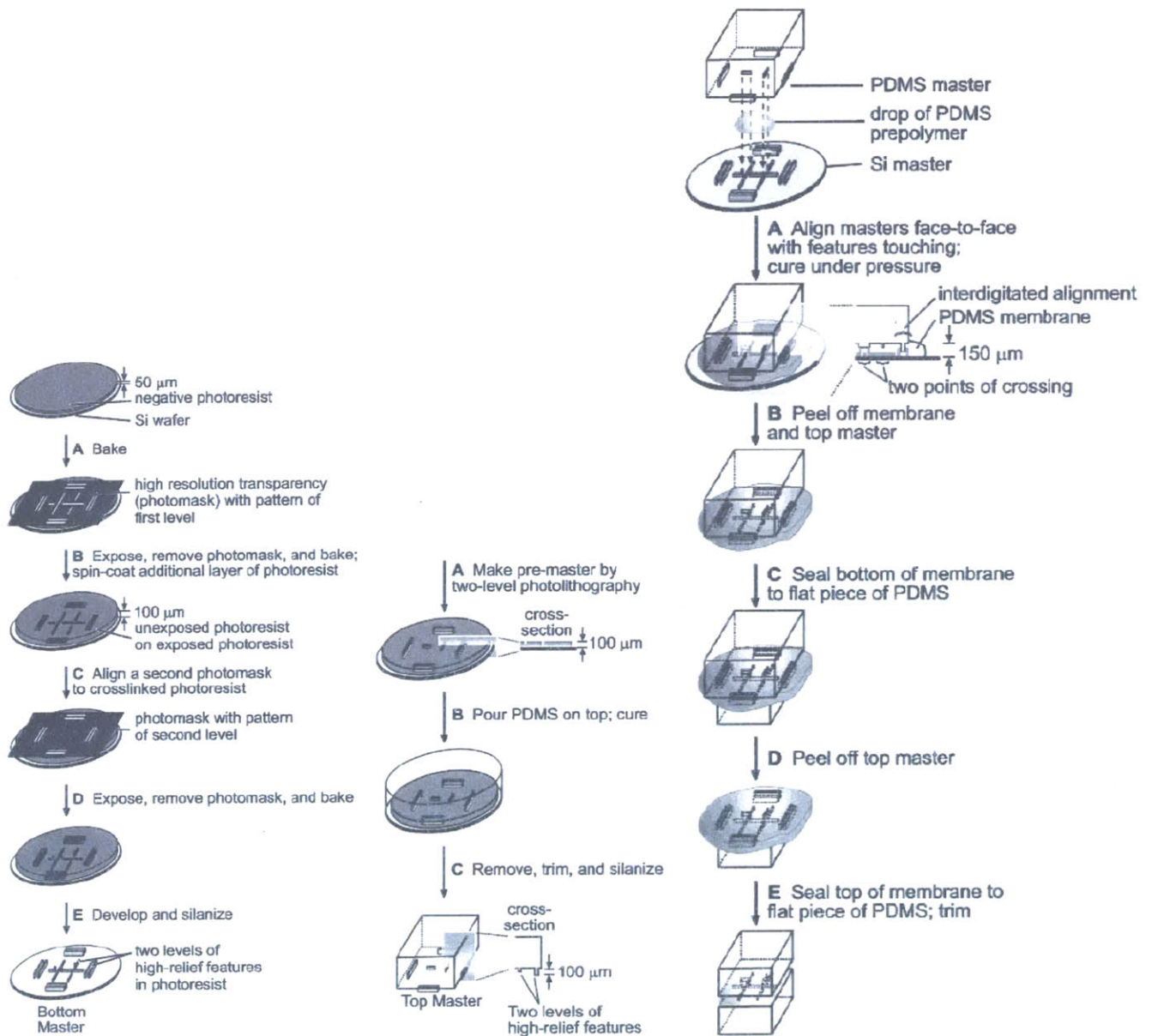E Seal top of membrane to
flat piece of PDMS; trim

Figure D-4: Whitesides Sandwich Layer Method [Anderson 2000].

The departure from the sandwich layer method in this design was the alignment features themselves. Whereas the original method used a wall-in-slot method, this was technically over-constrained, as discussed, in Section 5.2. Thus a simpler alignment scheme was selected, where four contact pads established the planar mate, restricting three degrees of freedom, and three cylinder-to-sidewall mates, restricting the other three, were employed. The layouts shown in Figure D-4 reflect these features. The circles on the top mold served as both the pads to establish the planar mate and as the cylinders to establish the other three mates. The sidewalls appeared in the middle mold, and these rested on the large rectangles on the bottom mold. After the bottom

184

layer was exposed, before the hard bake, a second layer of photoresist was spun on and soft baked. The middle layer was aligned to the bottom mold using the four cross structures, and then it was exposed again. The two were then jointly hard baked and exposes, creating the requisite multilevel mold for one side of the mechanical alignment. A solid model of the completed top and bottom molds is shown in Figure D-5.
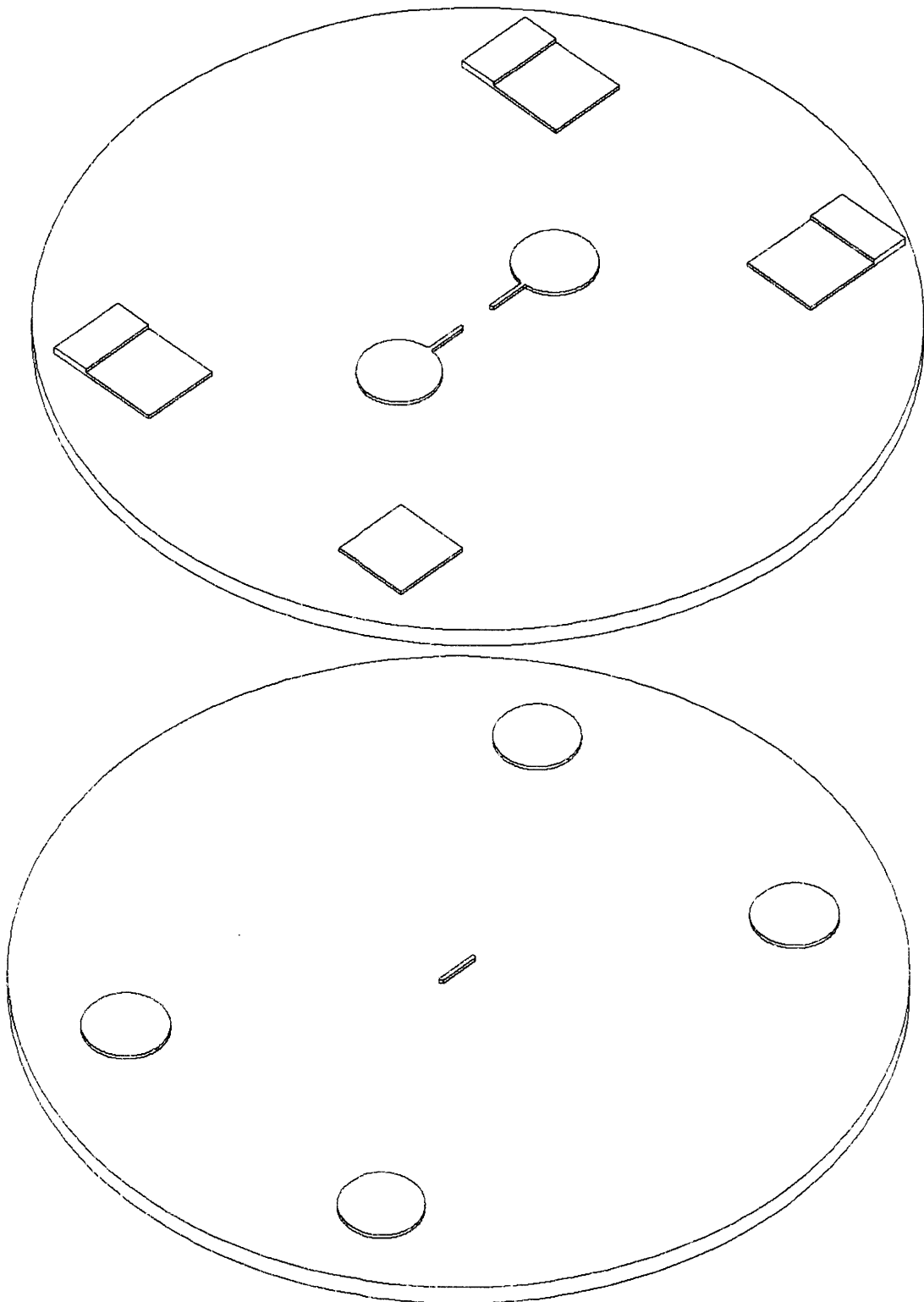
Figure D-5: Molds fabricated via photolithography (G1).

D.1.2 Drawbacks

The first problem with this method arose before PDMS was even introduced. The alignment of the second transparency mask, of the middle layer, to the exposed first layer of photoresist proved impossible given the design. The photoresist would stick to the transparency, making manipulation very jerky, as each move required un-sticking the mask, a process that disturbed the alignment greatly. Even when the top transparency was taped to a piece of glass it failed, as the middle of the mask would inevitably droop, causing it to contact the mask and stick. Also, the top mask was almost entirely dark-field, so it was very difficult to see through the mask to the faint features in the photoresist below. The alignment features themselves were even smaller than the sidewall opening, so it was effectively impossible to see enough to align the layers, had they not been sticking together.

Thus the first improvement was to change the design of the alignment features slightly, as well as switch from a transparency mask for the middle layer to a quartz mask with patterned chrome to serve as the masking material. The design for the quartz mask is shown in Figure D-6.
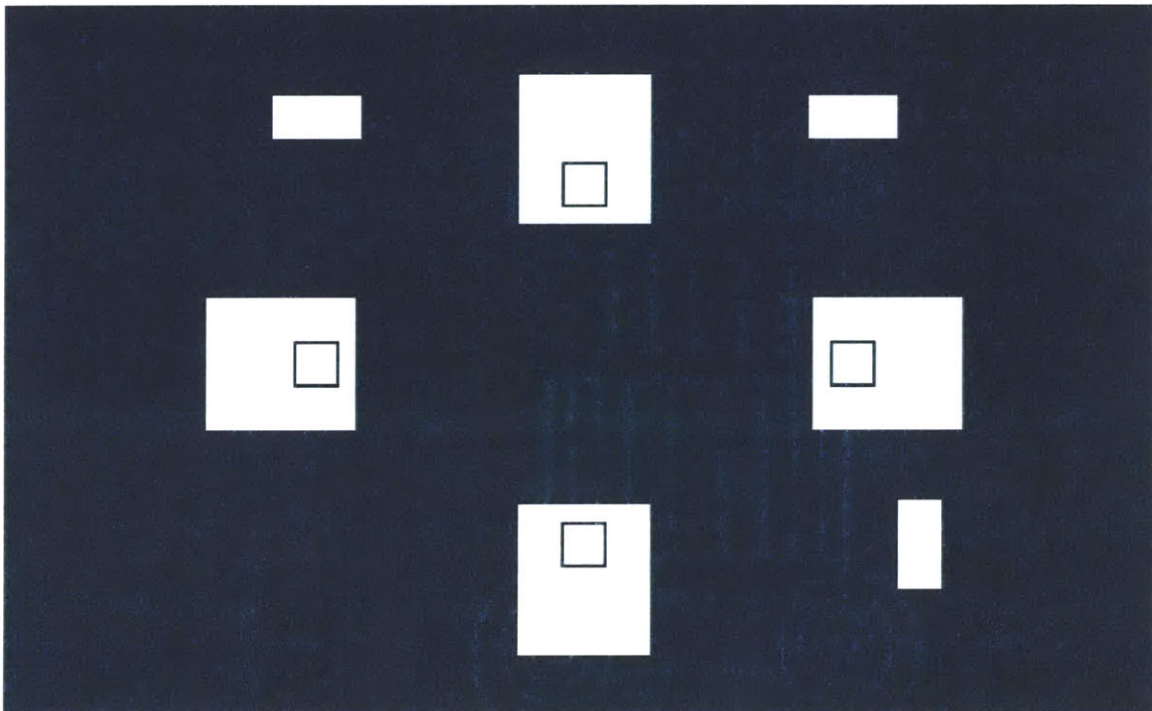

Figure D-6: Quartz Mask, G1.

The alignment features become windows with a box to fit the cross inside. Using this method, positioning became much more feasible. However, in at least two instances, there were still situations in which alignment was thought to be achieved, but after exposing, it appeared

that the alignment had somehow been disturbed between the final observation of the alignment and the actual activation of the exposure lamp.

As discussed in detail in Section 5.2, viscosity of the PDMS pre-polymer fights against the ability to easily align features together mechanically. That treatment was informed by the experiences in attempting to bring the features into alignment. The tiny size of the alignment features, and the even tinier contact area between the mate features, coupled with the tendency of the upper PDMS mold to deform, made the mechanical alignment of the molds nearly impossible. The first device fabricated with this method had the top channel missing the desired position by a significant amount, as shown in Figure D-7.
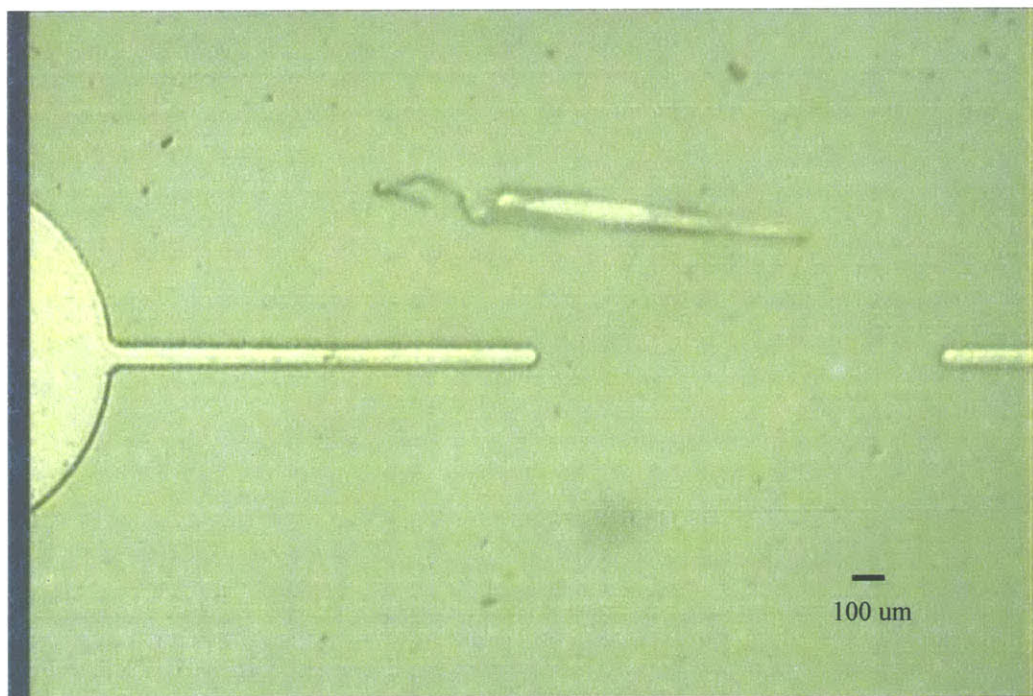

100 um

Figure D-7: Channel Misalignment, G1 Device.

An examination of the device showed that the problems started with the mold, for the sidewall failed to be correctly positioned to the bottom layer:
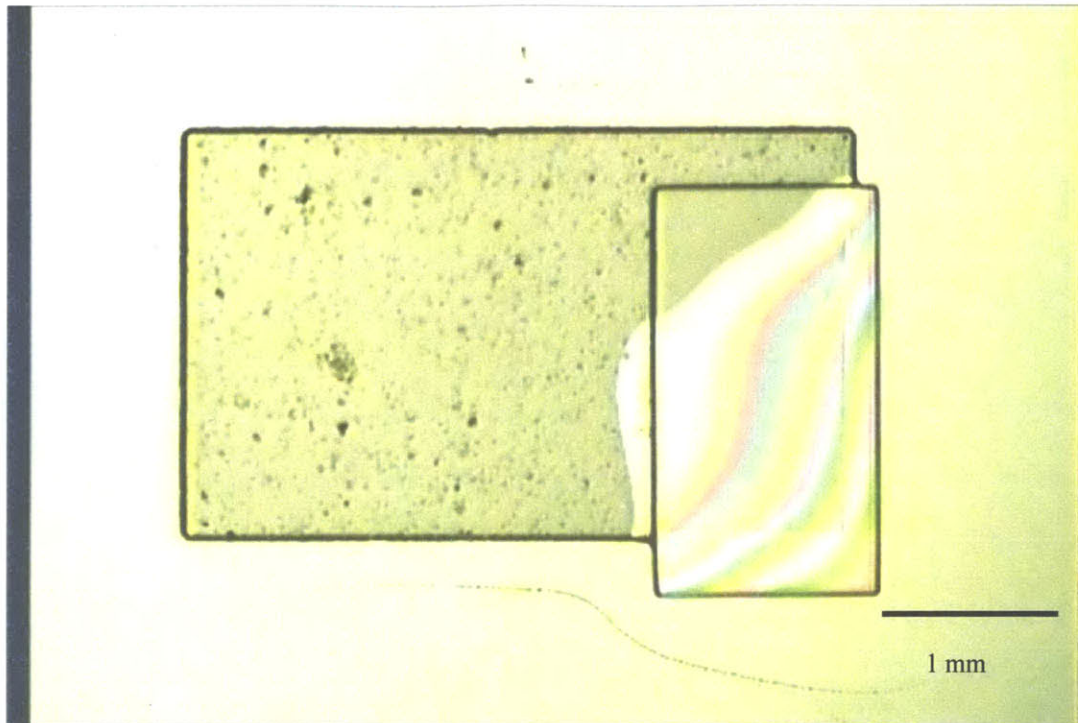
Figure D-8: Physical Alignment Feature Misalignment, G1.

This may have been due to some problems introduced by the alignment features becoming unaligned. The photographic evidence of this in Figure D-9:
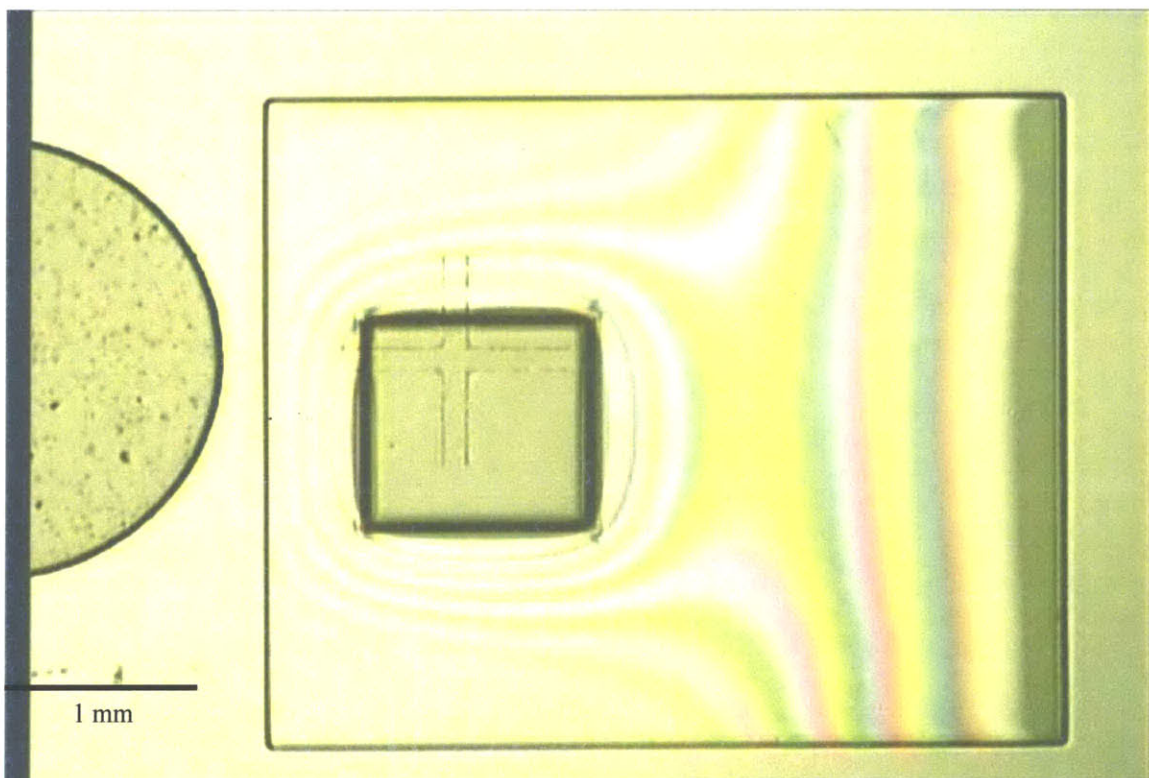

Figure D-9: Misalignment of Optical Alignment Features, G1.

189

It is unclear what caused this misalignment, because right before the exposure was performed, the features were properly aligned. But this was ultimately only a small problem, as the real problem was that the mechanical mates were impossible to achieve. A picture of what did result after the alignment was attempted is shown in Figure D-10.
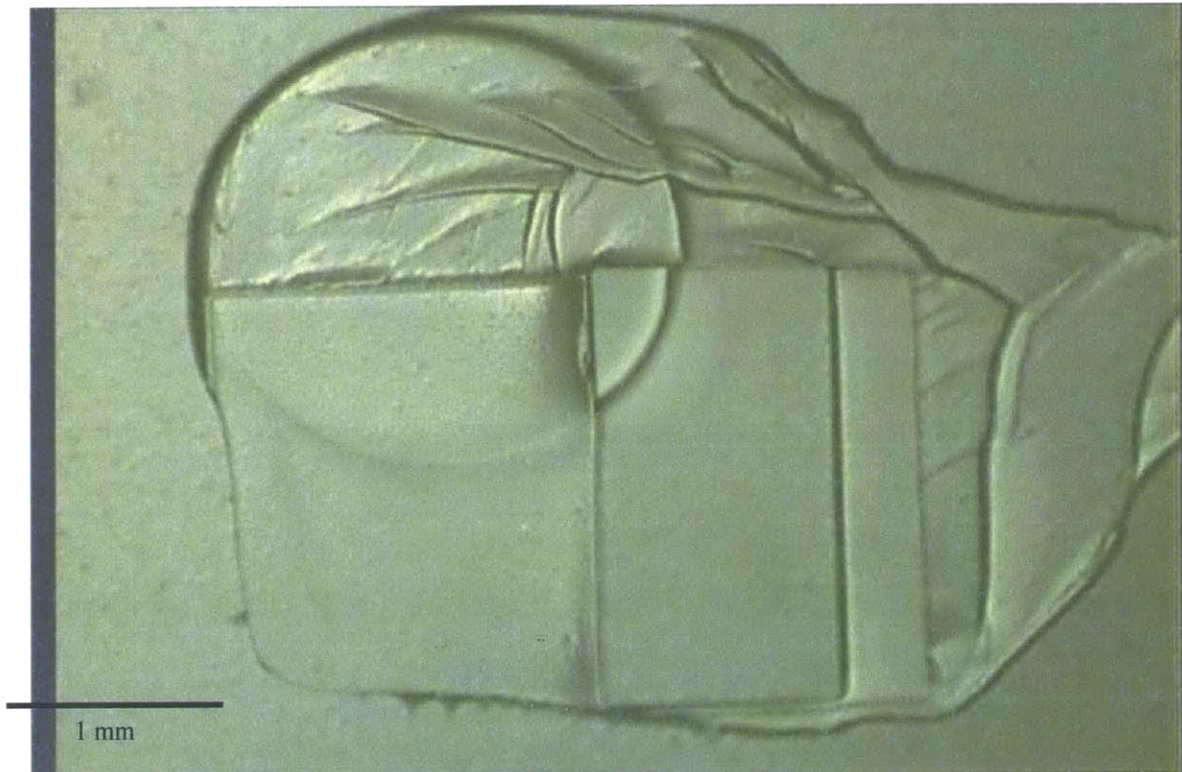

1 mm

Figure D-10: Combined Alignment Feature Mismatch, G1.

Even though the sidewall was indeed slightly out of position, this was not as much of a problem as the fact that the circular pad ended up atop the structure that it was supposed to be gently touching from the side.

As a result of these difficulties, this approach was abandoned.

D.2 G2

The next approach was to try to more-closely duplicate the sandwich layer method, using the wall-in-slot mates. This was the second generation device, or G2.

D.2.1 Design

This time, it was assumed that chrome mask would be employed, so the middle layer was never printed to transparency. The transparency design and chrome mask design are shown in Figure D-11 and Figure D-12.
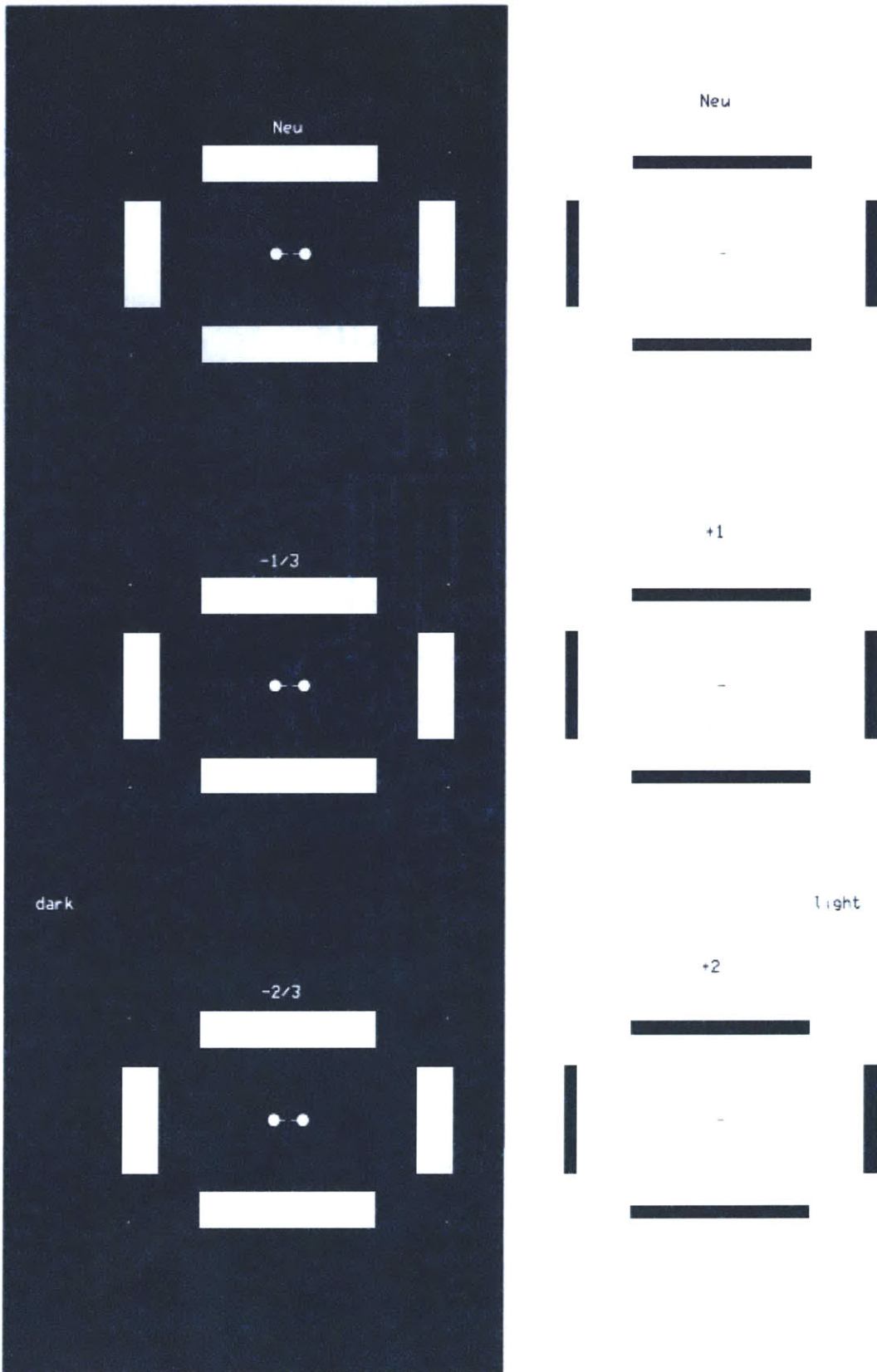
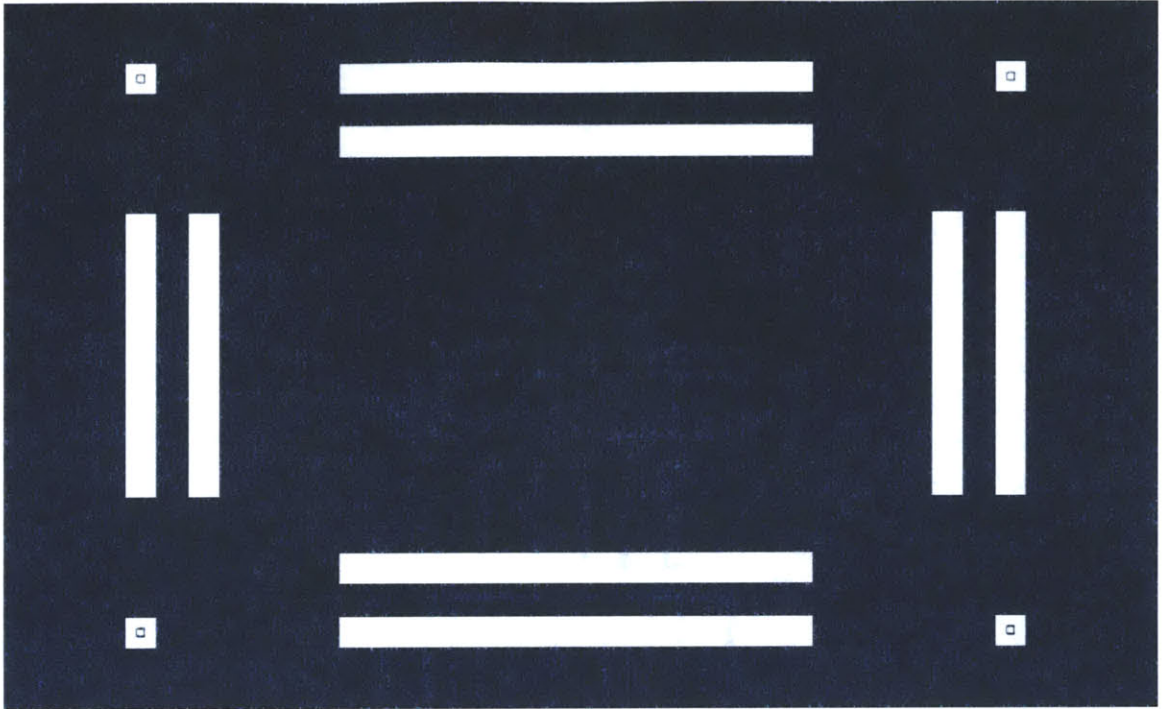**Figure D-11: Transparency Masks, G2.**

Figure D-12: Chrome Mask, G2.

The implementation of the overlap area sizes can be seen in the designs. A solid model of the new arrangement is shown in Figure D-13.
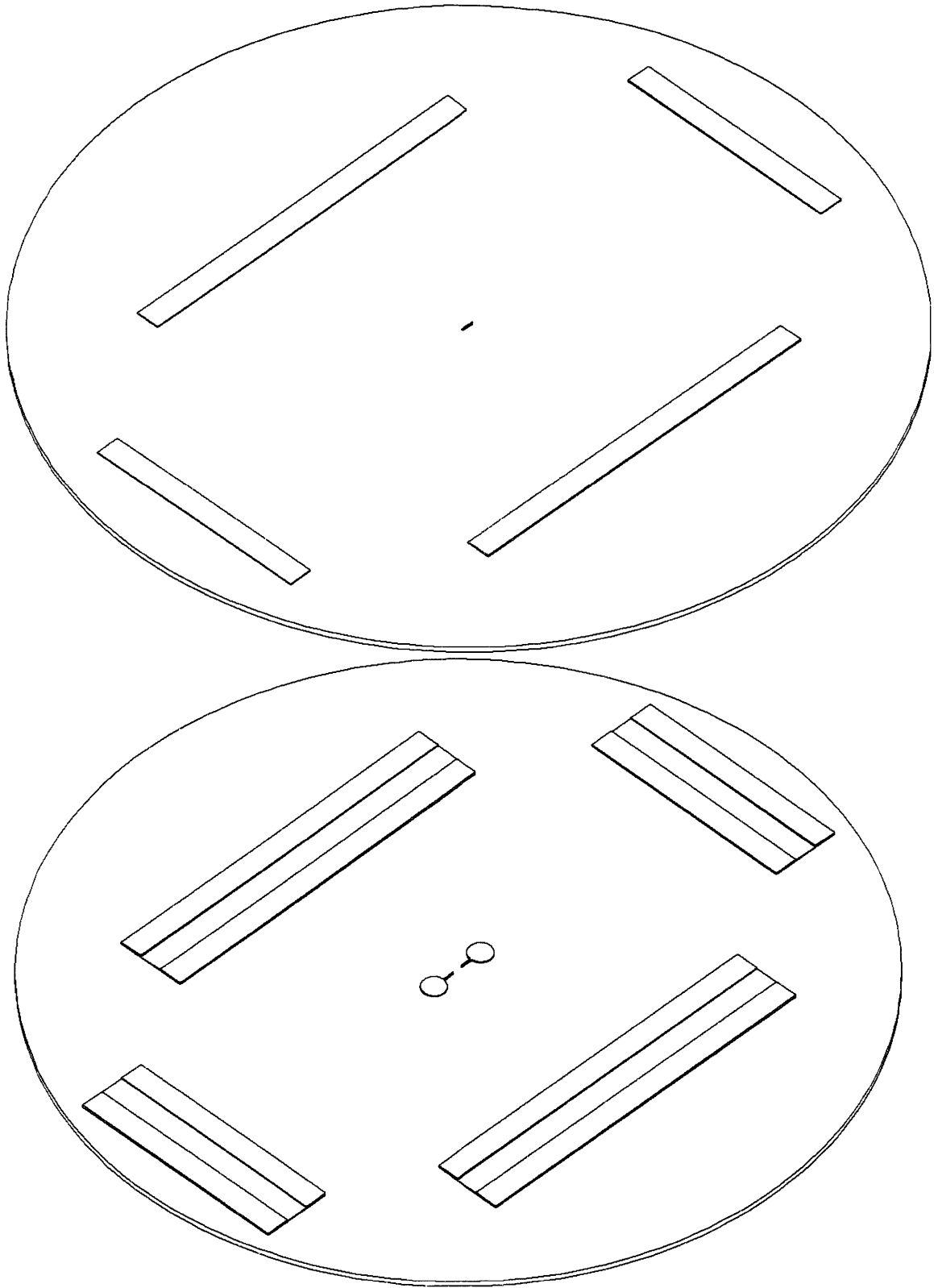
Figure D-13: Solid Model of the G2 Molds.

The approach was to take the completely opposite track than from G1: massive alignment features that would over-constrain the top mold, but hopefully simultaneously correctly position it in doing so.

In Anderson [2000], the method of joining, while using their slot features, is described as follows: "We placed the two masters face to face with a drop of PDMS prepolymer between. We aligned the features of the masters quickly and without magnification by manually sliding the top master over the prepolymer and bottom until its tall tracks slipped between the tall alignment tracks of the bottom master." It was hoped that this would be the case for this device as well.

D.2.2 Drawbacks of G2

Unfortunately, there were severe problems with this approach. The first device was attempted using only the smallest amount of PDMS necessary to cover the features, and then a large amount of pressure was applied during the cure. This seems to have had the unintended affect of deforming the top PDMS mold so that the features were not well transferred, and that the sandwich layer was exceedingly thin if not nonexistent. Two pictures of the first incarnation are shown in Figure D-14 and Figure D-15.
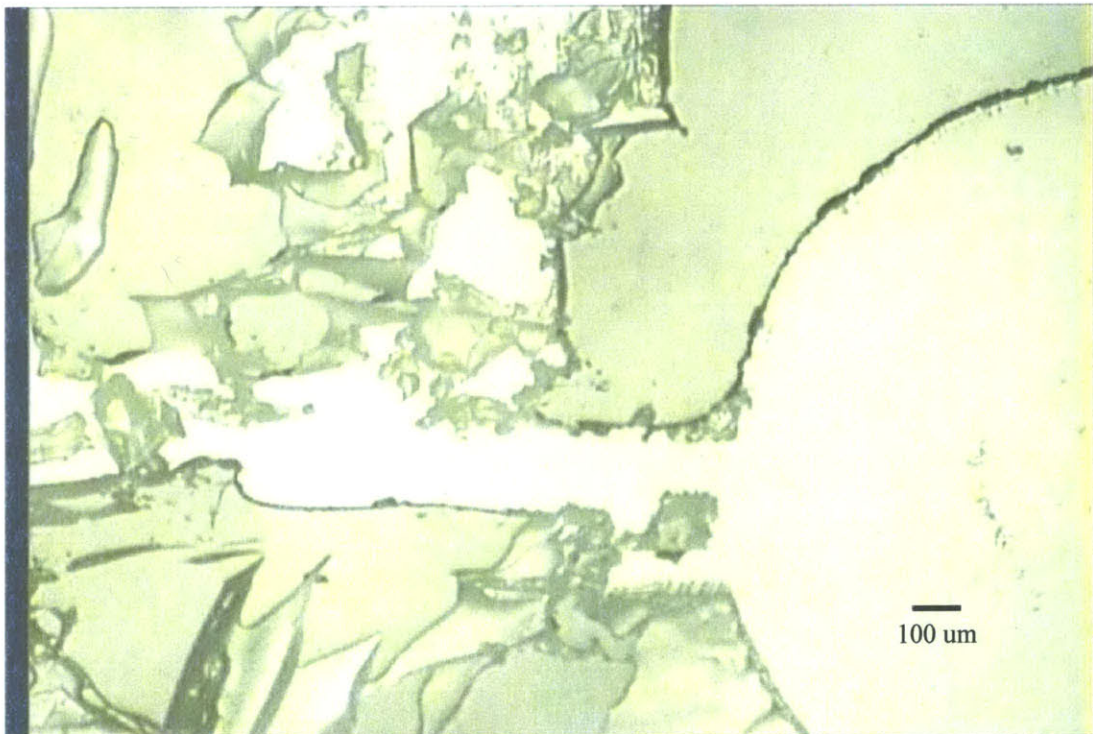

Figure D-14: The G2V1 Device, with obvious defects leading to device failure.
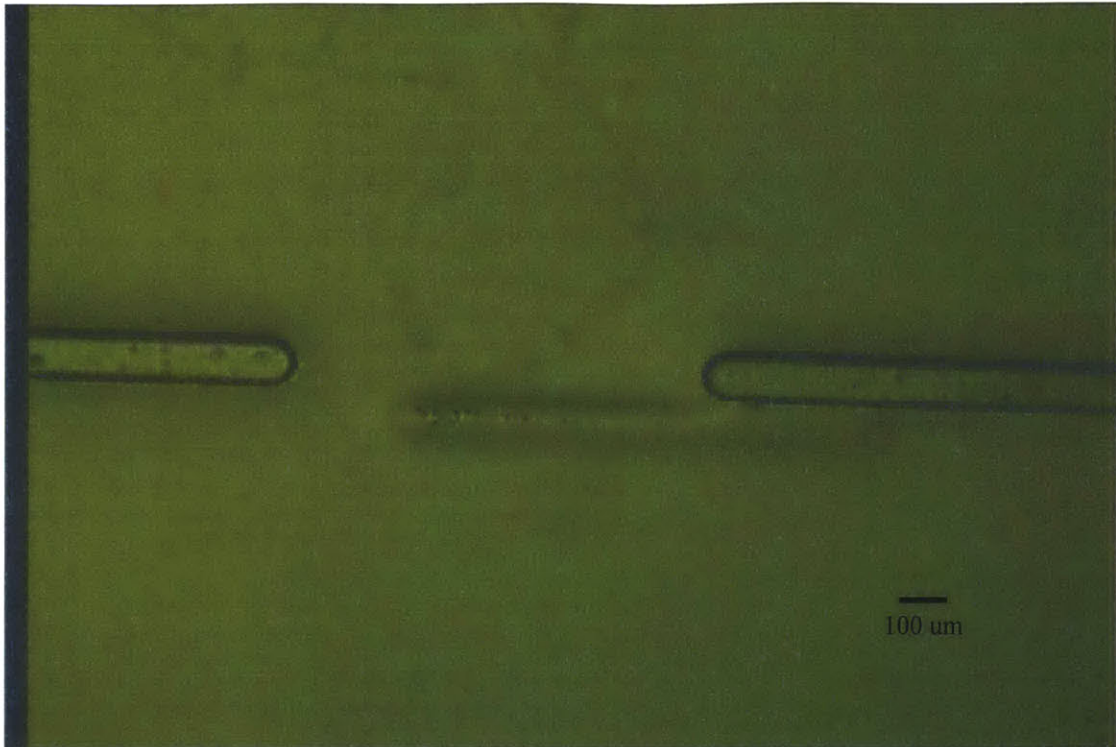
Figure D-15: The G2V1 bottom mold, after demolding, showing a shadow of where the top mold was in misaligned contact during molding of the sandwich layer.

Figure D-14 shows the thin layer as finally realized. The large striations shown are thought to be areas where the two molds were pushed together to the exclusion of the PDMS, or possibly places where the PDMS tore during one of its de-moldings because it was too thin.

Figure D-15 is more worrisome, as it shows the shadow of the top mold that was left on the bottom mold. The top channel yet again cleanly misses the proper position. Unlike the amount of PDMS used or the clamping force, this misalignment could have proved harder to correct, as ultimately proved to be the case.

The method was attempted again, using a flood of PDMS over the surface of the mold. This time there was no issue with complete exclusion of the PDMS, but rather the alignment again reared its head. The second version of G2, also called G2V2, is shown in Figure D-16. During the mold-to-mold alignment, the force of the walls in the slot could be faintly detected, but amid the large force being applied to keep mold halves together, it was very slight.
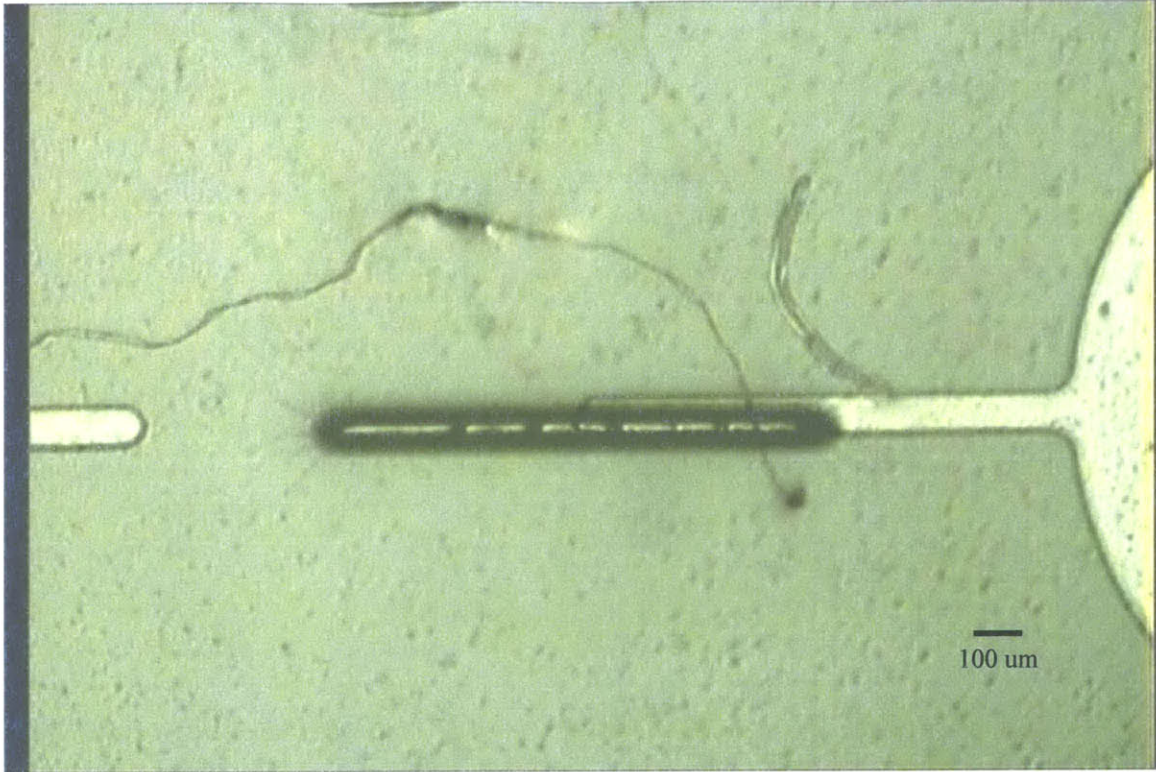
Figure D-16: The G2V2 Device, showing mismatch of the top channel as well as the possibility of flashing between the layers.

Beyond the obvious misalignment problem, the small bubble-like features at the surface of contact could be problematic. It is possible that they result from an in-complete sealing of the mold-halves. Similar to flash that appears in a injection molded part. The alignment was traced back to the alignment features, as shown in Figure D-17.

Figure D-17: The G2V2 Device Alignment Tracks, displaying mold overlap.
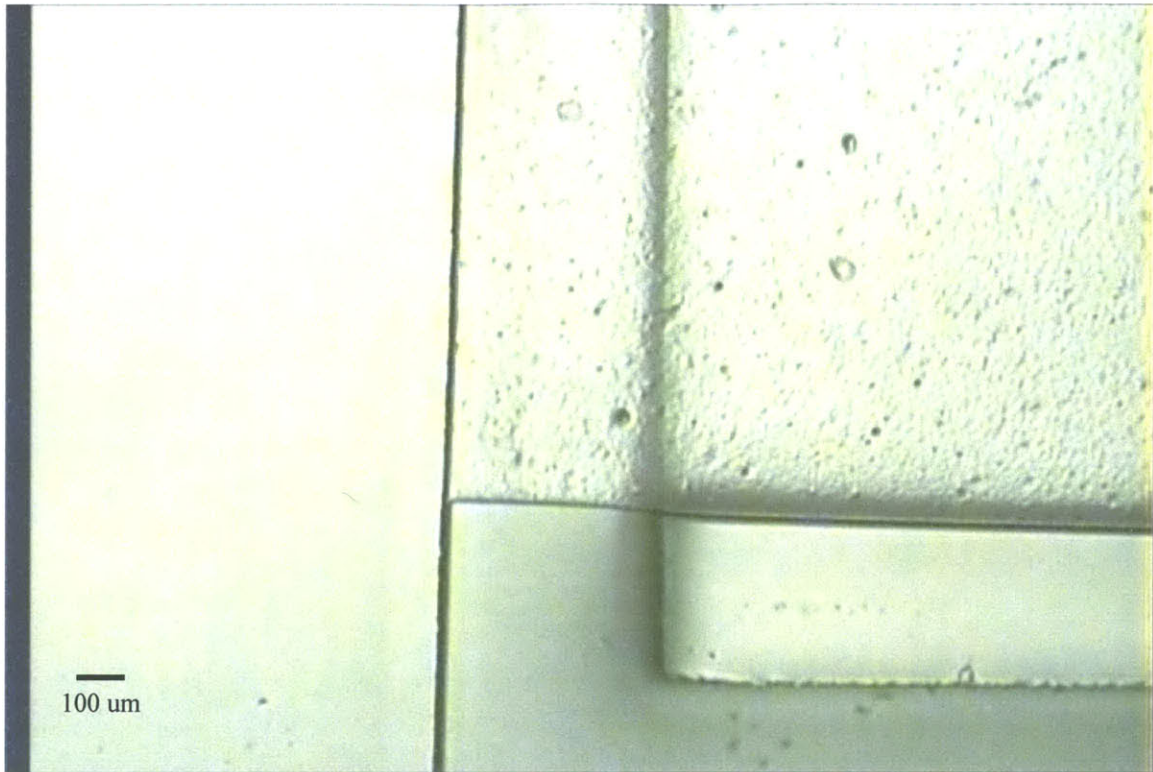
Unfortunately, this micrograph could not be "zoomed" out further to show the entire structures. What is shown here is the left end of the slot. Toward the bottom of the picture is the sidewall, and the misaligned rectangle is the top feature that was supposed to be neatly inside the slot. Here too, the low-profile features were taken to slipping on top of one another.

The method was attempted one last time, under the ideal conditions. The molds were meticulously positioned relative to one another, taking care to get the walls into the slots. Figure D-18 is of this G2V3 device.

The results are clear: even under the best-case positioning, the channel would not go where it was supposed to go. It is likely that this mismatch was not this great directly after aligning, but that it was introduced as the assembled molds and pre-polymer were moved from the alignment station into the oven. This underscored the point that alignment itself is only half the issue; the layers have to be correctly bonded once aligned, and if the process of bonding has the possibility of messing up the positioning, which did not take much disturbance in this case, the alignment was worthless.
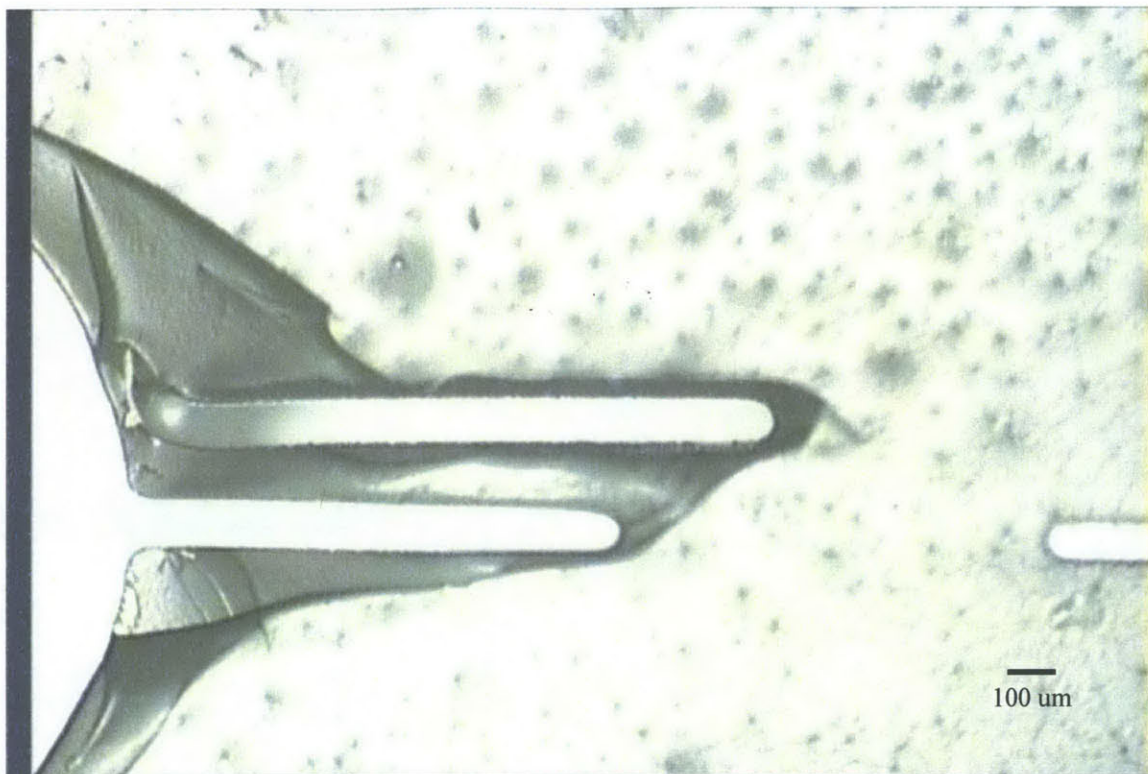
Figure D-18: The G2V3 Channels, with clear mismatch.

Another problem that this device displayed was at the tip of the top channel that ended up next to the reservoir. A picture at a higher magnification is shown in Figure D-19. The bizarre shape of this tip seem to indicate problems with the mold. The problem was traced back to the original SU-8 mold, which featured the channel in positive, which is to say a gap where the channel would ultimately be located. The intermediate mold transferred that shape into a negative, which was then used to create the final feature.

Figure D-19: The G2V3 Device, with Zoom on the misshapen tip of the top channel.

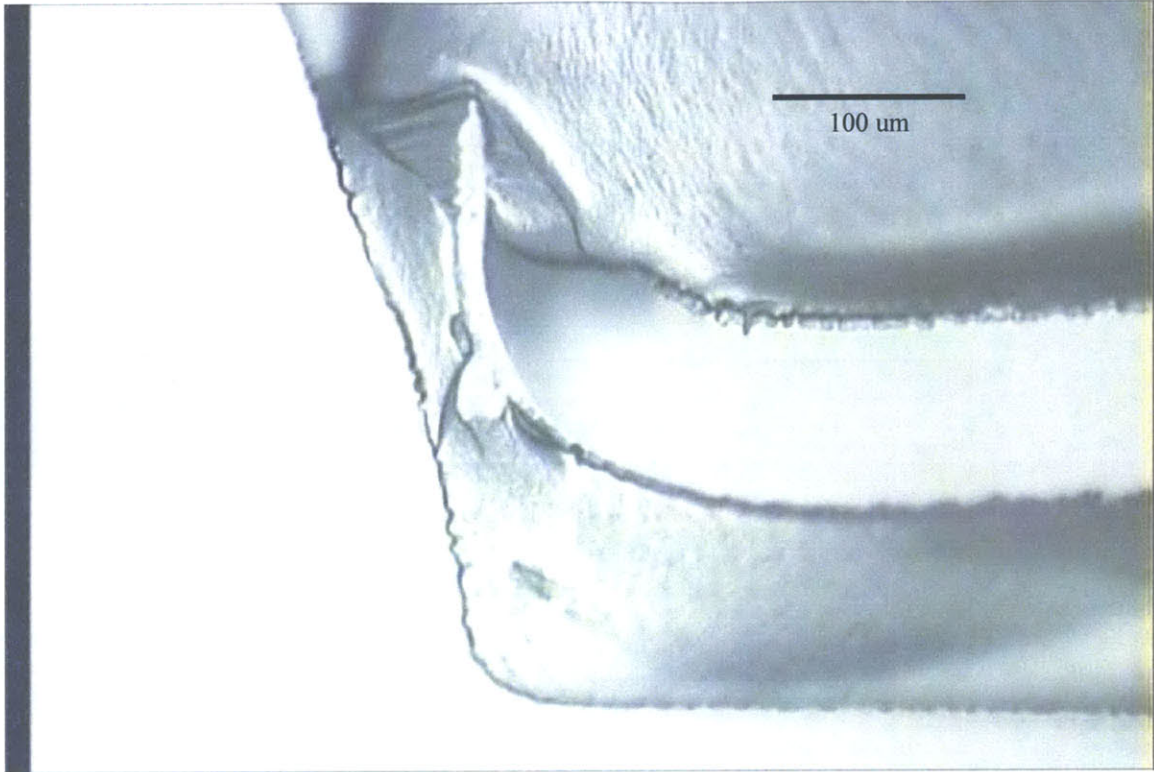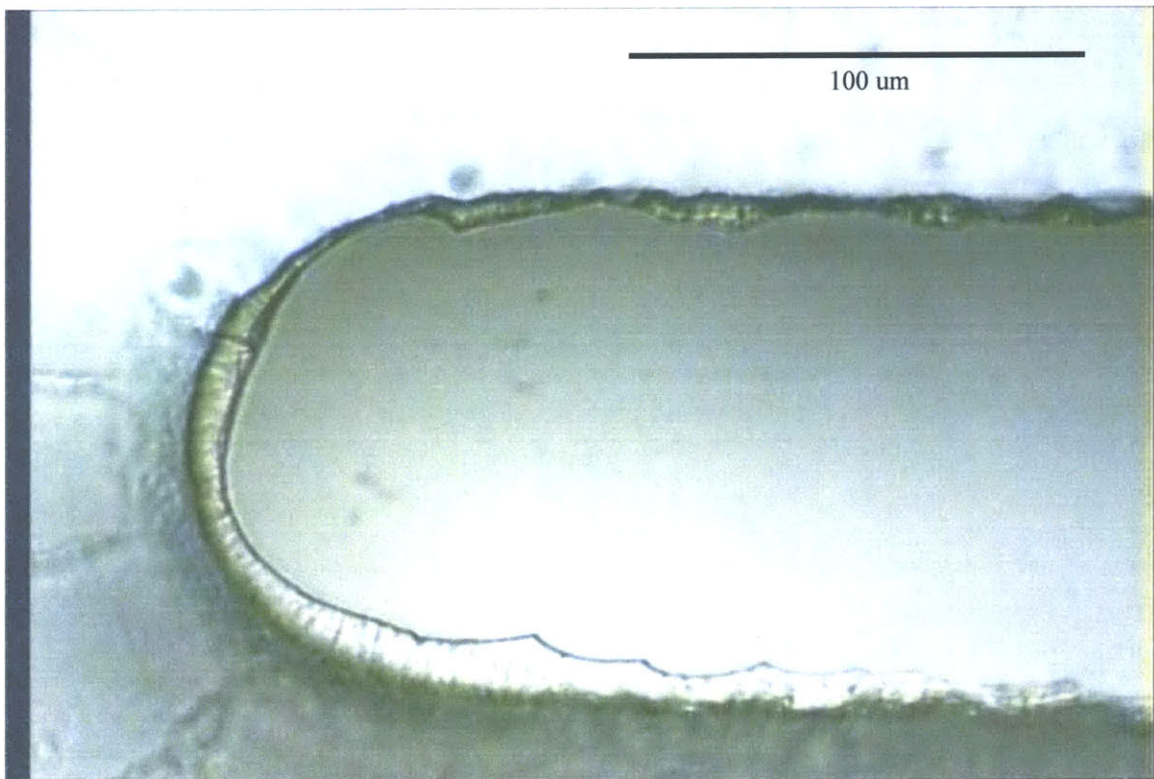**Figure D-20: SU-8 Mold, showing lip over the channel recess. This lip was actually less than initially detected; it seems the lip is fragile and tends to break off easily.**

Using a tight depth-of-focus, it was detected that the mold had a small lip over the channel. In cross section, it appeared to be roughly shaped like the diagram in Figure D-21.
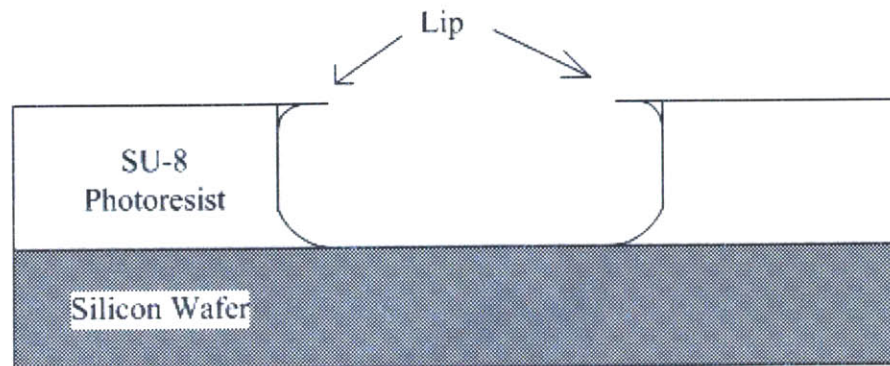
Figure D-21: Diagram of the Cross-Section of the Positive Channel in SU-8

It is unclear the cause of this lip, as thorough development of the photoresist failed to remove it. Perhaps it was a function of the photolithographic scattering, or a drying of the top surface of the photoresist. In any event, PDMS cast into this channel would have exactly the detached tip that would have lead to the odd shape shown in Figure D-19.

Almost all of these difficulties were due to the three-mask, mechanical alignment process, so this process was eliminated.

Appendix E: Test Platform Specifications

(From Harvard Appartus) Standard Infusion Only 2000 Syringe Pump

Specifications	702000
# of Syringes	2
Accuracy	0.35%
Average Linear Force	50 lbs
Communications	RS-232, TTL
Communications Level	2
Depth English	11 in
Depth Metric	27.9 cm
Display	Fluorescent, 2-line, 40 character
Flow Rate Maximum	220.82 ml/min
Flow Rate Minimum	0.0001 µl/min
Height English	6.3 in
Height Metric	15.9 cm
Input Power	0.5 A, 65 W
Motor	1/2 to 1/32 microstepping, microprocessor controlled, 1.8° step angle motor
Motor Stepper 1 Revolution of Lead Screw	800 at 1/2 stepping to 12,800 at 1/32 stepping
Net Weight English	10 lb
Net Weight Metric	4.5 kg
Non Volatile Memory	Storage of all settings
Pressure	Standard
Pump Configuration	Standard
Pump Function	Infusion Only
Pusher Travel Rate Maximum	190.676 mm/min
Pusher Travel Rate Minimum	0.18 µm/min
RS-232	RJ11-4 Connector
Reproducibility	0.05%
Step Rate Maximum	416.7 µsec/step
Step Rate Minimum	27.3 sec/step
Step Resolution	0.082 µm/step
Syringe Rack Type	Standard Rack
Syringe Size Maximum	140 ml
Syringe Size Minimum	0.5 µl
TTL	9-pin connector D-sub.

Type	Microprocessor multiple syringe, infusion only or infuse/withdraw, some models programmable from keypad
Voltage Range	Selectable, 95 to 130 VAC, 60 Hz or 220 to 260 VAC, 50 Hz
Width English	9 in
Width Metric	22.8 cm

3D INSTRUMENTS, LLC
Direct Drive Difference

DTG-6000
Digital Test Gauge

Features

➤ **Field Rugged** - 4 ½" 300 Series SS case with safety blow-out protection

➤ **Safe** - Intrinsically safe: design complies with requirements for use in Class 1, Group A,B,C and D areas (Approval Pending)

➤ **Precise Measurements** - 0.1% of reading accuracy for the range of 20-100% of span.

➤ **Versatile** - 9 pressure ranges to 5000 psig.. all ranges feature vacuum to 29.5" Hg

➤ **Temperature Compensation** - accuracy not de-rated over the range 14-122 deg F.

➤ **316 SS Sensors** - isolated pressure sensors are compatible with many corrosive media

➤ **High Resolution LCD** - oversized 0.65" digits enhance readability in poor lighting

➤ **Low Power Circuitry** - 3AA alkaline batteries provide for 1500 hours of continuous operation

➤ **Data Storage** - keypad addressable Hi/Lo pressure values

➤ **Field Re-Calibration** - Keypad re-calibratable using acceptable pressure calibration standards

PRODUCT DESCRIPTION

The DTG-6000 from 3D Instruments, a 4 ½" Digital Test Gauge, incorporates the ultimate in pressure measurement technology to address the calibration requirements of current process monitoring and control devices.

Outstanding pressure sensors from 0-15 to 0-5000 psi provide accuracy of 0.1% of reading from 20-100% of span. Temperature compensation circuitry maintains this accuracy over an operating temperature range of 14° to 122°F. Wetted components are 316SS for compatibility with many process fluids. A 5 digit LCD with 0.65" digits and high contrast provides for superior resolution and readability.

The DTG-6000 is housed in an electro-polished 300 series SS case with elastomeric seals. All controls including: Power, Zero, Eng. Units and Hi/Lo are selectable via the Lexan keypad for reliable operation in adverse weather conditions. To reduce maintenance, 1500 hour battery life is provided courtesy of a RISC (Reduced Instruction Set Computer) type microprocessor.

The combination of sophisticated precision pressure measurement technology, robust design and a wide array of pressure ranges makes the Digital Test Gauge family of pressure gauges the ideal choice to tackle your demanding pressure monitoring or Test and Calibration applications.

3D Instruments The "Direct Drive Difference" in Digital

MOUNTING FLANGE   **OPTIONS**   **DTG-CAL KIT**

3D Instruments The "Direct Drive Difference" in Digital

GENERAL SPECIFICATIONS

Accuracies: 0.1% of reading for 20-100% of span; 0.02% FS from 0-20% of span and 2% FS (FS=14.5 psi) for vacuum region includes all variations due to non-linearity, hysteresis, repeatability and temp. over the Operating range.

Ranges/Resolutions:

PSI	Resolution	Over Pressure (PSI)
0-15	0.001	100
0-30	0.001	100
0-100	0.01	200
0-300	0.01	600
0-500	0.01	1000
0-1000	0.1	2000
0-2K/3K	0.1	4500
0-5000	0.1	7500

Environmental:
Operating range: 14 to 122°F (-10 - 50°C)
Storage range: -4 to 158°F (-20 - 70°C)

Power:
3 x AA alkaline batteries deliver 1500 hours continuous service @68°F.

Display:
5 digit LCD, 0.65" high
Engr. Unit indication
Low Battery Indicator Battery Icon
Hi/Lo Pressure Icons
Dead Battery - dashed lines across display

Case:
300 Series Stainless Steel

Pressure Sensors:
Media compatibility: media compatible with 316SS. Display flashes at 110% FS.

Process Connection:
1/4" NPT (male) – 316 SS with integral sintered SS filter

Dimensions:
4.3"(W) x 2.46" (D) x 6.09"(L)

Weight:
22 oz (635 gms)

FEATURES

Selection of Engr. Units*:
PSI, mBar, Bar, kPa, kg/cm², inHg, mmHg, inH₂O, mmH₂O
*not all units enabled for all ranges

Power Management:
Auto shut-off after 20 min., if no keys are pressed. Field defeatable

Screen Update Rate:
3x per second

Hi/Lo:
Capture and query the High and Low pressure values

Tare:
0 to 100% FS zero offset capability

RS-232 (optional):
Special RS-232 cable is required

Mounting Flanges (optional):
Front or back 300 Series SS - welded on the DTG case

ORDERING INFORMATION

	①	②	③	④	⑤
	65514	– XX	B	XX	XXX

Example: 4 ½" DTG-6000 with 300 Series SS case, 0-3000 psi sensor no mounting flange, bottom ¼" NPT male fitting: 65514-33B55

① **Product Description:** 4 ½" DTG-6000 with 300 Series SS case

② **Pressure Range Codes:** (all ranges include vacuum measurement to: 29.5" hg)

15: 0-15 psig	23: 0-100 psig	27: 0-500 psig	32: 0-2000 psig	35: 0-5000 psig
21: 0-30 psig	26: 0-300 psig	29: 0-1000 psig	33: 0-3000 psig	

③ **Process Connection:** ¼" NPT male

④ **Connection Position and Mounting Flange Codes:**

15: Flange Front, Bottom Fitting   35: Flange Back, Bottom Fitting   55: Flange None, Bottom Fitting
25: Flange Front, Back Fitting   45: Flange Back, Back Fitting   65: Flange None, Back Fitting

⑤ **Option Codes:** leave blank if no options are required

PNO: DTG-Cal Kit #1 – includes a DTG-6000, Model 8110-300: 0-300 psi Pneumatic Handpump, Hose kit and Series-200 ABS waterproof carrying case

PRO: DTG-Cal Kit #2 – includes a DTG-6000, Model 8111-300: Vacuum/0-300 psi Duplex Handpump, Hose kit and Series-200 ABS waterproof carrying case

PUO: DTG-Cal Kit #3 – includes a DTG-6000, Model 8112-3000: 0-3000 psi Hydraulic Handpump, Hose kit and Series-200 ABS waterproof carrying case

GCO: NIST traceable Calibration Certificate w/data. A NIST traceable Certificate of Conformance is supplied with each unit.

RAA: Custom RS-232 cable (3D P/N: 4025-0005)

(from Acculab) VIC-303 Digital Scale

ACCULAB
sartorius group

- JUMP TO PRODUCT CATEGORY -   - JUMP TO SPECIFIC ITEM -

About   Home   Dealers   FAQs   Products   Service

Weigh The Difference

≫ VIC-Series 0.001g Precision Balances (NEW)

The new **VICON Series Milligram Balances** are ideal for Industrial, Laboratories, Research, Educational, Postal, and Speciality applications. Whether weighing multiple samples with totaled results, formulating a color, counting, percent weighing, specific gravity, or under pan weighing, Acculab has the answer in **VICON**. These new models feature a **flip-down protective cover**, **integrated cal-weights**, a **stainless steel pan** and **back-lit display**.

Standard features include:

- Made in the USA
- 4 models with milligram readability
- Protective flip-down and removable plastic cover for shipping protection and allows stackable storage
- Integrated external calibration weights
- Unique durable design for all applications
- Applications include: Counting, Percent Weighing, Totaling, Display Hold, Specific Gravity, Mass unit conversion
- 14 Mass unit conversions (g, oz, lbs, lbs:oz, dwt, ozt, grains, Newton, carats, Taels HK/Taiwan/Singapore/China, user defined)
- Optional RS-232 or USB interface kit (field installable)
- Parts counting with selectable reference sample (1-100)
- Included AC adapter
- External one button calibration with 3 weight options
- Lock down capability
- Two year manufacturer warranty

Individual Product Specifications

Model	VIC-123	VIC-303	VIC-2mg	VIC-4mg
Capacity	120g	300g	200g	400g
Readability	.001g		.005g	
Linearity (+/-)	3d		2d	
Repeatability (+/-)	2d		1d	
Calibration Weight	20g, 50g, 100g (100g weight included)		50g, 100g, 200g (2 100g weights included)	
Pan Size	4" dia.			
Power 100, 120, 220, 240 Volt	AC adapter			
Dimension WxHXD (includes cover)	6.8" x 3.7" x 9.8"			
List Price (USD)	$385.00	$465.00	$365.00	$425.00
Interface Options	RS-232 or USB (optional)			

(From Geneq)

Digital Thermohygrometer
Model Testo 625

FEATURES

The compact instrument with built-in humidity probe head for measuring air moisture and temperature. The large 2 line display shows humidity, wet bulb temperature or dewpoint as well as temperature. When measuring at hard-toaccess points, the humidity probe head can be easily removed and attached to the handle via the probe cable (accessory). Alternatively, the readings can be transmitted wirelessly over widedistances from the probe to the measuring instrument. To do this, the humidity probe head is attached to the radio handle (accessory) and the radio module (accessory) is added to testo 625.

COMPACT VANE ANEMOMETER

- Displays temperature and relative
- humidity / wet bulb temperature /dewpoint
- Max/min values
- Hold button to freeze readings
- Display light
- Auto Off function
- Patented humidity sensor
- 2 year guaranteed long-term stability
- TopSafe, instrument protection against dirt and knocks

Accessories	Part no.
Handle for plug-in humidity probe head for connection to testo 625, probe cable included	0430 9725
Case for measuring instrument and probes	0516 0210
TopSafe, protects from impact and dirt	0516 0221
Recharger for 9V rechargeable battery For external recharging of 0515 0025 battery	0554 0025
DKD calibration certificate/Humidity Electronic hygrometers; calibration points 11.3%RH and 75.3%RH at +25°C	0520 0206
ISO calibration certificate/Humidity	0520 0006

Electronic hygrometers; calibration points 11.3%RH and 75.3%RH at +25°C

testo 625, humidity/temperature measuring instrument, incl. plug-in humidity probe head, battery and calibration protocol

Part no.

0563 6251

SPECIFICATIONS		
Probe Type	**NTC**	**Testo humid. sensor cap.**
Meas. range:	-10 to +60 °C	0 to +100 %RH
Accuracy ±1 digit:	±0.5 °C	±2.5 %RH (+5 to +95 %RH)
Resolution:	0.1 °C	0.1 %RH
Oper. temp.:	-20 to +50 °C	
Storage temp.:	-40 to +85 °C	
Battery type:	Alkali manganese	
Battery life:	70 h (without radio operation)	
Dimensions:	18208064" M40"0"/> mm	
Weight:	195 g	
Material/Housing	ABS	
Warranty:	2 years	

Appendix F: Flow Rate/Pressure Drop Data

210

$y = 20.56x^2 + 126.05x - 12.50$

◆ -1/3 and Neu

$y = 2.17x^2 + 15.94x - 3.03$

◆ Neu and Neu

$y = 4.28x^2 + 22.45x - 7.23$

◆ -2/3 and +1

$y = 1.50x^2 + 16.39x - 7.72$

◆ -1/3 and +1

$y = 2.44x^2 + 7.65x + 0.36$

◆ Neu and +1

$y = 1.09x^2 + 15.34x - 6.21$

◆ -2/3 and +2

216

$y = 0.76x^2 + 15.06x - 5.96$

♦ -1/3 and +2

Pressure Drop in the Device (kPa)

Average Fluid Velocity (m/s)

$y = 0.71x^2 + 13.38x - 6.09$

♦ Neu and +2

Pressure Drop in the Device (kPa)

Average Fluid Velocity (m/s)

$y = 0.78x^2 + 8.84x - 2.15$

Pressure Drop in the Device (kPa)

Average Fluid Velocity (m/s)

♦ Control

2484-41